UNIVERSITY OF SOUTHAMPTON

FACULTY OF ENGINEERING AND THE ENVIROMNET

School of Civil Engineering

Effects of Temperature on the Adhesive Bonding in Steel Beams Reinforced with CFRP Composites

by

Ghayth Mohammed Hassein Abed

Thesis for the degree of Doctor of Philosophy

July 2012

UNIVERSITY OF SOUTHAMPTON

Abstract

FACULTY OF ENGINEERING AND THE ENVIRONMENT

Doctor of Philosophy

EFFECTS OF TEMPERATURE ON THE ADHESIVE BONDING IN STEEL BEAMS REINFORCED WITH CFRP COMPOSITES

By Ghayth Mohammed Hassein Abed

The use of carbon fibre reinforced polymer (CFRP) composites in strengthening and repairing steel beams and girders in existing structural bridges has become wide spread in recent years. Though the previous studies had showed significant improvement in the load carrying capacity and the fatigue life of the strengthened structures, they did not take into consideration the effects of extreme summer temperature on the behaviour of the reinforced structure because they were carried out at room temperature. The change of temperature affects the mechanical properties of the adhesive epoxy. Moreover, thermal stresses are induced in the adhesive bond due to the significant difference in the coefficients of thermal expansion between CFRP and steel materials. The main aspects investigated in this thesis are the changes in the adhesive mechanical properties due to the change in the temperature and the impact of these changes on the failure mechanism, the failure load, the fatigue life and the stresses distributions of steel beams strengthened with CFRP plates.

In order to achieve the aims of the research, the following procedures are carried out: First, tensile tests on adhesive specimens were carried out at different temperatures to investigate adhesive properties temperature dependency. Second, static tests were conducted on both double-lap shear and three-point bending specimens at temperatures ranging between 20 to 60 °C to examine the influence of temperature on the failure mechanism and the failure load. Third, an analytical model was developed to calculate the interfacial stresses in the reinforced beam by approximating the adhesive nonlinear behaviour at elevated temperatures with the elastic perfectly-plastic representation. Fourth, finite element analysis was conducted to validate the analytical results assuming bilinear elastic-plastic adhesive behaviour. Finally, fatigue tests were carried out on both double-lap shear and three-point bending specimens at different load and temperature ranges to identify their fatigue life temperature dependency.

Adhesive materials showed significant reduction in the strength and the stiffness coupled with nonlinear behaviour as the temperature reaches the adhesive glass transition temperature (T_g). Thus, the failure load and fatigue life of the strengthened structures were reduced significantly at T_g with a change in the failure mechanism. Both the analytical and finite element results were capable of defining the length of the plastic zone occurring at the plate end due to the high shear stress concentration. The length of the plastic zone depends on several parameters, including the elastic modulus and the thickness of the CFRP plate, the applied load and the temperature. The study of these parameters shows that it is possible to avoid CFRP plate debonding at extreme temperature by using thinner and longer CFRP plates with high modulus instead ultra-high modulus.

CONTENTS

List of figures

List of tables

DECLARATION OF AUTHORSHIP

I, Ghayth Mohammed Hassein Abed declare that the thesis entitled:

Effects of Temperature on the Adhesive Bonding in Steel Beams Reinforced with CFRP Composites

and the work presented in the thesis are both my own, and have been generated by me as the result of my own original research. I confirm that:

- this work was done wholly or mainly while in candidature for a research degree at this University;
- where any part of this thesis has previously been submitted for a degree or any other qualification at this University or any other institution, this has been clearly stated;
- where I have consulted the published work of others, this is always clearly attributed;
- where I have quoted from the work of others, the source is always given. With the exception of such quotations, this thesis is entirely my own work;
- I have acknowledged all main sources of help;
- where the thesis is based on work done by myself jointly with others, I have made clear exactly what was done by others and what I have contributed myself;
- parts of this work have been published as:

1. Abed, G. & Lee, M. (2011), "Effect of temperature variation on bond behaviour of steel beams strengthened with CFRP plates", *16th International Conference on Composite Structures (ICCS16), 28-30 Jun., Porto, Portugal.* Abstract and presentation
2. Abed, G. (2011), "The influence of temperature on steel structures strengthened with externally bonded CFRP Plates", in Advanced Composites in Construction *(ACIC 2011), 6-8 Sep., University of Warwick, UK.* Poster and presentation
3. Abed, G. and Lee, M. (2012), "Effect of temperature on fatigue behaviour of steel beam strengthened with CFRP plate", *The Third Asia-Pacific Conference on FRP in Structures (APFIS), 2-4 Feb., Japan*. Abstract accepted.

Signed: Ghayth M. H. Abed
Date: July 2012

Acknowledgements

I would first like to thank my supervisor, Professor Marcus Lee, for his support and patience supervision.

I wish to acknowledge the Erasmus Mundus programme (EM8) and the school of civil engineering for the financial support. A special thank you goes to Professor Janice Barton who allowed me to use the facilities in the Transport System Research Lab (TSRL). I would like to thank Dr. Steve Boyed and Dr. Jun Deng for supplying of the carbon fibre materials, and Sikadur Ltd Company for providing me with the adhesive materials without these contributions this research would not be completed.

I would also like to thank all the lab technicians at the University of Southampton, Mr. Rob Barnes, Mr. James Chitty and Mr. Clive Stafford, for helping me with various technical difficulties I faced during my experimental work. Especial thanks to my colleges in the TSRL lab for them advices and help in my tests, especially to Dr. Thomas Bostock for his help in my thermal tests.

Special thanks to Dr. Hassan Alfetlawi, Dr. Zuhair A. Amair and Mrs. Gillian Taylor for quickly proofreading and giving suggestions. I am thankful as well to all my friends for being there for me and for all motivations. Finally, I would like to thank my parents and my brother for their love, support and encouragement throughout my entire life.

Definitions and abbreviations

symbol	Description
A	Cross-sectional area
A_p	CFRP cross-sectional area
A_s	Steel cross-sectional area
a	Adhesive
b	Width
CFRP	Carbon Fibre Reinforced Polymer
E_a	Tensile elastic modulus of adhesive
E_p	Tensile elastic modulus of CFRP
E_s	Tensile elastic modulus of steel
G_a	Adhesive shear modulus
I_p	CFRP moment of inertia
I_s	Steel moment of inertia
L_p	CFRP plate length
L_s	Beam span length
L_1	Effective CFRP plate length
M	Bending moment
N	Longitudinal force/ number of cycles
p	CFRP plate
$P_{ult,T}$	Failure load at any temperature
q	Uniform load
S	Strain gauge
s	Steel beam
t_a	Thickness of the adhesive layer
t_p	Thickness of the CFRP plate

t_s	Thickness of the steel plate
T_g	Adhesive glass transition temperature
u	Longitudinal displacement
V	Shear force
v	Transverse displacement/Poisson's ratio
σ_a	Adhesive tensile strength
$\sigma_{a,plastic}$	Adhesive maximum normal strength
σ_p	CFRP tensile strength
σ_u	Steel ultimate strength
σ_y	Steel yield strength
α_p	CFRP coefficient of thermal expansion
α_r	Invar36 coefficient of thermal expansion
α_s	Steel coefficient of thermal expansion
$\tau_{a,plastic}$	Adhesive maximum shear strength
ε_y	Steel yield strain
γ	Shear strain
ΔT	Change in temperature

Chapter 1

1.1 Introduction

Sectional steels have been commonly used in the construction of many railway and highway bridges worldwide. These structures are in urgent need of retrofitting due to deterioration over time because of corrosion and fatigue. Unprotected steel corrodes and loses about 0.1 mm of thickness per year in a damp environment [1]. In addition, fatigue damage caused by cyclic loading leads to crack initiation and propagation, especially around the connections (bolted, riveted and welded). Furthermore, some of these bridges were constructed in a time where the permissible vehicle weights and train speeds were less than the current ones (44 tonnes across the EU, except in Sweden and Finland where 60 tonnes is allowed, 350 km/hr) [2, 3] which intensify the applied loads and vibrations on the bridge elements, thus reduced the expected life time of bridges. Therefore, there is an urgent need to strengthen and retrofit these bridges to ensure their safe use during the designed lifetime.

The conventional methods for repairing and strengthening metallic structures involve mechanical fasteners such as rivets and bolts, welding, and bonding a steel plate to the defective elements. The drawbacks of these methods are the development of local stresses around the drilled holes, the sensitivity of the welded joints to fatigue and the continuity of galvanic corrosion of the steel plate. The use of Carbon Fibre reinforced polymer (CFRP) composites in strengthening and repairing steel structures has become wide spread in recent years. CFRP composites adhesively bonded to steel members offer many advantages over steel plate bonding including high strength or high stiffness to weight ratios, excellent corrosion and fatigue resistance. In addition, CFRP is easy to handle and install. Thus, there is no need for lifting equipment, hence minimising traffic disruption and overall costs.

1.2 Identification of the problem

The mechanical properties of adhesive epoxies used to bond the CFRP composites to the steel beams in structural bridges are temperature dependent. Thus, the adhesive strength and stiffness reduce significantly when the temperature becomes close to a temperature known as the glass transition temperature (T_g). At T_g, the adhesive changes its nature from a hard (glassy) state to a flexible (rubbery) state [4]. Accordingly, the adhesive stress-strain behaviour changes from

linear elastic to nonlinear plastic [5]. More details about the temperature dependency of adhesive mechanical properties will be discussed in section 2.10 in Chapter 2.

In civil engineering applications, CFRP composites are bonded to steel structures using cold-cured adhesive epoxies. The T_g values of cold-cured adhesive epoxies range between 50-82 °C [4, 6]. The temperature of steel bridge components could exceed these values in the summer seasons [7, 8], causing premature CFRP debonding failure to occur. In addition, high thermal stresses are developed in the adhesive between a steel beam and a CFRP composite with the daily temperature variation due to the considerable difference in the coefficients of thermal expansion of the steel (10-12 $\times 10^{-6}$ \°C, [9]) and the CFRP (-1.7-1$\times 10^{-6}$ \°C, in the longitudinal direction of UD CFRP composites, [10]). These thermal stresses may exceed those produced by mechanical loading [11, 12]. The combined effects of the thermal stresses and adhesive softening at elevated temperatures may result in premature debonding failure [13].

1.3 Research objectives

The main objective of this research is to find out how temperature affects the strength and the fatigue life of steel beams strengthened with externally bonded CFRP plates.

Though much research [14-24] has achieved significant improvement in the strength and the fatigue life of strengthened steel beams and girders using externally bonded CFRP sheets or plates, they carried out their experiments at room temperature, hence they did not take into consideration the effects of extreme summer temperature on the behaviour of the strengthened structure. Moreover, several analytical solutions [11, 12, 25-30] have been developed to calculate the shear (τ) and the normal (σ) stresses within the adhesive layer between a steel beam and a CFRP composite. However, these solutions assumed linear elasticity and temperature independence of the adhesive material.

In order to avoid the drawbacks of the previous research, the researcher intends to conduct experimental tests and analytical and finite element (FE) analyses to evaluate the bond characteristics of CFRP strengthened steel at elevated temperatures. The experimental investigation will examine the behaviour of the double-lap shear specimens and the CFRP strengthened beams that are subjected to a static and a fatigue cyclic loading at elevated temperatures up to 60 °C. The analytical and FE analyses will be developed to calculate the shear and the normal stresses induced in the adhesive between a CFRP plate and a steel beam due to both thermal and mechanical loads. These analyses will take into consideration the changes in the adhesive properties with temperature and nonlinear behaviour. The nonlinear

stress-strain curves of the adhesive at elevated temperatures are simplified with both an elastic-perfectly-plastic approximation in the analytical model and with a bilinear elastic-plastic representation in the FE model.

1.4 Thesis outline

This thesis is composed of seven chapters.

Chapter 1 introduces the needs for strengthening steel bridges and the advantages of using CFRP composites, the problem identification and the objectives of this research. Chapter 2 reviews the previous work related to the impact of temperature on steel, adhesive and CFRP materials as well as on strengthened structures. Moreover, current analytical solutions to obtain the interfacial stresses of reinforced beam are discussed. Chapter 3 displays material mechanical and thermal properties of steel, CFRP and adhesive obtained from experimental tests at different temperatures. These properties are required for the analytical and the FE analyses that are used to calculate the shear and normal stresses in the adhesive between CFRP plate and steel beam. Chapter 4 presents the static test results carried out on double-lap shear specimens and CFRP strengthened steel beams at various temperatures. Chapter 5 introduces the analytical and FE analyses performed to calculate the shear and normal stresses induced in the adhesive for steel beams strengthening with CFRP plates under mechanical and thermal loads. Chapter 6 explores the fatigue tests results of double-lap shear specimens and reinforced bending beams at different cyclic loading ranges and temperatures. Finally, chapter 7 demonstrates the findings arrived at in this study as well as the recommendations and the further research.

Chapter 2

Background and literature review

2.1 Introduction

This chapter gives background information on the FRP composites and their usage as an external strengthening component in civil applications. In addition, the available design guidelines and the field applications are described. Following that, relevant research and information regarding the effect of temperature on the steel, on the adhesive and on the CFRP materials are discussed. Finally, the relevant experimental and analytical works on the effect of temperature on strengthened structures are reviewed.

2.2 Steel structures

Although steel material has been produced in Britain since 1860, it took about fifty years to entirely replace wrought iron bridges [27]. The mechanical properties of steel depend on the chemical composition, the heat treatment and the manufacturing process. Increasing the carbon percentage increases the strength of the steel but decreases its ductility. Modern steel is produced with a maximum carbon content of 0.25 per cent which provides the best combination of strength and ductility [27]. Developments in the manufacture and the control of quality and strength of steel materials have motivated engineers to create the most challenging and spectacular structures which are either difficult or costly to produce with other materials.

2.3 Fibre reinforced polymers

Fibre reinforced polymer (FRP) is a composite material that is composed of two components: fibre reinforcement and polymeric resin (matrix), as shown in Figure 2.1. The fibres enhance the strength and stiffness of the FRP composites whilst the matrix allows the load transfer between the individual fibres, and protects them from mechanical and environmental damage. The properties of the FRP composite depend on the properties of the matrix and the fibre as well as the fibre volume ratio and the fibre orientation. There are different types of FRP composites that often used in civil engineering applications such as: the glass fibre reinforced polymers (GFRP), the aramid fibre reinforced polymers (AFRP) and the carbon fibre reinforced polymers (CFRP). These types of composite have a wide range of material properties and prices.

CFRP composite is normally used in steel strengthening because its strength and stiffness are comparable to the steel material. There are three types of CFRP materials: normal modulus (CFRP) with a stiffness less than steel, high modulus (HM-CFRP) with a stiffness similar to steel, and ultra high modulus (UHM-CFRP) with stiffness higher than steel [31]. Therefore, HM-CFRP and UHM-CFRP are preferred in strengthening steel structures hence they will carry the stresses before the steel is yielded. The CFRP composites are supplied in the forms of pultruded plates and as preimpregnated (prepreg) or dry wrap sheets, as shown in Figure 2.2. CFRP pultruded plates are bonded to the structure using a two-part epoxy adhesive, while CFRP sheets are bonded using an epoxy resin by wet lay-up technique [32]. The properties of different types of CFRP sheets and plates supplied by SIKA are given in Table 2.1.

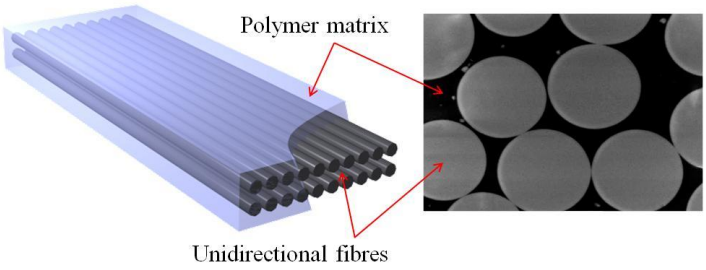

Figure 2.1: Schematic and microscopy image of FRP composite

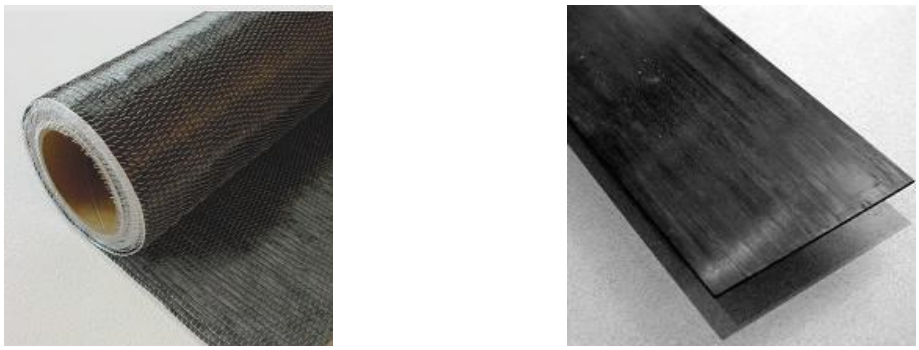

(a) Prepreg sheet (b) CRRP plate

Figure 2.2: CFRP products used in strengthening

Table 2.1: Properties of CFRP materials

Material	Tensile strength MPa	Elastic modulus GPa	Ultimate strain %
Sika Wrap 200C*	3900	230	1.5
Sika Wrap 201C*	4900	230	2.1
Sika Wrap 300C*	3900	230	1.5
Sika Wrap 300C Hi Mod NW*	2600	640	0.4
Sika CarboDur S**	2800	165	1.7
Sika CarboDur M**	2400	210	1.2
Sika CarboDur H**	1300	300	0.45

* Carbon fibre sheets, ** Carbon fibre plates

2.4 Composite vs steel plates bonding

Plate bonding is an effective technique for strengthening existing structures. This technique involves bonding a steel plate to the tension face of the beam by using an adhesive epoxy.

The earliest application of bonded steel plate to a concrete bridge took place in 1964 in Durban, South Africa [33]. Since then, the technique has received much attention and it has been used to repair and upgrade a variety of existing structures. In the UK, the first application of bonded steel plates on a concrete bridge was in 1975 at the Quinton interchange on the M5, south of Birmingham [34]. After it had been strengthened, the bridge demonstrated a significant increase in flexural stiffness and a reduction in crack opening under load. In 1995, cores were taken through the plates showed light corrosion of the steel beneath the adhesive [34]. Nevertheless the cohesive properties of adhesive materials were similar to their initial values and satisfactory structural performance was achieved in lap shear joints. Steel plate bonding technique was employed to strengthen Bures Bridge (cast-iron) in Suffolk, UK in 1991 [35]. The bridge capacity was raised from 7 to 40 tonnes after it had been strengthened.

Although this technique has proved efficiency in upgrading concrete and metallic structures, there are many problems associated with the use of steel plates:

- Installation of heavy steel plates requires expensive scaffolding and lifting equipment which may cause traffic interruptions.
- The difficulties of handling and mounting heavy steel plates result in restrictions on plate dimensions.
- The galvanic corrosion of the bonded steel plate is continuous.
- It is difficult to shape and fit steel plates on curved surfaces.

Therefore, it is necessary to adopt a technique which takes into account durable material and cost-effective reinforcing with minimum traffic disruption. Researchers investigated FRP composites as an alternative to the steel plate bonding. FRP composites have superior properties including high strength or high stiffness to weight ratios and excellent corrosion and fatigue resistance. Due to their lightweight, it is easy to handle and install without a need for lifting equipment hence minimising traffic disruption and overall costs.

The first research on the use of CFRP composites for reinforced concrete beams was carried out at EMPA (Swiss Federal Laboratories for Materials Testing and Research) [36].The first concrete bridge repaired with externally bonded CFRP stripes was the Ibach Bridge in Switzerland in 1991 [37]. The bridge was strengthened with three CFRP stripes of 2 mm thick and 5000 mm length. The loading test with an 84-tonne vehicle demonstrated that the restoration work was completely satisfactory.

In the UK, Oxford Brookes University carried out the first research on FRP plate bonding for concrete strengthening in the early 1990s under the supervision of the Joining Technology Research Centre [32, 38]. Furthermore, the ROBUST project was initiated in 1994 to investigate the viability of using CFRP and GFRP composites as an alternative to steel plates in strengthening of bridge. The project finding showed that FRP strengthening is more economical and durable than steel due to ease of transportation and handling and corrosion resistant. More details of the results of the entire project are available in Hollaway and Leeming [39].

Although the successful use of FRP composite for flexural and shear strengthening of reinforced concrete (RC) bridge structures, the use in strengthening of steel bridges is not as widespread as that for RC. This is because of a different and a more difficult set of problems [18, 40, 41]: first,

the failure mechanisms developed in the RC are different compared to that of steel, as FRP bonded concrete failed due to separation of concrete cover. Second, the high strength and stiffness of steel make it a more difficult material to strengthen therefore it requires composite material of same stiffness order to allow the load transfer from the beam to the reinforcement composite before steel has yielded such as UHM-CFRP.

2.5 Design guidelines for strengthening of steel structures using CFRP

Several design guidelines for the use of FRP in strengthening metallic structures have already been published throughout Europe as well as in the USA.

In 2001, the first design guidance "FRP composites-life extension and strengthening of metallic structures" was presented by the Institution of Civil Engineers in the United Kingdom [42]. The strength of a metallic structure strengthened with FRP materials was evaluated using a transformed section analysis in the elastic range and an elastic-plastic moment-curvature analysis beyond the elasticity. Suggestions for short-term and long-term behaviour were given. In addition, it included case studies of projects on the London Underground network.

In 2004, another design guideline for strengthening metallic structures using FRP materials was published in the UK (known as CIRIA C595) which covered design, installation and inspection [27]. In this guidance, sectional stress analysis was applied to calculate the amount of FRP material required to achieve the desired strength in a structural beam. An elastic analysis was proposed for brittle metallic structure, such as historical cast iron bridges, where the stress across the beam section is less than the yield stress. But elasto-plastic analysis was used beyond the elastic range for steel beams and steel-concrete composite girders, where the stress across the beam section at a point furthest from the neutral axis is equal to the yielding stress. According to the guidelines, debonding failure of the strengthening system can be prevented if the maximum principle stress in the adhesive joint does not exceed the strength of the adhesive obtained from lap-shear tests. In addition, this guidance suggests a load and material safety factors which should be included in the design. The material partial factor considered effects of environment (such as temperature and moisture) and time (such as creep and material degradation).

In 2007, Schnerch et al. (2007) proposed design guidelines for strengthening steel concrete composite beams with high modulus CFRP composites [43]. The guidelines are based on a moment-curvature analysis and load-deflection curves which satisfy the conditions of equilibrium and compatibility. The guidelines stated that the allowable increase of live load for

a strengthened girder should be selected to satisfy serviceability, safety and redundancy conditions. These are achieved by insuring that: first, the total service load of the strengthened beam, including the dead load and the increased live load, should not exceed 60 percent of the increased yield moment capacity of the strengthened beam; second, the total factored applied load should not exceed the ultimate capacity of the strengthened beam after applying an appropriate strength reduction factor; and finally, the combined effect of the dead load and increased live load should not exceed the capacity of the unstrengthened beam to ensure that the structure remains safe in the case of a possible loss of the strengthening system.

Recently, the Italian National Research Council published state-of-the-art guidelines on the design, installation and monitoring of an externally bonded FRP system for strengthening existing metallic structures [44]. The guidelines recommend the use of material partial factors to ensure structures safety. The stresses analyses are similar to those proposed by the CIRIA C595 guidance.

2.6 Metallic structures strengthened by CFRP composites

Several metallic beams in bridges and other structures have been strengthened with CFRP composite worldwide.

- In the UK, the Hythe bridge over the Thames river in Oxfordshire, Slattocks Canal bridge in Rochdale, Bow Road Bridge in East London and the Bid bridge in Kent were strengthened with normal modulus CFRP plates [18]. A London Underground steel bridge at Acton in West London was also strengthened with HM-CFRP plates to reduce the live load stresses by 25 percent and improve its fatigue resistance [45]. The King Street Railway Bridge in Mold was strengthened with CFRP laminate strips that helped strengthen six cast iron girders to allow 40 tonne vehicles to use the bridge [44]. The curved arch cast iron Tickford Bridge near Newport Pagnell was strengthened using 14 layers of prepreg CFRP sheets [44].

- In the USA, two bridges were strengthened using normal modulus CFRP plates in Delaware. The first bridge, 1-704 bridge, carries southbound I-95 traffic over Christina Creek with a single girder [17]. After the retrofitting, the measured strain in the tension flange of the steel girder was reduced by 15 percent and the girder stiffness was increased 12 percent. The second bridge, the Ashland bridge on State Route 82 over Red Clay Creek, had two steel strengthened girders to support part of the dead load after a new concrete deck was cast [46]. The girders of a three span

bridge over Walnut Creek in Pottawattamie County in Iowa were strengthened with normal modulus CFRP laminate plates [47]. The plates were bonded to both the bottom and top surfaces of the tension flanges at several locations of the positive moment regions. Load tests of the girders before and after the CFRP strengthening revealed similar measured strains in the steel tension flange of the girders. This was probably due to the relatively small amount of CFRP material installed and the low modulus of the CFRP selected. The Sauvia Island Bridge in Washington was strengthened using CFRP laminate strip bonded to an aluminium honeycomb core [48]. The aluminium core was added to increase the distance of the CFRP strip from the neutral axis of the steel beam thus increasing the stiffness of the member.

- In Italy, the Corona Bridge in Venice was retrofitted to reduce impact load damage. The cast iron arches were strengthened using aramid tri-axial sheets and mono-directional strips[44].

- In Japan, the Takiguchi Bridge in Tokyo was strengthened using UHM-CFRP laminates. The bridge girders were strengthened by bonding 4 mm thick laminates along the bottom of the tension flange.

2.7 Previous tests on steel beams and girders strengthened by CFRP composites

Mertz and Gillespie [40] investigated the effectiveness of using CFRP materials for rehabilitation of naturally deteriorated steel bridge girders. Steel girders deterioration was due to loss of cross-section area through corrosion. These girders were removed from a highway bridge in Pennsylvania (USA) after being demolished. The members retrofitted with five different schemes: First, composite plate was bonded to the bottom side of the tension flange. Second, aluminium honeycomb composite plate was adhered to the tension flange. Third, composite fabric was wrapped on the web of the beam down over the flange with a foam spacer. Fourth, E-glass pultruded channel was adhesively bonded and mechanically fastened to the beam flange. Finally, composite plate was bonded to the bottom and top sides of the tension flanges. Results showed that the flexural stiffness and strength increased considerably e.g., CFRP strips with 6mm-thick bonded to the top and bottom surfaces of the tension flange increased the strength and flexural stiffness to 65% and 27% of the original girders. Furthermore, result from two full-scale corroded steel girders with 6.4-m-long indicated an average of 25% increase in stiffness and a 100% increase in strength.

Another study was conducted by Miller et al. [17] on full scale corroded girders to investigate the potential of reinforcement with CFRP plates. Static three-point bending tests were performed on unreinforced girder to assess the decrease in strength and stiffness due to reduction of cross-section area. The results showed that the stiffness has been reduced and is ranging from 13% to 32%. The restoration of four girders consists of bonding 5.25 mm-thick CFRP plates to the soffit of the tension flange. Test results showed that the stiffness had increased in the range 10-37% due to retrofit. In addition, fatigue tests on small and large scale specimens had indicated that CFRP plate provides a good fatigue resistance. Liu et al [49] and Tavakkolizadeh and Saadatmanesh [50] conducted test on notched steel members retrofitted with CFRP strips. Notches were created using band saw across the bottom of the tension flange to simulate the corrosion. Test results showed significant increases in the strength and stiffness of notched beams.

Strengthening of undamaged steel-concrete composite girders through attaching different number of layers 1, 3, and 5 of 1.27 mm-thick CFRP plates to the tension flanges of the steel section was investigated by Tavakkolizadeh and Saadatmanesh [16]. Their results showed that ultimate load carrying capacity of the girders was significantly increased. However, their elastic stiffness was slightly increased. Furthermore, it was noted that efficiency of reinforcement was reduced as the number of layers of CFRP increased. Other researchers simulated beam damage by removing part of the sides of the tension flange (Tavakkolizadeh and Saadatmanesh [51], and Al-Saidy et al. [52]). Test results showed that the load carrying capacity of the girders was significantly increased, but the elastic stiffness was little increased. This was due to the CFRP composite having a lower elastic modulus than steel beams. In order to simulate severe service damage of the composite specimens, Sen et al. [53] overloaded steel-concrete composite beams until failure of the tension flange was induced and then the beams were reinforced with CFRP plates. Test results showed significant increases in the beams capacity. However the increases in the stiffness were relatively modest. The same authors suggested using mechanical anchorage at the CFRP plate end to prevent premature debonding failure.

The use of normal modulus CFRP and HM-CFRP sheets to restore artificially damaged steel-concrete composite beams was indicated by Shaat and Fam [54]. It was noted that flexural strength and stiffness of the composite girders were reduced by 60 and 54%, respectively due to complete cut in the tension flange at mid-span. However, restoration with CFRP sheets was able to recover original strength and stiffness. The failure mode of strengthened girder was debonding of normal modulus CFRP sheets, whereas rupture of the HM-CFRP sheets was observed.

Tavakkolizadeh and Saadatmanesh [15] conducted fatigue tests on steel beams strengthened with CFRP. Four-point bending tests were carried out on 21 notched steel beams strengthened with CFRP patches. The steel beams were tested with different constant stress ranging from 69 to 379 MPa, and from 5 to 10 Hz. The results showed that the CFRP strengthening extended the fatigue life by more than three times, and decreases the crack growth rate significantly.

Further studies regarding the performance of steel beams strengthened with CFRP under cyclic loads were reported by Täljstena et al. [24]; Kim and Harries [22] and recently Ghafoori et al. [23].

2.8 Existing analytical model

Many first-order analytical solutions have been developed to calculate the shear and the normal stresses within the adhesive layer between a steel beam and a strengthening composite. Smith and Teng [25] presented a general solution based on deformation compatibility approach for obtaining the shear and the normal stresses in the adhesive layer of a retrofitted beam. Their solution is applicable to beams made of any material strengthened with a thin plate and subjected to different loading cases. However, the bending moment in the adhesive layer was ignored in this model, and hence does not satisfy the equilibrium requirements. Denton [26] extended the solution presented by Smith and Teng to calculate the interfacial shear and normal stresses developed in the adhesive layer between the FRP plate and the beam due to differential thermal expansion. This model, however, does not consider the combined effects of the thermal and mechanical loads on the interfacial stresses, which is a realistic case of a retrofitted beam. Design guidance on the use of FRP to strengthen metallic structures is given in the CIRIA, C595 report [27]. This report analysed adhesive joint stresses based on two approaches: a stress-based approach and a fracture mechanics-based approach. Its analytical model concerned the interfacial stresses of retrofitted metallic structures due to both mechanical and thermal loadings and under all aspects of strengthening schemes including brittle (cast iron) and ductile (steel) metallic structures and non-prestressed and prestressed strengthening. Deng et al. [11] and Stratford and Cadei [12] also proposed an elastic bond stress analysis that predicted the shear and the normal stresses between a strengthened plate and a metallic beam under both mechanical and temperature loads.

All of the previous solutions, [11, 12, 25-27], assumed no variation in the interfacial stresses across the thickness of the adhesive layer and maximum shear stresses occur at the ends of the adhesive layer, thus violating the zero shear stress boundary condition. Therefore, several higher-order analyses have been proposed to overcome the limitations of the first-order

solutions. Rabinovich and Frostig [55] presented a high-order analytical solution based on equilibrium and deformation compatibility requirements for the analysis of concrete beams strengthened with FRP strips subjected to arbitrary distributed and concentrated loads and moments. Their model satisfied the free surface condition at the end of the adhesive layer, but the variation of the longitudinal stresses is ignored. Shen et al. [28] proposed a close form high-order solution for a beam or a slab bonded with a thin FRP composite or a steel plate subjected to a uniformly distributed load in combination with a uniform bending moment. This solution considered the variation of shear stresses across the adhesive thickness. Yang et al. [29] extended the Shen et al. approach to include arbitrary loading conditions for simply supported RC beams. The previous solutions, [28, 29, 55], are general in nature and can be applied to other types of composite materials. They consider mechanical loading only and do not include thermal loading. Yang et al. developed an analytical model to calculate the interfacial stress of a plated beam under symmetric thermal and mechanical loads [56]. The advantage of this model is the ability to predict the variation in the normal stresses between the plate-adhesive and the adhesive-beam interfaces. The computational complication of high-order solutions requires specialised computer packages to solve them, thus limiting their usage in design applications. Yang and Ye [30] presented a simple model that can be solved using an Excel spreadsheet and produces a good agreement with the high-order solutions. Their solution is general and can be used to analyse beams and plates of different types of materials under mechanical and/or thermal loads.

All of the first-order, [11, 12, 27, 30], and high-order, [30, 56], analytical solutions can calculate the interfacial stresses developed within the adhesive layer between a strengthening plate and a beam due to thermal and mechanical loading. But these solutions assumed that the adhesive material is linear elastic and its mechanical properties are temperature independent. Dawood and El-Tahan modified the analytical model proposed by Stratford and Cadei [12], taking into account the reduction in adhesive properties at elevated temperatures [13]. The stresses were calculated based on two criteria: the principle-stress criterion for linearly elastic adhesive behaviour (at room temperature), and the von-Mises criterion for elastic-perfectly-plastic adhesive behaviour (at elevated temperatures). Their model assumed that failure occurs if the maximum stresses exceed the adhesive strength. The failure load was calculated based on a moment-curvature analysis assuming complete interaction between the steel beam and the CFRP plate. Most recently, Stratford and Bisby [57] have recently presented a model which takes into consideration the variation in adhesive properties with temperature as well as non-uniform strain distribution along the bonded area. Thus, the bonded area was divided into two zones: purely elastic near the mid-span and elasto-plastic at the plate ends.

2.9 Steel thermomechanical properties

According to the Eurocode4 [58], the yield strength and the elastic modulus of structural steels reduce slightly at temperatures above 100 °C. The retention functions of the degraded yield strength (η_{f_y}) and Young's modulus (η_{E_s}) of steel section are given by empirical equations provided by AS4100 standard [59].

$$\eta_{f_y} = \frac{f_y(T)}{f_y(20\ ^oC)} = \begin{cases} 1 & 0 \le T \le 215 \\ (905 - T)/690 & 215 \le T \le 905 \end{cases} \quad (2.1)$$

$$\eta_{E_s} = \frac{E_s(T)}{E_s(20\ ^oC)} = \begin{cases} 1 + \left[T/\left(2000\ln(T/1100)\right)\right] & 0 \le T \le 600 \\ (690(1 - T/1000)/(T - 53.5) & 600 \le T \le 1000 \end{cases} \quad (2.2)$$

where T is the temperature and $f_y(T)$ and $E_s(T)$ are the yield strength and Young's modulus at any temperature.

According to Eq. (2.1), there is no reduction in the yield strength up to 215 °C. From these standards, the effects of extreme summer temperature of 60 °C, assumed in this research, on the steel mechanical properties are insignificant. Thus, steel Young's modulus value obtained from tensile test at room temperature (Chapter 3) will be used in the analytical and FE analyses at elevated temperatures (Chapter 5).

2.10 Adhesive thermomechanical properties

There are two types of adhesive polymers: thermoplastics (such as nylons and polyethylene) which melt on heating and solidify on cooling, and thermosets (such as epoxy and polyester) which cannot be melted or reshaped by reheating but just degrade. Polymer molecules chain together by primary strong covalent bonds, and secondary weak dipole interaction, hydrogen and Van der Waals bonds [60]. In addition to these bonds, thermosetting adhesive is heavily cross-linked during the polymerisation of its components (a resin and a hardener). The secondary bonds melt at high temperatures; hence the adhesive properties are reduced. The melting temperature is known as the glass transition temperature (T_g). The T_g depends on the curing temperatures and the moisture content. The post-curing at elevated temperatures of hot-cured epoxies can increase the T_g value. The moisture reduces the T_g due to plasticisation of the

adhesive with water uptake. De Nève and Shanahan [61] carried out viscoelasticimetric tests on small epoxy specimens ($130 \times 115 \times 5$ mm^3) exposed to 100% relative humidity at 70 °C. They indicated that the adhesive T_g value decreased from 126 to 77 °C after humid aging for about 53 days. The traditional methods for measuring T_g are the differential scanning calorimetry (DSC) [62], the dynamic mechanical thermal analysis (DMTA) [63], and the mechanical loading of bulk adhesive dogbone specimens. However, each method provides slightly different values of T_g e.g., the mechanical method gives different T_g values depending on the loading rate and the specimen configuration.

Hot and cold cured epoxies are widely used as an adhesive bonding agent or as a resin matrix material for FRP composites. The hot-cured epoxies lose their strength and stiffness above 200 °C [64]. However the cold-cured epoxies, often used in civil engineering applications because they do not require any curing equipment, have T_g values ranging from 50 to 82 °C [4, 6] which is not much in excess of the structure's temperature on hot summer days. Banea and Silva [65] carried out tests on two types of adhesives that are used in the automobile industry at temperatures of -40, 25, 60 and 80 °C. The adhesive showed large increases in ductility and reduction in strength and stiffness at 80 °C. However, a brittle failure occurred at higher strength and less strain at -40 °C. Al-shawaf [5] investigated the properties of three different types of adhesives that are commonly used in strengthening civil structures at temperatures ranging from -40 to 60 °C. Tensile tests on bulk specimens at different temperatures indicated that these adhesives exhibited a reduction in strength and stiffness with an increase of temperature.

The polymers modulus changes with temperature into four states: glassy, glass-transition, rubbery and viscous (see Figure 2.3) [60]. Details of these states and their analytical models are given by Ashby [60]. The model proposed by Mahieux and Reifsnider [66] to predict the reduction in composite properties with temperature validated the experimental results on different thermoplastic polymers [67]. Even below T_g, the modulus of an adhesive drops due to creeping of the secondary bonds [60], hence the adhesive properties are not only temperature-dependent but also time-dependent. DMTA tests on polyurethane adhesive at different heating rates showed that the adhesive modulus had a lower value for a lower heating rate at the same temperature [68]. The modulus variations with temperature were calibrated with a kinetic model proposed for FRP composites materials [69].

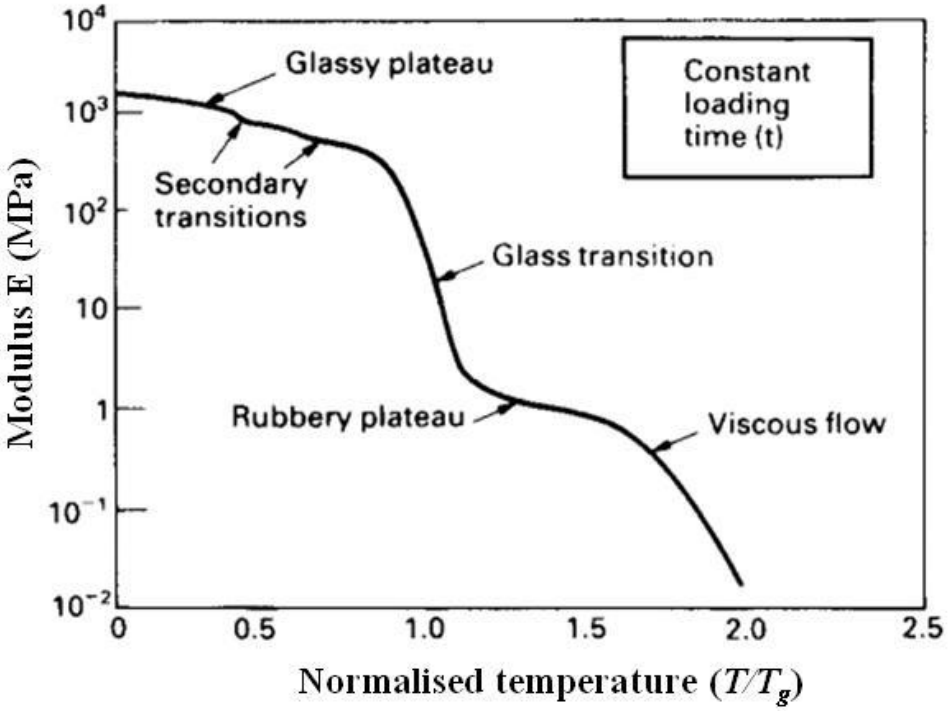

Figure 2.3: Change in the Young's modulus of thermoplastic polymer with temperature at a fixed loading time [60]

2.11 CFRP thermomechanical properties

As mentioned previously, CFRP composites are composed of a polymeric resin (matrix) material which is reinforced by carbon fibres. The carbon fibre is temperature resistant and the majority of its strength and stiffness can be retained up to 2000 °C [70]. However, the matrix loses the strength and stiffness once the temperature reaches its T_g. Thus, the ability of the matrix to transfer the forces amongst the fibres is lost which causes degradation in the mechanical properties of CFRP composites [60, 71]. It is important to mention that the T_g of the adhesive rather than the matrix should be taken in the design to avoid premature failure, especially if prefabricated (cured at elevated temperature) CFRP plates are bonded to steel structures using cold-cure adhesive epoxies [27].

Tensile tests carried out on CFRP bars at elevated temperatures showed very small reduction in the tensile strength and elastic modulus up to 100 °C [72, 73]. Cao et al. [74] investigated experimentally the tensile properties of CFRP, hybrid carbon/glass FRP and hybrid carbon/basalt FRP sheets impregnated with an epoxy resin adhesive at temperatures ranging from 16 to 200 °C. Test results showed that the tensile strengths decreased significantly when

the temperature exceeded the matrix T_g after which they remained constant up to 200 °C. The failure mode was also affected by increasing temperature where CFRP specimens failed in a brittle fracture at low temperatures and delamination between fibres occurred at increased temperatures.

Barker and Vangerko [75] carried out tests on both the unidirectional CFRP composites and the epoxy matrix to investigate changes in their elastic constants (Young's modulus, shear modulus and Poisson's ratio) within temperature ranges from -100 to 170 °C. The sensitivity of the elastic constants of the CFRP composite is closely related to the matrix temperature dependent. Below the transition temperature ($T_g \leq 120$ °C), the matrix is glassy and the elastic constants of the composite exhibited little change in value with temperature increases. In the transition region ($120 \leq T_g \leq 170$ °C), the matrix changes from a glassy to a rubbery state and thus the elastic constants decreased.

The effect of temperature on the mechanical properties of CFRP pultruded plates, widely used in externally strengthened steel structures, was experimentally investigated by Wang et al. [76]. The ultimate strength was found to reduce by approximately 50 % at 300 °C compared to that at room temperature. Different failure modes were also observed ranging from brittle fibre rupture at temperatures up to 50 °C, partial loss of epoxy matrix followed by plate rupture at temperature ranges from 97-308 °C, complete loss of all epoxy at about 400 °C and complete burning oxidation of the carbon fibres at 706 °C.

The typical relationship between the mechanical properties of FRP composite and temperature is shown in Figure 2.4 [77]. The figure shows that composite properties are not affected by an increase in temperature until a critical temperature (T_{cr}) has been reached, after which a significant decreased in the properties occurred due to softening of the resin matrix of the FRP composite. When the temperature reached the melting temperature (T_m), only the fibres carried the load therefore no further reduction in the properties occurred and they reached a residual value of (P_R).

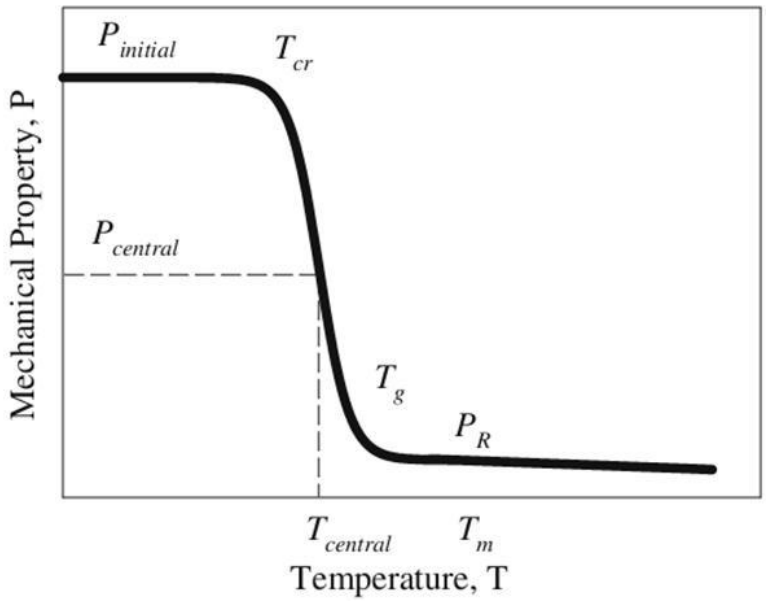

Figure 2.4: The relationship between the properties of FRP composites and temperature [77]

Many analytical models were developed to predict temperature-dependent mechanical properties for FRP composites which were reviewed comprehensively by Killer et al. [78, 79]. Mahieux and Reifsnider [66] proposed theoretical models to predict the reduction in any polymer matrix composite with changes of temperature. These models considered the effect of increasing temperature on the intermolecular bonds in the resin. They validated their model with experimental results on different thermoplastic polymers and composites [67]. Gibson et al. [80] extended the previous model to compute the reduction in FRP composite mechanical properties (e.g. strength, shear and elastic modulus) with temperature up to 200 °C considering the resin temperature dependency, as described by Eq. (2.3). This equation agreed well with the tests data on GFRP and FRP-to-FRP bond strength up to 200 °C [77]. In addition, it agreed with the results obtained from tensile tests on CFRP pultruded specimens up to about 400 °C [73].

$$P(T) = R_n \cdot \left(\frac{P_{initial} + P_R}{2} - \frac{P_{initial} - P_R}{2} \times \tanh\left(k_m .(T - T_{central})\right) \right) \tag{2.3}$$

Where $P(T)$ is a particular mechanical property at temperature T, $P_{initial}$ and P_R are the property value before and after transition (Figure 2.4), k_m is a constant related to the sharpness of the property degradation, $T_{central}$ is the temperature at which the property decreases rapidly and is not necessarily equal to T_g and R_n values depend on resin decomposition, which is equal to one when there is no decomposition loss and zero when the resin is completely vaporised.

Most recently, Bai et al. [69] presented a model to calculate stiffness variation of FRP composites with changes of temperature. Their model also considered the changes in viscosity of polymer resin at different temperatures in four states: glassy, leathery, rubbery and decomposed. Consequently, the elastic and shear modulus of FRP composites were described as a function of both temperature and viscosity at each state. Test results obtained from dynamic mechanical analysis (DMA) experiments on a pultruded GFRP laminate approved this model [69]. The same authors developed a model to describe the temperature and time dependent mechanical properties of FRP composite materials [81]. DMTA tests on pultruded GFRP laminates showed that the material properties degradation was influenced by the heating rate to which the material was subjected during thermal loading.

Although degradation in the mechanical properties of CFRP composites at warm temperatures is governed by T_g of the resin matrix, the CFRP pultruded plates used in this research have T_g typically about 190 °C due to post-curing at elevated temperatures [82], hence a maximum summer temperature of 60 °C would not influence the CFRP properties.

2.12 Steel structures temperature

Steel structure temperature is largely influenced by solar radiation, air temperature, wind speed and re-radiation. Some of the incident solar radiation may be lost by reflection, by convection and by re-radiation. The colour and texture of the surface determine the amount of reflected radiation. Heat energy lost by convection and re-radiation depends on the wind speed, the exposure of the surface and the difference in temperature between the surface and the surrounding air. In addition, structure temperature depends on the material thermal conductivity. The thermal conductivity of steel materials (43-54 W/m.°C, [83]) are 50 times greater than that of concrete materials (0.1-1.8 W/m.°C, [83]), and steel has a significant ability to transfer the heat rapidly. Therefore, steel structures exposed to direct sunlight on a warm summer day will become much hotter than the air temperature.

The temperature distribution through the decks of highway bridges is affected by air temperature, wind, humidity, intensity of solar radiation and material type [84]. Emerson [85] developed a method to calculate the distributions of the temperature within the decks of steel box and composite (concrete deck on steel beams) bridges during a 24 hour period of summer and winter time. Calculations and measurements showed that maximum temperature of the top surface of a steel box bridge deck was twice as high as the air temperature, and higher than the temperature of the composite deck. The same author [86] derived analytical equations to estimate the minimum and maximum bridge temperature based on minimum and maximum air

temperature over the United Kingdom. The minimum and maximum air temperatures were obtained from the meteorological office nearest to the location of the bridge. The maximum bridge temperature measured for a steel box bridge and a composite bridge during a 24 hour period of summer 1976 was around 50 °C [7].

Thus, extreme summer temperature may soften the adhesive used in bonding CFRP composites to steel beams when the temperature of the steel structure approaches the adhesive T_g.

2.13 Effect of temperature on strengthened structures

The effect of temperatures on FRP strengthened metallic structures was intensively investigated in the aerospace and automotive industries [87-89], but the adhesives and the temperature ranges used in these industries are different from those used in civil engineering applications. Therefore, there is limited information on the influence of temperature on the behaviour of adhesively bonded CFRP composites to steel structures in civil engineering applications.

2.13.1 FRP reinforced concrete structures

Although there have been many studies and applications of FRP composites in repairing and upgrading concrete structures, there is very little research concerning the effects of temperature on FRP reinforced concrete structures.

Blontrock [90] carried out double-lap shear tests on concrete specimens strengthened with externally-bonded CFRP laminates at various temperatures (20, 40, 55 and 70 °C). The result showed that increasing the temperature from 20°C to 40°C resulted in a significant increase in failure load (41%), while for a further increase in temperature a decreasing failure load was found. The first increase in failure load was due to the difference in coefficient of thermal expansions between the concrete and the CFRP, which may be induced thermal shear stresses opposite to mechanical thermal stresses. However, further increasing the temperature resulted in a decrease of the failure load due to adhesive softening. Similar results were obtained from the double-lap shear and three-point bending tests carried out by Klamer et al. [91].

Di Tommaso et al. [92] performed three-point bending tests on small-scale concrete specimens, without internal reinforcement, strengthened with normal (175 GPa) and high (300 GPa) modulus unidirectional CFRP laminates at -100, -30, 20 and 40 °C. Test results showed that increasing the temperature to 40°C decreased the failure load due to softening of the adhesive. The failure mode was changed from ductile at high to brittle at low temperatures. The same author presented a theoretical equation based on a kinematic model to calculate the shear

stresses between the laminate and the concrete, which had a good correlation with the experimental results.

The long-term behaviour of concrete specimens reinforced with two types of CFRP composites (composite A: tensile strength and elastic modulus of 3400 MPa and 235 GPa, respectively; composite B: tensile strength and elastic modulus of 1500 MPa and 235 GPa, respectively) and two types of resins (resin A: T_g is 50 °C; resin B: T_g is 75 °C) at elevated temperatures was investigated by Ferrier et al. [93]. Creep shear tests were carried out at 35 °C and stress of 0.8 MPa for composite A, and at 60 °C and stress of 0.35 MPa for composite B for a period of six months. Test results showed that the shear modulus reduced significantly with time for both composites, even composite B shows a better creep behaviour.

Aguiar et al. [94] investigated the effect of solar exposure on the adhesive shear strength as well as on the flexural capacity of CFRP strengthened concrete specimens. After 25 days of cyclical thermal exposures between 20 and 80 °C, compressive shear and bending tests were carried out at room temperature. Test results showed that the adhesive shear strength reduced significantly due to bond deterioration. Although the maximum bending moment capacity of the RC beam increased about 35-50% at 20 °C due to the CFRP strengthening, there was no apparent advantage in using CFRP reinforcement at 80 °C. However, the inclusion of polyurethane insulating materials showed a good protection to the strengthened RC beams.

Klamer et al. [95] had tested four-meter long reinforced concrete beams strengthened with CFRP plates of different lengths under four-point bending loads at 20, 50, and 70 °C. The failure loads of beams with long plates were not significantly affected by temperature since the plate ends were terminated close to the supports where the bending moment is lower. However, the load capacity for beams strengthened with shorter plates was dramatically reduced at 70 °C.

Most recently, experimental and theoretical analyses of RC beams strengthened with CFRP laminates subjected to cyclic loading at elevated temperatures were conducted by Huang et al. [96]. Tests were carried out at 5, 20, 50 and 80 °C at five load levels (25, 27.5, 30, 32.5, and 35 kN). The results showed that the fatigue lives of the CFRP strengthened beams decreased with temperature increasing at the same applied load.

2.13.2 FRP reinforced steel structures

The strengthening of civil engineering infrastructures with FRP composite was first applied on concrete structures and then it was extended to metallic structures with the development of the material properties of the CFRP composites. Although significant researches were performed on

the bond behaviour of FRP/steel systems at room temperature [97-105], few studies were conducted at elevated temperatures.

The adhesively bonded joints degraded with exposure to environmental conditions such as humidity, temperature, ultraviolet rays, oxidation, salt water and acid. Crasto and Kim [106] carried out tests on the CFRP double-lap shear specimens exposed to moisture at different temperatures. At lower temperatures, the failure load was larger for fully saturated specimens than for dry specimens. This was due to toughening of the adhesive by plasticisation. However, saturated specimens were weaker than dry specimens at higher temperatures, because the T_g may be reduced in the presence of the moisture in the adhesive. Clark [107] performed accelerated degradation single-lap shear tests on specimens fabricated by bonding CFRP and wrought-iron adherends. Specimens showed a significant loss in the apparent shear strength after they were exposed to distilled water for 1000 hours at an elevated temperature of 60 °C. A series of double-lap shear tests on CFRP/steel specimens preconditioned by immersion in saltwater spray and thermal cycles were conducted by Colombi et al. [108, 109]. The specimens were thermally cycled for different lengths of time in a range from -20 °C (6 hours) to +50 °C (6 hours). Test results showed that the joint strength was not significantly affected by the environmental conditioning. However, its ductility was decreased by up to 50% as compared to unconditioned specimens.

It is also important to note that an adhesive bond behaves very differently when subjected to one single environmental factor, than when it is subjected to a combination of type of exposure [110]. In addition to environmental exposures, the stresses to which the bond is subjected influence its lifetime. Zhang et al. [111] investigated the bond temperature dependency of adhesively bonded pultruded GFRP laminates. Tensile tests carried out on double-lap joints at a range of temperatures between -35 and 60 °C showed a significant reduction in the strength and the stiffness above T_g of the adhesive. In addition, the failure mode was changed from fibre-tear to adhesive failure with increasing temperature. The same authors conducted FE analyses to model the effect of temperature on joint stiffness considering the adhesive and the adherends' temperature dependencies. The FE results and the empirical models proposed by Mahieux et al. [66] and Gibson et al. [80] agreed well with the experimental results.

Ashcroft et al. [88] tested unidirectional CFRP double-lap shear joints under quasi-static loads at temperatures of -50, 22 and 90 °C which are experienced by aircraft. The results showed that the joints were stronger at 22 °C than at other temperatures. The mode of failure was also changed from cohesive failure at 90 °C to interlaminar failure of the middle adherend at -50 °C.

In addition, the same authors carried out fatigue testing on bonded joints at these temperatures up to one million cycles. The fatigue life of the bonded joint was temperature dependent and it decreased significantly at 90 °C. The fatigue failure observed at 22 °C was similar to that described for the quasi-static test.

Al-Shawaf et al. [112] investigated the bond behaviour of HM-CFRP/steel double-lap shear joints subjected to temperatures between 20 and 60 °C. The investigation was conducted to evaluate the effectiveness of CFRP materials for strengthening steel structures in civil engineering applications using three different epoxy resins. It was observed that failure mode and joint capacity are mainly governed by the operating temperatures as well as the epoxy type as each epoxy had different T_g. In addition, the strain distributions, the modes of failure, and the failure loads obtained from nonlinear FE analysis validated those from experimental tests [5].

Recently, Nguyen et al. [113] conducted experimental and modelling work to investigate the change of the mechanical properties of steel/CFRP double-strap joints with increased temperatures. Test results showed that the joint stiffness reduced by 20% at T_g and decreased further up to 80% at 20 °C above T_g. Similarly the joint strength decreased by 15% at the T_g. The effective bond length of the bonded joint increased with temperature and doubled when the temperature was near to T_g. In addition, they applied the model proposed by Bai et al. [68, 69] to describe temperature dependency of the adhesive into Hart-Smith model [114] to determine the change of the effective bond length and the joint strength with the temperature. They same authors extended the previous model to predict time and temperature dependent of the bonded joint [115].

Most recently, Stratford and Bisby [57] investigated the effect of elevated temperatures on the behaviour of steel beams strengthened with CFRP plates. Only half of the beam was heated up to the desired temperature while the rest of the beam was kept at room temperature. It was found that the slip at the plate end was significantly increased at higher temperatures until a debonding failure occurred. In addition, the failure load was reduced at elevated temperatures due to the increased deformation capacity of the adhesive and the reduced stiffness.

2.14 Conclusion

From the literature on the properties temperature-dependencies of steel, CFRP and adhesive, it can be concluded that the adhesive is the weakest part because it loses most of the strength and stiffness at the glass transition temperature (T_g). It is possible that the temperature of a structural steel on a hot summer day can exceed the T_g. In addition to temperature, the adhesive properties degrade with time due to creeping adhesive secondary bonds. Hence, the strength and the fatigue life of steel beams reinforced with externally-bonded CFRP plates may be affected by temperature and time. In the current literature the following areas are lacking:

- Limitation of the experimental tests on the CFRP strengthened beam subjected to a static load at elevated temperatures.
- The fatigue lives of steel beams strengthened with CFRP plates at elevated temperatures have not been studied yet.
- The available analytical and FE analyses to calculate the interfacial stresses within the adhesive layer between a steel beam and a CFRP composite assumed linear elasticity and temperature independence of the adhesive material.

Chapter 3

Materials properties at elevated temperatures

3.1 Introduction

The material properties of the steel, the adhesive and the CFRP used in this research are required in the analytical and the FE analyses (Chapter 5) to calculate the interfacial stresses in the adhesive between a CFRP plate and a steel beam. Some properties are provided by the manufacturer at room temperature only. Therefore, experimental tests are required to obtain material mechanical properties at different temperatures.

In this chapter, testing methods used to measure the tensile strengths and Young's moduli for steel, adhesive and CFRP materials are described. Moreover, test methods used to measure the coefficients of thermal expansion for the CFRP are illustrated. FE analysis is also employed on thick adherends lap-shear specimen to obtain adhesive shear modulus values at different temperatures. Also the reduction in the adhesive bond strength with temperature increase is examined. The results are discussed and the effects of temperature on the mechanical properties of adhesive are identified.

3.2 Steel

Hot rolled universal steel beams (127×76 UB13) are used in the static and the fatigue tests in this research.

3.2.1 Steel mechanical properties

The steel elastic modulus, yield stress and strain were obtained from tensile tests carried out on dogbone specimens. Steel properties temperature dependency and its coefficient of thermal expansion were taken from design standards [9, 58, 59].

3.2.1.1 Steel specimens preparation and test procedure

Three dogbone steel specimens were cut from the flange of a universal steel beam 127×76UB13. The specimens were given the serial numbers F1, F2 and F3. Linear strain gauge (10 mm long) was mounted in the middle of the specimen (see Figure 3.1) to measure the

longitudinal strain during loading. The specimens cross-sectional area are summarised in Table 3.1, and a specimen dimensional sketch is shown in Figure A.1 in Appendix A.

The tests were carried out on the specimens at room temperature according to BS EN ISO 6892-1 standard [116] to determine the elastic modulus E_s, the yield strength σ_y, the yield strain ε_y, and the ultimate tensile strength σ_u. The tests were performed in a displacement control mode at a rate of 2 mm/min using a hydraulic Instron universal test machine with a 100 kN capacity. Figure 3.2 shows the test setup. The load and the strains values were automatically recorded using a Vishay data logging system.

Figure 3.1: Strain gauges bonded on steel specimens

Figure 3.2: steel specimen loaded in tension

3.2.1.2 Test results

The stress-strain curves obtained from the tension specimens are shown in Figure 3.3. The relationships between stresses and strains are linear until steel yielding after which excessive strains occurred at the same stress. It was not possible to measure the failure strain because the strain gauges peeled away from the specimen surfaces soon after the yielding had occurred. However, the load and the extension data to failure was recorded for each specimen from the load cell and the change in the crosshead position (see Figure 3.4).

The average value of the steel Young's modulus (Es) obtained from three specimens at room temperature is 181 GPa, which is lower than the standard steel elastic modulus value of 205 GPa [117]. This is may be due to misalignment of the strain gauge or the specimen. Nevertheless, the value of steel elastic modulus obtained experimentally (181 GPa) will be used

to calculate the interfacial shear and normal stresses in a bonded joint and in a steel beam reinforced with a CFRP plate. The value of steel elastic modulus affects the value of the interfacial stresses, as stiffer steel beam carries more stresses than the CFRP plate thus lower interfacial stresses will be induced in the adhesive.

The failure modes for all tested specimens were ductile fracture after extensive localised plastic deformation (necking) in the middle, as shown in Figure 3.5. The mechanical properties obtained from the tests are summarised in Table 3.1. The details of the tensile strength and the elastic modulus calculations are described in Appendix A.

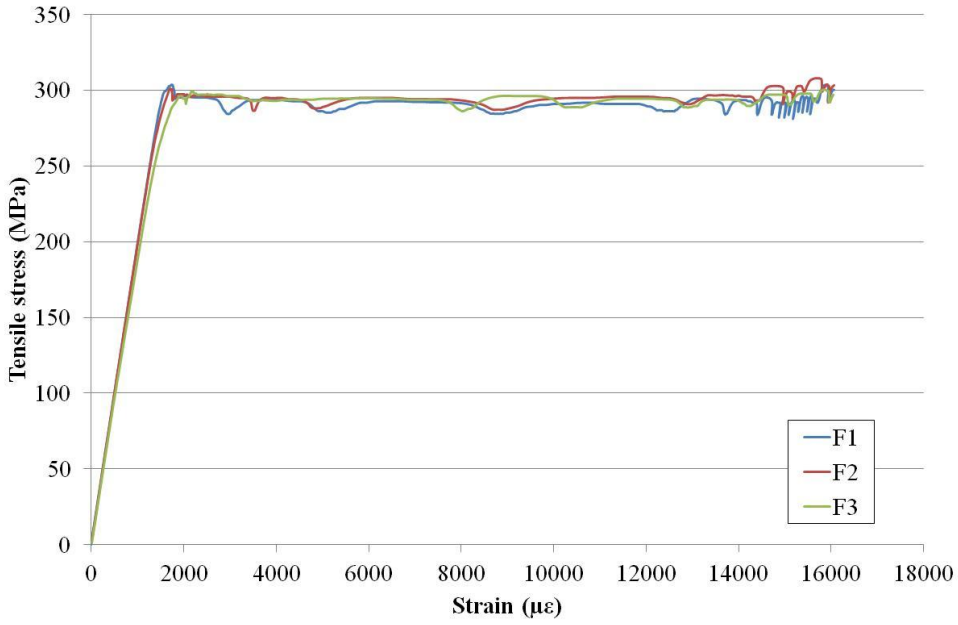

Figure 3.3: Stress-strain curves for the steel dogbone tension specimens

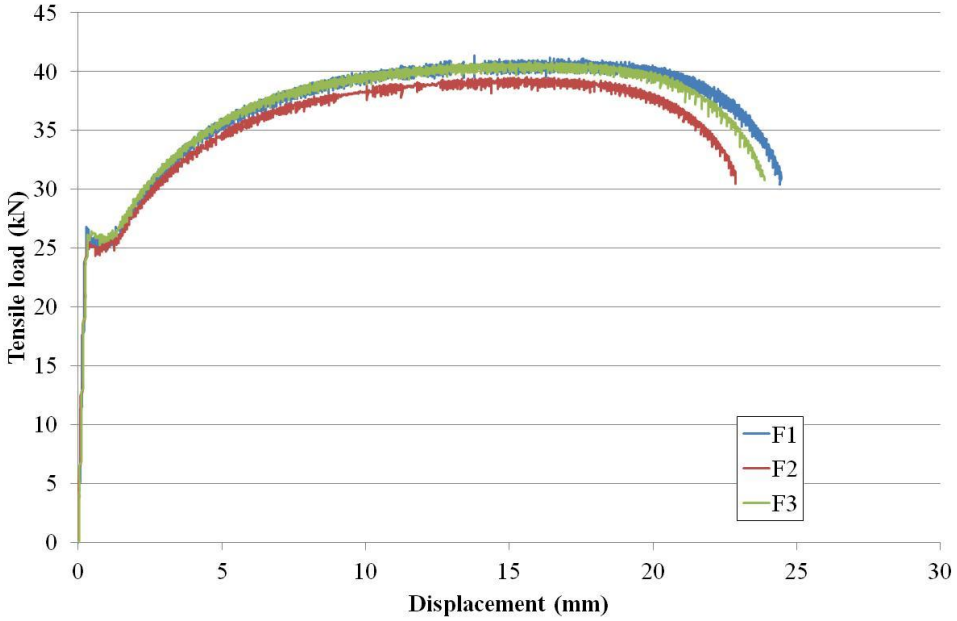

Figure 3.4: Load-displacement curves for the steel dogbone tension specimens

Figure 3.5: Fracture after necking in the middle of the steel dogbone tension specimens

Table 3.1: Summary of steel mechanical properties

Sample	Width (mm)	Thickness (mm)	Cross-sectional area (mm^2)	F_y / kN	ε_y / $\mu\varepsilon$	σ_y / MPa	F_u / kN	σ_u / MPa	E_s / GPa
F1	20.2	4.4	88.3	26.8	1762	304	41.4	468.5	191
F2	20.1	4.2	84.9	25.6	1717	301	39.5	465.2	182
F3	20.2	4.4	88.3	26.1	1959	296	40.8	462.4	169
Average	20.1	4.3	87.2	26.2	1813	300	40.6	465.3	181
St. dev.	0.04	0.09	1.9	0.6	128.8	3.8	0.9	3.1	11

3.2.2 Temperature dependency of structural steel mechanical properties

The steel yield strength and elastic modulus of structural steel reduce slightly at temperatures above 100 °C [58, 59]. Therefore, the effect of extreme summer temperature of 60 °C, assumed in this research, on the strength and stiffness of the steel can be ignored, as discussed previously in section 2.9 in Chapter 2. Thus, steel Young's modulus value used in the analytical and FE calculations at elevated temperatures is taken equal to that obtained from tensile test at room temperature.

3.2.3 Steel coefficient of thermal expansion (α_s)

Two values for the coefficient of thermal expansion of structural steel α_s, are recommended by Eurocode4 [9]: 10×10^{-6}/°C for the calculation of stresses in composite structures and 12×10^{-6}/°C for the calculation of a change in the length of a bridge. For calculations of the interfacial stresses using the analytical and FE models, the value of steel thermal expansion coefficient is taken equal to 10×10^{-6}/°C.

3.3 CFRP

Two different types of unidirectional CFRP pultruded plates were used in this research. First, CFRP strips with nominal dimensions of 38×6.5 mm, supplied by Exel Composites Ltd, were

used in the fabrication of the double-lap shear specimens. Their mechanical properties were given by Clarke [107]. Therefore, no additional tests were conducted to minimise laboratory work.

The second type of CFRP plate was fabricated from pre-impregnated (prepreg) laminates MTM 46/STS (24K), supplied by Advanced Composite Group (ACG, currently Umeco). MTM 46 is an epoxy resin matrix developed to produce high quality composite components using low pressures and temperatures. STS is a unidirectional carbon prepreg fibre. 24K refers to 24000 individual strands of carbon per fibre bundle. The fabrication was carried out in the Transport System Research Lab (TSRL) at the University of Southampton using an autoclave system. Details on the manufacturing of the CFRP plates are given in Appendix B. This plate was used for steel beam strengthening.

3.3.1 CFRP mechanical properties

Tensile tests were carried out on the CFRP specimens cut from the fabricated CFRP plates to obtain their tensile strength σ_p and Young's modulus E_p, since this data was not given by the manufacturer. Tests were also carried out at elevated temperatures of maximum value of 60 °C to determine the CFRP mechanical properties temperature dependency.

3.3.1.1 Specimen preparation and test procedure

The CFRP specimens were cut from a 750×450 mm CFRP panel using a mechanical saw. Each end of the CFRP specimen was reinforced by bonding a 2 mm thick aluminium tab on both sides (see Figure 3.6). Two 90° 2-element strain gauges (5 mm long) were mounted on either side of the specimen to measure the strains in the longitudinal and transverse directions during loading (Figure 3.6). The specimens were loaded in tension at a rate of 2 mm/min using the same testing machine described in the steel tension test in section 3.2.1.1.

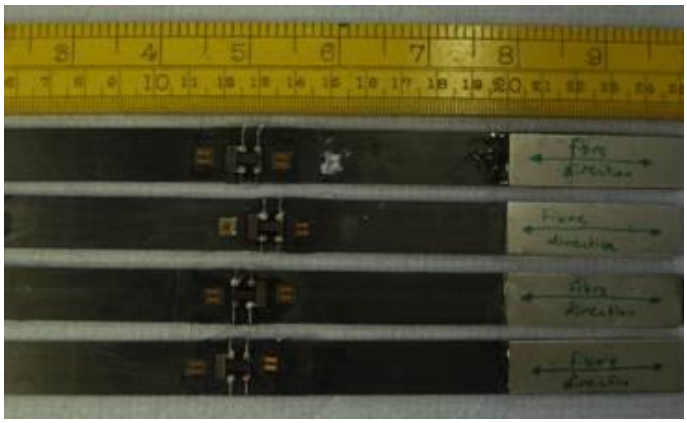

Figure 3.6: CFRP tension specimens with strain gauges and aluminium taps

3.3.1.2 Test results

The stress-strain curves obtained from the CFRP tension specimens instrumented with strain gauges are shown in Figure 3.7. The figure shows a linear relation between stress and strain until failure. The specimens failed suddenly with no sign of any plastic deformation. Figure 3.8 shows the shattered fibres of the specimens after testing. The average values of E_p and σ_p obtained from the tensile tests at 23 °C are 124 GPa and 1040 MPa, respectively. The Young's modulus value is lower than that of steel (181 GPa) which indicates that the CFRP is a normal modulus composite. Appendix C gives details of the tensile strength and the elastic modulus calculations.

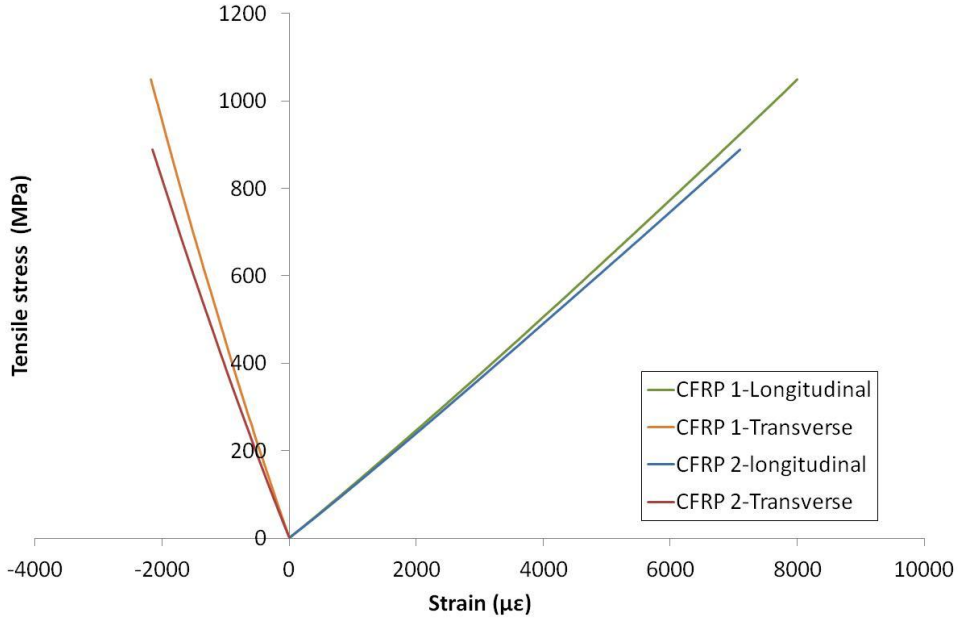

Figure 3.7: Stress-strain curves of CFRP specimens at 23 °C

Figure 3.8: CFRP specimens after the tensile tests at 23 °C

3.3.2 Temperature dependency of CFRP mechanical properties

The exposure to high temperature could possibly soften the resin matrix in the CFRP plate, thus, the CFRP elastic modulus and strength could be reduced. The epoxy matrix (MTM 46) used in this research has T_g of 190 °C after post-curing at 180 °C [82]. Therefore, the CFRP mechanical properties at the highest summer temperature of 60 °C will not be affected.

However, tensile tests were carried out on CFRP specimens at temperatures of 30, 40, 45, 50 and 60 °C to confirm the temperature effect on CFRP mechanical properties.

At least three specimens were tested to failure at each temperature. A thermal chamber was used to heat up the specimen to the desired temperature. To avoid stresses induced in the CFRP specimen during the heating process, the specimen was first clamped by the machine's top grip and heated up to the target temperature. It was then held at that temperature for 30 minutes to reach thermal stability. Then the specimen was clamped by the machine bottom grip and loaded to failure while the temperature was maintained.

3.3.2.1 Test results

The test results of the CFRP tension specimens at elevated temperatures are summarised in Table 3.2. The results are not consistent because each specimen may contain different amount of unidirectional fibres. This is due to misalignment that has occurred during fabricating of the CFRP plate by the stacking of seven layers of prepreg unidirectional laminates manually, or during the cutting of the CFRP specimens from the CFRP plate.

Selective stress-strain curves from 20 tension specimens at various temperatures are shown in Figure 3.9. The figure shows a linear relation between stress and strain until failure even at elevated temperatures. The effect of elevated temperature on CFRP mechanical properties is not obvious up to 60 °C, which is lower than the matrix T_g. Therefore, the CFRP mechanical properties are assumed to be temperature independent and the average value of E_p obtained from the test at the 23 °C is used in the analytical and the FE calculations at elevated temperatures.

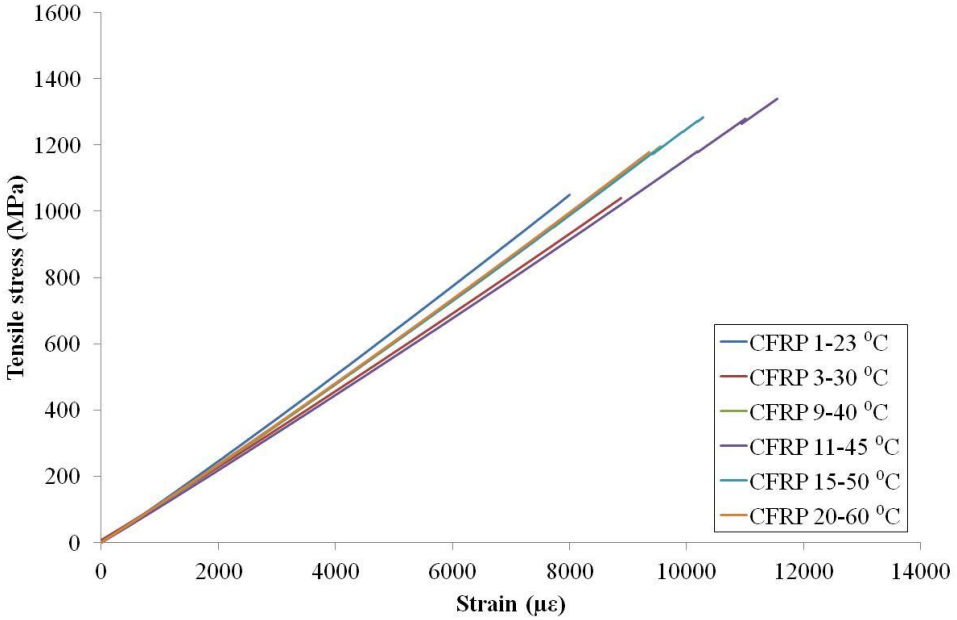

Figure 3.9: Stress-strain curves of selected CFRP specimens at different temperatures

Table 3.2: Mechanical properties of CFRP at different temperatures

Temperature °C	Average elastic modulus (E_p) /GPa	Average tensile strength (σ_p) /MPa	Modulus standard deviation (E_p) /GPa	Strength standard deviation (σ_p) /MPa
23	124	1040	13.1	2.7
30	107	1219	98.8	14.0
40	114	1349	120.5	7.8
45	117	1324	99.3	9.6
50	116	1309	21.4	8.8
60	121	1371	143.5	2.3

3.3.3 CFRP coefficient of thermal expansion (α_p)

In the absence of the CFRP coefficient of thermal expansion α_p value, the two different techniques discussed below were used to determine α_p in the fibre longitudinal direction. The value of α_p which is required in the analytical and the FE analyses (Chapter 5).

3.3.3.1 Specimen preparation and test procedure

The vitreous silica dilatometer method was used to determine the linear thermal expansion of three CFRP specimens ($60 \times 10 \times 1.5$ mm dimension). In this method, the change in the specimen length is measured as a function of temperature while it is subjected to a constant heating or cooling rate [118]. Test using this method was not successful to measure the CFRP thermal expansion due to the limitation of the dilatometer sensor, which was only able to measure thermal expansion greater than 1×10^{-6}/°C. Therefore, a more accurate method is required since the coefficient of thermal expansion of CFRP in the longitudinal direction is expected to be smaller than 1×10^{-6}/°C. The technique addressed by Lanza di Scalea [119] using identical strain gauges bonded onto two specimens was followed. One of the specimens (the reference material) has a known coefficient of thermal expansion, and the second one (the test material) has an unknown coefficient of thermal expansion. The principle of this method is that the difference in the value of coefficient of thermal expansion for the test and the reference materials, at any common temperature, is equal to the change in the electrical resistance of the strain gauges. The reference material is nickel-iron alloy containing 36% nickel, known commercially as Invar36, which has a very low linear thermal expansion coefficient. The test specimen is a CFRP specimen cut from the same tension specimens with a nominal dimension of $25 \times 15 \times 3.2$ mm. The Invar specimen was cut from a 15 mm diameter rod.

The coefficient of thermal expansion of the test material relative to that of the reference material at the same heating rate, assuming zero strain gauge transverse sensitivity (k_t), is obtained from Eq. (3.1):

$$\alpha_p - \alpha_r = \frac{(\varepsilon_p - \varepsilon_r)}{\Delta T} \tag{3.1}$$

where α_p and α_r are, respectively, the coefficient of thermal expansion of the CFRP and the reference materials, ε_p and ε_r are, respectively, the thermal strains from the gauges mounted on test and reference materials and ΔT is the change in temperature.

A half-Wheatstone bridge circuit was employed to connect the gauges. This circuit ensures that the gauges output are electrically subtracted and automatically compensated [120]. Details of the half-bridge circuit can be found in Kreuzer [121]. The sketch of the circuit is shown in Figure 3.10.

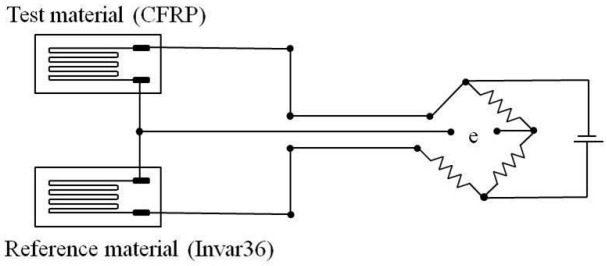

Figure 3.10: Half-Wheatstone bridge circuit for measuring CFRP thermal expansion coefficient

Three thermocouples (type J) were used to record the oven, CFRP and Invar36 temperatures. Preliminary heating cycles were performed at 0.5, 0.3 and 0.1 °C/min to determine an optimal heating rate that ensured thermal equilibrium, minimum thermal hysteresis and low residual stresses in the specimens. It was found that a heating rate of 0.1 °C/min is an ideal to maintain a linear response in the temperatures of the CFRP and the Invar36 with the oven temperature. This is shown in Figure 3.11 which shows similar temperatures measured on both the CFRP and the oven, but the Invar36 temperature was lower than the oven temperature by about 1 °C. However, the difference in the CFRP and the Invar temperatures remained constant as the temperature increased.

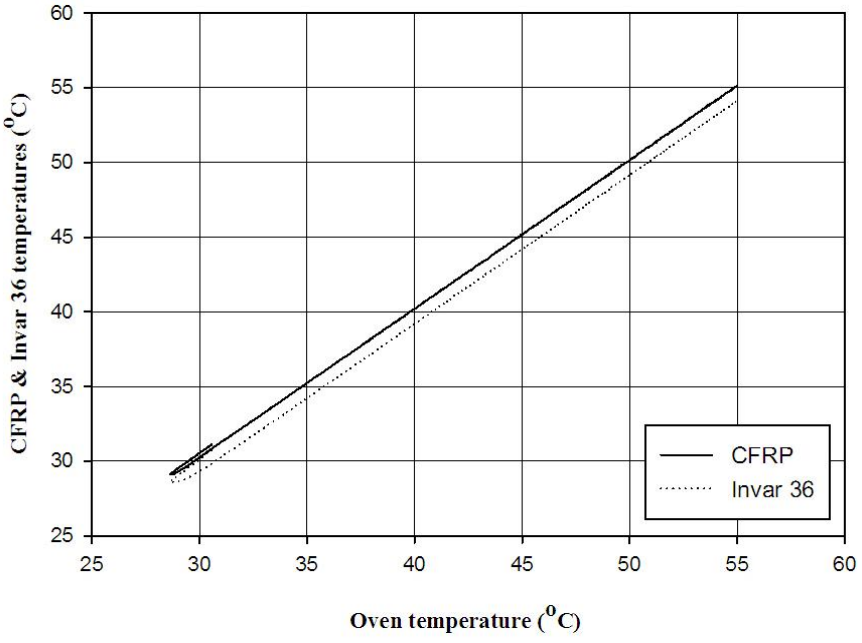

Figure 3.11: CFRP and Invar36 temperatures as a function of oven temperature

3.3.3.2 Test results

Figure 3.12 shows the thermal strains recorded on the CFRP and Invar36 specimens as a function of the oven temperature. The difference between CFRP and Invar36 strains ($\varepsilon_p - \varepsilon_r$) plotted against the oven temperature is shown in Figure 3.13. The plot has a scatter due to the small thermal strain values of the CFRP and Invar36. The least-square method is used to fit a linear regression. The slope of the line $(\varepsilon_p - \varepsilon_r)/\Delta T$ is computed within temperature ranges from 35 to 75 °C. The linear thermal expansion coefficient α_r of Invar36 over temperature ranges from 20 to 100 °C is 1.5×10^{-6}/°C [122]. The slope and α_r value are applied in equation (3.1) to calculate the α_p in the longitudinal fibres direction. Thus, the CFRP coefficient expansion obtained is equal to 0.34×10^{-6}/°C.

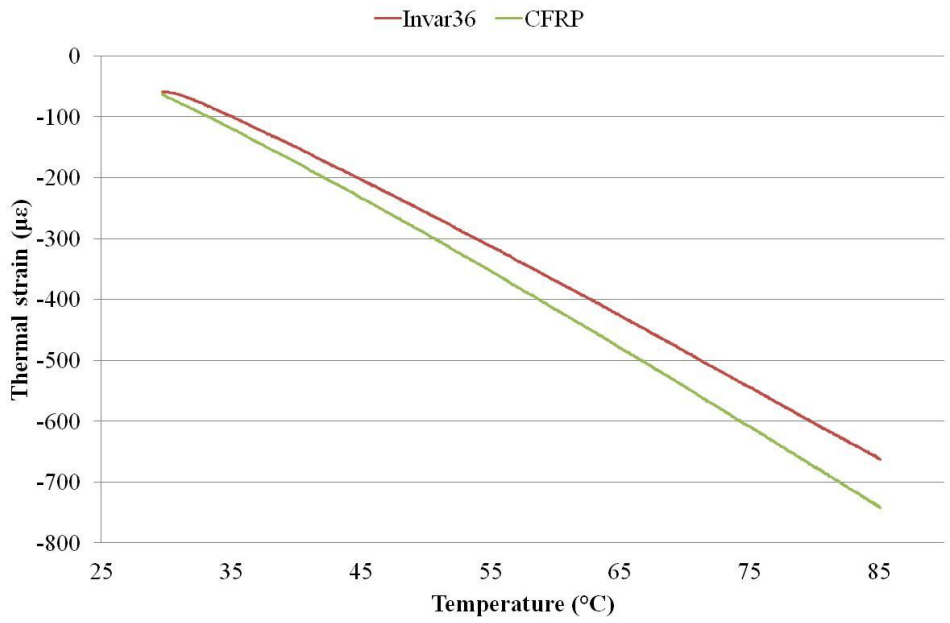

Figure 3.12: Thermal strains of CFRP and Invar36 relating with oven temperature

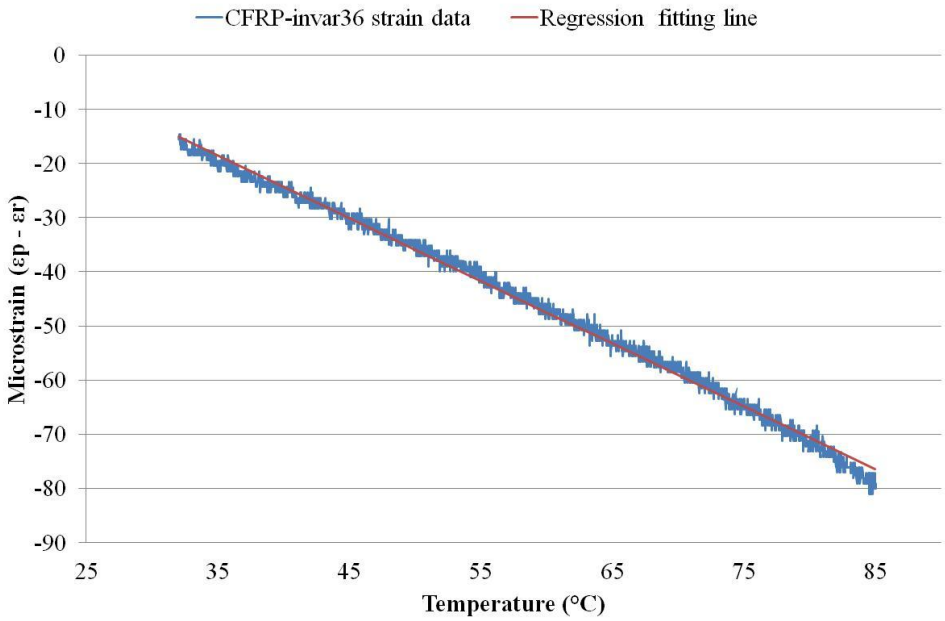

Figure 3.13: Least-square fitting line to the difference in CFRP and Invar36 thermal strains

3.4 Sikadur-30 adhesive

Sikadur-30 is a solvent free epoxy adhesive which is commonly used in bonding reinforcement of concrete and steel structures due to many advantages that can be summarised as follows: First, it can be mixed and applied easily. Second, it can be cured at room temperature. Third, it has a high mechanical strength and high creep resistance. Fourth, it hardens without shrinkage and finally, it is an excellent adhesion in damp conditions. This adhesive consists of two components: the epoxy resin (part A) and the hardener (part B) which are mixed together in a weight proportion of 3:1.

3.4.1 Adhesive tensile properties

Sikadur-30 adhesive mechanical properties are given by the manufacturer at room temperature only. Therefore, tensile tests were carried out on adhesive dogbone specimens at different temperatures to obtain their Young's modulus (E_a) values at these temperatures.

3.4.1.1 Specimen preparation and test procedure

Bulk adhesive dogbone specimens were made using a multi-cavity flexible silicon mould. The quality of the fabricated adhesive specimen depends on the amount of air bubbles formed during

mixing or during casting. Air bubbles cause stress concentration in the specimen and thereby initiate premature failure. Precautionary steps were taken to fabricate high density specimens with minimum air bubbles. These steps can be summarised as follows: First, the mould was sprayed with three layers of bond release agent prior to the pouring in of the adhesive to ensure easy removing of the specimen after cured. Second, the two-part adhesive was placed in a plastic bag and mixed together till it reached consistency in colour. The plastic bag was vacuumed during the mixing process to remove any air entrapment (Figure 3.14a). Third, mixed adhesive was poured into the mould (Figure 3.14b). The mould was vibrated to ensure complete filling. Finally, the top face of the adhesive was covered with a non-stick foil and a thick plate was pressed against the mould using four G clamps (Figure 3.14c). The covering was removed after 24 hours and the specimens were then left for a week at room temperature to be fully cured. Figure 3.14d illustrates ready adhesive dogbone specimens.

Tensile tests were carried out on the adhesive dogbone specimens according to BS EN ISO 527-2 [123] to determine their elastic modulus, ultimate tensile strength, and Poisson's ratio. The tests were carried out under displacement control mode at a rate of 1 mm/min using Instron 5569 machine with a maximum load capacity of 50 kN. Each specimen was bonded with 2 mm long rosette strain gauges to obtain the transverse and the longitudinal strains to calculate the Poisson's ratio. To carry out tests at high temperatures, the same environmental chamber described in section 3.3.2 was used to heat the specimen to the desired temperatures. The test setup including the thermal chamber is shown in Figure 3.15.

(a)

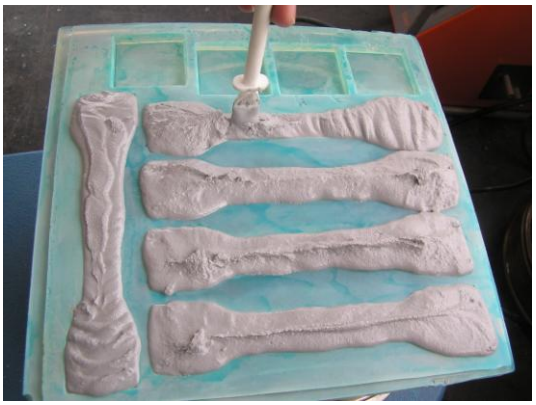

(b)

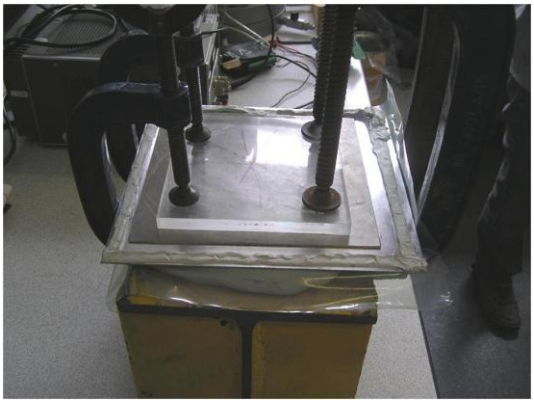

(c)

(d)

Figure 3.14: Fabrication steps of bulk adhesive dogbone specimens: (a) vacuum and vibration of the mixture, (b) adhesive casting in the mould, (c) pressed mould and (d) ready samples

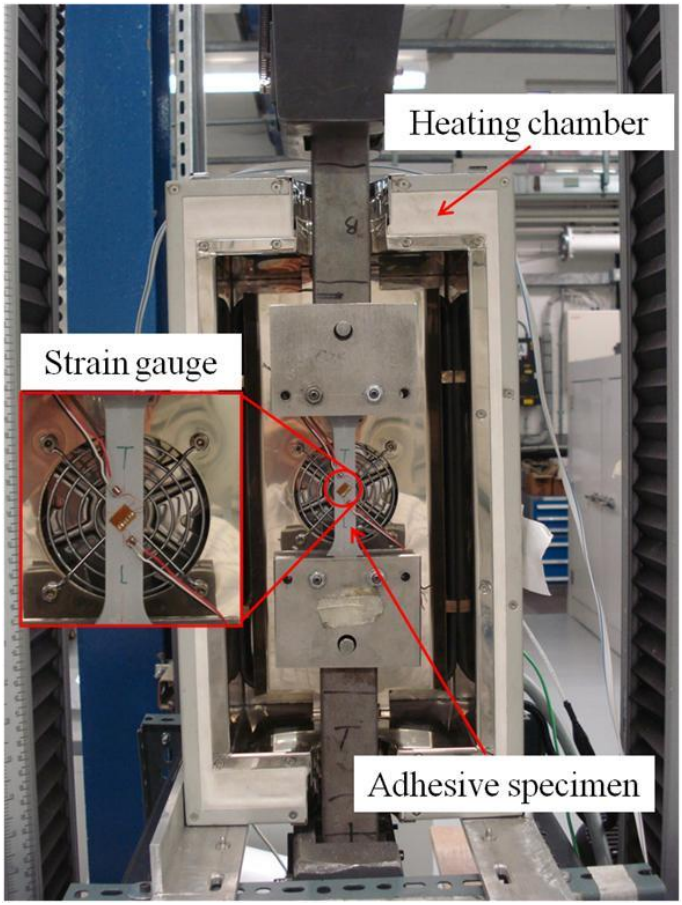

Figure 3.15: Adhesive tensile test setup with environmental chamber

3.4.1.2 Test results

The stress-strain relationships for eighteen adhesive tension specimens are shown in Figures D.1 in Appendix D. Some specimens contained air bubbles thus they broke at lower tensile load. Selective stress-strain curves at different temperatures are shown in Figure 3.16. The curves have the same trends of the results obtained by AL-Shawaf [5]. The adhesive tensile strength is reduced and nonlinear stress-strain behaviour is observed when the temperature becomes close and above T_g. The relationship between the stress and the strain at elevated temperatures is fitted with a polynomial curve from which the tangent at the origin represents the Young's modulus. Variations in adhesive modulus and tensile strength with temperature are presented in Figure 3.17 and Figure 3.18, which indicate significant reduction in both the strength and stiffness as the temperature increased from 40 to 45 °C.

The value of the T_g was defined from the relationship between the adhesive elastic modulus and the temperature, which is the midpoint temperature for the reduction in the elastic modulus. Figure 3.17 gives a T_g value of about 43±1 °C which is lower than the value provided by the manufacturer (62 °C) [124]. This is may be due to the fact that the testing method used by the manufacturer [124] was different than the one used in this research [123]. In addition, post-curing of adhesive epoxies at elevated temperatures could increase T_g values [4, 82] i.e., the tested specimens were cured at room temperature while the manufacturer specimens were cured at 45 °C [124]. The reason of curing the adhesive, the double-lap shear and the reinforced beam specimens at room temperature is due to the similarity in practical applications. It is important to mention that the value of T_g depends on the heating and loading rates. Therefore it cannot be an exact value.

The average values of E_a and σ_a obtained from adhesive tension specimens at 20 °C are 12.06 GPa and 27.60 MPa which agree with the manufacturer datasheet [124]. The test results of Sikadur-30 adhesive at different temperatures are summarised in Table 3.3. Details of the calculations for the tensile strength and elastic modulus are given in Appendix D.

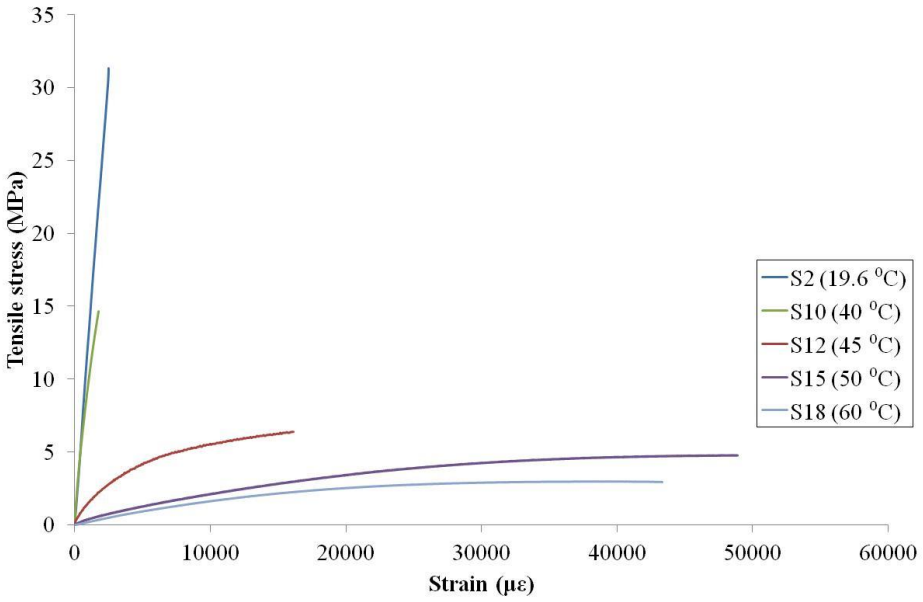

Figure 3.16: Selective stress-strain curves of Sikadur-30 adhesive at different temperatures

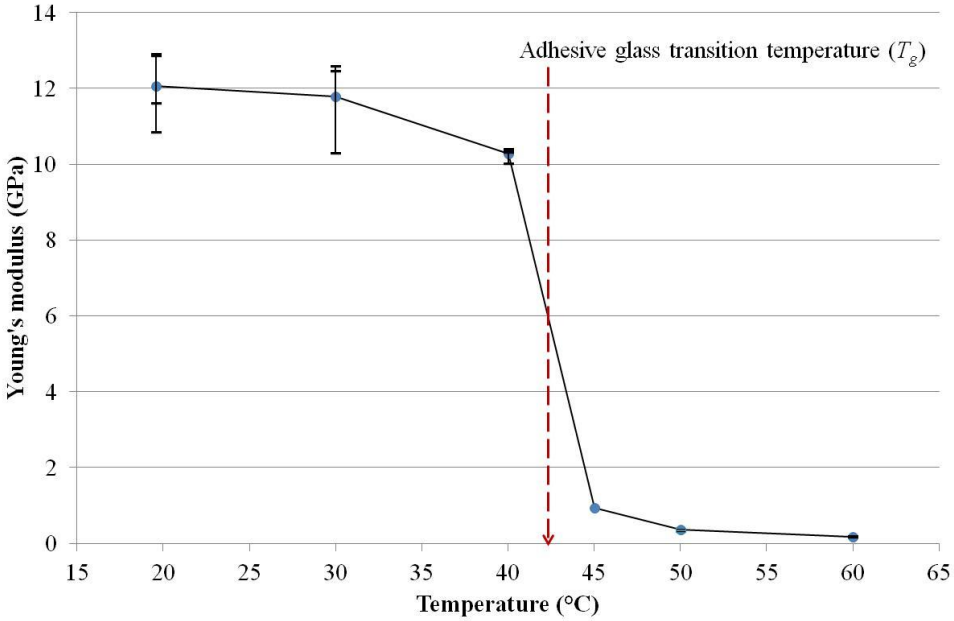

Figure 3.17: Sikadur-30 adhesive Young's modulus as a function of temperature

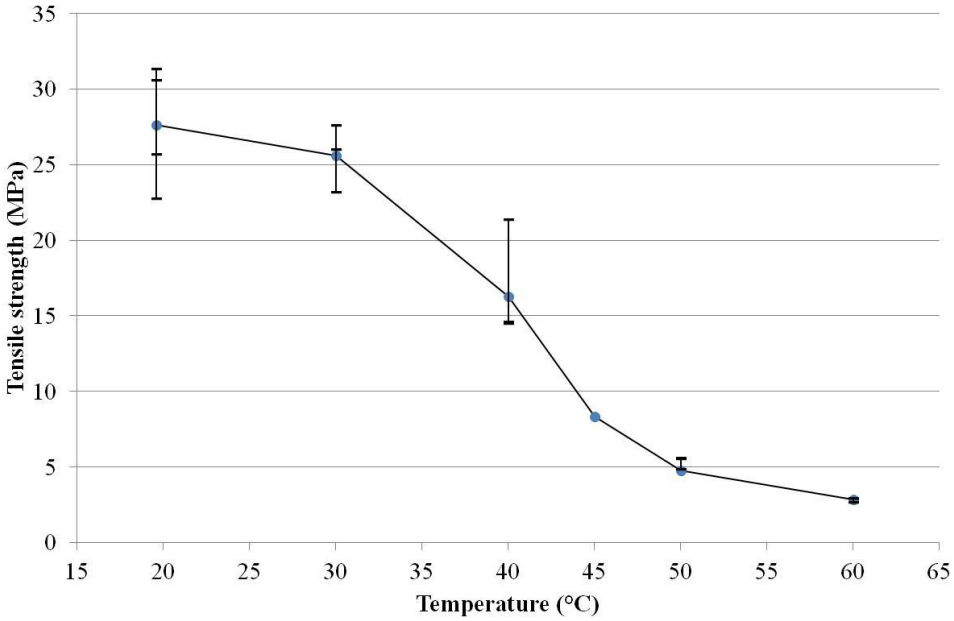

Figure 3.18: Sikadur-30 adhesive tensile strength as a function of temperature

Table 3.3: Mechanical properties of Sikadur-30 adhesive at different temperatures.

Temperature °C	Average tensile strength (σ_a) /MPa	Normalised strength %	Average elastic modulus (E_a) /GPa	Normalised modulus %	Poisson's ratio (ν)
20	27.6	100	12.1	100	0.21
30	25.6	93	11.8	98	0.22
40	16.3	59	10.3	85	0.24
45	8.4	30	0.9	8	0.29
50	4.8	17	0.4	3	0.32
60	2.9	10	0.2	2	0.39

3.4.2 Adhesive shear properties

The adhesive shear modulus (G_a) is required in the analytical model to calculate the interfacial stresses in the adhesive between the CFRP plate and the steel beam. This will be discussed in details in Chapter 5. Thick adherends lap-shear tests (TAST) [125] were carried out at elevated temperatures using the same environmental chamber described earlier. The strains along the bonded joint were recorded using a digital image correlation system and the load was obtained from a testing machine. The tests were unsuccessful because of the low quality captured images caused by the limitations and reflections of the light for the specimen placed inside the thermal chamber.

However, the TAST specimen was modelled using two dimensional (2D) FE analysis using ABAQUS software [126]. The dimensions, the boundary conditions and the applied loading of TAST specimen are shown in Figure 3.19. Very fine mesh toward the joint ends was applied (minimal element size of 0.25 mm), see Figure 3.20, because of the concentration of stresses at the discontinuity. The adhesive layer was divided into eight layers through the thickness which allowed the stresses and the strains data to be obtained along a path created in the middle layer, as shown in Figure 3.20.

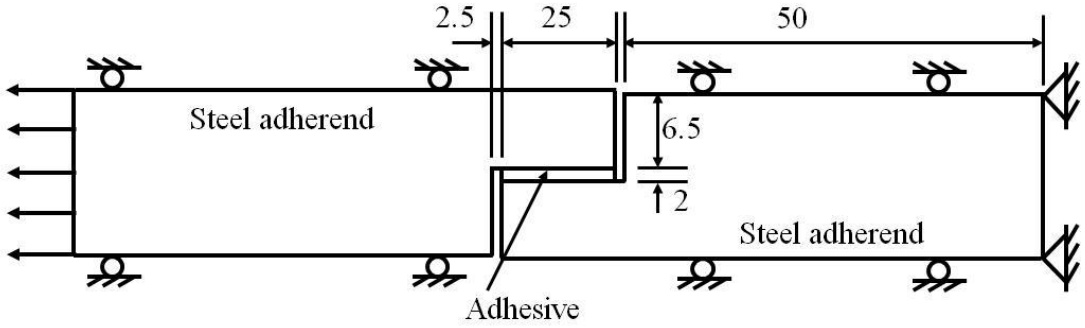

Figure 3.19: Sketch of the thick adherend shear test (TAST) specimen employed in FE analysis showing the boundary conditions and dimensions (in mm)

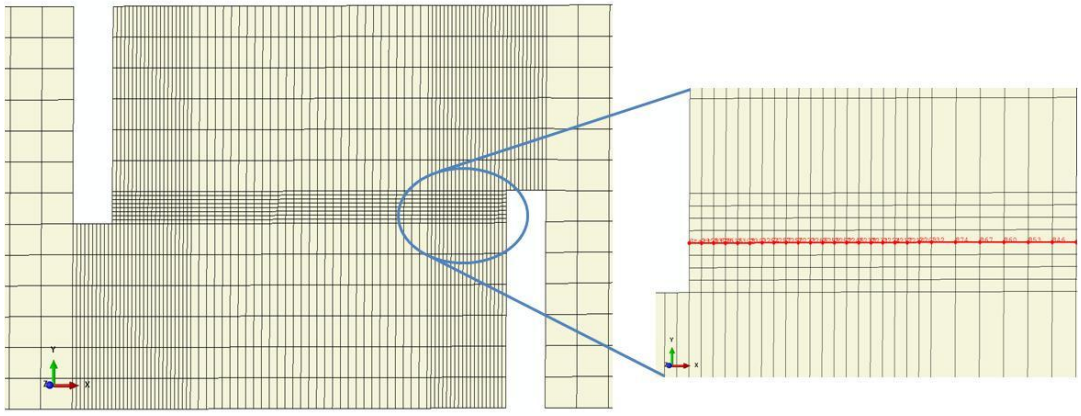

Figure 3.20: Mesh details of the thick adherend shear test (TAST) specimen and middle path

The FE model assumed linear elastic behaviour for steel adherends and applied the same material properties (E_s, v) obtained from the steel dogbone tension tests summarised in Table 3.1. These properties were assumed to be temperature independent, as discussed previously in section 3.2.2. The adhesive nonlinearity at elevated temperature (see Figure 3.16) was approximated with bilinear elastic-plastic model, as shown in Figure 3.21. The first line starts from the origin with a slope (E_1) equal to adhesive Young's modulus (E_a). The second line has a slope (E_2) which is defined by using the yield stresses and plastic strain at failure obtained from fitting a line on the actual stress-strain curve. The slopes (E_1 and E_2) are defined in ABAQUS software using the elasticity and the plasticity options. In the elasticity option, the Young's

modulus and Poisson's ratio are required (see Table 3.3). In the plasticity option, the stress and the plastic strain at failure are set, as summarised in Table 3.4. At each temperature, different adhesive elastic and plastic values were used similar to those obtained from the adhesive dogbone tensile test. Thus, the FE analysis considered both the temperature dependency of adhesive properties and nonlinearity behaviour.

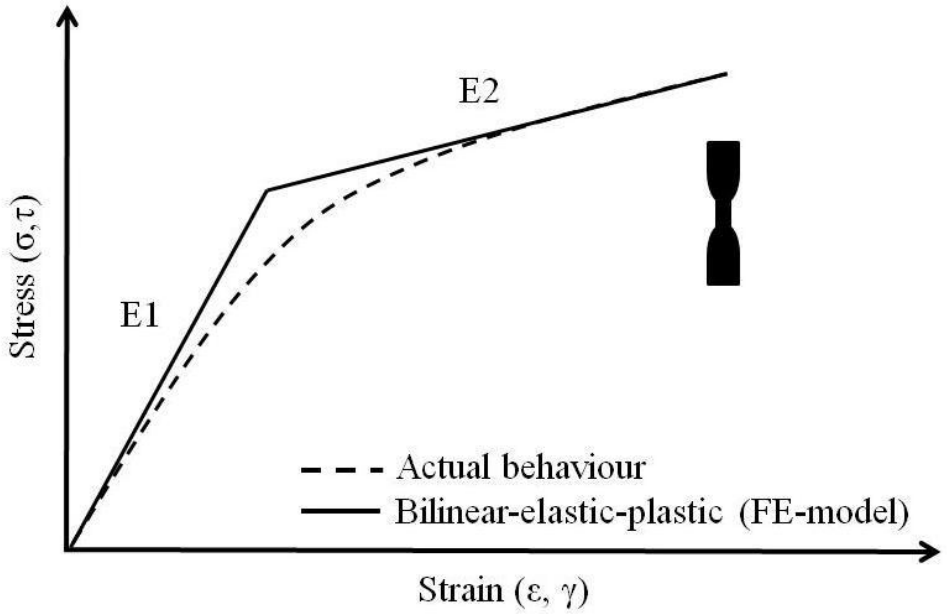

Figure 3.21: Idealisation adhesive stress-stain curve with bilinear model for FE analysis

Table 3.4: Adhesive plastic properties used in the FE-modelling

Temperature ° C	Yield stress MPa	Plastic strain
20	27.1	0.00
	27.6	0.000050
30	11.1	0.00
	25.6	0.001790
40	9.0	0.00
	16.23	0.000942
45	2.8	0.00
	8.4	0.013264
50	2.0	0.00
	4.8	0.033909
60	1.3	0.00
	2.9	0.018566

3.4.2.1 Test results

Figure 3.22 shows the contour plots of the TAST bonded joint loaded at 0.013 kN at different temperatures. At 20 °C, the adhesive is stiff and strong, hence, results in adherends distortion due to a bending moment (Figure 3.22a). However, at 45 °C, the adhesive is soft and weak causing the adherends to slip without bending (Figure 3.22b). The model was created as one part, and then the part was partitioned into different regions. The material properties and the mesh sizes of each region were defined. The interfaces between these regions are strongly connected with solid elements, thus the adhesive and adherends stay connected after loading. Therefore, high stresses concentration and bending of the adhesive at the adherends ends occurred at 20 °C (Figure 3.22a). However, the used model is aimed to obtain the adhesive shear stress-strain curves not to detect crack propagation. It is recommended to use cohesive element to avoid stress concentrations at the ends of adherends. ABAQUS [126] software offers a library of cohesive elements to model the strength of interfaces in adhesive joints.

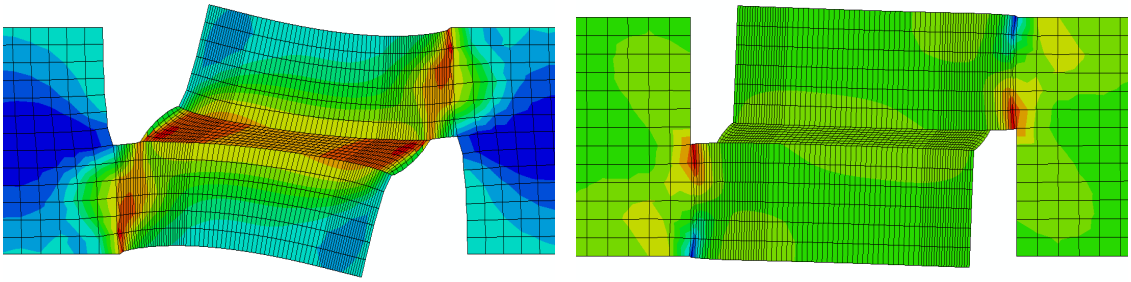

(a) 20 °C (b) 45 °C

Figure 3.22: Shear stresses of the thick adherend shear test (TAST) loaded 0.013 kN

The distributions of the shear stresses along the bonded joints at various temperatures at 0.013 kN are shown in Figure 3.23. The maximum shear stress occurred at 40 °C due to the combined effects of the thermal and mechanical stresses.

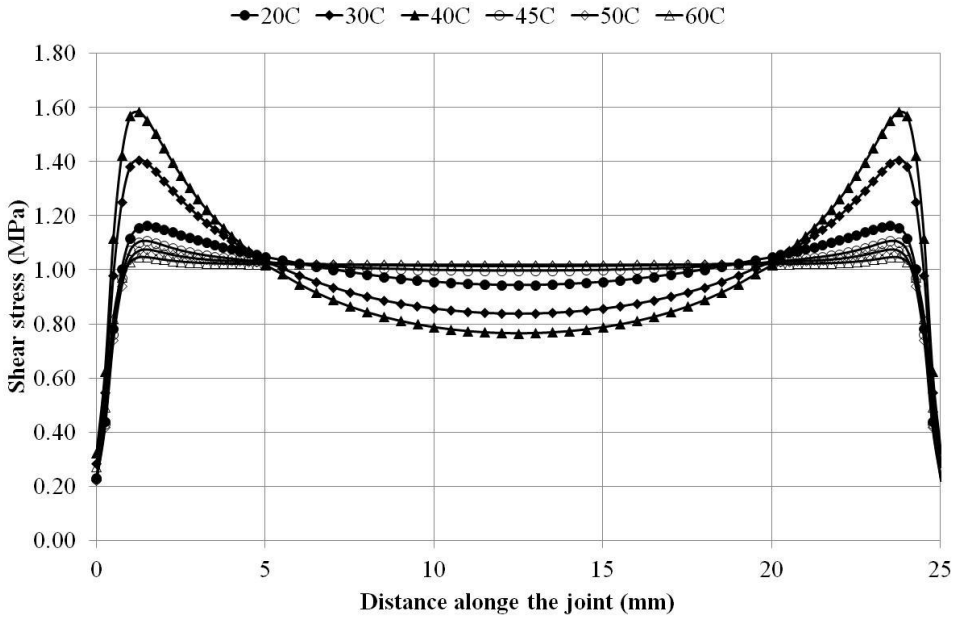

Figure 3.23: Shear stresses along the TAST joint loaded under 1 kN

The relationships between the shear stress and shear strain at different temperatures were obtained by applying various tension loading levels till the joint reaches full plasticity. Figure 3.24 shows the shear stress-strain curves for Sikadur-30 adhesive at different temperatures. The shear stress-strain relationship was linear with small expansion to failure at 20 °C, but it became bi-linear (not nonlinear) at elevated temperatures. This is because the adhesive nonlinear stress-strain curves (Figure 3.16) were approximated in ABAQUS software by elastic and plastic lines (Figure 3.21). The stress-strain data were taken from an element at the centre of the TAST specimen. Therefore, the stress and the strain data were not representing the mean adhesive response along the bonded length. Also, changing the geometry of the TAST specimen especially the adhesive thickness may affect the shear stress-strain behaviour. These limitations in the analyses are out of the scope of this research.

The relationship between the shear stress and the shear strain at elevated temperatures is fitted with a polynomial curve from which the tangent at the origin represents the shear modulus (G_a). The same value of shear modulus was obtained from Eq. (3.2), as the elastic modulus (E_a) and Poisson's ratio (ν) at each temperature were taken from Table 3.3. The G_a values are summarised in Table 3.5.

$$G_a = \frac{E_a}{2(1+\nu)} \tag{3.2}$$

Table 3.5: Adhesive shear modulus obtained from FE analysis

Temperature ° C	Shear modulus (G_a)/ MPa	Normalised modulus %
20	4983	100
30	4832	97
40	4145	83
45	360	7
50	136	3
60	65	1

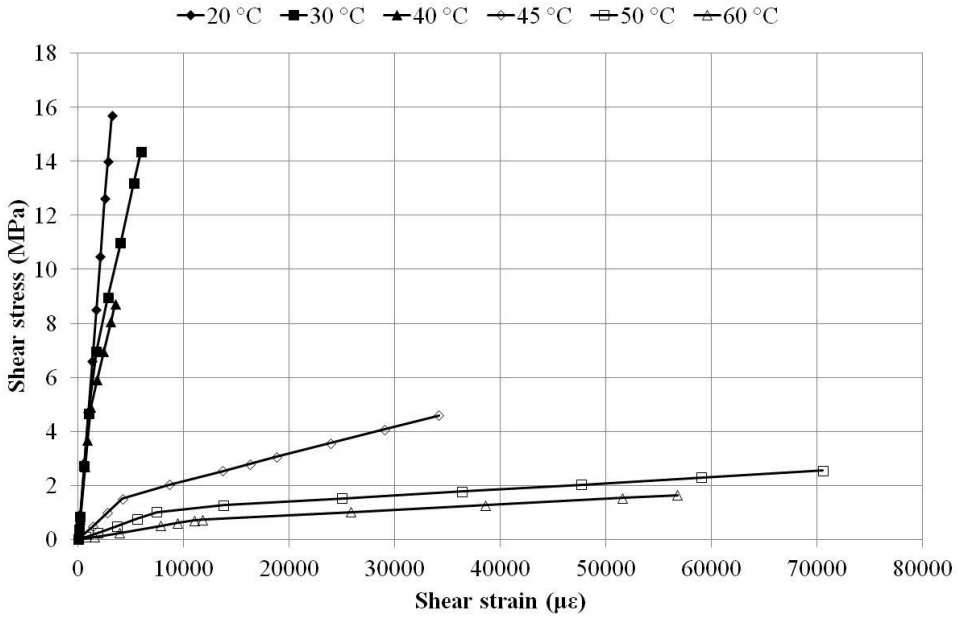

Figure 3.24: Shear stress-strain curves for Sikadur-30 adhesive at different temperatures obtained from FE analysis

3.4.3 Bond Interface strength

To examine the changes in adhesive bond strength and failure mode with temperature, pull-off tests were carried out at 20, 40, 50 and 60 °C.

3.4.3.1 Specimen preparation and test procedure

Mild steel was used to fabricate the specimens because it has a higher stiffness than the adhesive ($E_s/E_a = 15$). The specimens consist of cylindrical steel dollies cut from 20 mm diameter steel rods and steel plates with a cross-sectional dimension of 38×13 mm cut from a steel bar. The dollies and the steel plates were bonded together using Sikadur-30 adhesive (Figure 3.25). The adherends faces were first grit blasted to remove any rust and introducing a rough surface for better bonding. Then, the surfaces were wiped with acetone to remove any oil or grease. The adhesive was applied to both adherends and then they were pressed together. Spherical glass balls of 1 mm diameter (ballotini) were added to the adhesive mixture to ensure a uniform thickness of the adhesive layer between the adherends. Minimum amount of spherical glass

balls, 1% in weight of the mixed adhesive, should be added to avoid stress concentration. The specimens were cured for at least three days at room temperature before testing.

A heating system is designed to carry out the test at elevated temperatures, as shown in Figure 3.26. The heating system consists of a square steel plate containing two big holes and a small one. Two pin heaters are inserted inside the big holes and a thermocouple is inserted in the small one. The pull-off specimen was fixed to the square plate using two bolts. As the electrical current passed through the heaters, the plate was heated up. The specimen then was warmed up due to heat conductivity. To increase thermal conductivity, a layer of thermally conductive paste was applied between the plate and the specimen. A plate thermocouple was attached to the specimen to control its temperature before loading. The specimen was loaded at a rate of 2.5 mm/min to failure. Four specimens were tested at each target temperature (20, 40, 50 and 60 °C) according to the recommendations mentioned in BS EN 1542 [127].

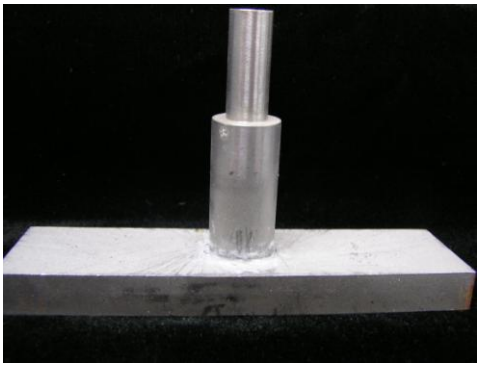

Figure 3.25: Pull-off test specimen

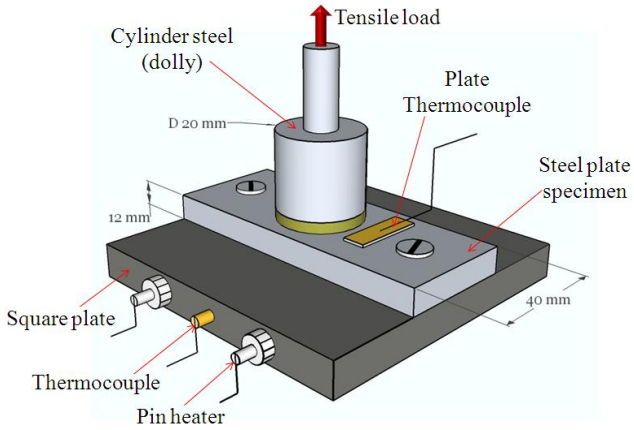

Figure 3.26: Schematic of heating system set up with pull-off specimen

3.4.3.2 Test results

The average bond strength value at room temperature is 16.2 MPa, which it is lower than the manufacturer value (>21 MPa, [124]). This may be due to the different surface preparation and testing method (DIN EN 24624, [128]) carried out by the manufacturer. Nevertheless, the test results indicated a reduction in the adhesive bond strength with temperature, as summarised in Table 3.6. The relationship between the adhesive bond strength and temperature is shown in Figure 3.27. The failure mode was also changed with temperature. While a cohesive failure

occurred within the adhesive leaving a thick layer of adhesive on both adherends at 20 °C, an adhesive failure occurred at the interface between the adhesive and the steel plate at 60 °C, leaving a very thin layer of adhesive attached to it, as shown in the sketch in Figure 3.28.

Table 3.6: Sikadur-30 adhesive bonding strength

Sample	Temperature °C	Pull-off tensile load kN	Adhesive bond strength MPa	Average adhesive bond strength MPa
S1	20	5.45	17.3	16.2
S2	20	5.07	16.2	
S3	20	4.80	15.3	
S4	20	5.09	16.2	
S5	40	3.16	10.1	11.5
S6	40	3.51	11.2	
S7	40	3.99	12.7	
S8	40	3.75	11.9	
S9	50	2.31	7.4	8.1
S10	50	2.55	8.1	
S11	50	2.59	8.3	
S12	50	2.75	8.8	
S13	60	1.48	4.7	4.5
S14	60	1.50	4.8	
S15	60	1.26	4.0	
S16	60	1.44	4.6	

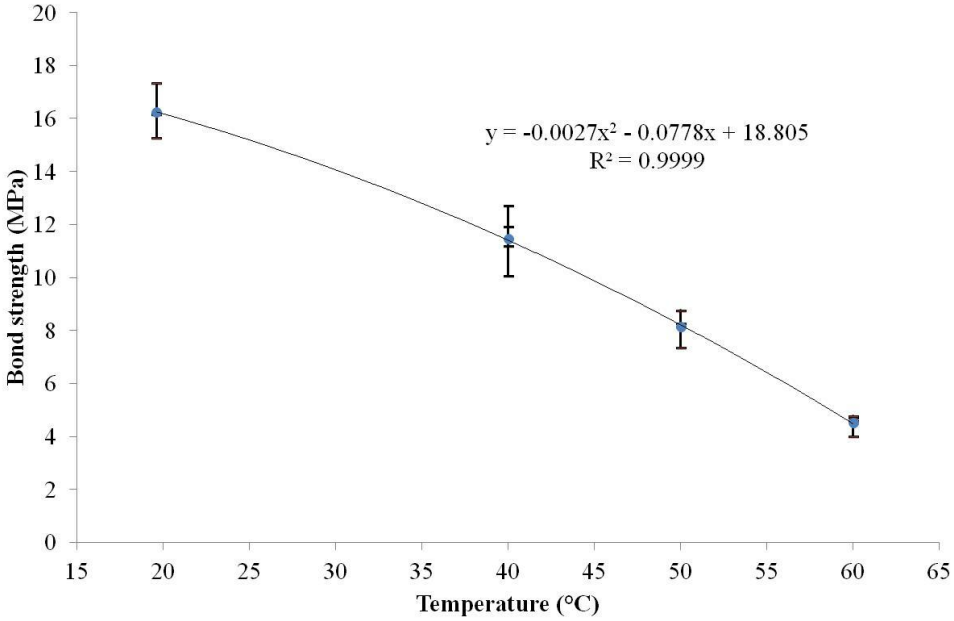

Figure 3.27: Adhesive bond strength (pull-off test) as a function of temperature

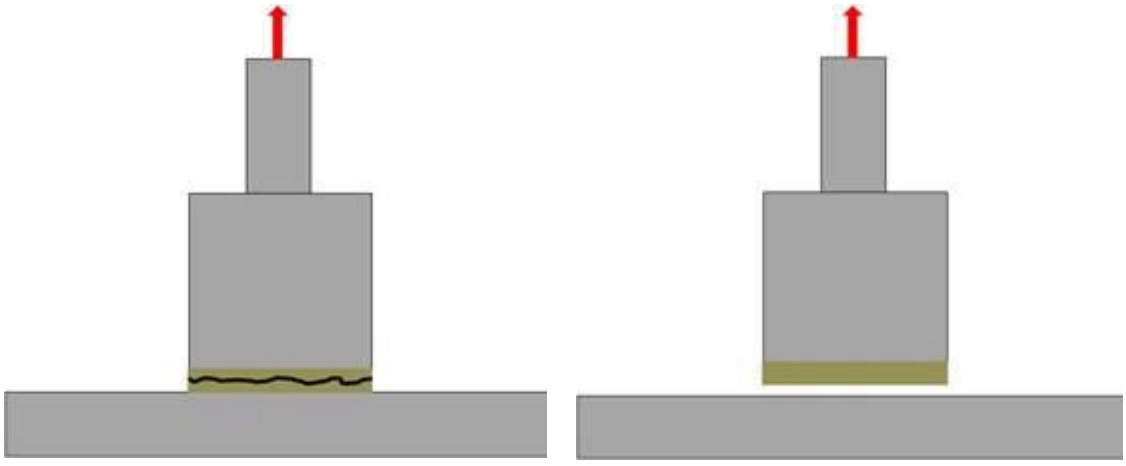

(a) (b)

Figure 3.28: Failure modes in adhesive pull-off test: (a) cohesive failure at 20 °C, and (b) adhesive failure at 60 °C

3.5 Conclusion

The steel, CFRP and adhesive properties at different temperatures were obtained from experimental tests and FE analyses. These data are required in the analytical and the FE analyses to calculate the interfacial stresses in the adhesive between a CFRP plate and a steel beam (Chapter 5).

According to the literature, steel mechanical properties are slightly reduced above 100 °C. Tensile test carried out on the CFRP pultruded specimens at different temperatures up to 60 °C showed that the CFRP properties were not considerably influenced by these temperatures because the CFRP matrix softened above 190 °C. The Sikadur-30 adhesive epoxy was the weakest material and its mechanical properties reduced with temperature. Tensile tests on adhesive dogbone specimens at elevated temperatures showed a significant reduction in the strength and the elastic modulus when the temperature exceeded the adhesive glass transition temperature (T_g) which was about 43±1 °C. In addition, the relationship between the stress and strain became nonlinear with temperature increase.

The adhesive shear modulus values at different temperatures were obtained from the FE analyses carried on thick adherends lap-shear specimens. The shear modulus decreased with temperature increase. Finally, the bond strength of the steel/steel bonded joint decreased with temperature and the failure mode changed from cohesive failure below T_g to adhesive failure above T_g.

Chapter 4

Behaviour of bonded joints under static loading at elevated temperatures

4.1 Introduction

Although much research has been performed on steel beams strengthened with CFRP composites at room temperature, only limited work has been done up to now at elevated temperatures. Generally, the temperature of steel structures over the summer season may exceed 50 °C in the UK [7] or even higher in other countries [8]. Temperature change affects the strength and stiffness of the adhesive bond which may influence the failure load and the failure mode of CFRP strengthened structures as well as the stress distribution along the bonded area.

This chapter presents experimental tests carried out on double-lap shear specimens loaded in tension and CFRP reinforced beams loaded in bending. These tests were performed under static loads at temperatures ranging from room temperature up to 60 °C. Furthermore, FE analyses were conducted on a double-lap shear joint to obtain the adhesive maximum shear and normal strengths at different temperatures. These strengths will be required to calculate the interfacial stresses developed in the adhesive between a CFRP plate and a steel beam (Chapter 5). The time and the temperature dependencies of the bonded shear joint were also investigated. Finally, three-point bending tests were carried out on steel beams reinforced with CFRP plates at different temperatures. The effects of elevated temperatures on the flexural capacity of CFRP strengthened beams were evaluated.

4.2 Shear test

Lap shear tests are most widely used by researchers to evaluate the bond characteristics between a steel and a CFRP composite, because they are easier to prepare and test than flexural beam tests [31]. The double-lap shear specimens are preferable to the single-lap shear specimens as they eliminate the bending of the adherends at the discontinuity due to eccentric loading [114, 129]. In this research, double-lap shear specimens were fabricated and then tested in tension after heated up to target temperatures: 24, 30, 40, 45, 50 and 60 °C. Specimens were named in the form of SS N-T, where the first letter ‘S’ refers to static test and the second letter ‘S’ stands for shear test. The number ‘N’ denotes the test number and the number ‘T’ refers to the testing

temperatures. For example, SS 8-45 represents static test on double-lap shear specimen number eight at 45 °C.

4.2.1 Specimen preparation

Each specimen consisted of two 13 mm thick steel inner plates and two 6.5 mm thick CFRP cover plates bonded together using Sikadur-30 adhesive, as shown in Figure 4.1. The thickness of the steel adherend is twice the CFRP adherend in order to avoid the steel yielding at the CFRP plate ends. The width of both the steel and the CFRP plates are 38 mm. The total length of the specimen is 450 mm (Figure 4.1) to ensure fitting inside the thermal chamber. The CFRP plates were cut to the required lengths using a mechanical saw.

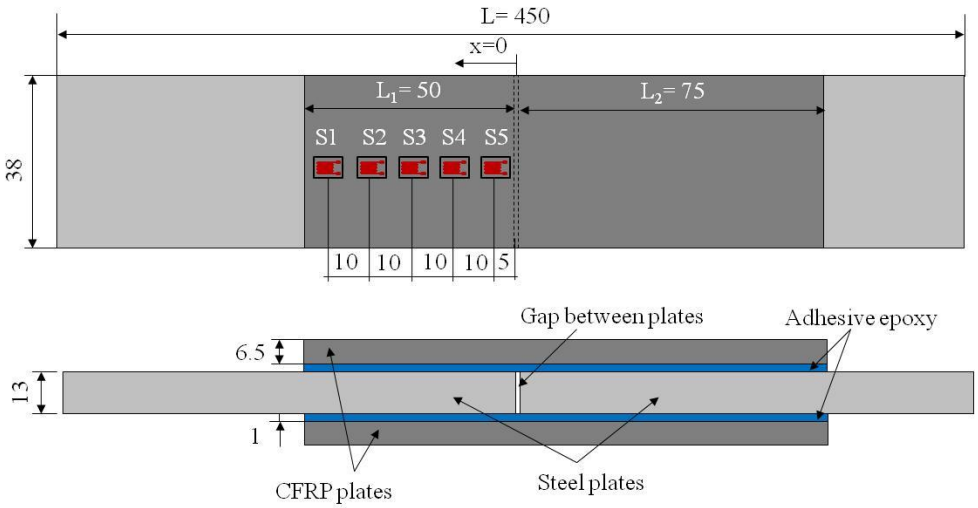

Figure 4.1: Schematic of the double lap shear specimen shown the dimension and the locations of strain gauges (All dimension in mm)

The preparation processes of double-lap shear specimens included several steps: Firstly, the steel plate's surfaces were grit-blasted to remove any rust and to introduce rough surfaces for better bonding (Figure 4.2a). Then, the surfaces were cleaned using a vacuum to remove any dust and sanding debris, and after that the surfaces were wiped with acetone to remove any contaminants and oil. They were cleaned in one direction with a tissue which was used once only, so that contaminants could not redeposit. The CFRP plate was manufactured by Excel composite Ltd with a peel-ply layer on both surfaces to keep the surfaces clean and protect the CFRP fibres from damage during transportation and handling. The peel-ply layer has a rough texture which creates a non-smooth CFRP surface after it is removed. Therefore, no additional

roughening was required to improve the CFRP plate surfaces for better bonding. Secondly, the steel plates were marked to ensure correct fitting of the adherends, as shown in Figure 4.2b. Thirdly, Teflon tapes were applied to one end of each steel plate to prevent end-to-end bonding (see Figure 4.2b), thus allowing the load to be transferred by shear along the bonded joint rather than a tensile load between the steel adherends. Fourthly, a layer of mixed adhesive was applied on the CFRP plate directly after the peel-ply layer was removed. Another layer of adhesive was applied on the steel plate surfaces. The adhesive was spread on both adherends by laying more adhesive along the centre than the outer edges (Figure 4.2c) to allow air trapped between the adherends to escape when they were pressed together. Finally, the CFRP plates were placed on the steel plates at pre-marked locations (Figure 4.2b) and pressed together using two G-clamps (Figure 4.2d). To ensure a uniform thickness of adhesive layer, spherical glass balls of 1 mm diameter (ballotini) were added to the adhesive mixture (1% in weight). The specimens were cured for at least three days at room temperature before testing.

(a)

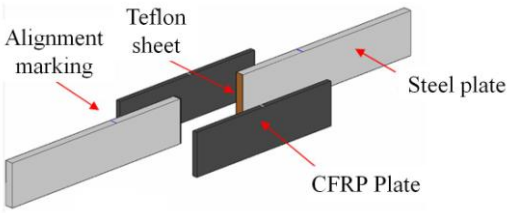

(b)

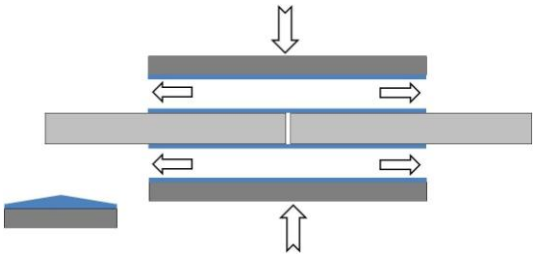

(c)

(d)

Figure 4.2: Double-lap shear specimen fabrication processes: (a) steel plate before and after grit blasted, (b) marking and alignment, (c) adhesive application and (d) clamping and curing.

To ensure the occurrence of the debonding failure at only one side of the bonded joint, the bonded length L_1, the effective length, was designed to be shorter than the bonded length L_2 by 25 mm (see Figure 4.1). Five electrical resistance strain gauges (2 mm long) were bonded along the centre line of the shorter plate length to measure the strains on the outer surface of the CFRP plate, as shown in Figure 4.3. Bonding strain gauges is both labour intensive and time consuming. Therefore, for each temperature groups, one specimen was selected and bonded with five strain gauges. Thus, the strain distribution along the bonded joint and the failure strain were recorded for selected specimens only (see Table 4.2). Gauge numbers and locations from the mid-joint are illustrated in Figure 4.1.

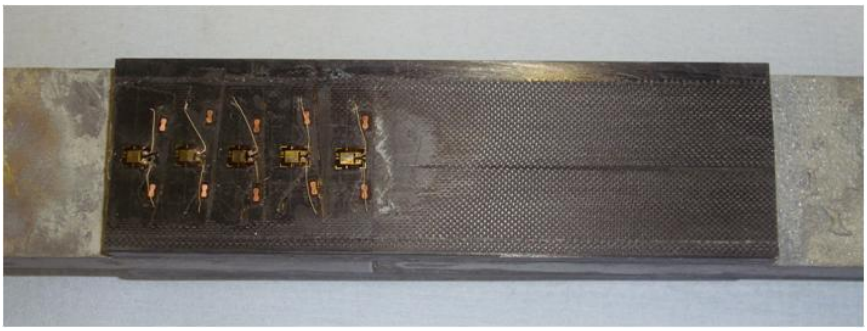

Figure 4.3: Strain gauges mounted on double-lap shear specimen

4.2.2 Test setup

Before testing, the excess adhesive at the edges and the plate ends of the double-lap specimens were removed to eliminate any variability of the results due to different adhesive fillet sizes. Each specimen was loaded in tension to failure using a hydraulic universal testing machine with a maximum capacity of 100 kN. Tests were carried out at elevated temperatures by using the same thermal chamber shown in Figure 3.15 in Chapter 3. Specimens tested at high temperatures were first heated up to the target temperature then loaded to failure. To avoid internal stresses induced in the specimen during the heating-up process due to thermal expansion, the specimen was first clamped by the machine's top grip only. It was then heated up to the required temperature and held for 30 minutes to ensure uniform temperature distribution across the specimen. Then the bottom grip was clamped and the specimen was loaded to failure. All the specimens were tested under displacement control with a loading rate of 1 mm/min. The loads and the strains data were automatically recorded during loading using a Vishay data acquisition system.

4.2.3 Test results and discussion

In this section, the effects of temperature on the failure load, the failure mode and the strain distribution along the bonded plate of the double-lap shear specimens are discussed. The dependency of the failure load on the time and on the temperature is also presented. The maximum adhesive shear and normal strengths at various temperatures are calculated from FE analyses on double-lap joints, which are required in the analytical calculation of the interfacial stresses for the reinforced beam (as will be discussed in Chapter 5).

4.2.3.1 Failure load

The failure loads of the double-lap shear specimens at different temperatures are summarised in Table 4.1.

Table 4.1: Failure load of double-lap shear specimens at different temperatures

Sample	Temperature °C	Ultimate failure load ($P_{ult,T}$)/ kN	Average failure load ($P_{average}$)/kN
SS 1-24	24	89	90
SS 2-24	24	88	
SS 3-24	24	93	
SS 4-30	30	83	88
SS 5-30	30	93	
SS 6-40	40	64	73
SS 7-40	40	82	
SS 8-45	45	64	64
SS 9-50	50	62	62
SS 10-60	60	41	41

The variation in the average failure load and the temperature for double-lap shear joint is presented in Figure 4.4. The figure indicates that the joint capacity decreases with increasing temperature. This is due to the reduction in strength and stiffness of the adhesive with temperature (Table 3.3 in Chapter 3).

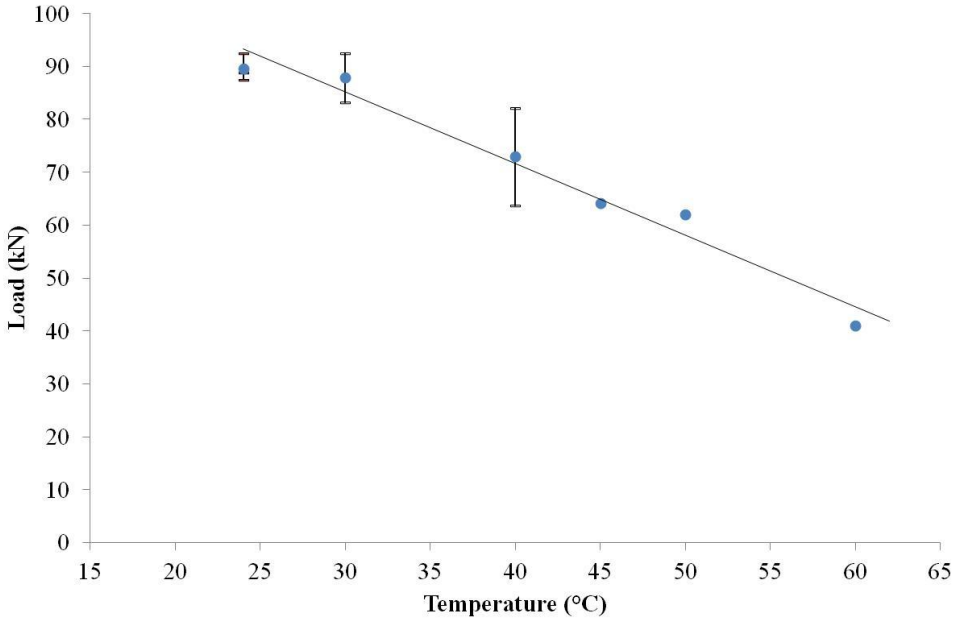

Figure 4.4: Variation in the failure load of double-lap shear joint with temperature

Linear regression analysis was used to produce the following best-fit line between the failure load and the temperature (with a correlation coefficient of R^2=0.97):

$$P_{ult,T} = 125.87 - 1.3558T \tag{4.1}$$

where $P_{ult,T}$ is the failure load at any temperature T.

This equation is not a general solution to calculate the failure load of double-lap shear joint at different temperatures of due to limitation in the number of tested specimens.

The plots of the load versus the displacement obtained from double-lap shear specimens at different temperatures are shown in Figure 4.5 (a to d). The relationship between load and displacement was linear at 24 °C, but became nonlinear at elevated temperatures. This is due to

the change in the adhesive properties from the glassy state to the rubbery state (softens) associated with a reduction in the strength and stiffness (weaken) as the temperature increased.

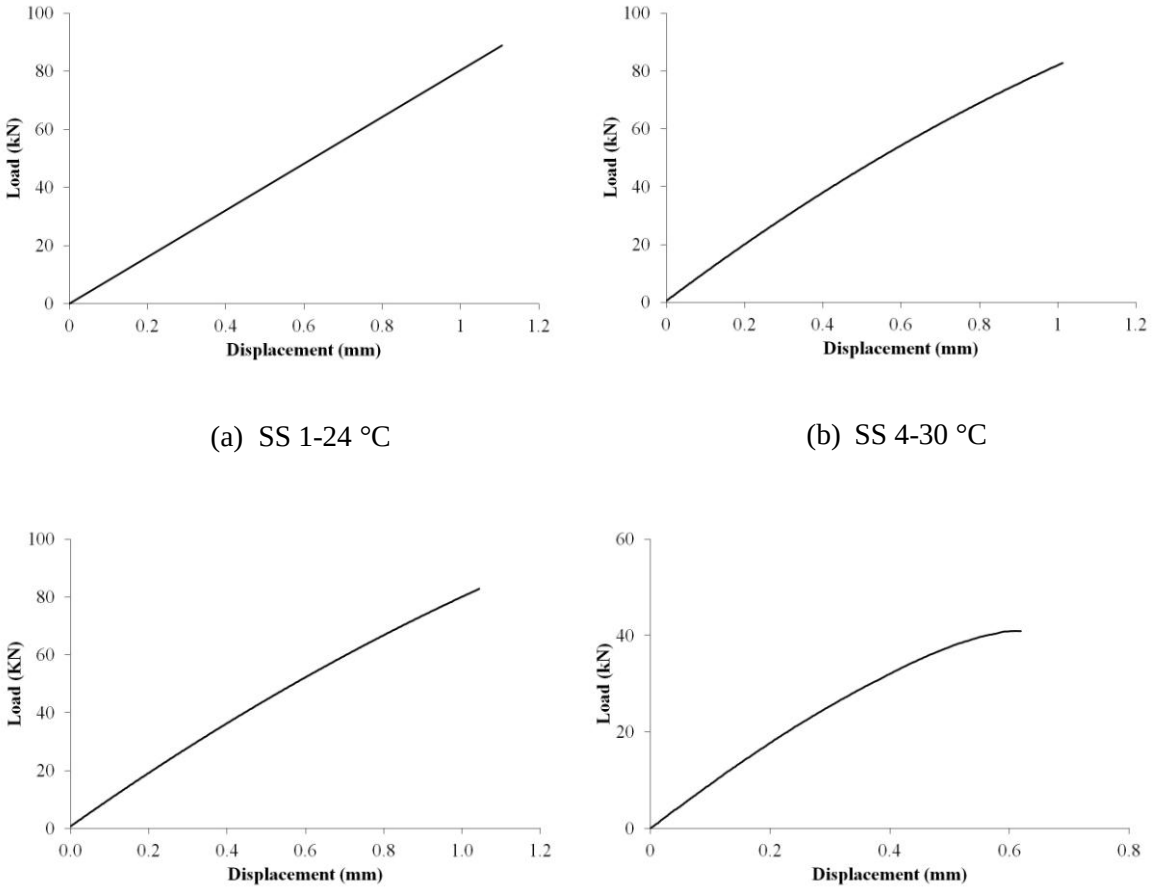

(a) SS 1-24 °C

(b) SS 4-30 °C

(c) SS 7-40 °C

(d) SS 10-60 °C

Figure 4.5: Comparison the load-displacement curves for the double-lap joint at different temperatures

4.2.3.2 Failure modes

Zhao and Zhang presented six possible failure modes that may occur in CFRP strengthened steel specimens subjected to a tensile load [31]: (a) between steel/adhesive interfaces (adhesive failure); (b) through the adhesive layer (cohesive failure); (c) between CFRP/adhesive interfaces (adhesive failure); (d) CFRP delamination; (e) CFRP rupture; and (f) steel yielding. The mode of failure depends on the ratio of modulus of elasticity of the CFRP to steel, the properties and the thickness of the adhesive and the CFRP materials and the temperature.

Two types of failure were observed from the tested double-lap shear specimens at different temperatures. At 24 °C, combined failure modes (a) and (c) was observed, as shown in Figure 4.6a. However, failure type (c) occurred at 60 °C, where both CFRP plates were separated from the adhesive layer, as shown in Figure 4.6b. The steel yielding failure (f) did not occur as the steel plate elastic modulus and thickness were larger than that for the CFRP plate ($E_s t_s \rangle E_p t_p$). The CFRP rupture failure (e) did not occur because the CFRP tensile strain at mid-joint was smaller than failure strain, as will be discussed in section 4.2.3.3.

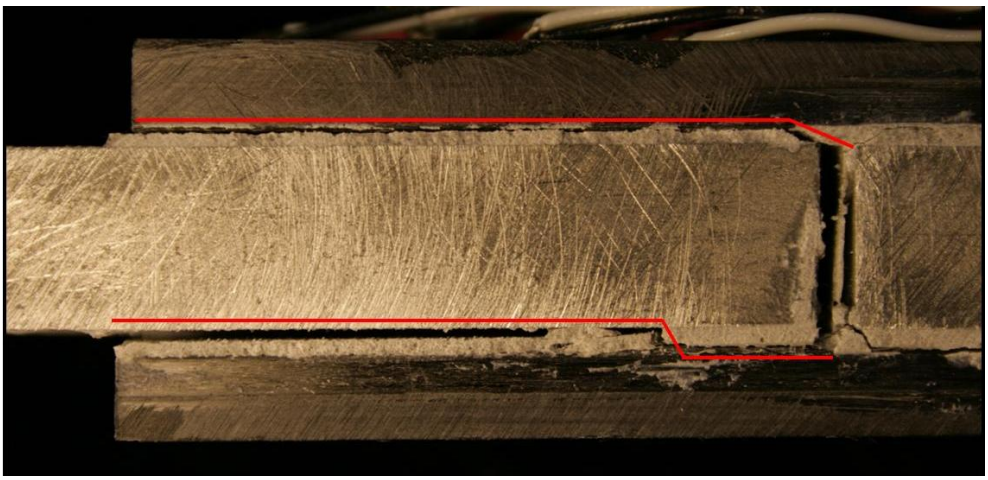

(a)

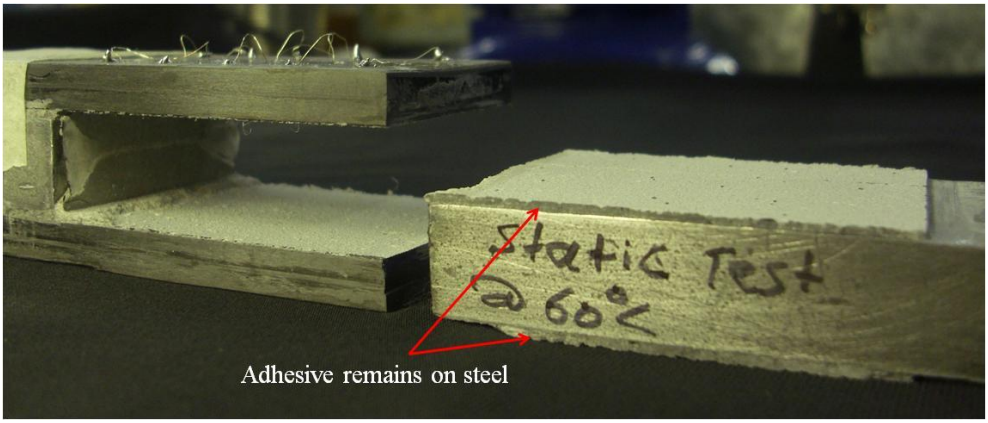

(b)

Figure 4.6: Static failure modes for double-lap shear specimens (a) combined between steel/adhesive and CFRP/adhesive interfaces at 24 °C and (b) between CFRP/adhesive interfaces at 60 °C

4.2.3.3 Strain distribution

The tensile strain in the CFRP plate at mid-joint of a double-lap specimen ($x = 0$, Figure 4.1) is calculated as follows:

$$\varepsilon = \frac{P_{ult,T}}{2 \times A_p \times E_p} \tag{4.2}$$

where $P_{ult,T}$ is the failure load of a double-lap joint at any temperature (Table 4.1), A_p is the CFRP cross-sectional area (38 mm $\times$ 6.5 mm, Figure 4.1) and E_p is the CFRP elastic modulus (158 GPa, as reported by Clarke [107]).

The CFRP tensile strain at failure load calculated from Eq. (4.2) corresponds with that measured by the strain gauge (S5, Figure 4.1) located 5 mm from the mid-joint, as summarised in Table 4.2. Tensile tests carried out by Clarke [107] on CFRP specimens gave the tensile failure strain of 6500 $\mu\varepsilon$, which is larger than the failure strain calculated at the mid-joint of the double-lap shear specimens. Thus, the CFRP rupture failure (e) at mid-joint did not occur, as the CFRP plate expanded by about 18% of its failure strain.

Table 4.2: Failure strain of double-lap shear specimens at different temperatures

Sample	Temperature °C	Failure load ($P_{ult,T}$)/ kN	CFRP tensile strain recorded by strain gauge (S5) $\mu\varepsilon$	CFRP tensile strain calculated by Eq. (4.2) $\mu\varepsilon$
SS 3-24	20	92.5	1080	1185
SS 5-30	30	92.5	1176	1186
SS 7-40	40	82.2	977	1053
SS 8-45	45	64.1	888	821
SS 9-50	50	62.1	779	795
SS 10-60	60	41.1	441	526

The strains distribution captured along the CFRP plate for double-lap shear specimens at different loading levels (the ratio of the applied load to the ultimate failure load) are presented in Figures 4.7 to 4.10.The figures showed that maximum tensile strain occurred near the mid-joint

(measured by strain gauge S5) and decreased gradually to negative (compressive) strain near to the plate end (measured by strain gauge S1). The negative strain is due to bending of the CFRP plate end (as will be shown in Figure 4.22) caused by the normal stress at the plate end.

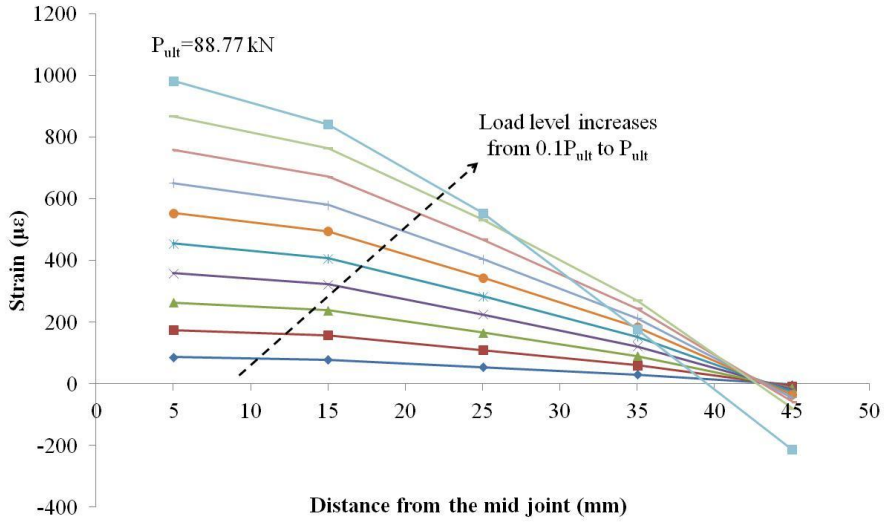

Figure 4.7: Strain distributions along CFRP plate bonded length at 24 °C (SS 1-24)

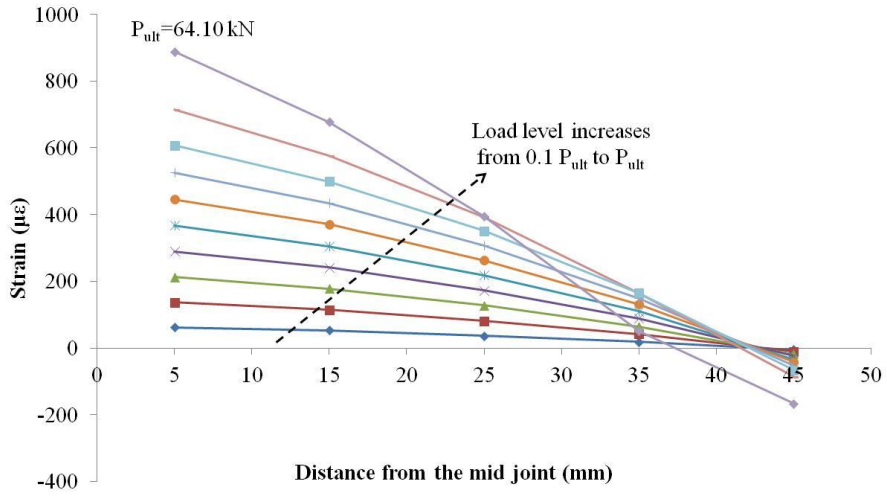

Figure 4.8: Strain distributions along CFRP plate bonded length at 45 °C (SS 8-45)

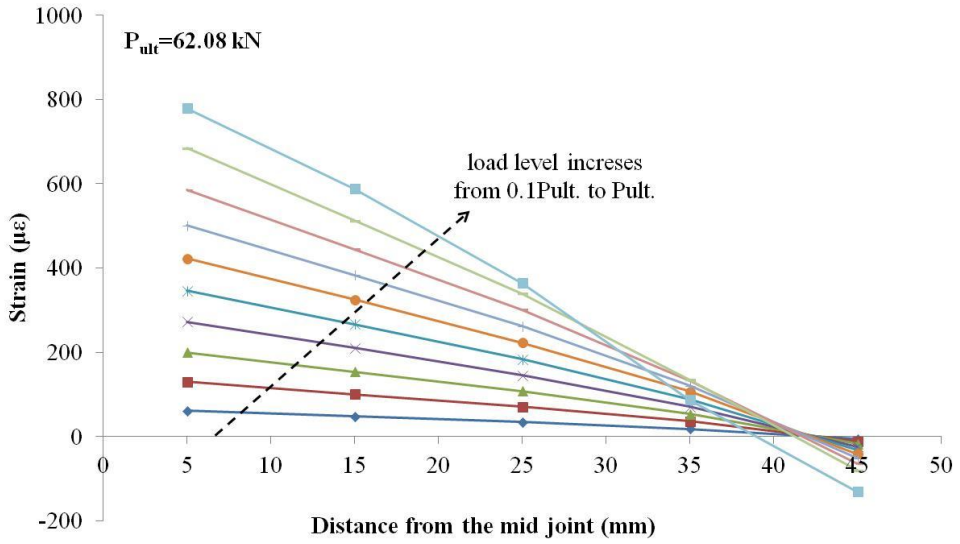

Figure 4.9: Strain distributions along CFRP plate bonded length at 50 °C (SS 9-50)

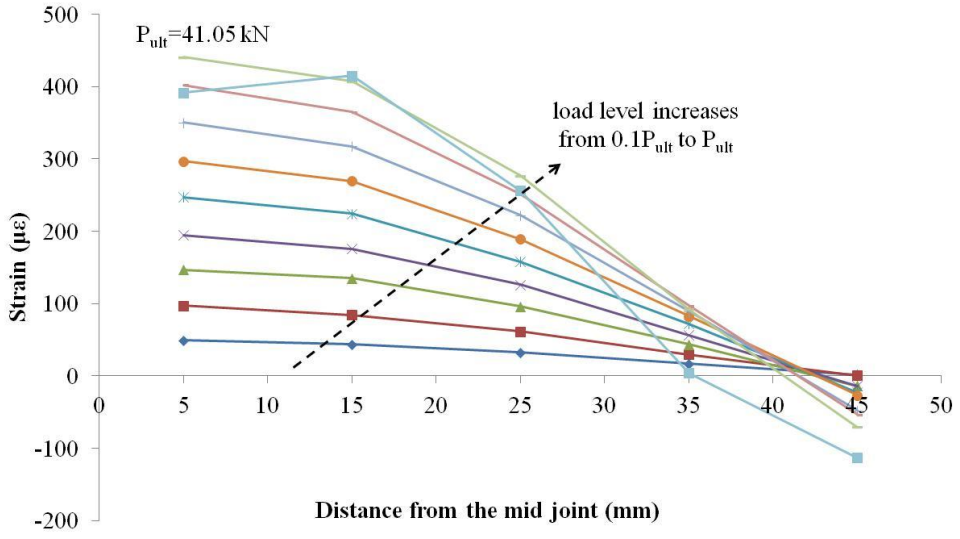

Figure 4.10: Strain distributions along CFRP plate bonded length at 60 °C (SS 10-60)

The relationship between the strains at different locations on the CFRP surface and the applied load at 24 °C are shown in Figure 4.11. The strains measured by strain gauges (S1-S5, Figure 4.1) bonded at different locations along the CFRP plate changed linearly with the load. The strains were positive (tension) at all locations, but near to the plate end (S1) the strain was negative (compressive) due to plate bending. The strains dropped suddenly in a very short time (less than 0.1 second) indicating abrupt debonding.

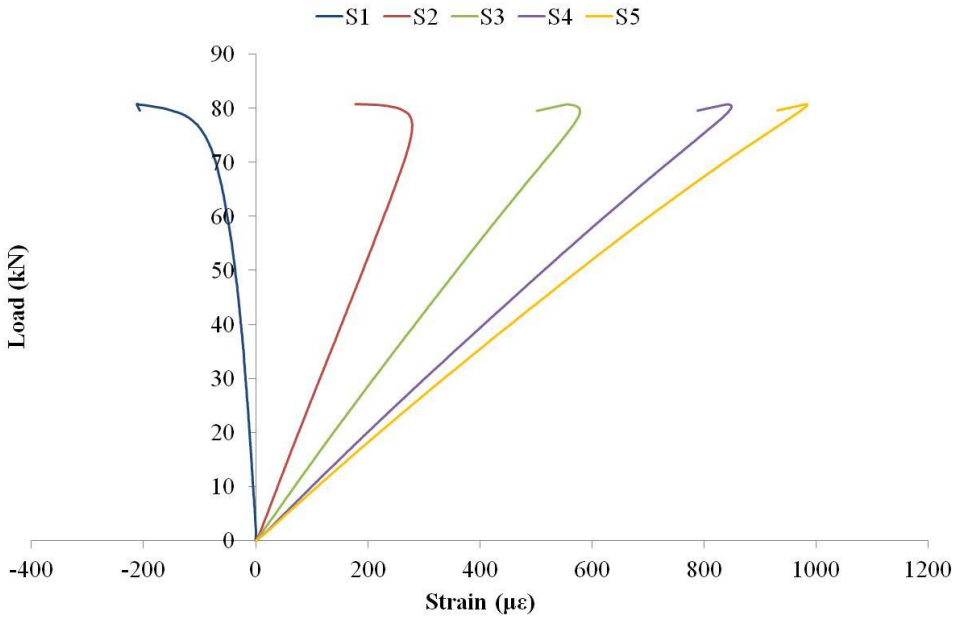

Figure 4.11: Strains versus load at different locations along CFRP plate surface at 24 °C

Comparisons of the strains measured by gauges S1 to S5 (Figure 4.1) for different specimens at various temperatures are shown in Figures 4.12 to 4.16. The figures show that the strains values at any location along the CFRP plate surface were greater at 24 °C than at higher temperatures. This is due to the softening of the adhesive with temperature thus the stresses transferred from the steel plate to the CFRP plates were decreased. Figure 4.12 shows that the load varied linearly with the strain near the plate end (S1) at 24 °C before reaching a plateau, but a nonlinear relationship was observed at 60 °C. However, the relationships between the loads and the strains at other locations were linear to failure (Figures 4.13 to 4.16).

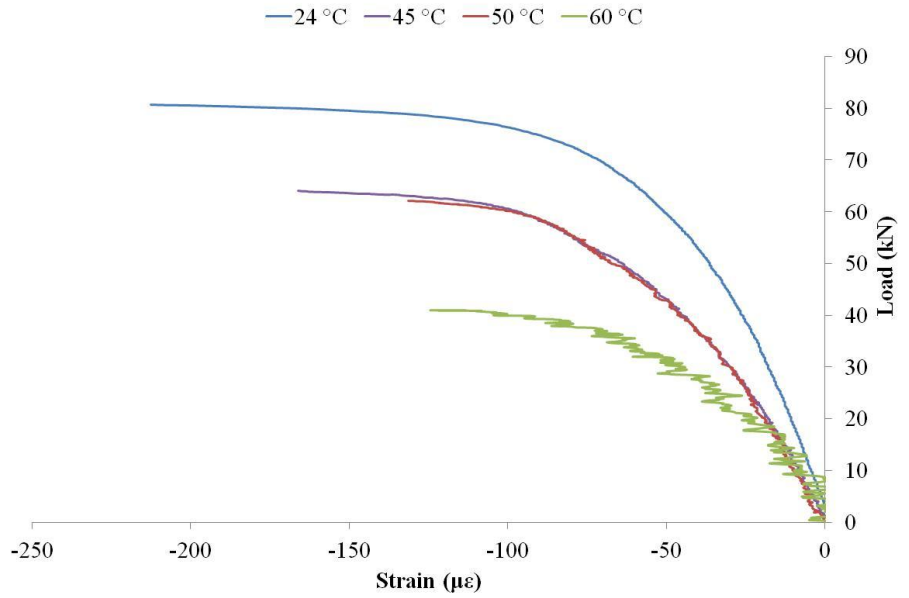

Figure 4.12: Strain measured by strain gauge S1 (45 mm from mid-joint) at different temperatures

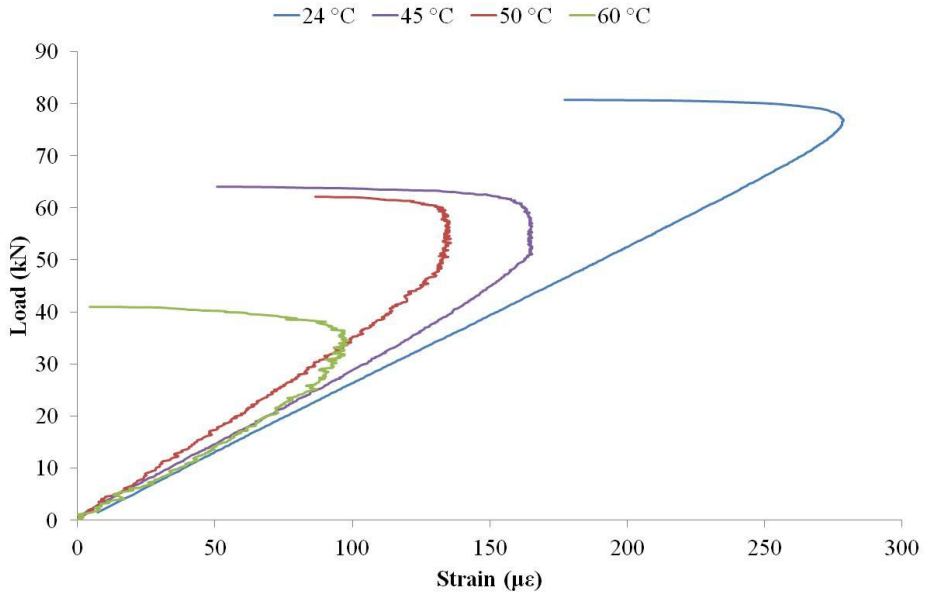

Figure 4.13: Strain measured by strain gauge S2 (35 mm from mid-joint) at different temperatures

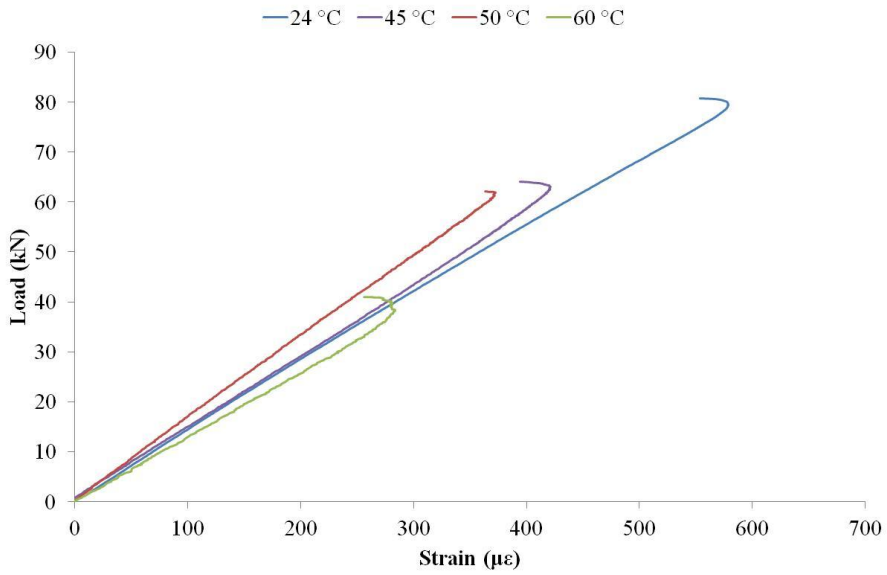

Figure 4.14: Strain measured by strain gauge S3 (25 mm from mid-joint) at different temperatures

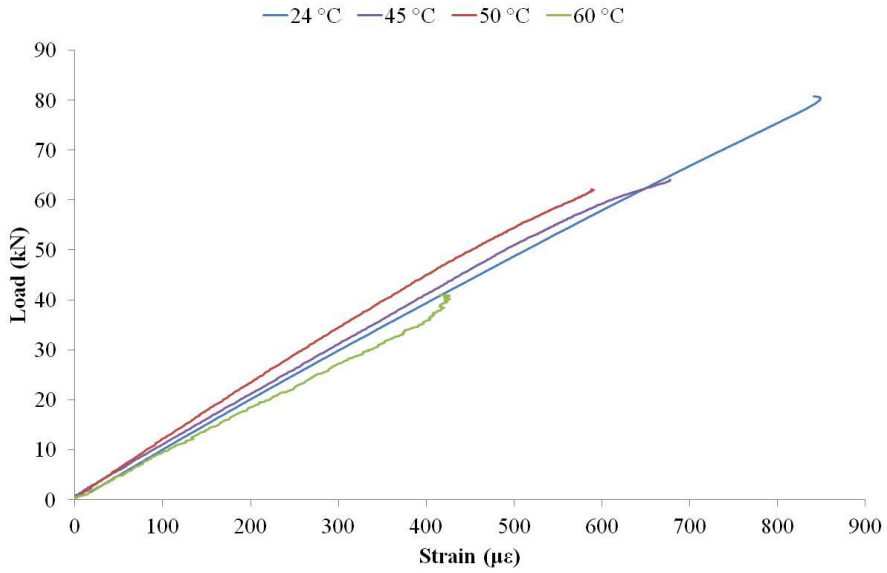

Figure 4.15: Strain measured by strain gauge S4 (15 mm from mid-joint) at different temperatures

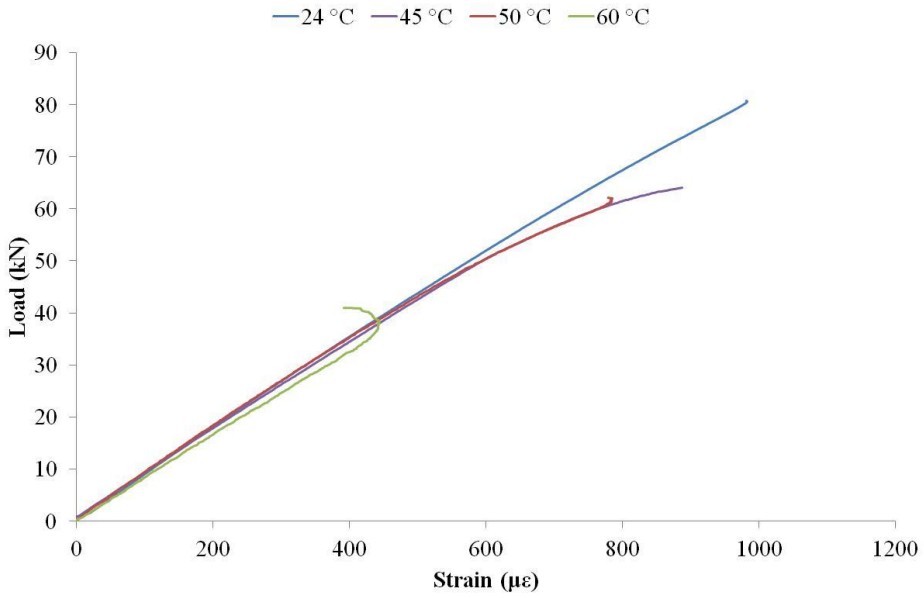

Figure 4.16: Strain measured by strain gauge S5 (5 mm from mid-joint) at different temperatures

4.2.3.4 Creep tests

Creep tests were carried out on double-lap shear specimens subjected to various loading levels of the average static failure load at 40 °C (Table 4.1). The temperature of 40 °C was chosen in this test, as it is below adhesive T_g, and it is frequently reached by steel structures in summer time. In the test procedure shown in Figure 4.17, the specimens were heated to 40 °C, and then loaded to certain levels of the average static failure load at 40 °C while temperature was maintained. To ensure thermal stabilisation, the specimen was held at 40 °C for 30 minutes before being loaded. Then, the tensile load was applied at a rate of 1 mm/min to 34, 44, 54 and 68% of the static failure load and held to failure. The time was recorded starting from the applied load to the debonding failure. Table 4.3 summarised test results including the applied load and the failure time. The results show that the time to failure of double-lap joint decreases with increasing loading level, as shown in Figure 4.18. The figure shows that a sudden failure occurred after less than 1 minute when the specimen was loaded to 68% of the static failure load, but the failure time increased to 1 hour after the loading level was reduced by 34 %. Thus, the strength of a bonded joint is dependent not only on temperature but also on time. This is

because the properties of adhesive are time and temperature dependent even below T_g, as mentioned in the literature in section 2.10. Therefore, the CFRP strengthened structures time and temperature dependencies must be taken into consideration to avoid sudden failure.

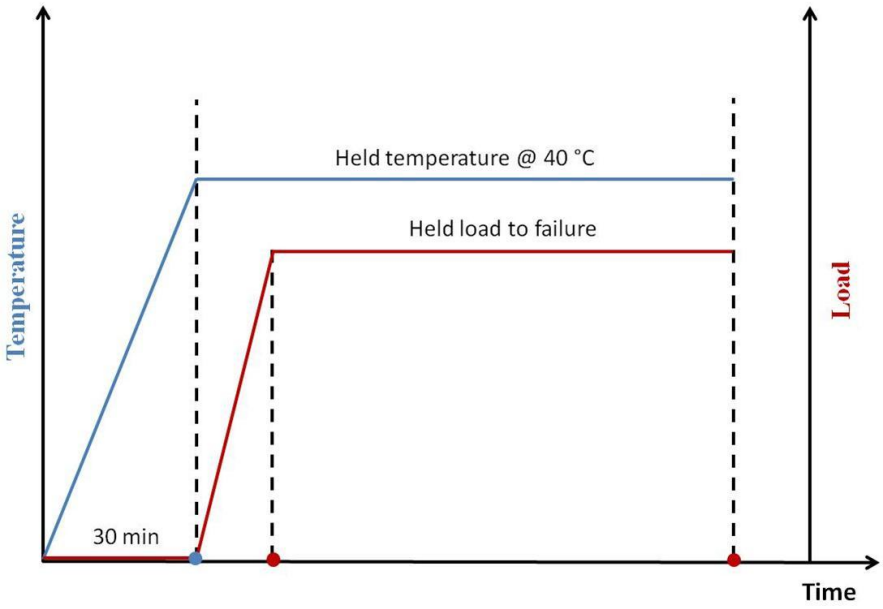

Figure 4.17: Sketch of heating and loading process in the time-temperature test

Table 4.3: Failure load time dependent

Temperature °C	Loading level ($P/P_{static,40°C}$) %	Load kN	Failure time min
40	34	24.65	60.57
40	44	32.87	9.09
40	54	41.09	7.57
40	68	49.30	0.88

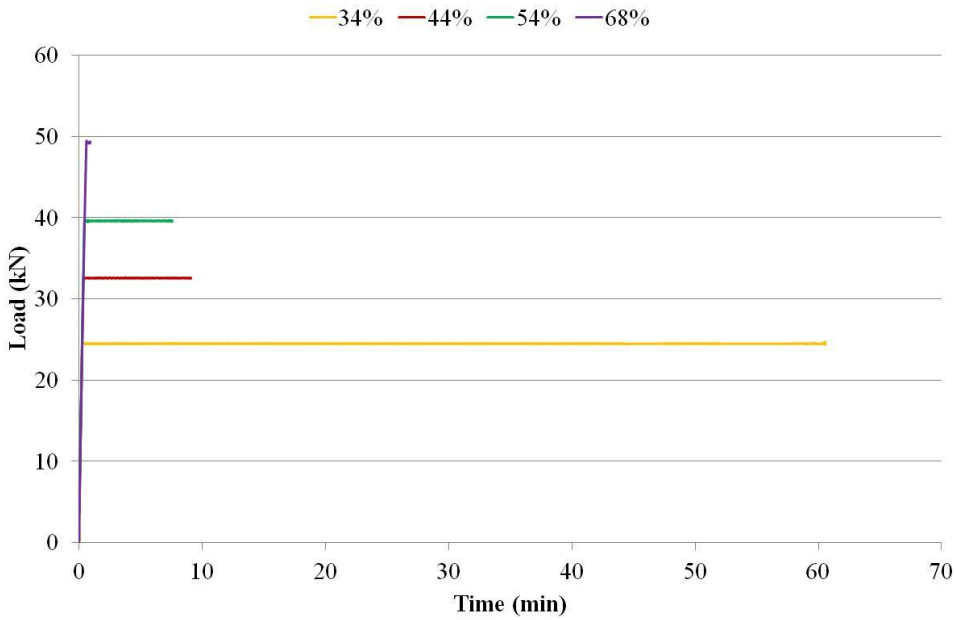

Figure 4.18: Time to failure of double-lap shear joint at 40 °C

4.2.3.5 Finite Element model for the double-lap shear joint

Nonlinear FE analysis was conducted on a double-lap shear specimen to investigate the distribution of the shear and normal stresses in the adhesive along the bonded joint. In addition, the maximum adhesive shear and normal strengths were calculated at different temperatures, which will be required in the analytical calculations of the interfacial stresses developed in the adhesive between a CFRP plate and a steel beam, as will be discussed in Chapter 5.

The double-lap shear specimen was modelled using two-dimensional (2D) FE analysis using ABAQUS software [130]. The model was constructed using 8-node bi-quadratic reduced integration elements. The geometry of the model was similar to that of the test specimen (Figure 4.1), but only a quarter of the specimen was modelled due to symmetry, as shown in Figure 4.19. The top and bottom faces of the steel plate were restrained in the y direction only to ensure that the steel plate only moved in the x direction. The end of the CFRP plate was restrained in the x direction. The adhesive layer was divided into five layers through the thickness which allowed the shear and normal stresses to be acquired from a path created in the central elements. Fine mesh was applied towards the adherend ends due to concentration of the stresses at the discontinuity (Figure 4.20).

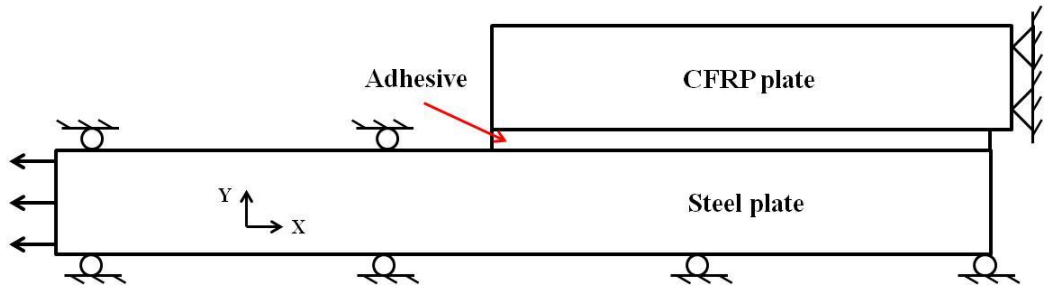

Figure 4.19: Boundary conditions and loading on a quarter of the double-lap shear specimen applied in the FE-model.

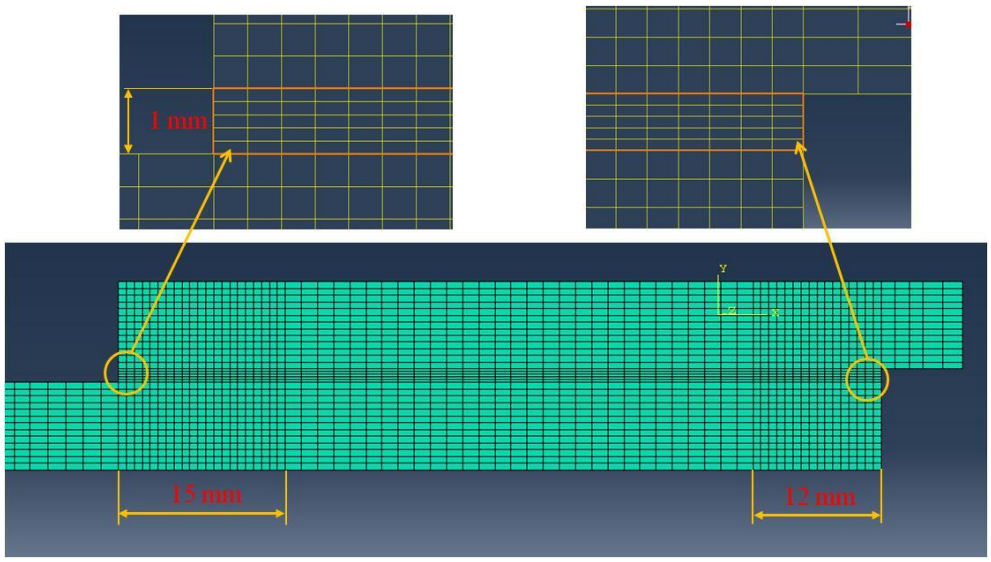

Figure 4.20: Overview of the mesh on a quarter of the double-lap shear specimen applied in the FE model with a close-up view of the adhesive layers near the adherends ends.

The steel and the adhesive properties used in the FE model were based on values obtained from experimental tests (reported in Tables 3.1, 3.3 and 3.4 in Chapter 3), and the properties of the CFRP were given by Clarke [107]. The steel and the CFRP materials were modelled as linear elastic and their properties were temperature-independent, as discussed previously in sections 3.2.2 and 3.3.2 in Chapter 3. The adhesive stress-strain relationship was linear elastic at room temperature, but became nonlinear at elevated temperatures. The nonlinearity behaviour was approximated with a bilinear elastic-plastic model (see Figures 3.16 and 3.21 in Chapter 3). A

detail of the bilinear fitting curve was previously discussed in section 3.4.2 in Chapter 3. Thus, the FE analyses included both the adhesive temperature dependency and the nonlinearity behaviour.

Although the mechanical properties of unidirectional CFRP composites in the normal direction are different than those in the transfer direction (anisotropic), the model assumed that the CFRP composite material was isotopic for simplicity. This assumption may affect slightly the longitudinal stress than the transverse stress, as the applied load was within the fibres direction. The FE model was first validated by comparing the strain data measured by five strain gauges bonded along the CFRP plate surface with the strain data obtained from the FE analyses at the same locations. As the strain data obtained from FE analyses agreed well with those measured experimentally for specimens loaded at room temperature (Figure 4.21), the model was further used to calculate the shear and normal stresses within the adhesive.

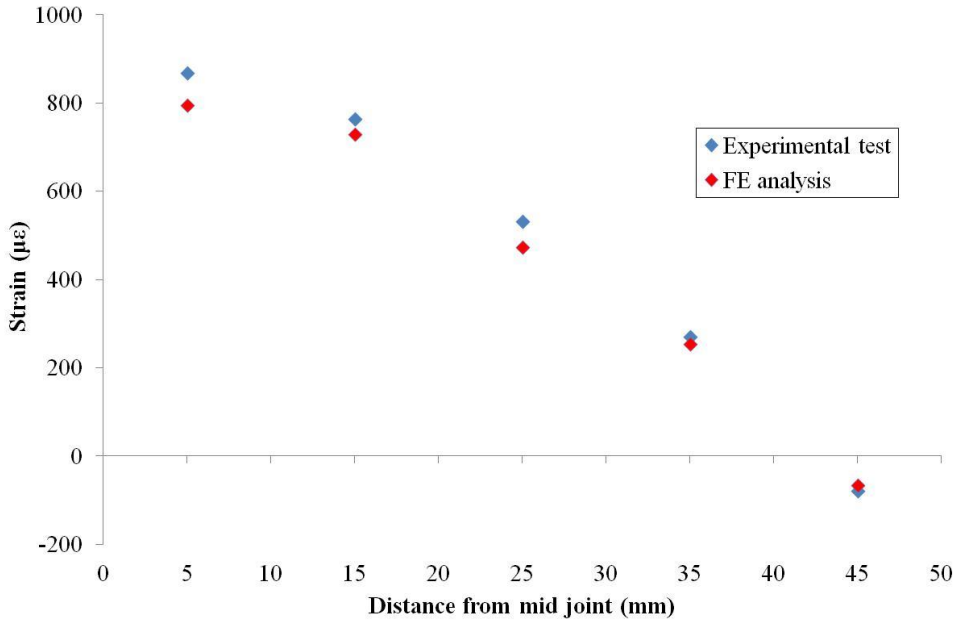

Figure 4.21: Comparison of the strains obtained from the FE analyses and the experimental test at 20 °C

Figure 4.22 shows the comparison between the deformed and undeformed models confirming CFRP plate end bending due to high normal stresses. Therefore, a negative strain measured experimentally by strain gauge (S1) as shown in Figure 4.12. The Von-Mises stresses were higher near mid-joint especially at the upper interface, as shown in the contour in Figure 4.23.

This was due to the dissimilarity between the stiffness of the steel ($E_s = 180.60\,\text{GPa}$) and the stiffness of the CFRP ($E_p = 158\,\text{GPa}$). Therefore, the CFRP plate extends more than the steel which results in severe plastic deformation in the adhesive at mid-joint, which agreed with the analysis of Hart-Smith imbalanced adherends stiffness [114].

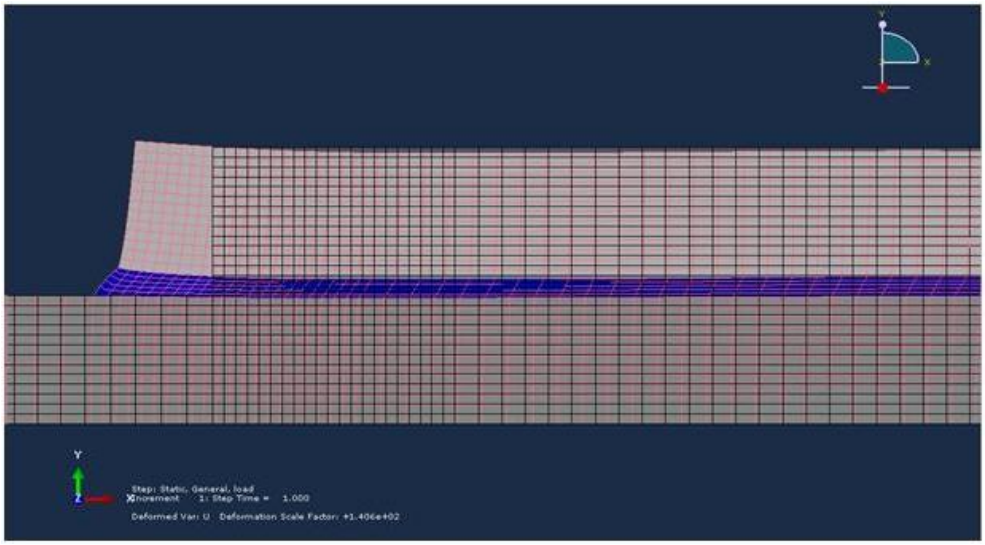

Figure 4.22: The CFRP plate end bent due to the high normal stresses

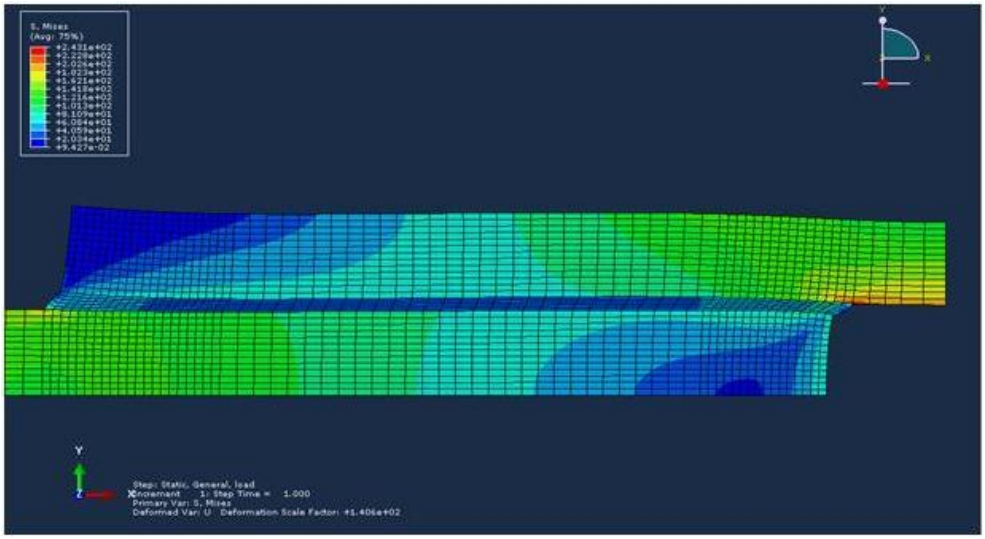

Figure 4.23: Von-Mises stress concentrated at mid-joint

The distributions of Von-Mises, shear, and normal stresses in the adhesive along the bonded joint subjected to different load levels at 20 °C are shown in Figures 4.24 to 4.26, respectively. The figures show non-uniform stress distributions along the bonded joint. The stresses were high at adherends discontinuities and reduced to minimum at 25 mm from mid-joint, which divided the bonded joint into two zones: plastic zones near the adherends ends and an elastic zone in the middle of the bonded joint. The plastic zones grew as the load increased until full plasticity occurred. Figure 4.24 shows that the plastic zone length at the mid-joint was larger than that at the CFRP plate end. Thus, debonding failure was initiated at mid-joint as shown in Figure 4.23.

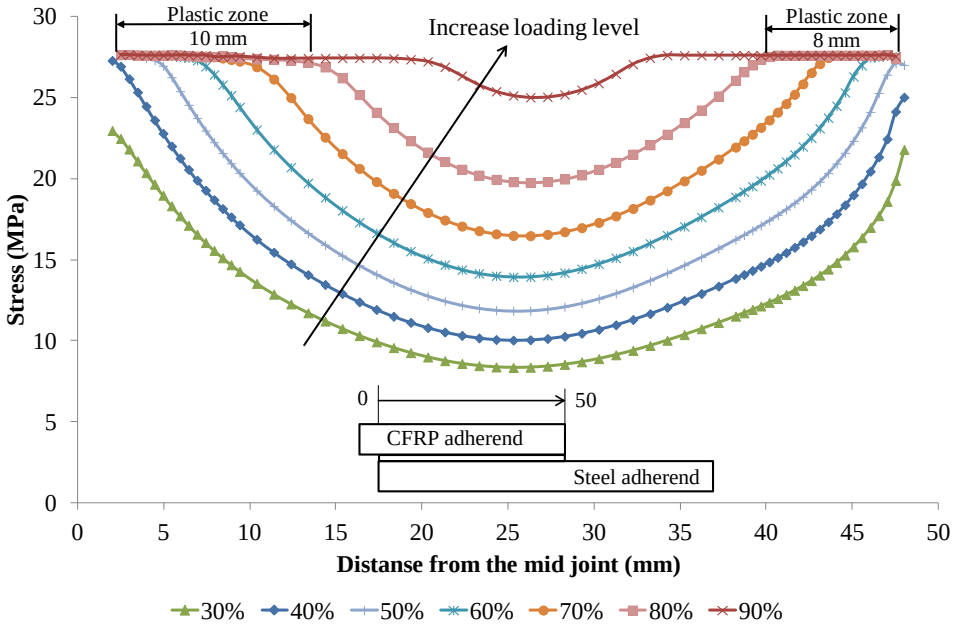

Figure 4.24: Distribution of Von-Mises stresses at different levels of the average failure load (20 °C)

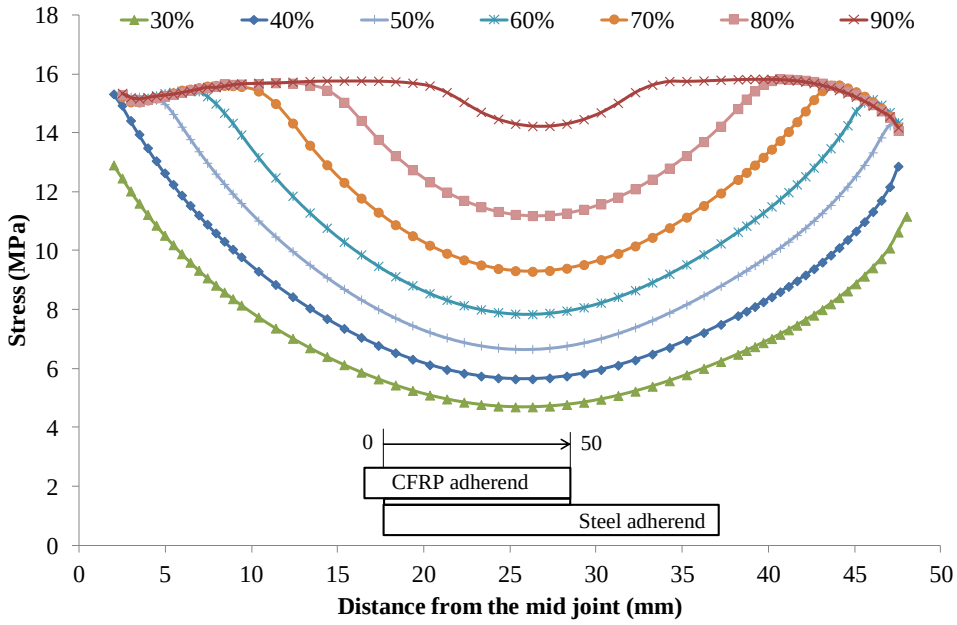

Figure 4.25: Distribution of shear stresses at different levels of the average failure load (20 °C)

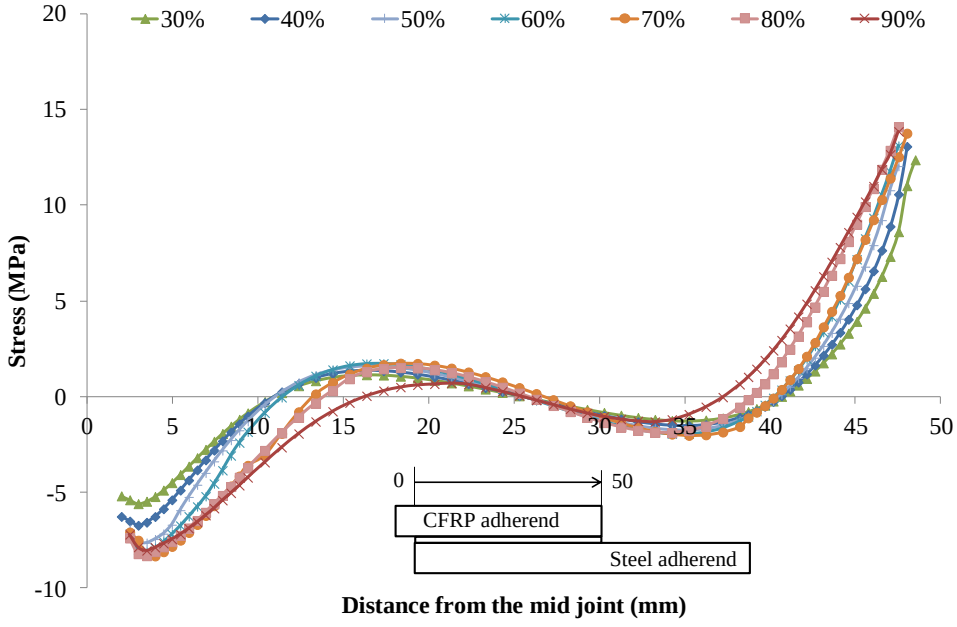

Figure 4.26: Distribution of normal stress at different levels of the average failure load (20 °C)

The length of the plastic zone at the higher loads just before failure was obviously long, although the adhesive is elastic and brittle at 20 °C (Figure 3.24). This is because the properties of the adhesive at 20 °C were defined in the FE model using elasticity and plasticity options (Table 3.4). The elasticity option defines only the elastic modulus and the Poisson ratio, where the plasticity option identifies the maximum strength that the adhesive could reach before failure. Figure 4.27 shows that the shear strains along the bonded joint are within the elastic shear strain limitation (Figure 3.24).

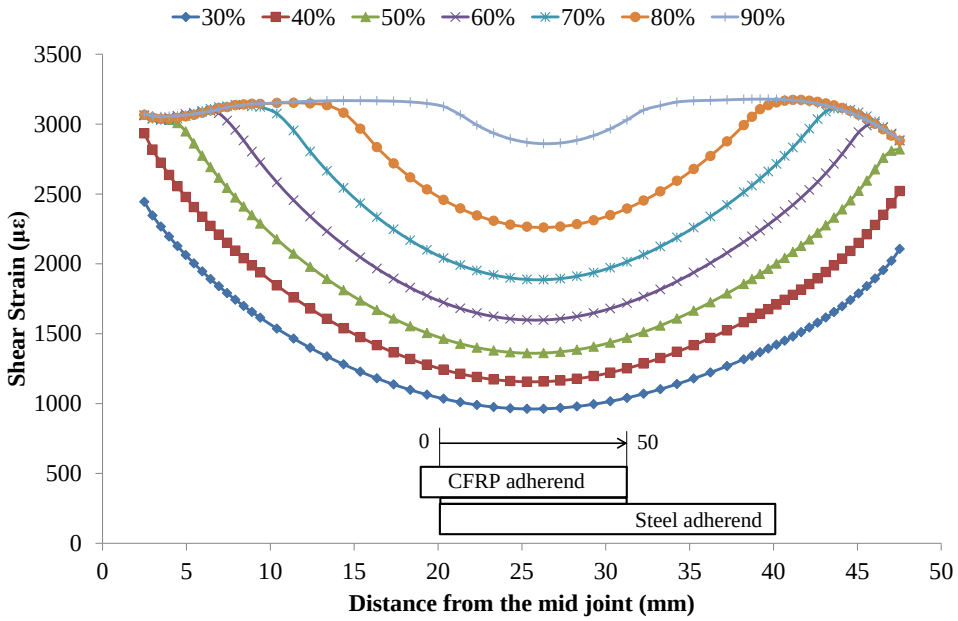

Figure 4.27: Distribution of shear strains at different levels of the average failure load (20 °C)

Thermal stresses were developed within the adhesive layer to the significant difference in the coefficients of thermal expansions for the steel (10×10^{-6}/°C) and the CFRP (0.34×10^{-6}/°C). Figure 4.28 shows that the thermal shear stresses for bonded joint without mechanical loading were higher at the adherends discontinuity and reduced to zero in the middle of the bonded joint. The maximum shear stress of 6.6 MPa occurred as the temperature increased from 20 to 40 °C. Above 40 °C the thermal shear stress was decreased due to the significant reduction in the adhesive (strength and the) stiffness at T_g (Table 3.3 in Chapter 3).

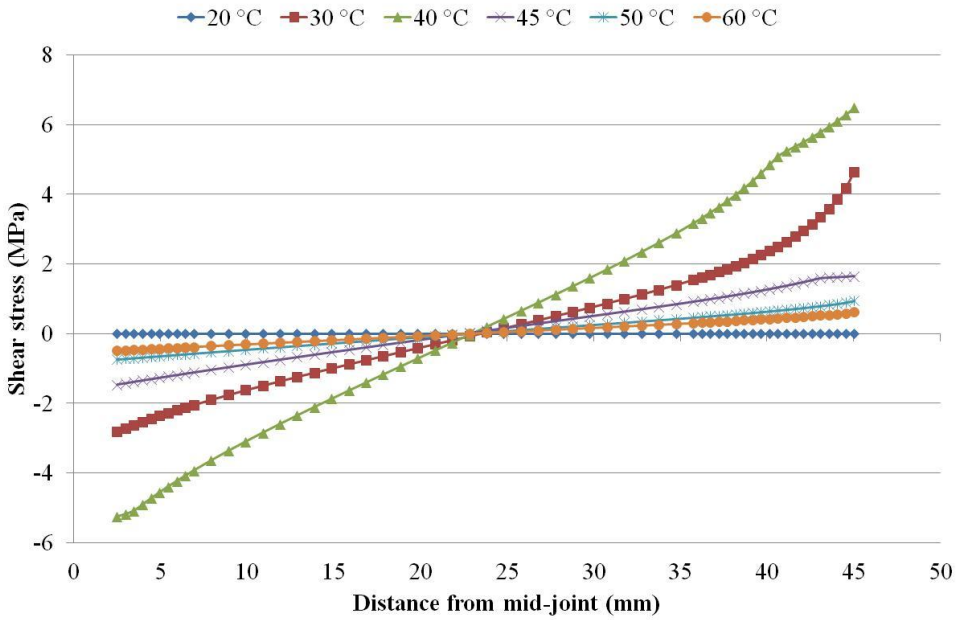

Figure 4.28: Thermal stresses in the adhesive layer at different temperatures (without load)

The behaviours of the double-lap joint under both mechanical and thermal loads were also considered in the FE analysis. At each temperature, different load levels were applied until the joint reached the shear plasticity at the discontinuity. The distributions of the shear and the normal stresses along the adhesive bondline at selected load levels at different temperatures are shown in Figure 4.29 and Figure 4.30, respectively. The figures show a reduction in the adhesive maximum shear and normal strengths with temperature increases, hence the joint strength decreases at elevated temperatures. The maximum values of the adhesive shear and normal strengths at different temperatures obtained from FE-model (Figure 4.29 and Figure 4.30) are summarised in Table 4.4 . These values will be used in the analytical equations (Eqs. 5.24 and 5.37 given in Chapter 5) for calculating the interfacial stresses developed in the adhesive layer of the CFRP reinforced beams.

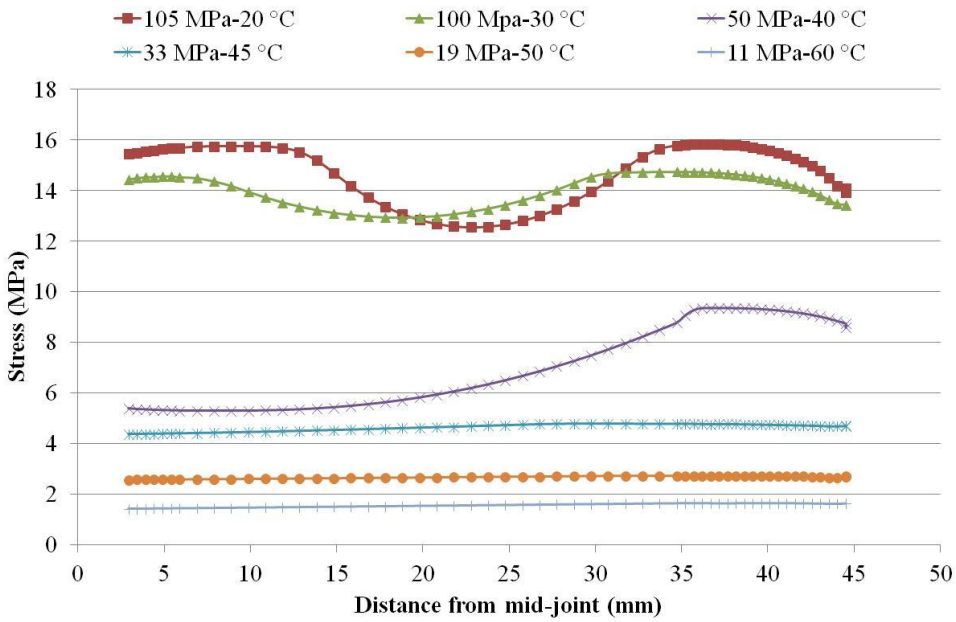

Figure 4.29: Distribution of shear stresses at different load levels and temperatures

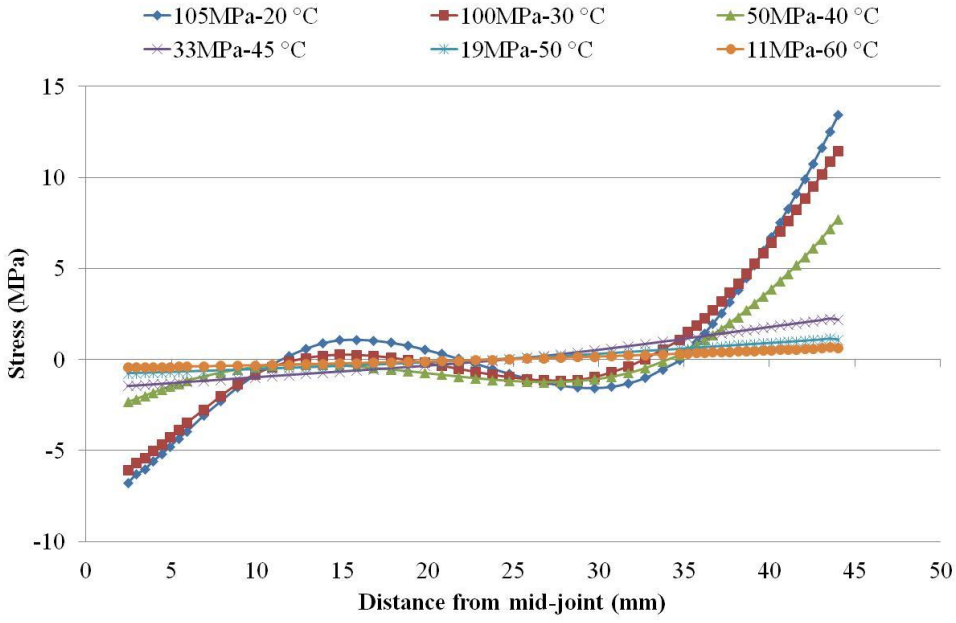

Figure 4.30: Distribution of normal stresses at different load levels and temperatures

Table 4.4: Adhesive maximum shear and normal strengths

Temperature °C	Maximum shear strength ($\tau_{a,platsic}$)/ MPa	Normalised shear strength %	Maximum normal strength ($\sigma_{a,platsic}$)/ MPa	Normalised normal strength %
20	15.8	100	13.4	100
30	14.7	93	11.5	45
40	9.4	59	7.7	57
45	4.8	30	2.3	17
50	2.7	17	1.2	9
60	1.6	10	0.7	5

4.3 Bending test

Three-point bending static tests were carried out on steel beams (127×76UB13, 1200 mm long) reinforced by bonding CFRP plates at different temperatures. Tests were carried out in three phases: First, unstrengthened beam was tested as a control specimen. Second, three specimens reinforced with different CFRP plate lengths, 450, 600, and 700 mm, were tested at room temperature to failure. Third, four beams reinforced with 700 mm CFRP plate lengths were tested at elevated temperatures (35, 42, 45 and 60 ℃) to failure.

Beam specimens were named in the form of SB N-T, where the letter 'S' refers to the static test and the letter 'B' stands for bending test. The number 'N' denotes the length of the CFRP plate in mm. The number 'T' refers to the testing temperatures. e.g., SB 450-20 represents the static bending test on a beam specimen bonded with a 450 mm CFRP plate length at 20 °C.

4.3.1 Specimen preparation

Each hot-rolled steel beam, 127×76UB13, was 1200 mm long with measured average yield strength of 300 MPa and average elastic modulus of 180 GPa, as reported in Table 3.1 in Chapter 3. Transverse stiffeners of 4 mm thick steel plates were welded at the mid-span under the loading point to prevent local buckling of the flange (Figure 4.34). The CFRP plates were cut from CFRP panels fabricated previously (see Appendix B) to the same width as the beam

flange (76 mm) and to various required lengths. The CFRP average tensile strength and average elastic modulus were 1040 MPa and 124 GPa, as given in Table 3.2 in Chapter 3. Sikadur-30 adhesive epoxy was used to bond the CFRP plate to the steel beam. The preparation processes of the strengthened specimens are shown in Figure 4.31 (a to d). The procedure was the same as that for the double-lap shear specimens described in Section 4.2.1. A uniform pressure was applied by G-clamps through a 25×75 mm wooden plate (Figure 4.31c). A minimum of six clamps were used over the length of the CFRP to ensure correct alignment and a uniform adhesive thickness between the CFRP plate and the steel beam. The excess adhesive along the longitudinal sides and the ends of the plates from pressing the adherends together was scraped off (Figure 4.31d). Specimens were cured for at least three days at room temperature before testing.

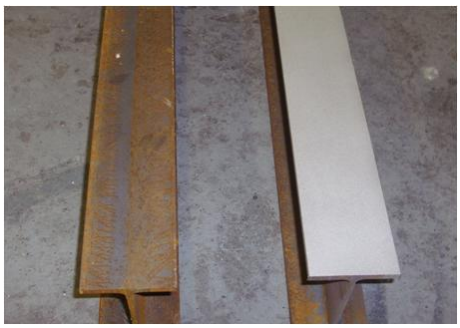

(a)

(b)

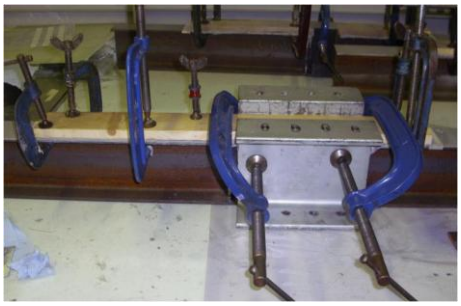

(c)

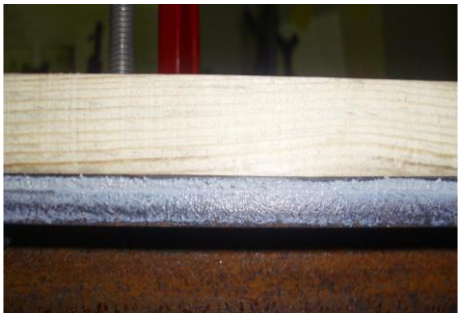

(d)

Figure 4.31: Installation steps of CFRP plate to steel beam: (a) steel beam before and after grit-blasting, (b) adhesive application on both adherends, (c) applying pressure using G-clamps on the CFRP plate, and (d) scraping off the excess adhesive from all edges.

4.3.2 Thermal chamber

To carry out the tests at elevated temperatures, a thermal chamber was constructed to house the test specimen. Phenolic foam insulation boards and slotted steel angles were used in the fabrication. Figure 4.32 shows a photograph of the specimen inside the thermal chamber, and a schematic of the heating system is shown in Figure 4.33. A fan-heater system was used to provide hot air to heat the specimen. The hot air was circulated from one end of the chamber to the other end using an isolated tube. The air temperature was monitored by a temperature controller installed inside the chamber (Figure 4.33). In addition, two type K thermocouples were mounted on the bottom flange to ensure a uniform temperature distribution along the beam length.

Figure 4.32: Specimen setup inside thermal chamber

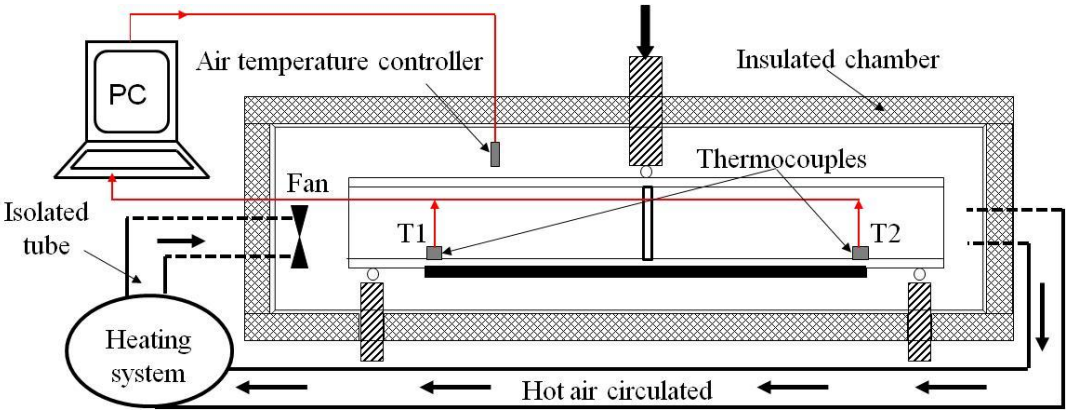

Figure 4.33: Schematic of heating system setup

4.3.3 Instrumentation and testing

A beam strengthened with a 700 mm CFRP plate length was bonded with seven 2 mm long strain gauges along the centre line of the CFRP plate to measure the strain distribution on the outer surface of the CFRP plate, as shown in Figure 4.34. In addition, three 5 mm long strain gauges were mounted to the middle of the steel beam, two on the internal face of the top and the bottom flanges and one at the centre of the beam web (Figure 4.35). Also a linear potentiometer was used to measure the beam deflection at mid-span, as shown in Figure 4.34. The load, the deflection, the strains and the temperatures were automatically recorded every 0.1 second by a data logging system.

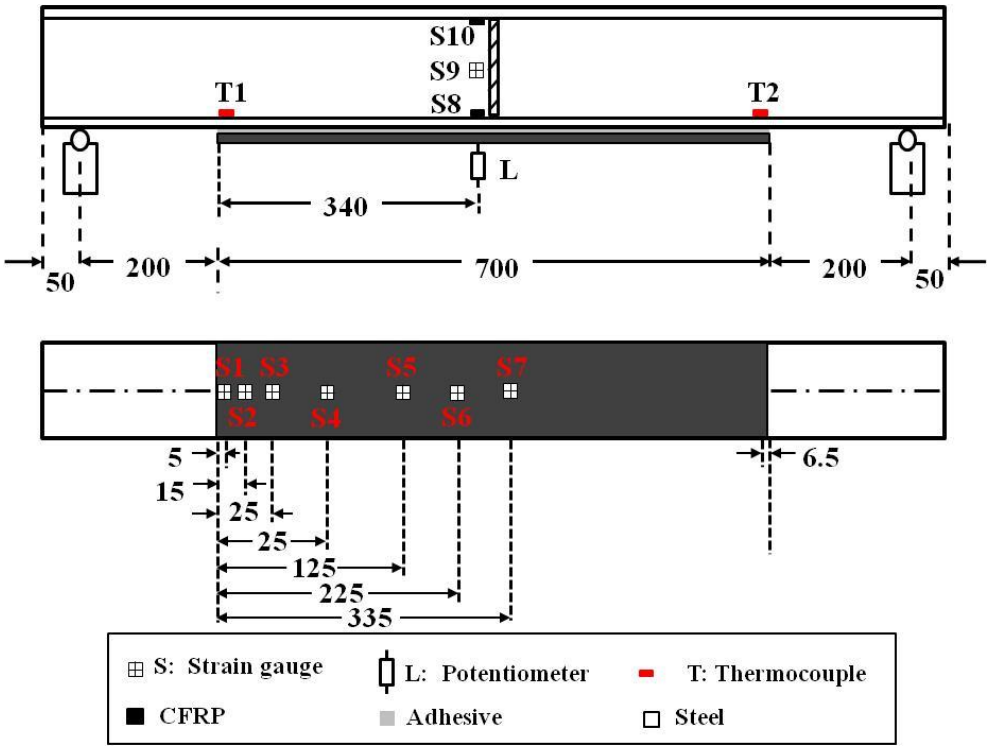

Figure 4.34: Numbering and location of strain gauges, thermocouples and potentiometer

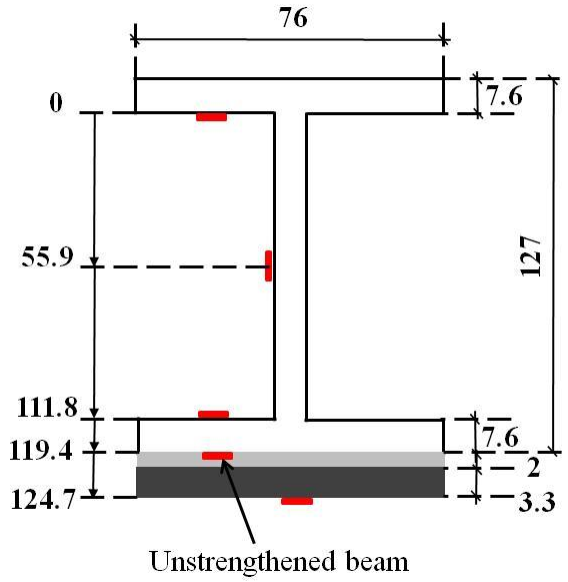

Figure 4.35: Location of strain gauges at mid-span measured from the bottom face of top flange

Tests were carried out using a servo-hydraulic machine with a maximum capacity of 500 kN under displacement control with a stroke rate of 0.05 mm/sec. A schematic of the test setup is shown in Figure 4.36. The load was applied to the middle of the beam through a steel roller placed on the top flange. The beam was supported on two rollers placed 1100 mm apart (Figure 4.36), which allowed the beams to behave in a simply supported manner. Lateral bracing was provided near to the supports to prevent the beam from falling to the sides.

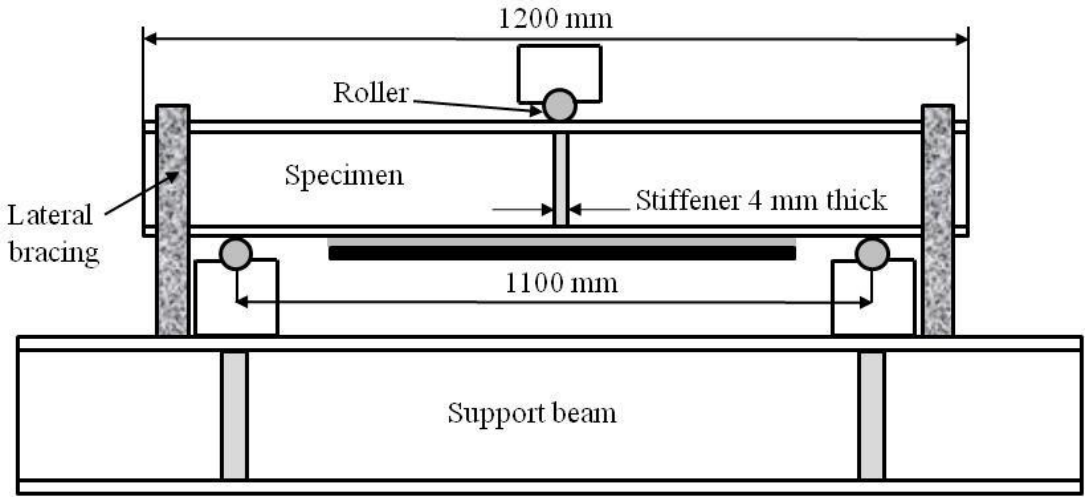

Figure 4.36: A Schematic of three-point bending test setup

Each specimen was heated up to the desire temperature and held for 45 minutes to reach a uniform temperature distribution along the beam. The thermal soaking time of 45 minutes was determined by measuring a dummy beam specimen. The beam was heated up to 45 °C and held at this temperature while the strains along the CFRP plate and mid-span were recorded, as shown in Figure 4.37. The figure indicates that strains at different locations had reached a plateau after 20 minutes. However, the difference in temperature measured at the plate ends by the thermocouples (Figure 4.34) was 0.5 °C after 45 minutes.

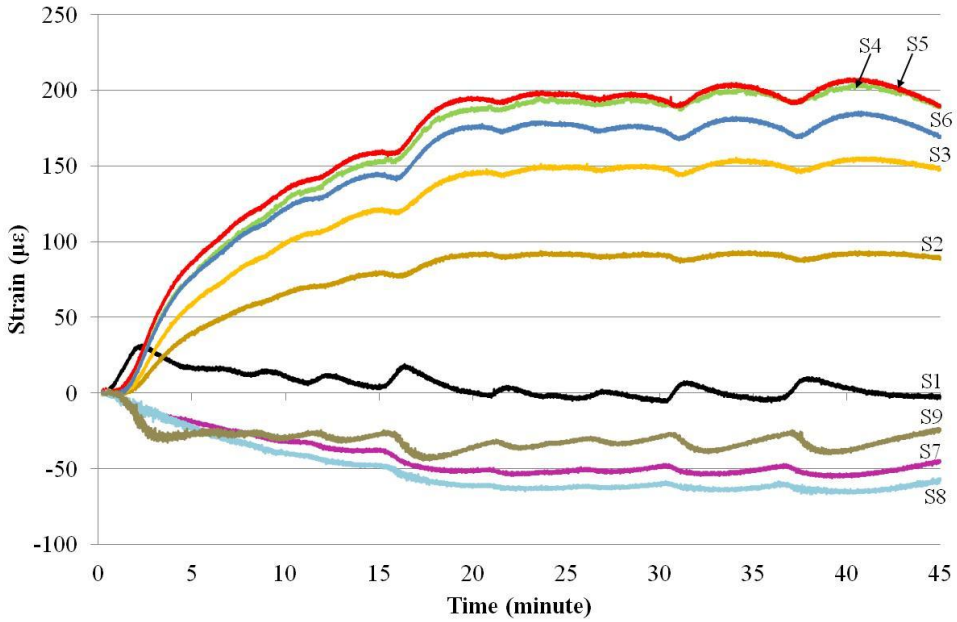

Figure 4.37: Thermal strain for SB 700-45 specimen during heating process

4.3.4 Test results and discussion

The test results are summarised in Table 4.5 including: the failure loads, the normalised failure load (the percentage between the failure load for the strengthened beam to the unstrengthened beam), the increase in the failure load due to strengthening, the maximum mid-span deflection when the CFRP debonded and the modes of failure.

Table 4.5: Three-point bending test results

Specimen	CFRP plate length mm	Failure load kN	Normalised failure load %	Increase in failure load %	Max. mid-span deflection mm	Failure mode
SB 000-20	Unstrengthened	130.48	100	0	41.74	d
SB 450-20	450	135.40	104	4	10.64	$a^{(S/A) > (C/A)}$
SB 600-20	600	174.80	134	34	26.31	$a^{(S/A) \ll (C/A)}$
SB 700-20	700	176.00	135	35	27	$a^{(C/A)}$
SB 700-35	700	163.19	125	25	22.65	$a^{(C/A)}$
SB 700-42	700	152.23	117	17	26.33	$a^{(S/A) > (C/A)}$
SB 700-45	700	150.62	115	15	21.66	$a^{(S/A) \gg (C/A)}$
SB 700-60	700	131.01	100	0	6.00	$a^{(S/A)}$

(d) steel beam top flange yielding, (a) debonding at the plate end, (S/A) steel/adhesive interface and, (C/A) CFRP/adhesive interface

4.3.4.1 Failure loads

Test results show that the flexural capacity of the strengthened beams increased (by 4, 34 and 35%) with increasing the CFRP plate lengths (450, 600 and 700 mm). This is because the ends of the longer plate located in low bending moment regions compared to the shorter plate hence the interfacial stresses at these ends were smaller. Thus, 700 mm CFRP plate length was chosen for strengthening beams that tested at elevated temperature. Figure 4.38 shows the relationships between the load and the mid-span deflection for beams strengthened with different CFRP plate lengths at 20 °C. The figure shows that failure load increased with the plate length. Also the reinforced beams yielded at a higher flexural load compared to unstrengthened beam.

Although the capacity of the beam was increased by 35% at 20 °C, the capacity of the reinforced beam decreased again with temperature increases (Table 4.5). About 50% of the increased capacity decreased around the T_g . The beam lost totally the benefit of CFRP plate reinforcement at 60 °C and the load-deflection curve became similar to that of the unstrengthened beam. Figure 4.39 shows the relationship between the loads and the mid-span deflections for beams reinforced with 700 mm CFRP plate length at different temperatures.

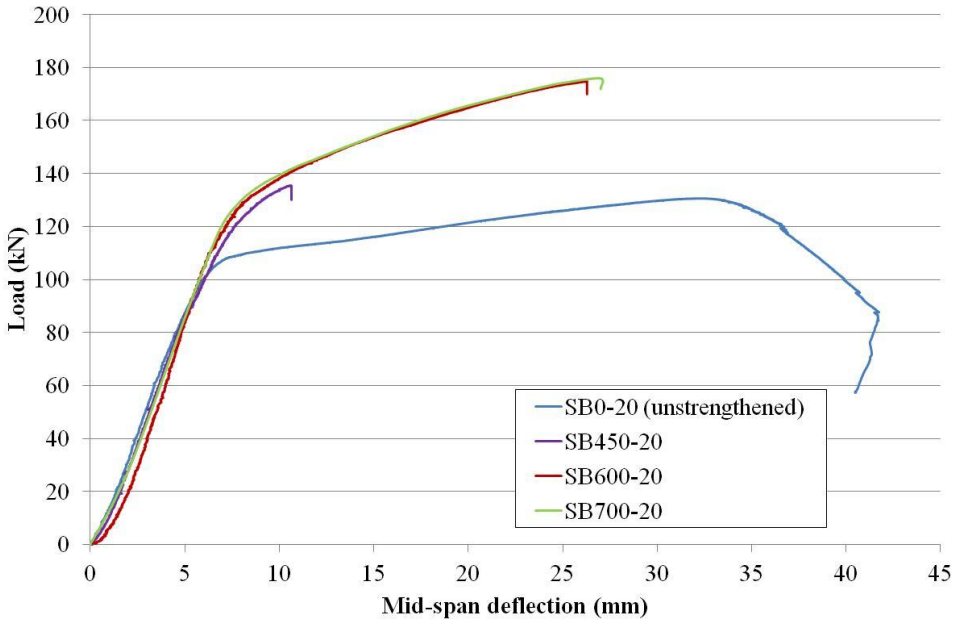

Figure 4.38: Comparison of the load versus the mid-span deflection for reinforced beam with different CFRP plate lengths tested at 20 °C

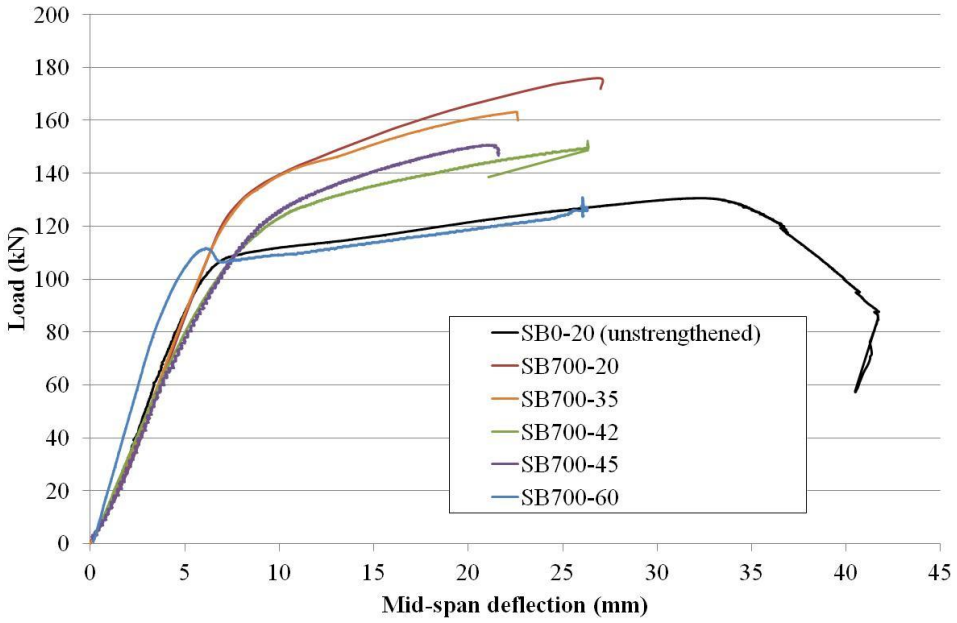

Figure 4.39: Comparison of load vs. mid-span deflection for beams reinforced with 700 mm CFRP plate at different temperatures

The relationship between the percentage of the flexural load of beams strengthened with 700 mm CFRP plates at any temperature to that at 20 ° ($P_{(T)} / P_{(20\ ^oC)}$) and the temperature is presented in Figure 4.40. The figure indicates that beam flexural capacity decreased with temperature increases. Linear regression analysis was used to produce the following best-fit line:

$$P_{(T)} / P_{(20\ ^oC)} = 113.87 - 0.6442 \times T \quad , \quad (R^2 = 0.9885) \tag{4.3}$$

where $P_{(T)}$ are the failure loads any temperatures (T)

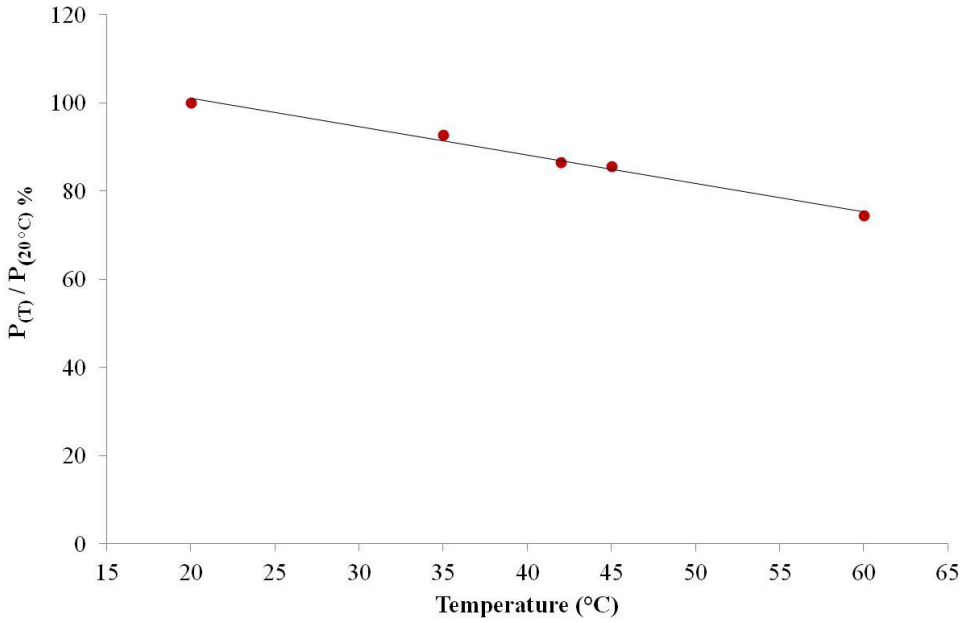

Figure 4.40: The relationship between the percentage of failure load for reinforced beam and the temperature

4.3.4.2 Beam stiffness

There was no increase in the stiffness of the reinforced beam because the elastic modulus of the CFRP was lower than that of the steel. Thus, the initial load verses mid-span deflection curves for all the reinforced beams were similar to that of unstrengthened beam, except for SS 700-60. However, the yield loads for the reinforced beams were increased compared with the

unstrengthened beam due to the contribution of the CFRP plate in carrying part of the applied load on the beam.

4.3.4.3 Failure modes

The possible failure modes of CFRP strengthened steel beams subjected to a flexural load [27, 131] include : (a) debonding at the plate end between steel/adhesive interfaces (S/A) and/or between CFRP/adhesive interfaces (C/A); (b) rupture of CFRP at mid-span; (c) delamination of CFRP plate; (d) local buckling of strengthened beam. The type of failure depends on the mechanical properties (CFRP and adhesive strength and stiffness), the geometrical properties (CFRP and adhesive thickness, plate length and plate end preparation), and the temperature. Two failure modes observed from the tested beams were types (a) and (d), as summarised in Table 4.5.

The failure mode of the unstrengthened beam was type (d), where the top flange yielded due to high compression applied load, as shown in Figure 4.41. Failure type (a) occurred in all the reinforced specimens. However, failure varied from S/A to C/A depending on the CFRP plate length and temperature. The failure modes for the beams strengthened with different lengths of CFRP plate at 20 °C are shown in Figure 4.42. The figure indicates a change in failure mode from both S/A and C/A to C/A only due to increase the CFRP plate length from for 450 to 700 mm. The effect of temperature on the failure modes of the beams strengthened with 700 mm CFRP plates is shown in Figure 4.43. The mode of failure transferred from C/A to S/A when temperatures increased from 20 °C to 60 °C. The change in the failure mode is due to softening of the adhesive. At the highest temperature of 60 °C, the adhesive degraded leaving a thin layer of adhesive on the steel beam, as shown in Figure 4.44. This type of failure was also indicated in the pull-off test illustrated previously in section 3.4.3 in Chapter 3.

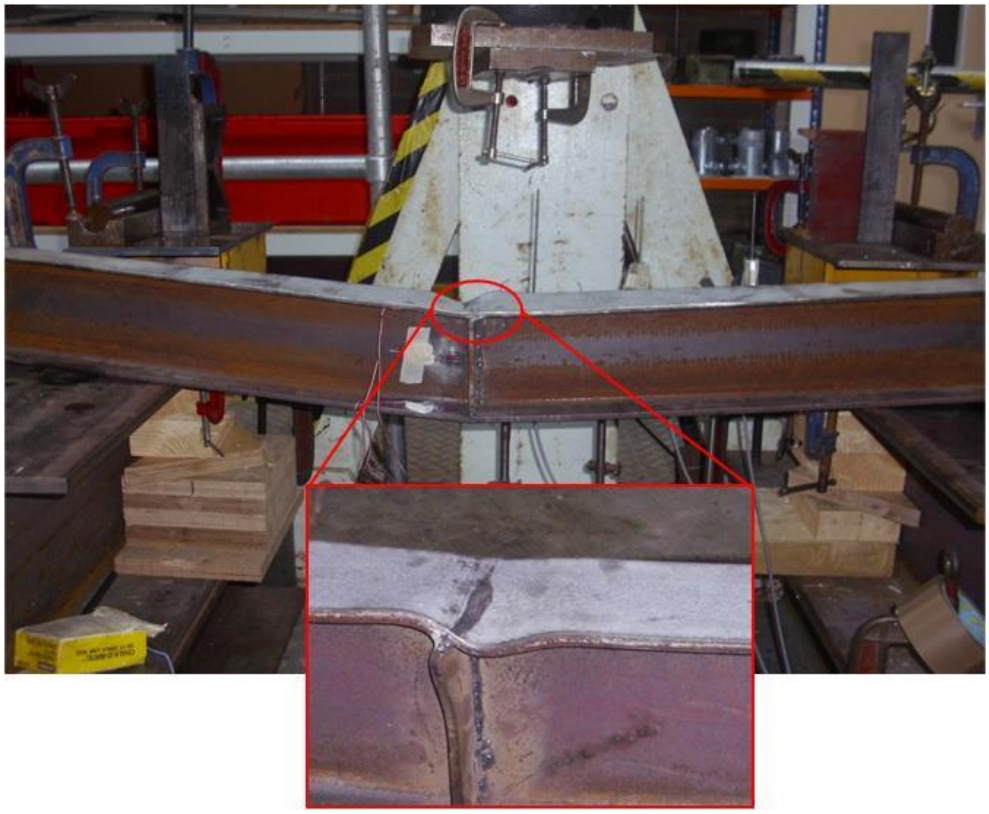

Figure 4.41: Top flange yielded for the unstrengthened beam (SB 000-20)

Figure 4.42: Failure mode of strengthened beams with different lengths of CFRP plate at 20 °C

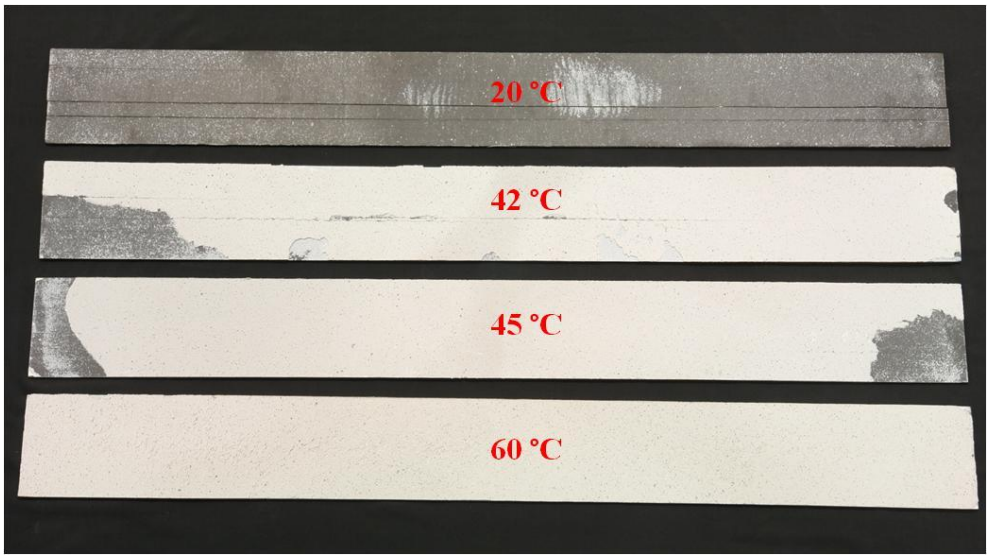

Figure 4.43: Failure mode of strengthened beams with 700 mm CFRP plate at various temperatures

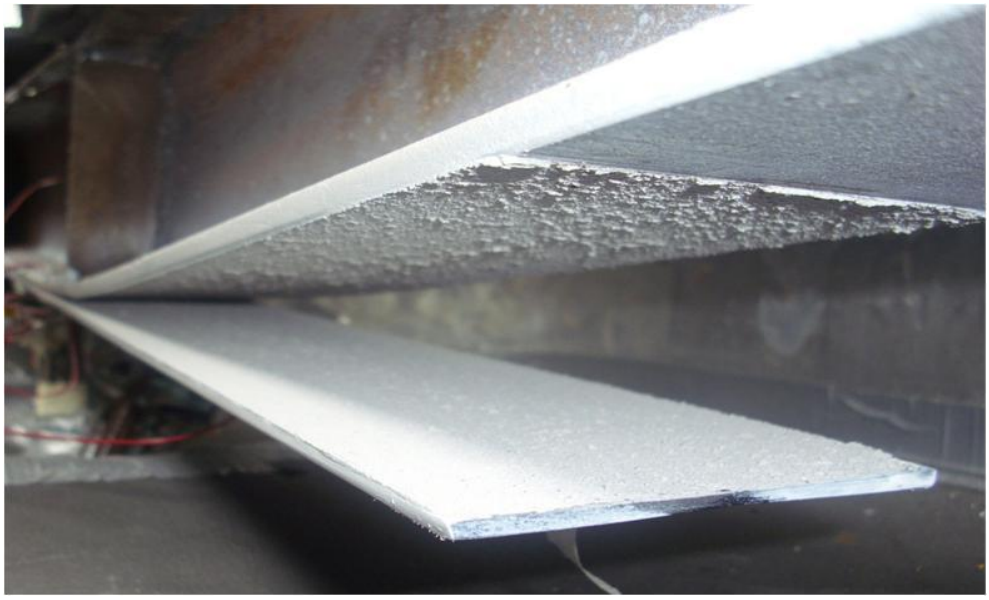

Figure 4.44: Adhesive epoxy degraded at 60 °C leaving a thin layer on the steel beam

4.3.4.4 Strain distribution

The relationship between the load and strains at mid-span for the unstrengthened beam (SB 000-20) is shown in Figure 4.45. The figure indicates that the steel has first yielded (steel yielding strain is 1812 $\mu\varepsilon$, Table 3.1 in Chapter 3) at the inner face of the top flange (S4) at about 76 kN due to the high compression load. Then, the outer face of the bottom flange (S1) yielded at about 89 kN followed directly by the yielding of the inner face of the bottom flange (S2) at 105 kN. Finally, the web yielded at 116 kN at which the entire mid-span beam yielded (Figure 4.38).

The entire mid-span for the strengthened beams with 450, 600 and 700 mm CFRP plates yielded at about of 123.5, 131, 136.5 kN, respectively, as shown in Figures 4.45 to 4.47. The figures indicate that beams strengthened with the shorter plates (SB 450-20 and SB 600-20) reached yielding at the top flange at a relatively very low load level of 70 and 78 kN, respectively. Then, yielding propagated through the web toward the bottom flange (at 123.5 and 131 kN). However, the beam strengthened with 700 mm CFRP plate (SB 700-20) yielded at the entire mid-span at about the same flexural load level (136.5 kN). This indicates that a longer plate carried more load than a shorter plate before debonding as the plate terminated in a lower bending moment region.

The strains distributions along the centre of the CFRP plate for SB 700-20 specimens at different load levels are shown in Figure 4.49. The figure shows that the strains along the plate increased gradually with the load until the beam started to yield at 136.5 kN, then the strain near mid-span (S5-S7) increased rapidly with the load. This is because the elastic modulus of the CFRP plate is lower than that of the steel which means that the plate starts to contribute to carrying more loads after the steel beam has yielded. The strains measured across the mid-span (S7-S10) for the SB 700-20 specimen at different load levels are shown in Figure 4.50. The figure shows that the strains distributions became nonlinear after the steel had yielded. The distributions of strains along the CFRP plate and at mid-span at different load levels and temperatures for the other reinforced specimens can be found in Appendix E.

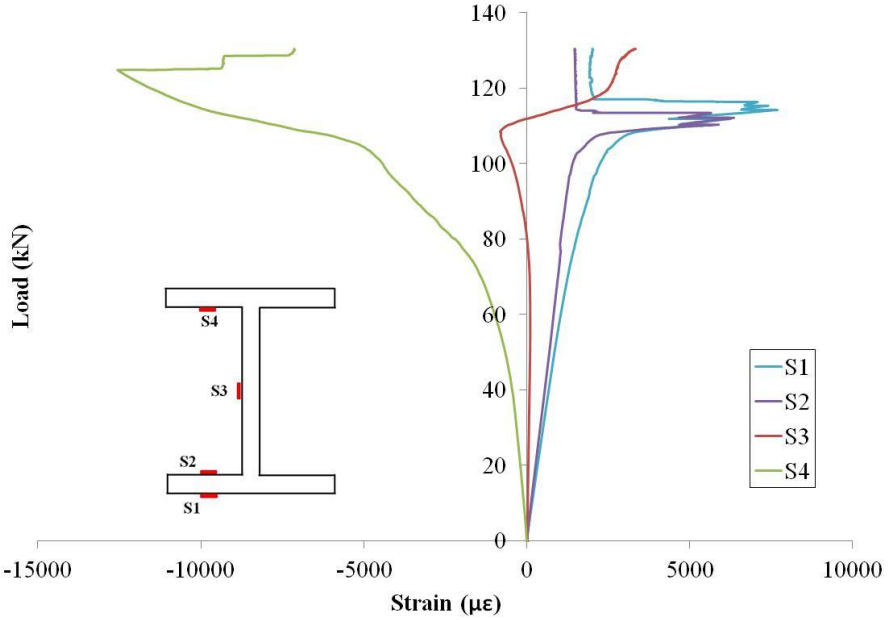

Figure 4.45: Strain verses load plots at mid-span for unstrengthened beam (SB 000-20)

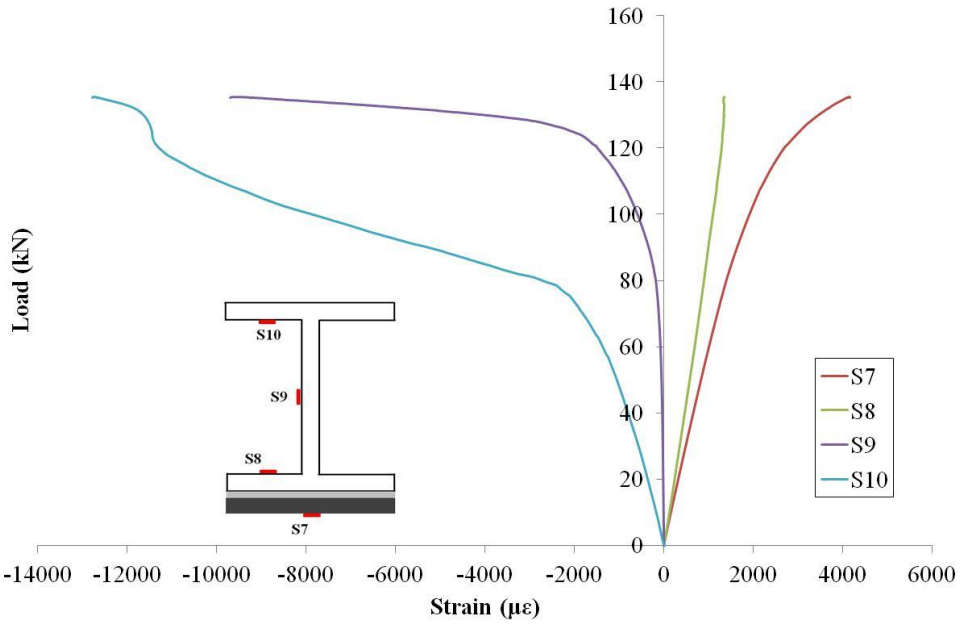

Figure 4.46: Strain verses load plots at mid-span for strengthened beam (SB 450-20)

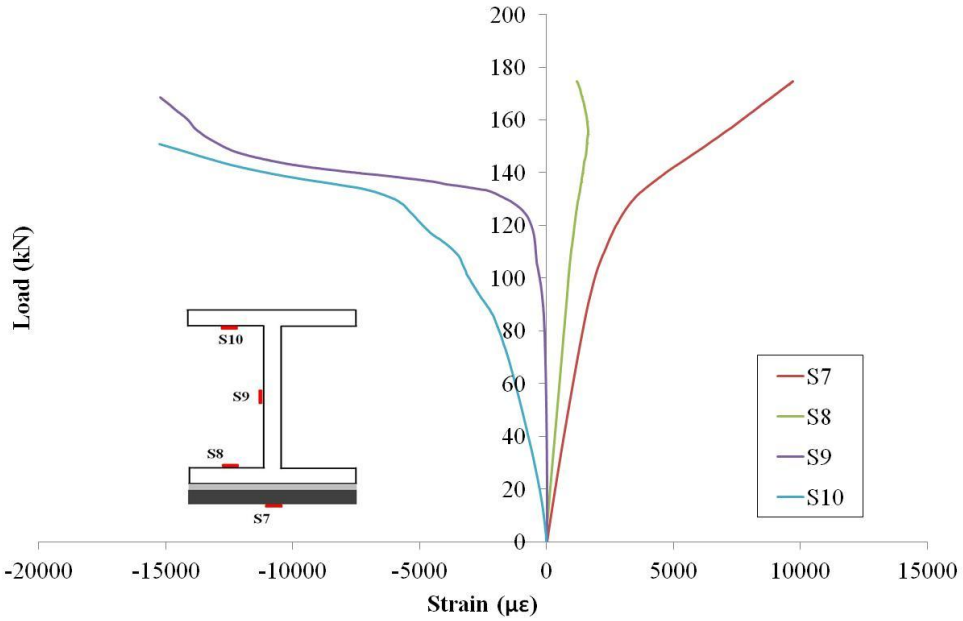

Figure 4.47: Strain verses load plots at mid-span for strengthened beam (SB 600-20)

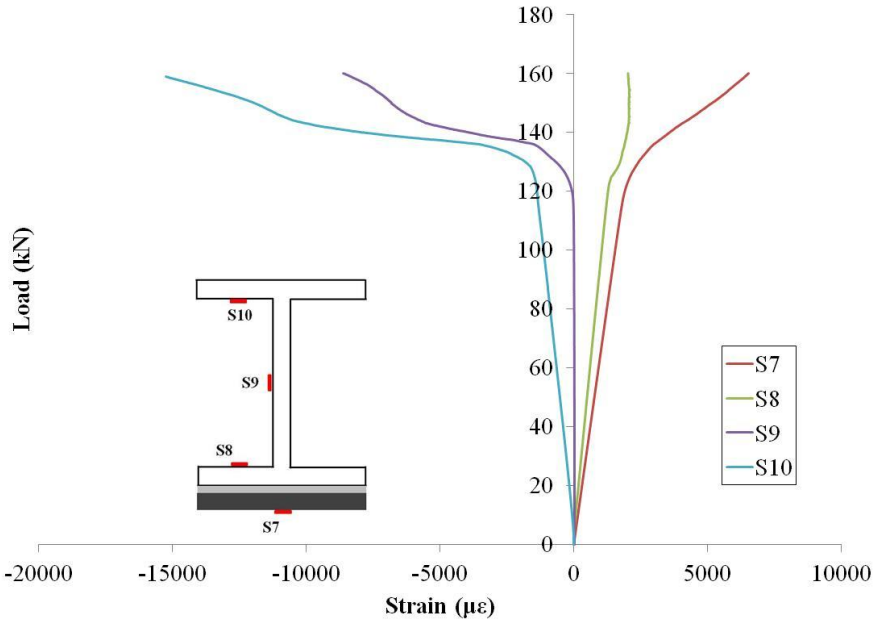

Figure 4.48: Strain verses load plots at mid-span for strengthened beam (SB 700-20)

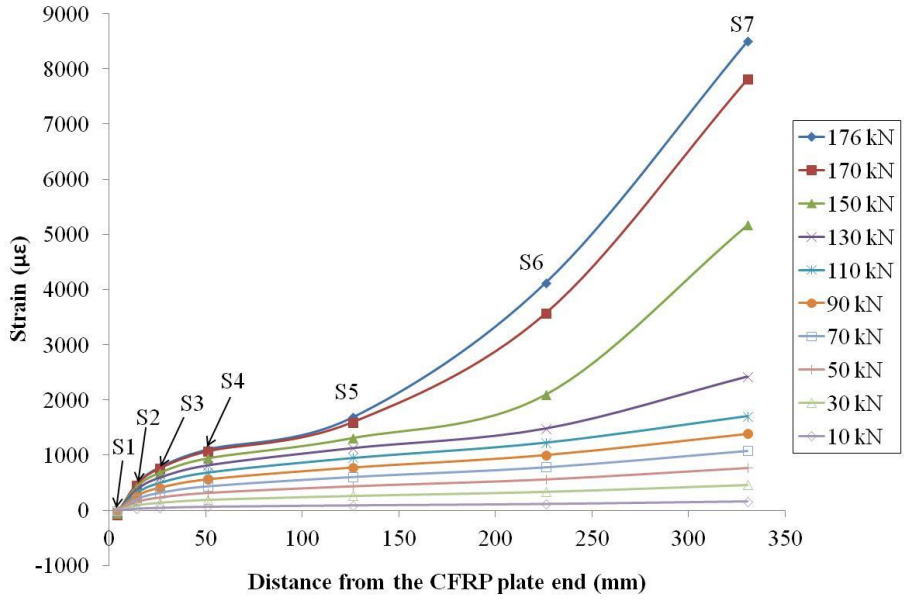

Figure 4.49: Strain distribution along CFRP plate at different load levels for SB 700-20 specimen

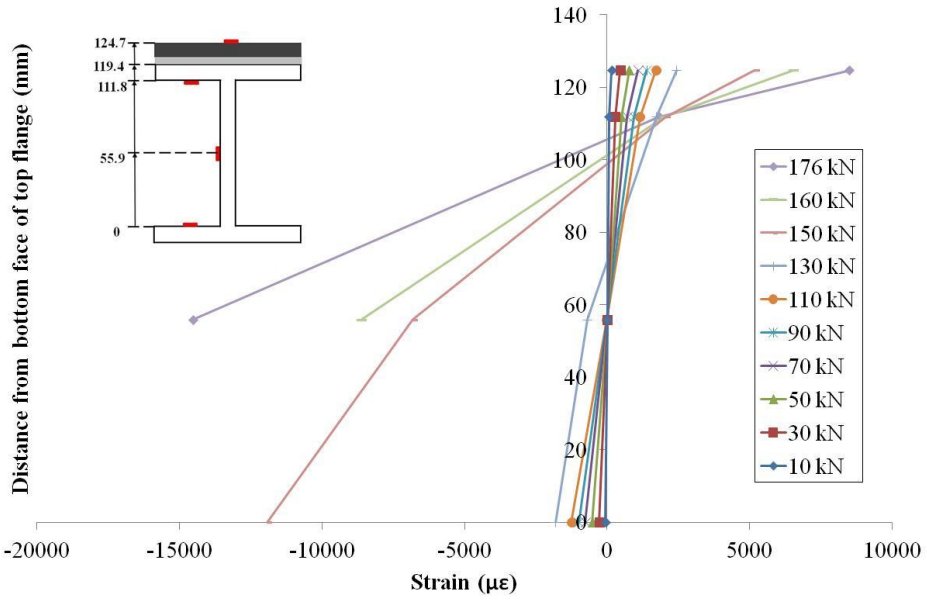

Figure 4.50: Strain distribution across mid-span of SB 700-20 specimen at different load levels

Comparison of the strain distribution across the mid-span for beams strengthened with different CFRP plate lengths with the unstrengthened beam subjected to 110 kN is shown in Figure 4.51. The unstrengthened beam was yielded across the entire mid-span, except at the web. The strains were reduced at the bottom flange but not at the top flange after bonding 450 and 600 mm CFRP plates. However, the beam reinforced with 700 mm CFRP plate kept the strain across the entire mid-span less than that yielding limitation. Thus, the beam was yielded at a higher flexural load before the CFRP plate was debonded.

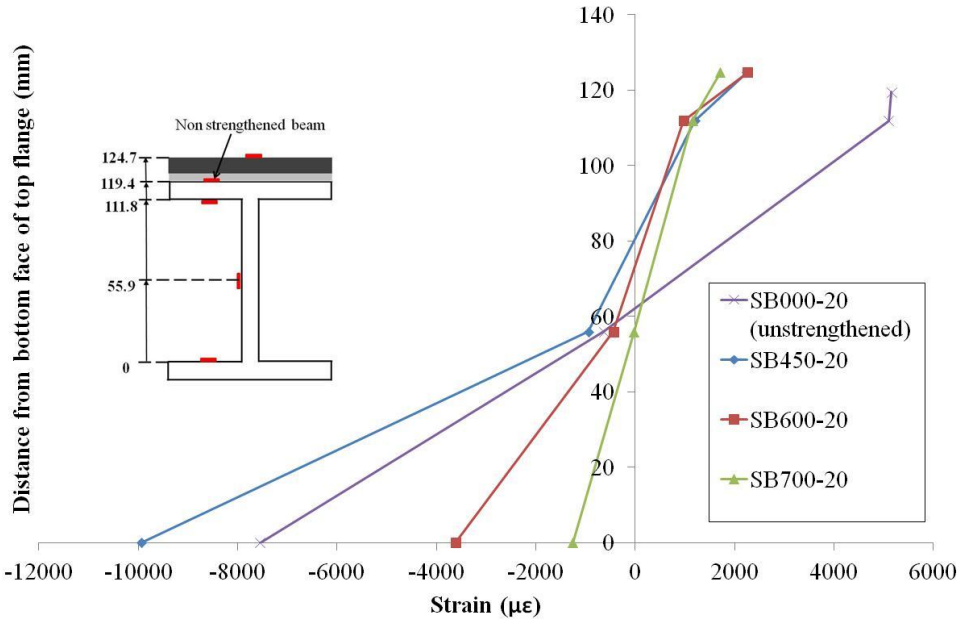

Figure 4.51: Strains across mid-span for strengthened beam loaded under 110 kN at 20 °C

Effects of temperature on the strains distributions at mid-span for beams strengthened with 700 mm CFRP plates at 42 and 45 °C are shown in Figure 4.52 and Figure 4.53, respectively. The beams were firstly yielded at the top flange then the yielding continued through the web toward the bottom flange, which was similar to the behaviour of a beam reinforced with a shorter plate. Comparison of the strain distribution across the mid-span for the strengthened beams subjected to 110kN at different temperatures with a SB 450-20 specimen is shown in Figure 4.54. The figure shows that the strains across mid-span for SB 700-20 were under the yielding limitation, but the strains were increased significantly, especially at the top flange, when the temperature was increased to around T_g. Thus, the strains distributions at the web and the bottom flange for SB 700-42 and SB 700-45 specimens were similar to those of SB 450-20. This was due to adhesive softening and weakening at elevated temperatures hence the load transferred from the

beam to the plate was reduced causing mid-span to yield in the same manner as the shorter plate.

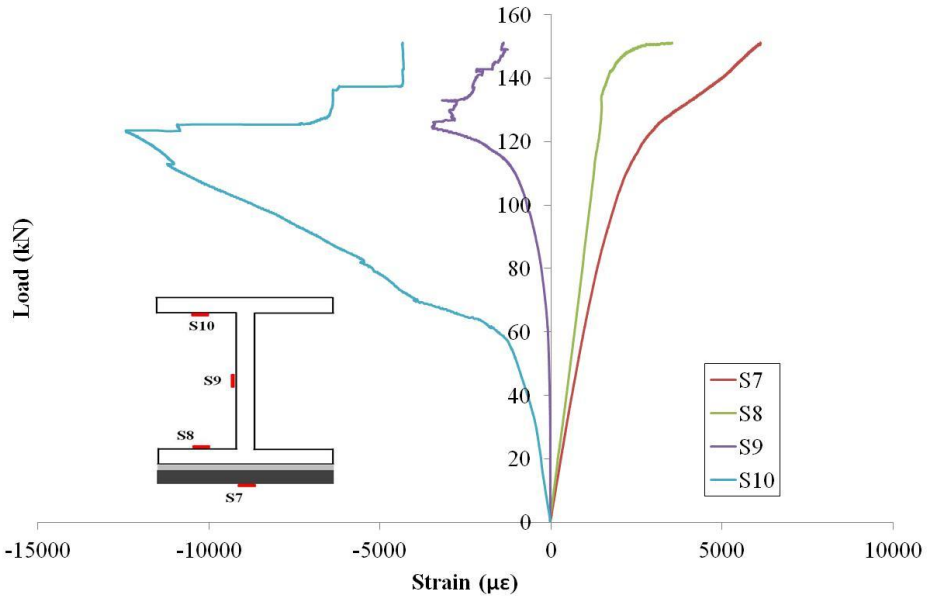

Figure 4.52: Strain verses load plots at mid-span for strengthened beam (SB 700-42)

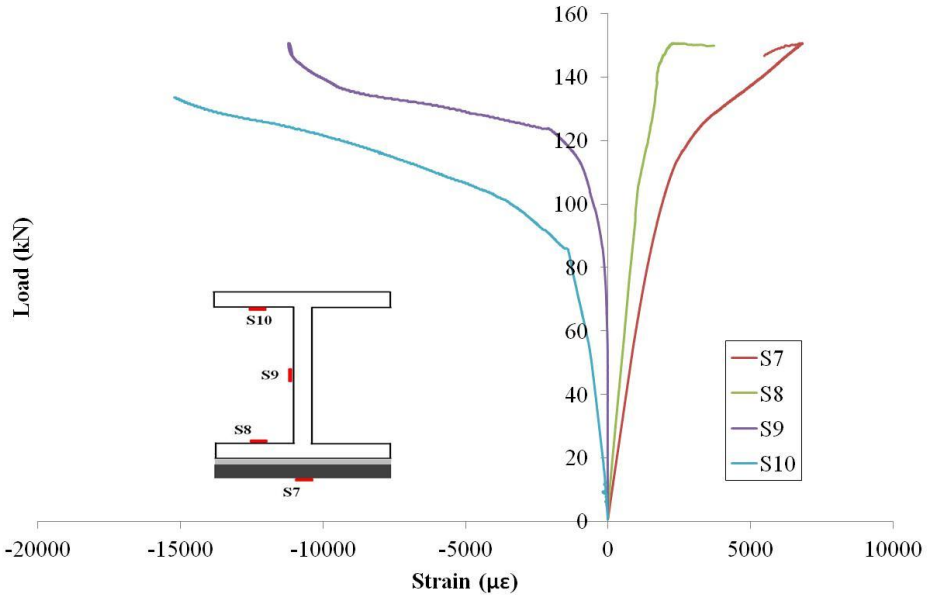

Figure 4.53: Strain verses load plots at mid-span for strengthened beam (SB 700-45)

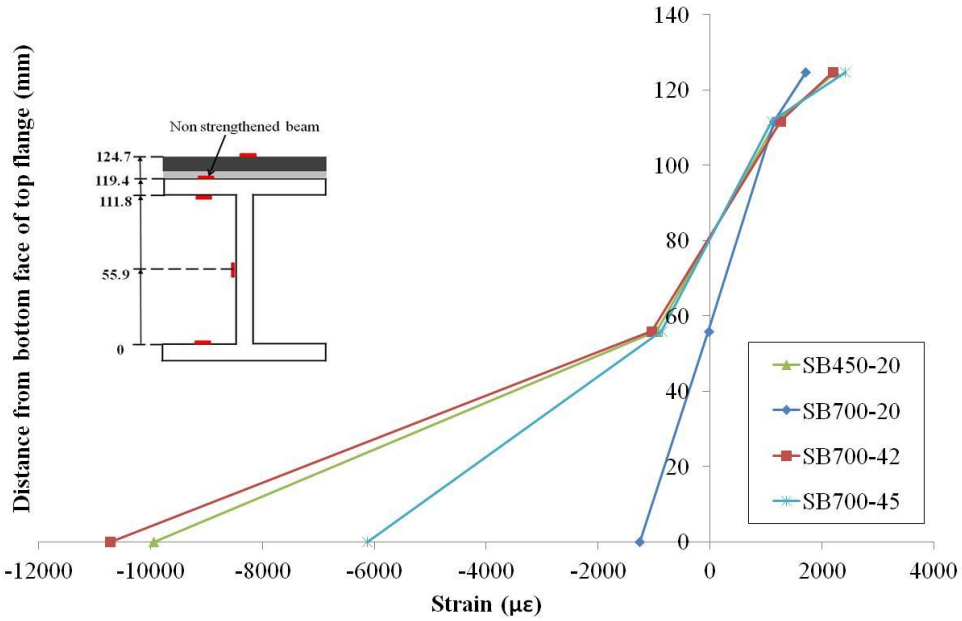

Figure 4.54: Strains across mid-span for strengthened beam loaded under 110 kN at different temperatures

4.4 Conclusion

In this chapter, experimental tests on both double-lap shear specimens and CFRP reinforced beams subjected to a static load were carried out at temperature ranges from 20 to 60 °C. In addition, creep tests on double-lap shear specimens subjected to different load levels were performed at 40 °C. Also FE analyses were conducted on the double-lap shear joints to calculate the adhesive shear and normal strengths at these temperatures range.

Test results showed that the joint capacity of the double-lap shear specimens decreased with temperature increase. The average failure load decreased from 90 to 41 kN when the temperature increased from 24 to 60 °C. In addition, the failure mode was changed from combined failures between steel/adhesive and CFRP/adhesive interfaces at 24 °C to CFRP/adhesive interfaces failure at 60 °C. Creep tests carried out on the double-lap shear specimens loaded at 40 °C showed that the bonded joint failed after one hour at 34% of the average static failure load. However a sudden failure occurred after one minute by doubling the percentage of the applied load. This is because the properties of the adhesive material are time

and temperature dependent (as mentioned in the literature in section 2.10).Therefore, the combined effects of time and temperature on adhesively bonded joints should be taken in consideration in the design.

The strains measured along the CFRP plate of the double-lap joint showed a good agreement with those obtained from the FE model, thus the model was further used to calculate the shear and normal strengths within the adhesive at different temperatures. The shear and the normal stresses obtained from FE model were the highest at the plate end and the mid-joint exceeding the adhesive elastic limitation, thus, plastic zones were developed. The length of the plastic zone increased with the applied load and the temperature.

The flexural capacity of steel beams strengthened with different CFRP plate lengths increased with the length of the plate at 20 °C. This is because a longer plate reduced the moment at the plate ends and thus the stresses at theses ends were reduced. Although the beam capacity increased by 35% after bonding 700 mm CFRP plate, the capacity decreased with temperature increasing due to softening of the adhesive e.g., at 60 °C, the benefit of CFRP plate bonded to the beam disappeared and the failure load of strengthened beam became equal to that of unstrengthened beam. In addition, the failure mode of the strengthened beams was changed from CFRP/adhesive to steel/adhesive as the temperatures increased from 20 °C to 60 °C. The stiffness of retrofitted beams did not increased due to low Young's modulus of the CFRP compared to that of the steel.

The strains measured at mid span indicated that the SB 450-20 specimen first yielded in the top flange at about 70 kN. Then, the yielding propagated through the web toward the bottom flange at 123.5 kN, while the entire mid-span for the SB 700-20 specimen yielded at the flexural load of 136.5 kN. However, the strains distributions across the mid-span for SB 700-42 and SB 700-45 specimens became similar to the strains for SB 700-20. This is due to softened of the adhesive and hence the load transferred from the beam to the CFRP plate reduced.

Chapter 5

Stress analysis of steel beam strengthened with CFRP plate at elevated temperatures.

5.1 Introduction

The applied load on a strengthened beam is transferred from the beam to the CFRP plate by the shear and the normal stresses developed in the adhesive bond. These stresses concentrate at the plate ends [19, 132] and hence premature debonding failure of the plate from the beam may occur before the beam reaches its full bending capacity. To avoid this failure mode, knowledge of the interfacial stresses at the plate ends is necessary.

Several analytical and finite element (FE) solutions were developed to calculate the shear (τ) and the normal (σ) stresses within the adhesive between a beam and a FRP composite. But these solutions assumed linear elasticity and temperature independency of the adhesive. However, tensile test results on adhesive dogbone specimens (reported in Chapter 3) showed significant reduction in adhesive strength and stiffness coupled with nonlinear behaviour at elevated temperatures. Therefore, these solutions are not suitable at elevated temperatures.

This chapter presents analytical and FE models that calculate the shear and the normal, or peel, stresses developed in the adhesive between a steel beam and a CFRP plate due to both thermal and mechanical loads. These solutions take into consideration adhesive properties temperature dependency as well as nonlinearity behaviour along the bonded plate. The nonlinear stress-strain behaviours of the adhesive at elevated temperatures are simplified with an elastic-perfectly-plastic approximation in the analytical model and with a bilinear elastic-plastic representation in the FE model.

5.2 Stress analysis

The shear and the normal stresses within the adhesive layer between a steel beam and a CFRP plate under both thermal and mechanical loads were calculated from both analytical and finite element (FE) models. The adhesive properties at elevated temperatures used in these models were given previously in Tables 3.3 to 3.5 in Chapter 3.

5.2.1 Analytical and FE models at elevated temperatures

The analytical model proposed by Deng et al. [11] (Deng et al. model) is adopted in this research to calculate the shear and normal stresses developed in the adhesive between a CFRP plate and a steel beam, because it considers both mechanical and thermal loads. Although their model calculates thermal stresses due to differential thermal expansion between steel and CFRP materials, it assumes that adhesive material is linear elastic and its mechanical properties are temperature independent. Disregarding the nonlinearity behaviour and temperature dependency would cause the interfacial stresses at the plate ends to increase continuously exceeding the maximum adhesive (strength) strengths, as shown in the sketch in Figure 5.1.

The modification on the Deng et al. model presented in this research approximates the adhesive nonlinear stress-strain curve (actual behaviour) with an elastic-perfectly-plastic representation (analytical model), see Figure 5.1. The interfacial stresses along the bonded plate are obtained from an elastic analysis taking in consideration the change in adhesive shear modulus value with temperature (Table 3.5 in Chapter 3). Then, these stresses were curtailed at the maximum shear and normal strengths that obtained from FE analyses on the double-lap shear specimen (Table 4.4 in Chapter 4). This approximation does not satisfy all the compatibility and equilibrium conditions of the elastic bond stress distribution, thus the stresses obtained from the analytical model were different from that obtained from the FE analysis. Thus, the shear stress obtained from the analytical model increases until reaching a maximum adhesive shear strength ($\tau_a = \tau_{a,plastic}$) at distance ($x = Q$, defined as the length of the plastic zone) from the plate end.

In addition, FE model was employed, using ABAQUS software [126], to calculate the interfacial stresses in the CFRP bonded beam. The model approximates the adhesive nonlinear curve with bilinear elastic-plastic representation (Figure 5.1). Details of fitting the bilinear elastic-plastic model with the nonlinear curve were discussed previously in section 3.4.2 in Chapter 3. The shear stress in the adhesive along the bonded plate obtained from the FE model was larger than those calculated by the analytical model hence developed slightly longer plastic zone. This is because the analytical model assumed linear elasticity of the adhesive along the entire bonded plate thus the shear stress concentrated near the plate ends. Nevertheless, the difference in the plastic zone obtained from the analytical and the FE models was insignificant. The difference depends on the applied load and the temperature.

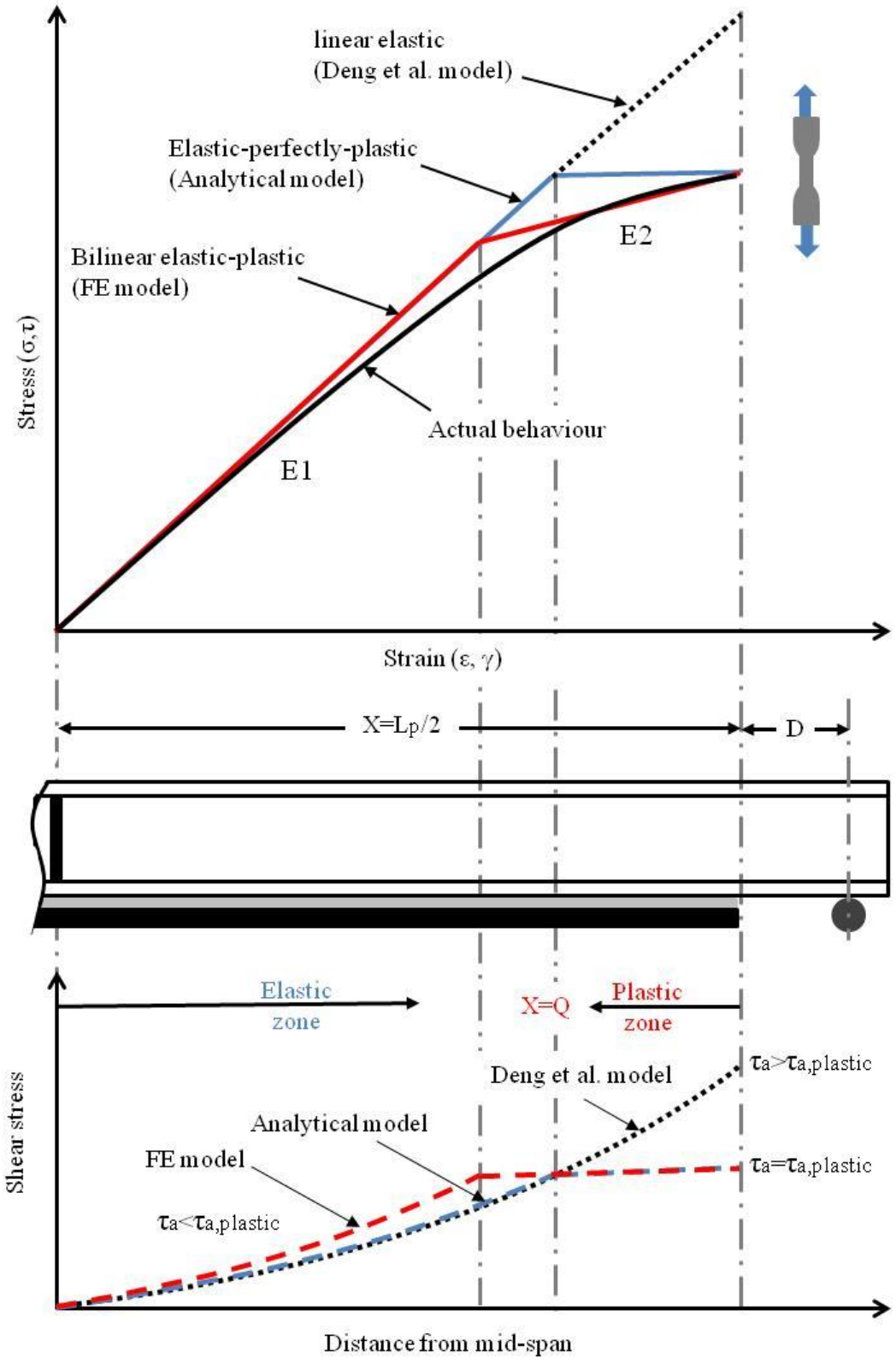

Figure 5.1: Representative sketch of adhesive stress-strain behaviour and shear stress distribution at elevated temperatures

The derivation of the equations for the shear and the normal stresses proposed by Deng et al. [11] are given in sections 5.2.1.1 and 5.2.1.2. The modifications suggested by the researcher are presented in Eqs (5.24 and 5.37).Figure 5.2 shows the parameters used in the derivative. The steel, the adhesive and the CFRP plate are denoted by s, a and p respectively; where M, V and N are the bending moment, the shear force and the axial force; and t is the thickness of the strengthening components; L_s and L_p are the beam span and the plate length, respectively. The τ and σ are the shear and the normal stresses in the adhesive layer, respectively. These equations apply to a steel beam reinforced with a CFRP plate without taper.

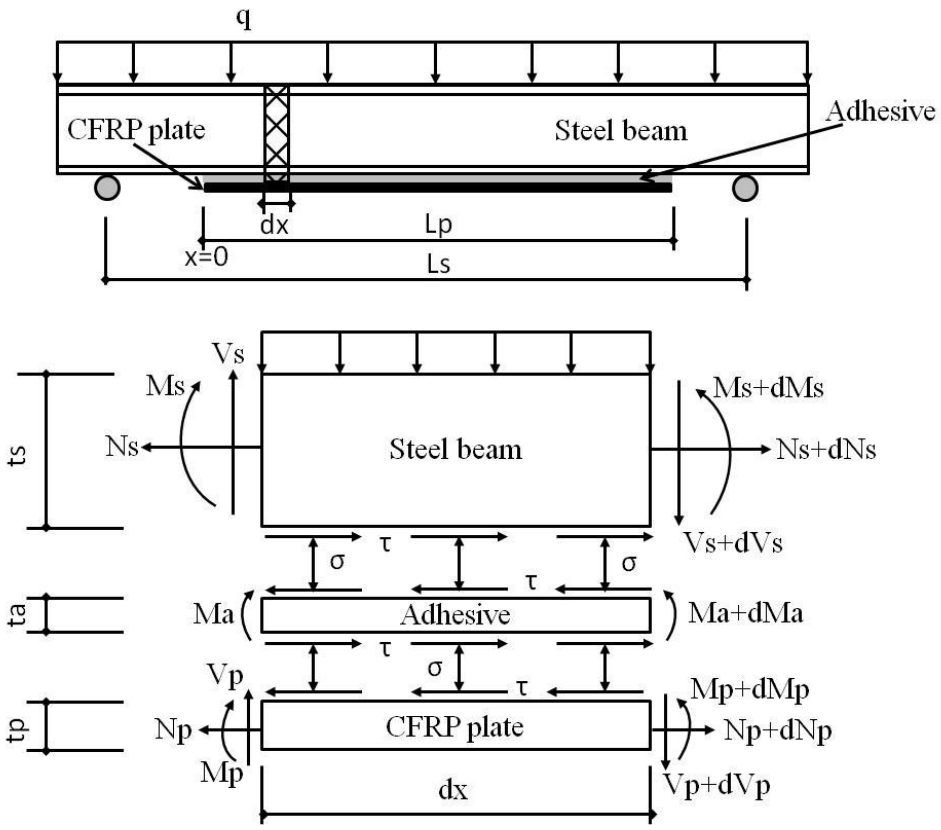

Figure 5.2: Geometry and definition of the strengthened beam and a segmental element of length dx

5.2.1.1 Shear stresses

Referring to Figure 5.2, equilibrium of the CFRP plate element, of length dx and width b, in the horizontal x-direction is

$$(N_p + dN_p) - N_p - \tau b dx = 0 \tag{5.1}$$

which gives the shear stress

$$\tau = \frac{1}{b}\frac{dN_p}{dx} \tag{5.2}$$

The equilibrium of the CFRP plate element in the vertical y-direction is

$$(V_p + dV_p) + \sigma b dx - V_p = 0 \tag{5.3}$$

which gives the normal stress

$$\sigma = \frac{-1}{b}\frac{dV_p}{dx} \tag{5.4}$$

In the same way, the equilibrium of the steel beam element in the x and y directions can be expressed, respectively, as:

$$\tau = \frac{-1}{b}\frac{dN_s}{dx} \tag{5.5}$$

and

$$\sigma = \frac{1}{b}\left(\frac{dV_s}{dx} + q\right) \tag{5.6}$$

For the combined cross-section, the force equilibrium in the horizontal direction and the moment equilibrium give, respectively:

$$N_s = -N_p \tag{5.7}$$

and

$$M(x) = M_s + M_p + M_a - N_s(\frac{t_s}{2} + t_a + \frac{t_p}{2}) \tag{5.8}$$

where $M(x)$ is the applied bending moment.

$$M_a = -\int_0^x \tau(t) t_a dt = t_a N_s \tag{5.9}$$

The bending of the CFRP plate is assumed to be zero, i.e. $M_p = 0$, in the shear stress calculation, thus Eq. (5.8) substituted with Eq. (5.9) gives

$$M_s = N_s(\frac{t_s + t_p}{2}) + M(x) \tag{5.10}$$

Assuming the adhesive deformed linearly, the shear strain γ can be written as

$$\gamma = \frac{du(x,y)}{dy} + \frac{dv(x,y)}{dx} \tag{5.11}$$

where $u(x,y)$ and $v(x,y)$ are the longitudinal and the transverse displacements at any point in the adhesive layer, respectively. Thus the adhesive shear stress is given as

$$\tau = -G_a\left[\frac{du(x,y)}{dy} + \frac{dv(x,y)}{dx}\right] \tag{5.12}$$

Differentiating Eq. (5.12) with respect to x gives

$$\frac{d\tau}{dx} = -G_a\left[\frac{d^2u(x,y)}{dydx} + \frac{d^2v(x,y)}{dx^2}\right] \tag{5.13}$$

The shear stress is assumed to be constant through the thickness of the adhesive, and $u(x,y)$ in the adhesive varies linearly

$$\frac{du}{dy} = \frac{1}{t_a}(u_s - u_p) \tag{5.14}$$

Differentiating Eq. (5.14) with respect to x gives

$$\frac{d^2u}{dydx} = \frac{1}{t_a}(\frac{du_s}{dx} - \frac{du_p}{dx}) \tag{5.15}$$

where u_s and u_p are the longitudinal horizontal displacements at the beam-adhesive interface and at the plate-adhesive interface, respectively, which can be written in term of strains

$$\varepsilon_s(x) = \frac{du_s}{dx} = \alpha_s\Delta T + \frac{M_s t_s}{2E_s I_s} + \frac{N_s}{E_s A_s} \tag{5.16}$$

and

$$\varepsilon_p(x) = \frac{du_p}{dx} = \alpha_p\Delta T - \frac{M_p t_p}{2E_p I_p} + \frac{N_p}{E_p A_p} \tag{5.17}$$

where α_s and α_p are the thermal expansion coefficient of the steel beam and the CFRP plate, respectively. ΔT is the uniform change in temperature. E, I and A are the elastic modulus, the second moment of inertia and the cross-sectional area, respectively.

Substituting Eqs. (5.16) and (5.17) into Eq.(5.15) gives

$$\frac{d^2u}{dydx} = \frac{1}{t_a}\left[(\alpha_s - \alpha_p)\Delta T + \frac{M_s t_s}{2E_s I_s} + \frac{N_s}{E_s A_s} - \frac{N_p}{E_p A_p}\right] \tag{5.18}$$

Substituting Eqs. (5.7) and (5.10) into Eq. (5.18) gives

$$\frac{d^2u}{dydx} = \frac{1}{t_a}\left[(\alpha_s - \alpha_p)\Delta T + \frac{\left[M(x) + N_s(t_s/2 + t_p/2)\right]\ t_s}{2E_s I_s} + N_s\left(\frac{1}{E_s A_s} + \frac{1}{E_p A_p}\right)\right] \tag{5.19}$$

Disregarding the adhesive bending deformations, i.e. $\frac{d^2v(x,y)}{dx^2} = 0$, and Eq. (5.13) becomes

$$\frac{d\tau}{dx} = -\frac{G_a}{t_a}\left[(\alpha_s - \alpha_p)\Delta T + \frac{\left[M(x) + N_s(t_s/2 + t_p/2)\right]\ t_s}{2E_s I_s} + N_s\left(\frac{1}{E_s A_s} + \frac{1}{E_p A_p}\right)\right] \tag{5.20}$$

Differentiating Eq. (5.20) with respect to x and substituting Eq. (5.5) gives

$$\frac{d^2\tau}{dx^2} = \lambda^2\tau - g\lambda^2 M'(x) \tag{5.21}$$

where

$$\lambda = \sqrt{\frac{G_a b}{t_a}\left[\frac{(t_s + t_p/2)t_s}{2E_s I_s} + \frac{1}{E_s A_s} + \frac{1}{E_p A_p}\right]} \tag{5.22}$$

and

$$g = \frac{G_a}{\lambda^2} \frac{t_s}{2 t_a E_s I_s} \tag{5.23}$$

$M'(x)$ is the first derivative of the moment distribution $dM(x)/dx = V$. Integrating Eq. (5.21) two times with respect to x gives the general solution of adhesive shear stress:

$$\tau(x) = c_1 e^{\lambda x} + c_2 e^{-\lambda x} + g M'(x) \leq \tau_{a,platsic} \tag{5.24}$$

To identify the integration constants (c_1 and c_2), two boundary conditions are applied:

- The shear stress at mid-span ($x = L_p / 2$) is equal to zero, if the beam is symmetric

$$\tau(L_p/2) = c_1 e^{\lambda L_p/2} + c_2 e^{-\lambda L_p/2} + g M'(L_p/2) = 0 \tag{5.25}$$

- The longitudinal force ($N_s = d\tau/dx$) at the end of the plate ($x = 0$) is zero, substituted in Eqs. (5.20) and (5.24), respectively, gives

$$\frac{d\tau(0)}{dx} = -\frac{G_{a(t)}}{t_a}\left[(\alpha_s - \alpha_p)\Delta T + \frac{M(0) t_s}{2 E_s I_s}\right] = c_1 \lambda - c_2 \lambda + g M''(0) \tag{5.26}$$

Solving Eq. (5.25) and Eq. (5.26) gives

$$c_1 = \frac{-\frac{1}{\lambda} e^{-\lambda L_p/2}\left\{\frac{G_a}{t_a}\left[(\alpha_s - \alpha_p)\Delta T + \frac{M(0) t_s}{2 E_s I_s}\right] + g M''(0)\right\} - g M'(L_p/2)}{e^{\lambda L_p/2} + e^{-\lambda L_p/2}} \tag{5.27}$$

$$c_2 = \frac{\frac{1}{\lambda} e^{\lambda L_p/2} \left\{ \frac{G_{a2}}{t_a} \left[(\alpha_s - \alpha_p)\Delta T + \frac{M(0) t_s}{2 E_s I_s} \right] + gM''(0) \right\} - gM'(L_p/2)}{e^{\lambda L_p/2} + e^{-\lambda L_p/2}} \tag{5.28}$$

5.2.1.2 Normal stresses

Assuming normal stress is constant through the thickness of the adhesive layer gives

$$\sigma(x) = \frac{E_a}{t_a}\left(v_p(x) - v_s(x)\right) \tag{5.29}$$

where E_a is the elastic modulus of the adhesive, v_s and v_p the transverse displacements at the bottom of the steel beam and the top of the CFRP plate, respectively, which are given by:

$$\frac{d^2 v_s(x)}{dx^2} = \frac{1}{E_s I_s} M_s(x) \tag{5.30}$$

and

$$\frac{d^2 v_p(x)}{dx^2} = \frac{1}{E_p I_p} M_p(x) \tag{5.31}$$

The moment equilibrium of the element in Figure 5.2 gives

$$(M_s + dM_s) - M_s - (V_s - dV_s)dx + \frac{1}{2}(\sigma b - q)(dx)^2 + \tau b(t_s/2)dx = 0 \tag{5.32}$$

Substituting Eq. (5.6) into Eq. (5.32) gives

$$\frac{dM_s}{dx} = V_s - \tau b t_s/2 \tag{5.33}$$

Similarly,

$$\frac{dM_p}{dx} = V_p - \tau b t_p / 2 \tag{5.34}$$

Differentiating Eq. (5.29) three times with respect to x and substituting Eqs. ((5.30), ((5.31), ((5.33) and ((5.34) gives

$$\frac{d^3\sigma(x)}{dx^3} = \frac{E_a}{t_a}\left[\frac{1}{E_p I_p}(V_p - \tau b t_p / 2) - \frac{1}{E_s I_s}(V_s - \tau b t_s / 2)\right] \tag{5.35}$$

Differentiating Eq. (5.35) with respect to x gives

$$\frac{d^4\sigma(x)}{dx^4} + \frac{E_a b}{t_a}\left(\frac{1}{E_s I_s} + \frac{1}{E_p I_p}\right)\sigma(x) - \frac{E_a q}{t_a E_s I_s} - \frac{E_a b}{t_a}\left(\frac{t_s}{2E_s I_s} + \frac{t_p}{2E_p I_p}\right)\frac{d\tau(x)}{dx} = 0 \tag{5.36}$$

Assuming that $d^5\tau/dx^5 = 0$ and that the normal stress approaches zero for large values of x, the general solution to Eq. (5.36) is

$$\sigma(x) = e^{-ßx}\left(s_1 \cos(ßx) + s_2 \sin(ßx)\right) + m_1\frac{d\tau}{dx} + m_3 q \le \sigma_{a,plastic} \tag{5.37}$$

where

$$ß = \sqrt[4]{\frac{E_a b}{4t_a}\left(\frac{1}{E_s I_s} + \frac{1}{E_p I_p}\right)} \tag{5.38}$$

$$m_1 = \frac{E_p I_p t_s / 2 - E_s I_s t_p / 2}{E_s I_s + E_p I_p} \tag{5.39}$$

$$m_3 = \frac{E_p I_p}{b(E_s I_s + E_p I_p)} \tag{5.40}$$

The shear force and the bending moment are zero at the ends of the CFRP plate, hence these boundary conditions give

$$\frac{d^2\sigma(0)}{dx^2} = \frac{E_a}{t_a}\left[\frac{1}{E_p I_p} M_p(0) - \frac{1}{E_s I_s} M_s(0)\right] = \frac{E_a}{t_a}\frac{1}{E_s I_s} M(0) \tag{5.41}$$

and

$$\frac{d^3\sigma(0)}{dx^3} = m_2 \tau(0) - \frac{E_a}{t_a}\frac{1}{E_s I_s} V(0) \tag{5.42}$$

where

$$m_2 = \frac{E_a b}{t_a}\left(\frac{t_s}{2E_s I_s} - \frac{t_p}{2E_p I_p}\right) \tag{5.43}$$

and from Eq. (5.37) for x=0

$$\frac{d^2\sigma(0)}{dx^2} = -2s_2 ß^2 + m_1 \frac{d^3\tau(0)}{dx^3} \tag{5.44}$$

$$\frac{d^3\sigma(0)}{dx^3} = 2\,ß^3(s_1 + s_2) + m_2\frac{d^4\tau(0)}{dx^4} \tag{5.45}$$

Combining Eqs. (5.41) with (5.44), and (5.42) with (5.45), respectively, give

$$s_1 = \frac{1}{2\,ß^3}\left(m_2\tau(0) - m_1\frac{d^4\tau(0)}{dx^4}\right) - \frac{m_1}{2\,ß^2}\frac{d^3\tau(0)}{dx^3} - \frac{E_a}{2\,ß^3 t_a}\frac{1}{E_s I_s}\left(V(0) + ßM(0)\right) \tag{5.46}$$

and

$$s_2 = \frac{m_1}{2\,ß^2}\frac{d^3\tau(0)}{dx^3} + \frac{E_a}{2\,ß^2 t_a}\frac{1}{E_s I_s}M(0) \tag{5.47}$$

The modifications also considers the variation in adhesive mechanical properties with temperature, which was not taken in Deng et al. analyses [11]. Thus, the parameters in Eqs. (5.22), (5.23), (5.27), (5.28) (5.38), (5.43), (5.46) and (5.47) change with temperatures because they depend on the adhesive elastic modulus (E_a) and shear modulus (G_a). The values of these moduli at different temperatures were given in Tables 3.3 and 3.5 in Chapter 3.

5.2.2 Finite element model at elevated temperatures

Three-dimensional (3D) FE analysis was used to model a simply supported beam bonded with a CFRP plate by epoxy adhesive and subjected to an uniform load. The model was analysed using the ABAQUS software [126].

5.2.2.1 Boundary conditions

A quarter of the reinforced beam was modelled due to symmetry of the geometry, the load and the boundary conditions. Figure 5.3 shows the restrained nodes along the symmetric axes to ensure the symmetry, where U and UR are the linear and the rotation displacements. X, Y and Z are the coordinate axes defined in ABAQUS as 1, 2 and 3, respectively. The line of nodes at 50 mm away from the end of the beam was restrained in the Y direction ($U2 = 0$) to give the simply roll-supported conditions (Figure 5.3).

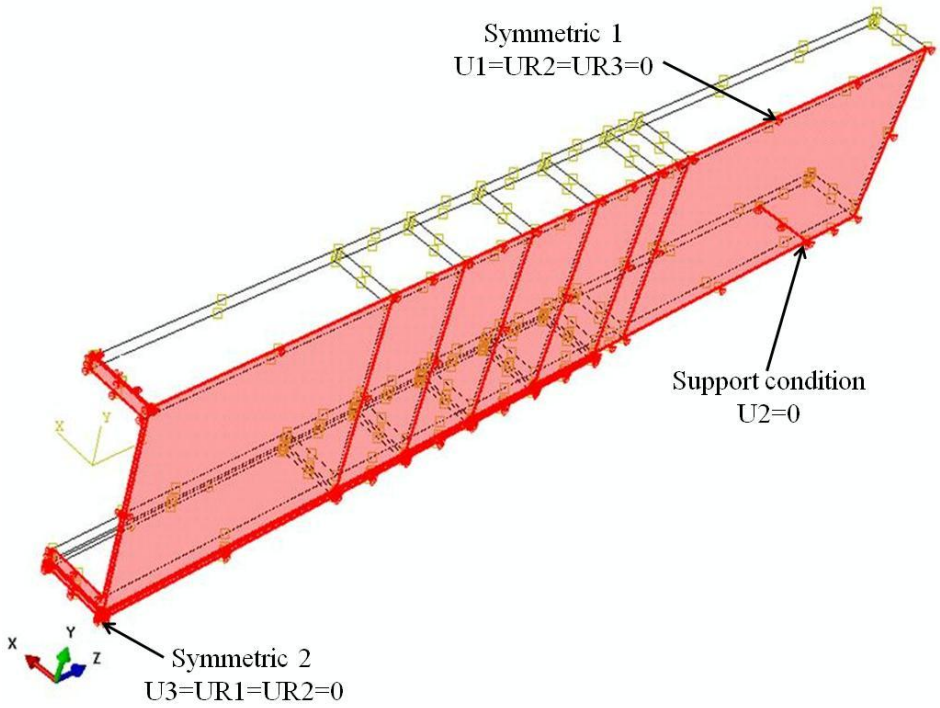

Figure 5.3: Boundary conditions of a quarter beam

5.2.2.2 Meshing

All the materials were simulated using 8-node linear brick 3D stress elements (C3D8R), which have reduced integration with hourglass control to prevent shear locking. Very fine mesh size was employed at the plate end due to high stress concentrations. Figure 5.4 shows the finite element mesh produced for this model. The 2 mm adhesive thickness was divided into eight layers to allow the stress and the strain data to be taken from a path created at the central elements (Figure 5.4).

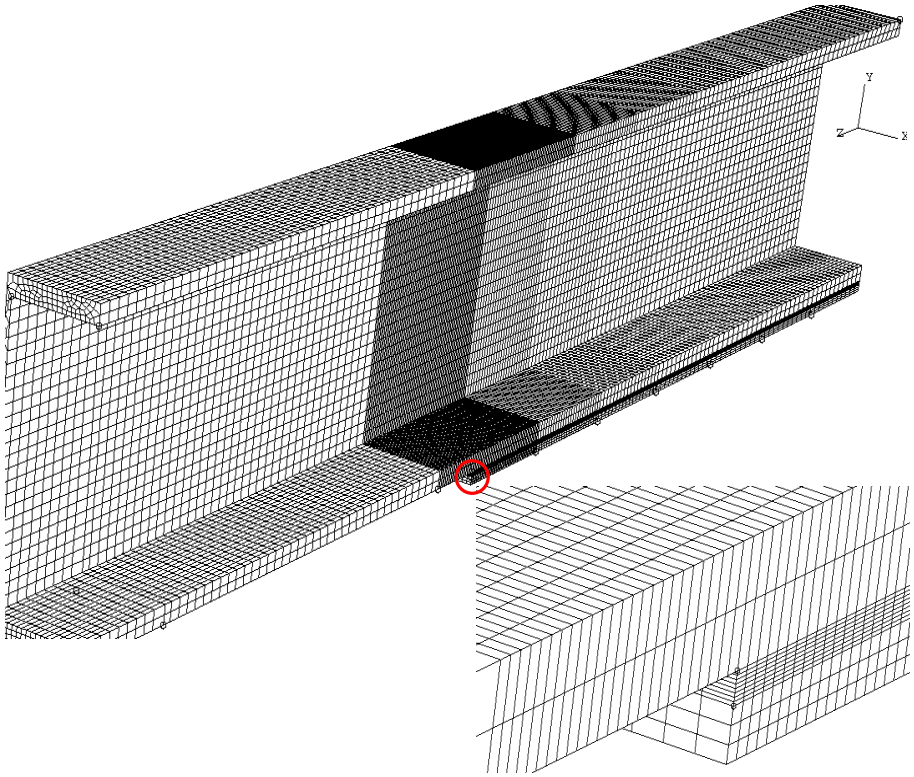

Figure 5.4: Mesh details of a quarter beam

5.2.2.3 Material models

In ABAQUS, material data is given as true stress and logarithmic strain which means that the stress and strain obtained from experimental tests (known as nominal or engineering stress and strain) have to be converted before they used in the FE model. The ABAQUS manual [126] gives the equations to calculate the true stress (σ_{true}) from the nominal stress ($\sigma_{nom.}$) and the true strain (ε_{true}) from the nominal strain ($\varepsilon_{nom.}$), as following:

$$\sigma_{true} = \sigma_{nom.}(1+\sigma_{nom.}) \tag{5.48}$$

$$\varepsilon_{true} = \ln(1+\varepsilon_{nom.}) \tag{5.49}$$

The material properties of the steel and CFRP are assumed to be linearly elastic and temperature independent. Table 5.1 summarises the properties of the steel and the CFRP plate employed in

the FE model. These data were obtained from experimental tests and design standard, as discussed previously in Chapter 3.

Table 5.1: Steel and CFRP material properties used in FE modelling

Properties	Steel	CFRP
Elastic modulus GPa	181[(a)]	124[(c)]
Poisson ratio	0.3	0.3
Coefficient of thermal expansion /°C	10×10^{-6} [(b)]	0.34×10^{-6} [(d)]

(a) average value obtained from mechanical test described in Sec. 3.1.1, Chapter 3; (b) according to BS EN 1994-2 [9]; (c) average value obtained from mechanical test described in Sec. 3.2.1, Chapter 3; (d) test described in Sec. 3.2.3, Chapter 3.

The adhesive nonlinear behaviour at elevated temperatures is approximated with a bilinear elastic-plastic model. Details of defining adhesive bilinear curve in ABAQUS were described in section 3.4.2 in Chapter 3.

5.2.2.4 Beam specification

The dimensions used in the FE model were the same as the tested beams. The beam span (L_s) was 1100 mm and the CFRP plate length (L_p) was 700 mm. The plate width was 76 mm, the same as that of the beam flange, and the thickness was 3.2 mm.

5.3 Results of analytical and finite element solutions

The interfacial shear and normal stresses of the strengthened steel beam subjected to a thermal load only calculated using the analytical and the FE models are compared. Figure 5.5 shows the shear and the normal stresses obtained from these solutions compared to Deng et al. model after the temperature increased from 20 °C to 50 °C (without external load). It can be seen that the shear and the normal stresses at the plate end calculated by Deng et al. are significantly higher than those obtained from the analytical and the FE solutions. This is because Deng et al. model did not take the change in adhesive Young's modulus with temperature into account. The maximum values of the thermal shear and normal stresses calculated from the analytical model agree well with those obtained from the FE model. The distributions of thermal shear and normal stresses calculated from the analytical and FE models at different temperatures are

shown in Figure 5.6 and Figure 5.7, respectively. The figures illustrate the shear and the normal stresses reached a peak at 40 °C, but they reduced at higher temperatures. This is due to the significant reduction in the elastic modulus and strength of the adhesive above 40 °C. The maximum values of the thermal shear and normal stresses at different temperatures are lower than the maximum adhesive shear and normal strengths at these temperatures, presented in Table 4.4 in Chapter 4. This confirms that CFRP plate debonding will not occur due to temperature increases only.

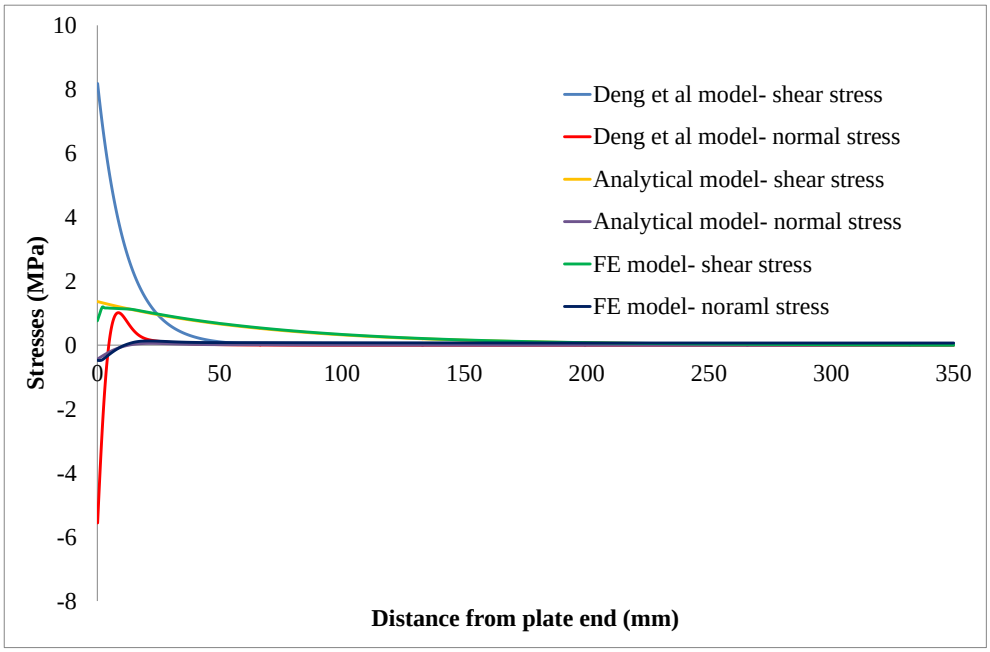

Figure 5.5: Comparing thermal stresses calculated from different models ($\Delta T = 30\ ^{o}C$)

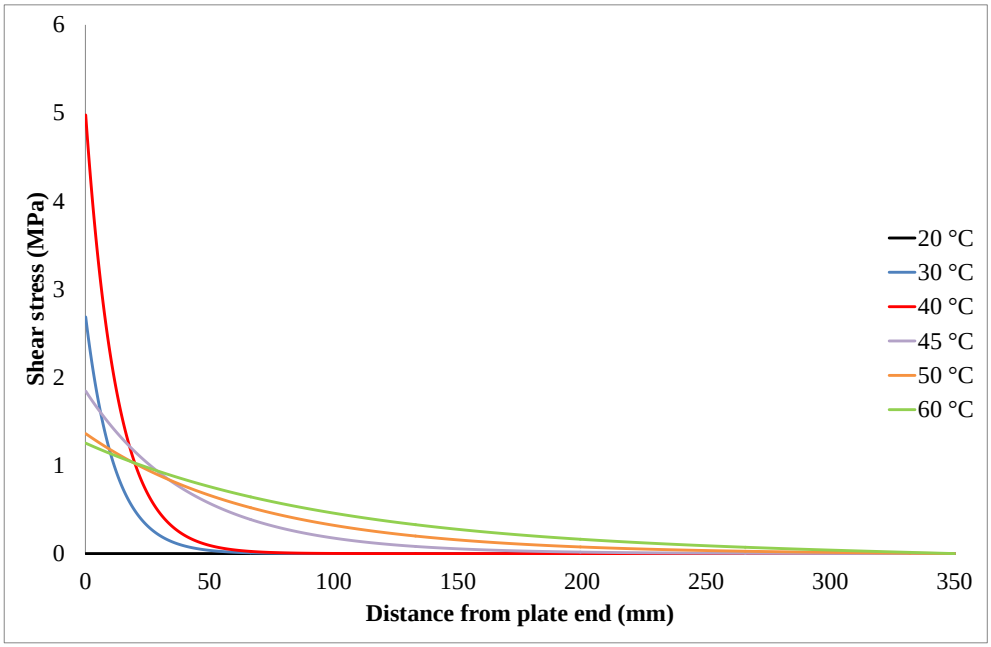

Figure 5.6: Shear stresses developed due to temperature increases

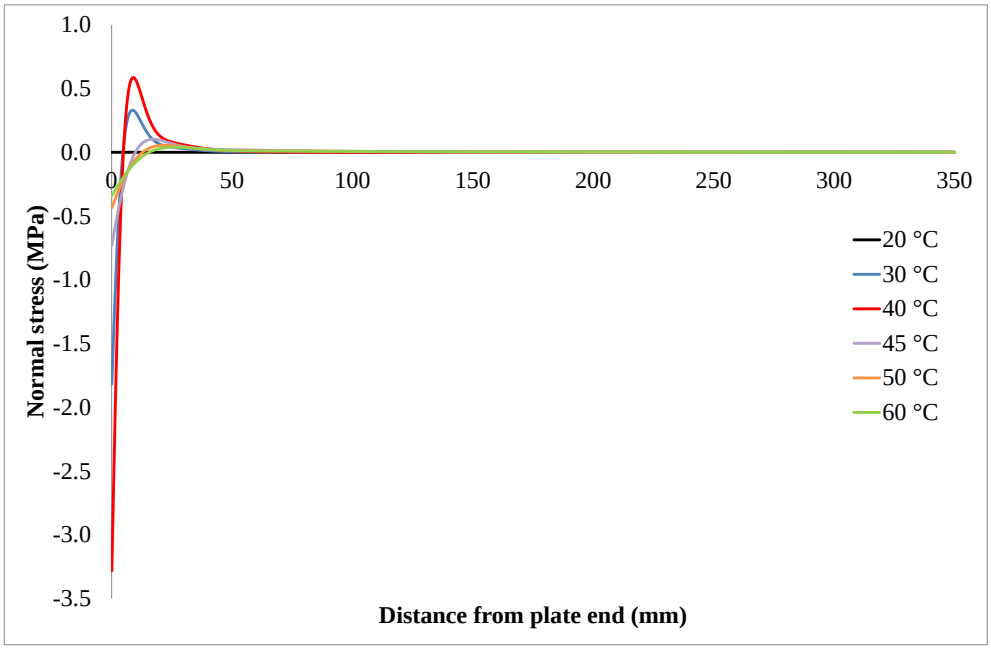

Figure 5.7: Normal stresses developed due to temperature increases

The slip deformation of the CFRP plate end increases significantly above 40 °C due to softening of the adhesive. Figure 5.8 shows the CFRP plate end slips obtained from the FE model at the same load level below and above the T_g value. The figure demonstrates a high slip of the CFRP plate at 45 °C compared to that at 40 °C.

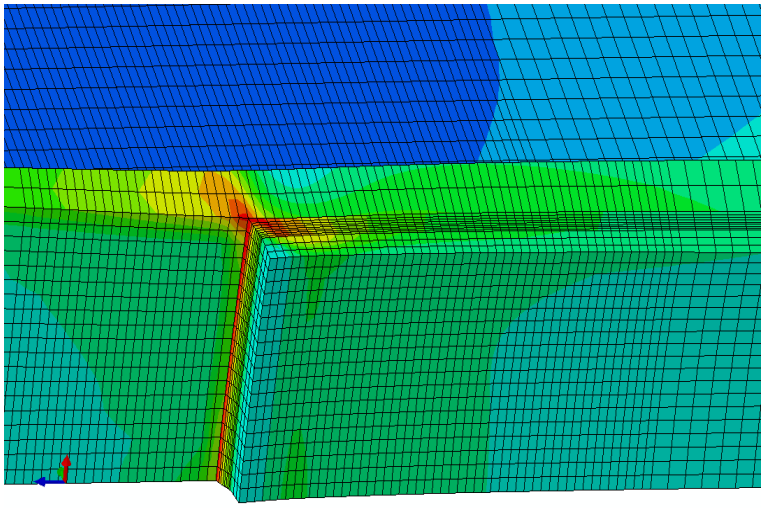

(a)

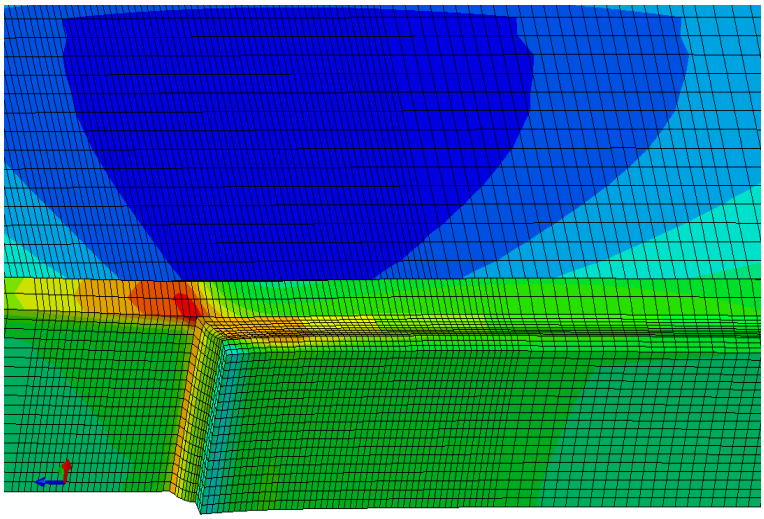

(b)

Figure 5.8: Slip of the CFRP plate end at (a) 40 °C and at (b) 45 °C under the same load level

The shear and normal stresses for reinforced beam subjected to a uniform load of 216 N/mm (90% of the failure load at 60°C) at different temperatures are calculated using the analytical and the FE models. Figure 5.9 shows a good agreement between the analytical and the FE shear and normal stresses distributions at 20 °C. However, the shear stress distribution at elevated temperatures obtained from the FE model was a little higher from that obtained from the analytical model, as shown in Figures 5.10 and 5.11. Thus, the longer plastic zone was obtained from the FE model than the analytical model (Figure 5.1). This is due to the difference in the strain value at which plasticity in the adhesive starts as the Deng et al. model assumed linear elasticity along the entire bonded plate thus the shear stress concentrated near the plate ends.

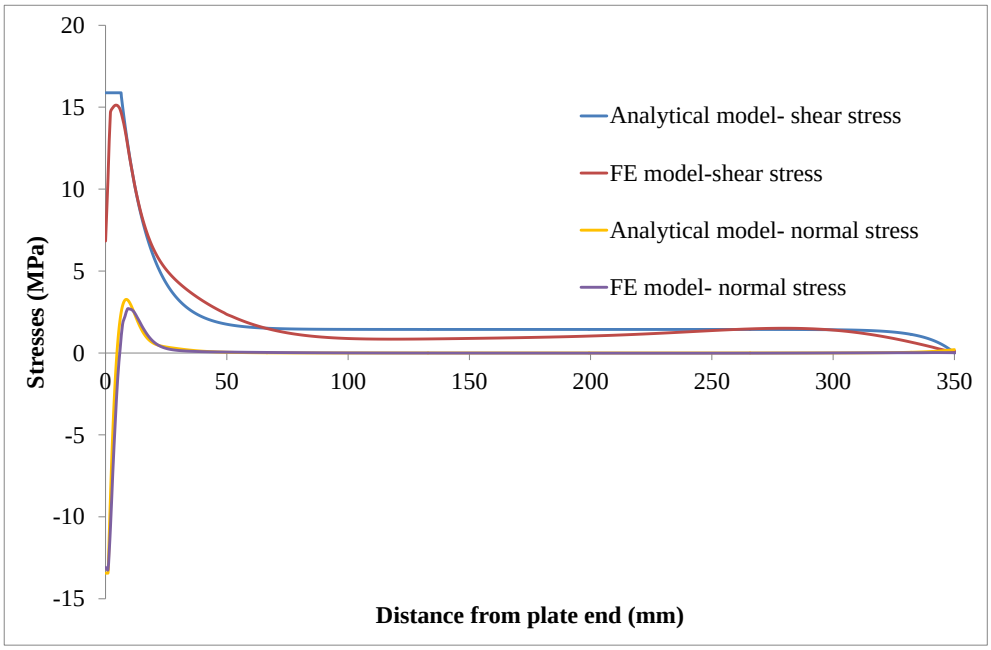

Figure 5.9: Comparison of stresses under concentrated load of 216 N/mm at 20 °C

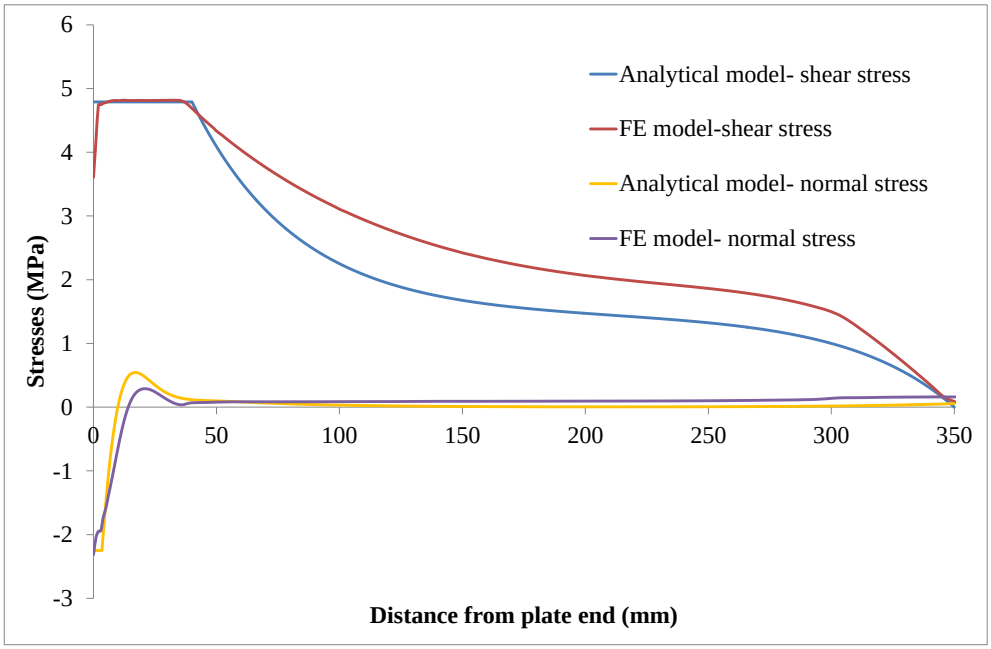

Figure 5.10: Comparison of stresses under concentrated load 216 N/mm at 45 °C

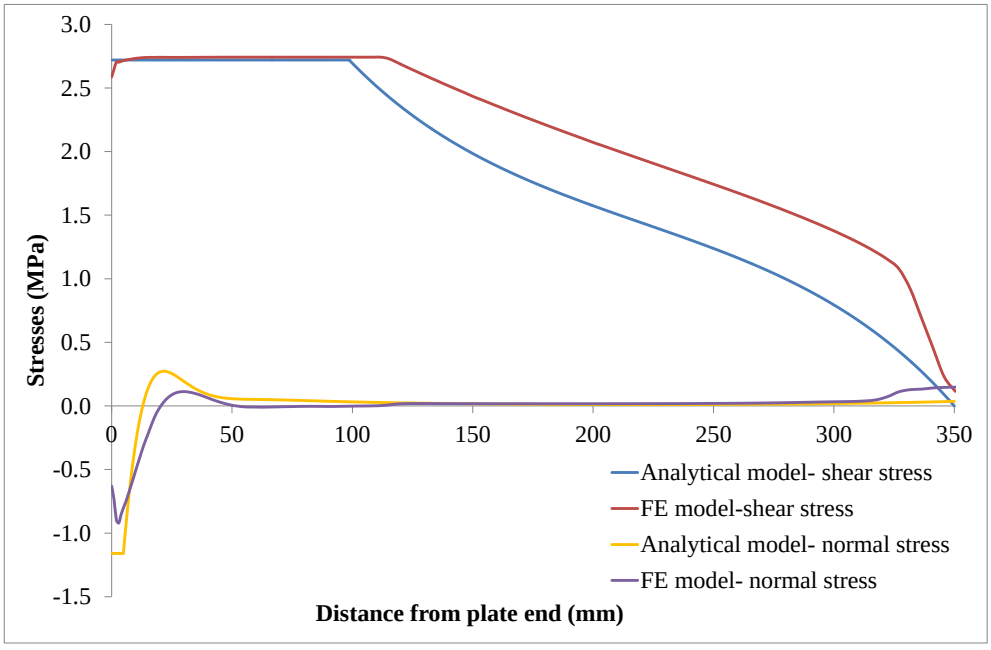

Figure 5.11: Comparison of stresses under concentrated load 216 N/mm at 50 °C

5.4 Parametric study

The maximum shear stress at the plate end is dependent on different parameters such as the elastic modulus of the CFRP plate, the thickness of CFRP plate, the load and the temperature. Thus, the length of the plastic zone changes with these parameters. As the adhesive used in this research lose most of its strength and stiffness at 45 °C, the changes in these parameters were studied using the analytical solution at this temperature under 273.82 N/mm.

5.4.1 CFRP plate modulus

The modulus was varied from modulus of CFRP plate ($E_p = 124 \quad GPa$) up to three times the modulus of steel ($3E_s$, as in the case of ultra high modulus CFRP). Figure 5.12 shows that the length of the plastic zone increases significantly with a higher CFRP modulus. This is because a stiffer CFRP plate carried more load from the beam compared to a normal modulus plate, thus a higher shear stress developed at the plate end which induced longer plastic zone.

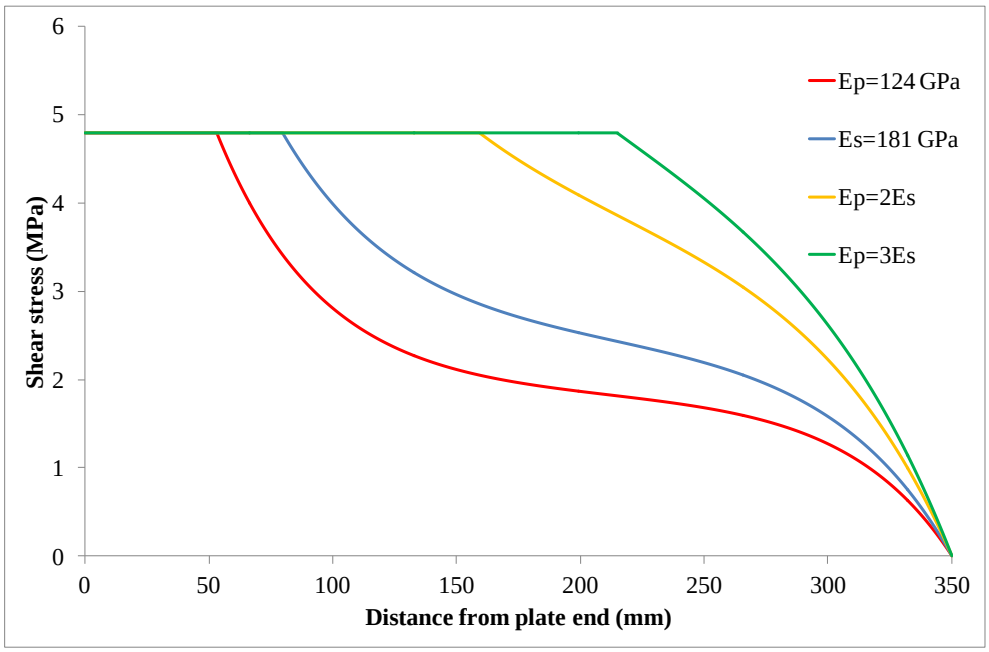

Figure 5.12: Variation of the plastic zone length with CFRP plate Young's modulus (45 °C)

5.4.2 CFRP plate thickness

The effect of increasing the thickness of the CFRP plate on the shear stress distribution and the plastic zone length was investigated at 45 °C. The shear stress distribution and the length of the

plastic zone was first calculated using the average thickness of the CFRP plate ($t_p = 3.3 \ \ mm$). Then the analyses were carried out using different plate thicknesses. Figure 5.13 shows that the length of the plastic zone increases with the CFRP plate thickness. The length of the plastic zone can be reduced to less than half (from 53.4 mm to 20 mm) by reducing the plate thickness to 1.5 mm.

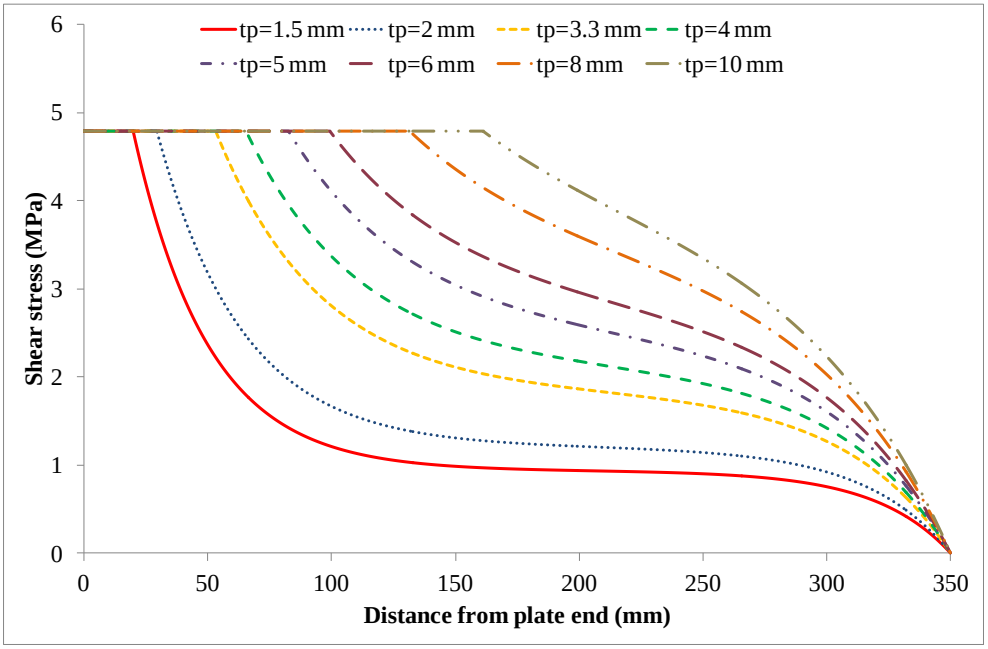

Figure 5.13: Variation of the plastic zone length with the thickness of the CFRP plate (45 °C)

5.4.3 Applied load and CFRP plate length

The length of the plastic zone depends on the maximum shear stresses at the plate end and it can be reduced by reducing the applied load. In addition, extending the CFRP plate into the area of lower bending moment may reduce the length of the plastic zone. Figure 5.14 shows the relation between the plastic zone length with both the normalised load (percentage of applied load to failure load) and the length of the CFRP plate. The figure shows that the length of the plastic zone reduces with increasing the CFRP plate length. The length of the plastic zone increase dramatically with the percentage of applied load in the shorter the CFRP plates comparing to the longer plate. Thus, it is possible to avoid CFRP plate debonding at T_g by increasing the plate length.

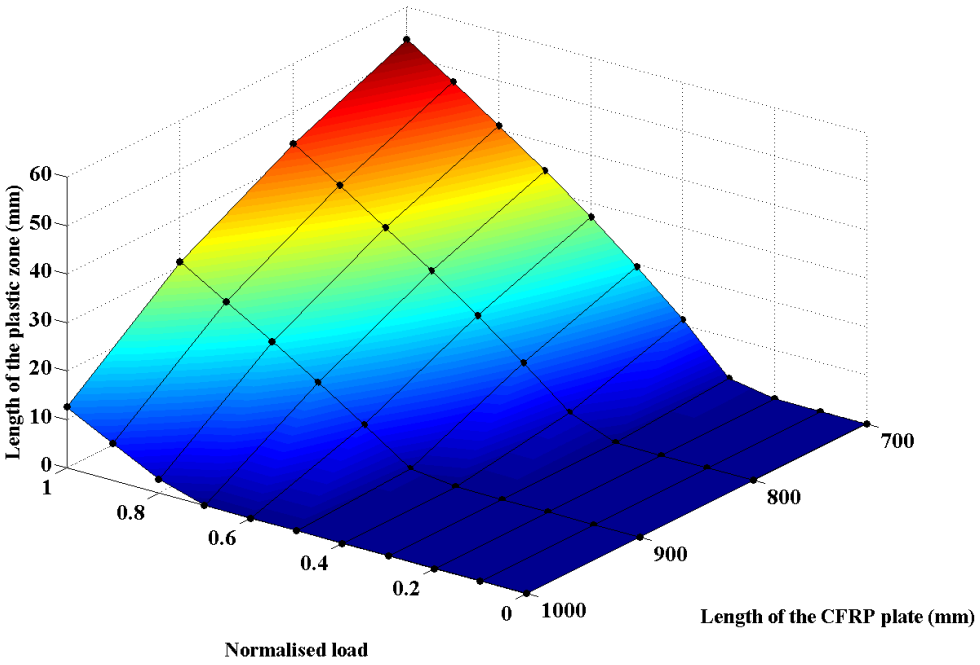

Figure 5.14: Plastic zone length as a function of load and CFRP plate length (45 °C)

5.4.4 Temperature and CFRP plate length

The variation in the length of the plastic zone with temperature and the CFRP plate length was investigated under 240 N/mm uniform load. Figure 5.15 shows that the plastic zone length can be reduced significantly with increasing the CFRP plate length. The shortest CFRP plate has significantly increased the plastic zone length with temperature increases compared to that with a longer plate. Thus, it is possible to avoid CFRP plate debonding at elevated temperature by increasing the plate length.

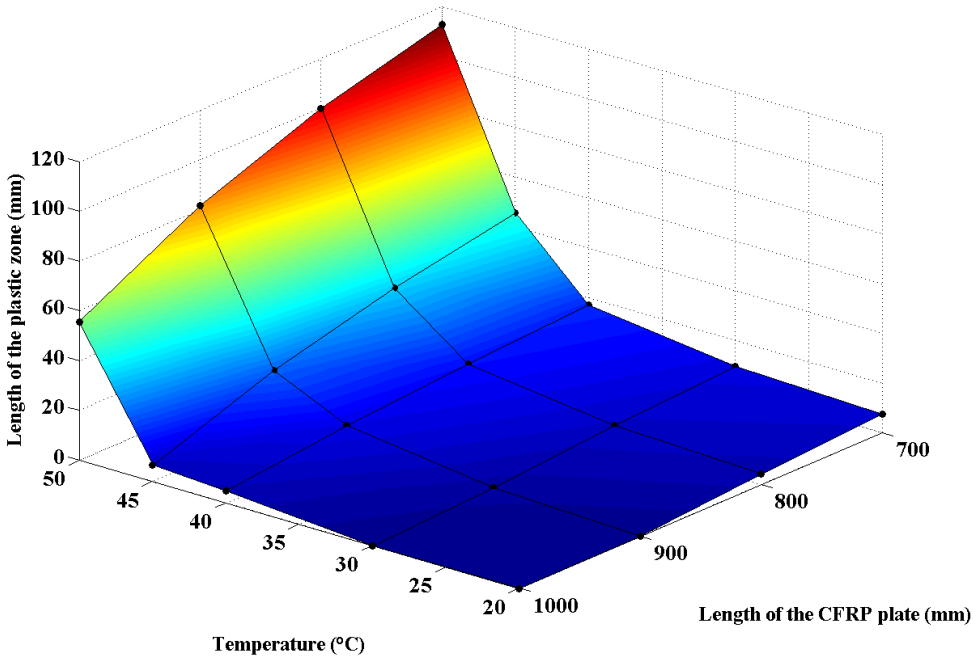

Figure 5.15: Plastic zone length as a function of temperature and CFRP plate length (240 N/mm)

5.5 Conclusion

In this chapter an existing analytical model was modified to calculate the interfacial stresses in the adhesive between a steel beam and a CFRP plate. The modification considered the variation of the adhesive properties with temperatures as well as the nonlinearity behaviour along the bonded plate. In addition, FE analyses were employed to validate the analytical results.

The analytical model suggested by Deng et al. assumed that adhesive material was linear elastic and its mechanical properties were temperature independent thus the interfacial stresses at the plate ends increased continuously exceeding the maximum adhesive strength strengths. Two modifications on their model were suggested in this research: First, the adhesive properties temperature dependency was taken into consideration. Second, the stresses at the plate end were equalised to the adhesive strengths obtained from FE analyses on double-lap shear joint. The modified model showed that the stresses at the plate ends were high and reached adhesive maximum strengths thereby plastic zones at these ends developed. FE analyses validated well the analytical model for a reinforced beam subjected to thermal loads only. However, the shear stress distribution and the length of the plastic zone obtained from the FE analyses was slightly larger from those obtained from the analytical model for a reinforced beam subjected to mechanical and thermal load. This is because the analytical model assumed linear elasticity of the adhesive along the entire bonded plate thus the shear stress concentrated near the plate ends.

The length of the plastic zone was dependent on several parameters including, the elastic modulus, the thickness and the length of the CFRP plate, the applied load and the temperature. Studying these parameters showed that stiffer CFRP plate may debond earlier than normal stiffness plate because the shear stress increased with the CFRP plate stiffness and thus the length of the plastic zone. The length of the plastic zone decreased to less than a half by reducing the plate thickness from 3.3 to 1.5 mm due to the reduction in the stresses at plate ends. Increasing the load or the temperatures increased the length of the plastic zone. But, increasing the plate length reduced significantly the plastic zone even at temperature above the T_g . Thus, it is possible to avoid CFRP plate debonding at high temperature by selecting longer CFRP plate.

Chapter 6

Behaviour of bonded joint under fatigue cyclic loading at elevated temperatures

6.1 Introduction

Steel beams and girders strengthened with CFRP composites expose to cyclic loadings caused by the daily traffic passages which may affect the adhesive bond at the plate ends. Although several fatigues tests carried out on damaged and non-damaged steel beams reinforced with prestressed and non-prestressed CFRP composites had shown an improvement in the fatigue life at room temperature[15, 17, 20, 22-24], to date there is no available research on the fatigue behaviour of steel beams reinforced with CFRP composites at elevated temperatures. Because of this knowledge gap, urgent research is required to ensure this strengthening method can be safely used.

This chapter reports on a series of experimental tests carried out on double-lap shear specimens and CFRP reinforced beams at different cyclic loading levels and temperatures to investigate their fatigue lives temperature dependency. In addition, the effect of plate lengths on the fatigue life of double-lap shear specimens was examined. The shear and the normal stresses for reinforced beams at different cyclic loading levels and temperatures were obtained from FE analyses.

6.2 Shear test

Fatigue tests were carried out on the double-lap shear specimens. The preparation and fabrication processes of the specimens followed the same procedure previously mentioned in section 4.2.1 in Chapter 4. The shorter length of the CFRP plate L_1 (see Figure 4.1, Chapter 4) was 50 mm for all specimens, except for only two specimens which were extended to 60 and 70 mm, respectively.

Specimens were named in the form of FS N1-N2-T, where the letter ‘F’ refers to fatigue test and the letter ‘S’ stands for shear test, the numbers ‘N1-N2’ denote minimum and maximum tensile loads respectively, and the last number ‘T’ refers to the testing temperature. For example, FS 1-

10-24 represents the fatigue test on a double-lap shear specimen subjected to minimum and maximum tensile loads of 1 and 10 kN, respectively, carried out at 24 °C.

6.2.1 Test setup

Fatigue tests were carried out using the same hydraulic universal testing machine and the thermal chamber used in the static tests described in section 4.2.2 in Chapter 4. Specimen tested at elevated temperatures was initially heated up to the target temperature and held for 30 minutes to ensure thermal stabilisation before cyclically loaded to failure. All specimens were subjected to sinusoidal waveform cycles at a frequency of 5 Hz. Different cyclic loading ranges were applied to the specimens while the load ratio ($R = P_{max} / P_{min}$) was kept constant at 0.1, as summarised in Table 6.1. In each test, the cyclic load was applied continuously until the CFRP plate was debonded. If the debonding was not achieved after one million cycles, the fatigue test stopped and then a static load was applied until failure.

Table 6.1: Minimum and maximum tensile loads applied on double-lap shear specimens

Loads (P_{min} ; P_{max})/ kN		ΔP ($P_{max} - P_{min}$)/ kN	Load ratio ($R = P_{max} / P_{min}$)/ %
1	10	9	0.1
2	20	18	0.1
3	30	27	0.1
3.5	35	31.5	0.1
4	40	36	0.1
5	50	45	0.1

6.2.2 Test Results and discussion

The effects of temperature on the fatigue life, the stress distribution and the failure mode of the double-lap shear specimens are discussed in this section. In addition, the influence of increasing the CFRP bonded length on the fatigue life is examined

6.2.2.1 Fatigue life of the double-lap shear specimens

Fatigue test results for the double-lap shear specimens are summarised in Table 6.2.

Table 6.2: Failure load of double-lap shear specimens at different temperatures

Sample	Temperature/ °C	Load ranges ($P_{min} - P_{max}$)/ kN	Normalised Loads ($P_{max} / P_{static,\ ave.}$)/ %	Number of cycles (N)	Reduction in number of cycles %
FS 1-10-24	24	1-10	11	10^6	/
FS 2-20-24	24	2-20	22	10^6	/
FS 3-30-24	24	3-30	33	10^6	/
FS 3.5-35-24	24	3.5-35	39	252033	/
FS 4-40-24	24	4-40	45	59181	/
FS 5-50-24	24	5-50	56	6261	/
FS 1-10-40	40	1-10	14	10^6	0
FS 2-20-40	40	2-20	27	10^6	0
FS 3-30-40	40	3-30	41	28869	97
FS 4-40-40	40	4-40	55	2343	96
FS 5-50-40	40	5-50	69	989	84
FS 3-30-45	45	3-30	47	4806	99
FS 4-40-45	45	4-40	62	1560	97
FS 3-30-40[(a)]	40	3-30	/	979811	2
FS 3-30-40[(b)]	40	3-30	/	10^6	0

(a) CFRP plate effective length is 60 mm; (b) CFRP plate effective length is 70 mm

The results show that the fatigue life of the bonded joint decreased as either the load or the temperature increased. Increasing the load intensified the stresses in the adhesive at the discontinuities (plate end and mid-joint) thus developed longer plastic zones at the adherends ends (as will be discussed in section 6.2.2.3). The normalised applied loads (the percentage of the maximum cyclic applied load to the static average failure load given in Table 4.1 in Chapter 4) versus the numbers of cycles to failure at 24 and 40 °C are shown in Figure 6.1. the figure shows that the bonded joint held one million cycles at 24 and 40 °C by decreasing the normalised load from 33 to 27 %.

Regression analysis was used to give the best fit normalised load versus the number of cycle lines at 24 and 40 °C as follows:

$$P_{\max} / P_{static,\ ave.} = 93.689 - 4.387 \ln(N) \quad , \quad R^2 = 0.996 \quad @24\ ^oC \tag{6.1}$$

$$P_{\max} / P_{static,\ ave.} = 101.42 - 5.5191 \ln(N) \quad , \quad R^2 = 0.937 \quad @40\ ^oC \tag{6.2}$$

where $P_{\max}$ is the maximum value of cyclic load, $P_{static,\ ave.}$ is the average static failure load given in Table 4.1, and N is the number of cycles. These equations are not a general solution to calculate the failure life of a double-lap shear joint at different temperatures as they are applicable only to the tested specimen's specifications.

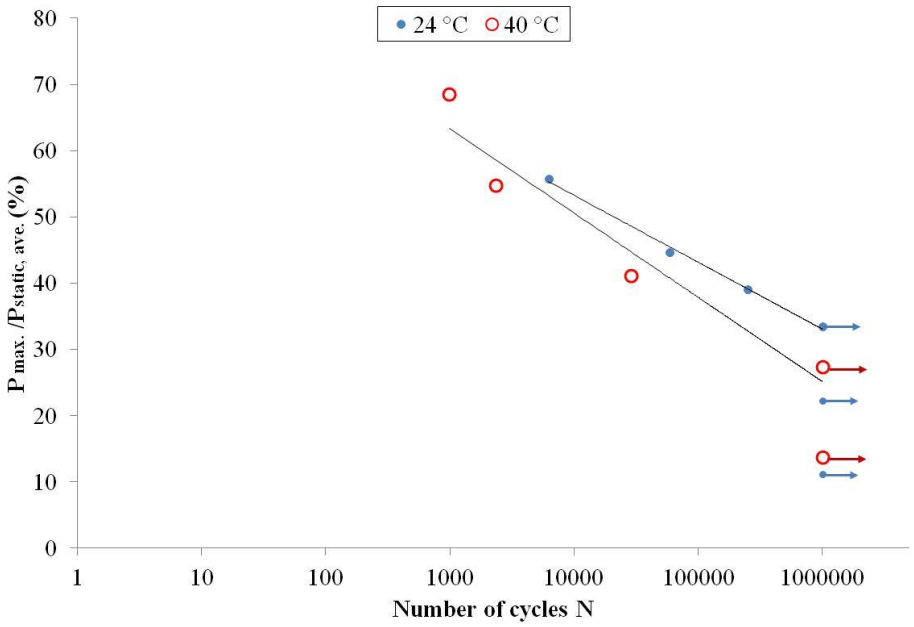

Figure 6.1: The normalised applied load versus the number of cycles curves for double-lap shear specimens at 24 and 40 °C

The fatigue lives of the bonded joints were significantly decreased by increasing the temperature at the same applied loads. This is because of the reduction in the strength and stiffness of the adhesive with temperature increases thus increased the length of the plastic zone (as will be discussed in section 6.2.2.3). The temperatures versus the number of cycles to failure of double-lap shear specimens subjected to a maximum applied load of 30 and 40 kN, respectively, are shown in Figure 6.2.

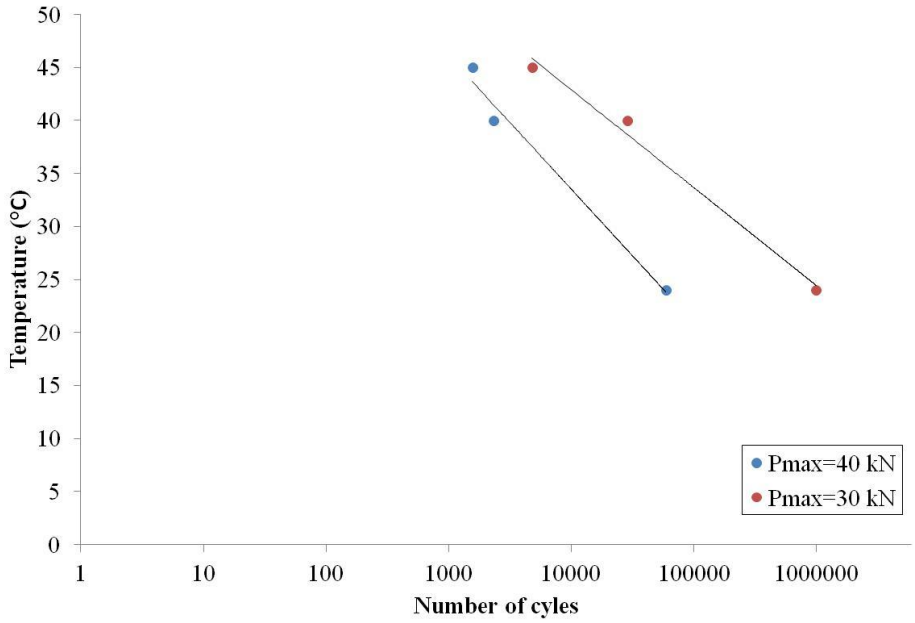

Figure 6.2: The temperature versus the number of cycles curves for double-lap shear specimens at two different maximum applied loads

6.2.2.2 Effect of joint bonded length on the fatigue life

Most recently, Nguyen et al. [113] indicated that the effective bond length of steel/CFRP double strap joints subjected to static loading doubled when the temperature exceeded adhesive T_g. According to them finding, fatigue tests were carried out on two specimens fabricated with longer CFRP bonded plates of 60 and 70 mm to investigate the effect of bonded length on the fatigue life at elevated temperature. These specimens were subjected to minimum and maximum loads of 3 to 30 kN, respectively, while the temperature was held at 40 °C. The chosen loading range and the temperature were similar to that for the specimen FS 3-30-40 (bonded with a 50 mm CFRP plate) to compare the improvement in the fatigue life due to increasing the CFRP plate length.

Test results showed that the number of cycles increased from 28869 to 979811 cycles when the CFRP plate length was increased from 50 to 60 mm, and no fatigue failure occurred up to one million cycles by bonding the 70 mm CFRP plate (see Table 6.2). Thus, the fatigue failure of a bonded joint at an elevated temperature can be prevented by increasing the CFRP plate length. This is because the average shear stress along the bonded joint and the plastic zone decreased with increasing the plate length, as will be discussed in section 6.2.2.3.

6.2.2.3 Stress analysis of the double-lap shear specimens

The distributions of the shear and normal stresses along the bonded joint at different fatigue cyclic loading and temperatures were obtained from the FE model previously discussed in section 4.2.3.5 in Chapter 4. Figures 6.3 to 6.6 show the distributions of the shear and the normal stresses at the minimum and maximum cyclic applied loads at 20 and 40 °C. The analysis carried out at 20 °C instead of 24 °C because the adhesive mechanical properties implemented in ABAQUS model was measured at 20 °C (Table 3.3 in Chapter 3). Nevertheless, the adhesive elastic modulus was not significantly reduced up to 40 °C.

The maximum shear and normal stresses concentrated at the CFRP plate end and the mid-joint exceeding the adhesive elasticity limit and thus created plastic zones. The stress analyses show the following results:

- The length of the plastic zones increased with both the applied load and the temperature. The load increased the stresses while the temperatures softened the adhesive.

- The fatigue life at the same applied load decreased significantly with increase the temperature due to the reduction in the shear strength of the adhesive thus the plastic zone increased. E.g, at 20 °C, the adhesive along the bonded joint subjected to 30 kN was elastic (Figure 6.3), however about 25 mm from the plate end of the adhesive became plastic due to increasing the temperature to 40 °C at the same applied load (Figure 6.5).

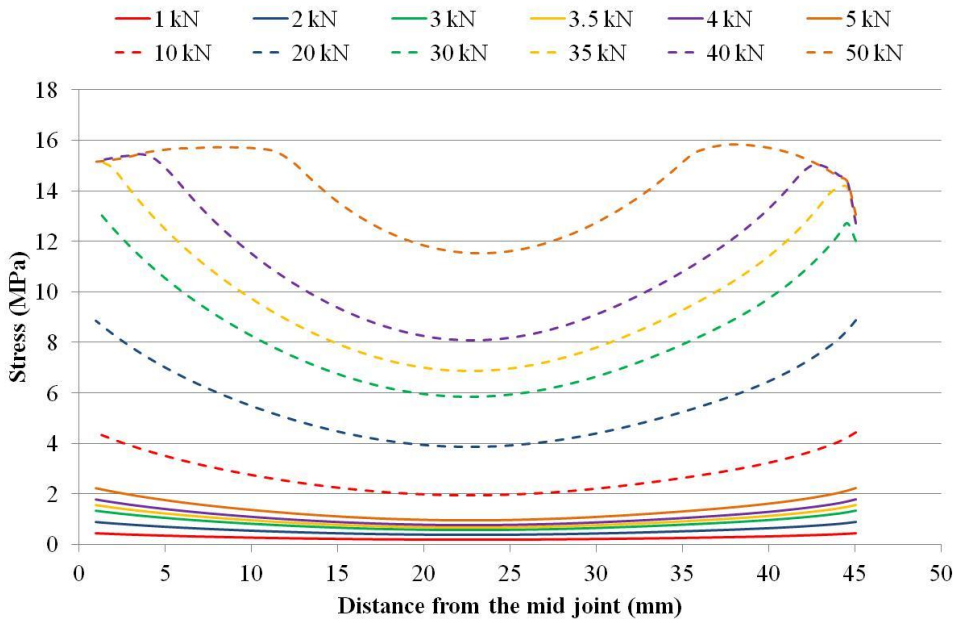

Figure 6.3: Distribution of shear stresses at the minimum and maximum cyclic loads at 20 °C

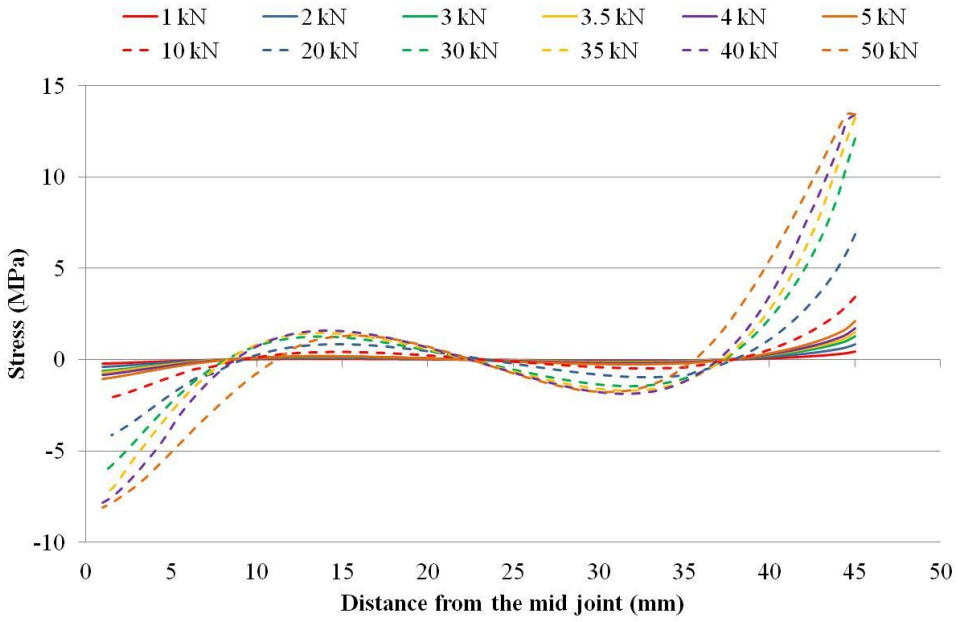

Figure 6.4: Distribution of normal stresses at the minimum and maximum cyclic loads at 20 °C

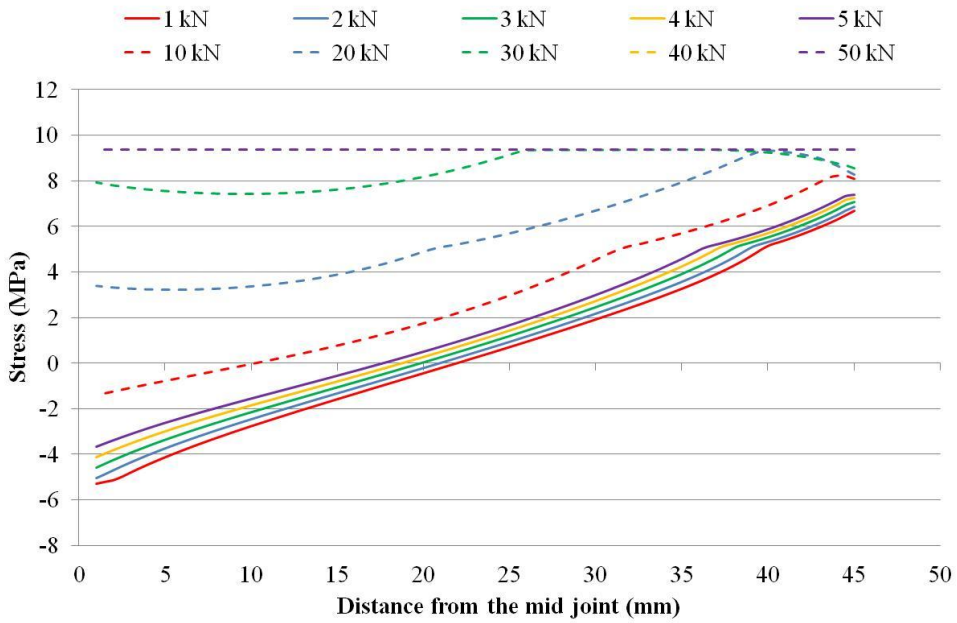

Figure 6.5: Distribution of shear stresses at the minimum and maximum cyclic loads at 40 °C

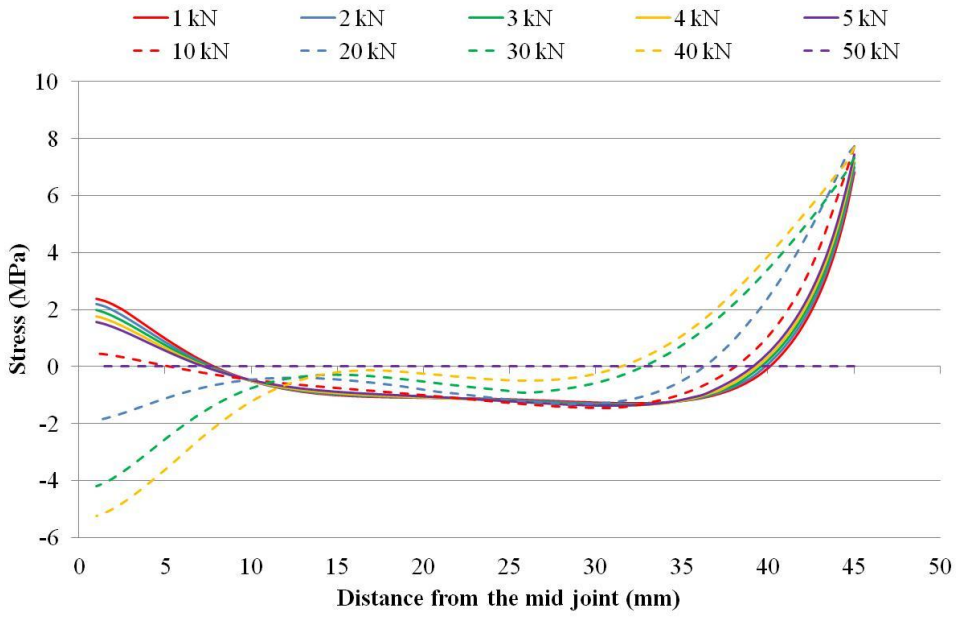

Figure 6.6: Distribution of normal stresses at the minimum and maximum cyclic loads at 40 °C

The distribution of the shear stresses for specimens bonded with 50, 60 and 70 mm CFRP plate lengths at the maximum cyclic loading of 30 kN and 40 °C is shown in Figure 6.7. The figures indicated that the specimen bonded with a 50 mm plate had an average shear stress of 8.43 MPa along the bonding joint and a longer plastic zone about 25 mm. Thus, it had a short fatigue life and failed after 28869 cycles (FS 3-30-40 in Table 6.2). However, increasing the bond length to 60 and 70 mm reduced the average shear stresses to 7.08 and 6.18 MPa and the plastic zone length to around 14 mm. Thus, the fatigue life of the longer bonded plate increased, as already discussed in section 6.2.2.2. The distribution of the normal stresses for bonded joints with different plate lengths is shown in Figure 6.8. The figure shows that the normal stresses were higher at the plate end and mid-joint than at the middle of the bonded joint.

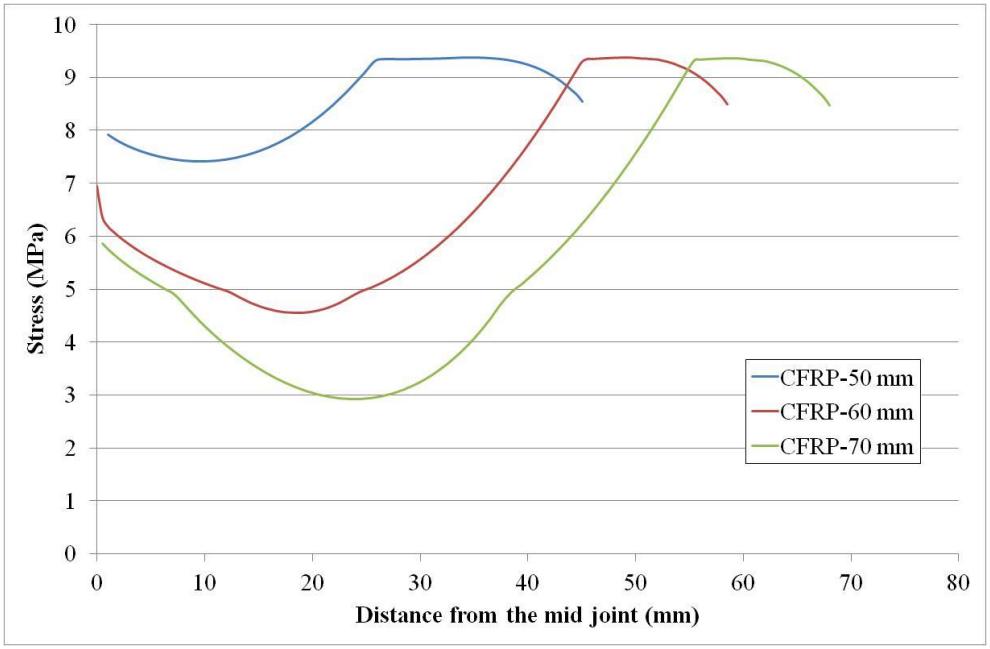

Figure 6.7: Distribution of shear stresses for different CFRP plate lengths at a maximum cyclic load of 30 kN and 40 °C

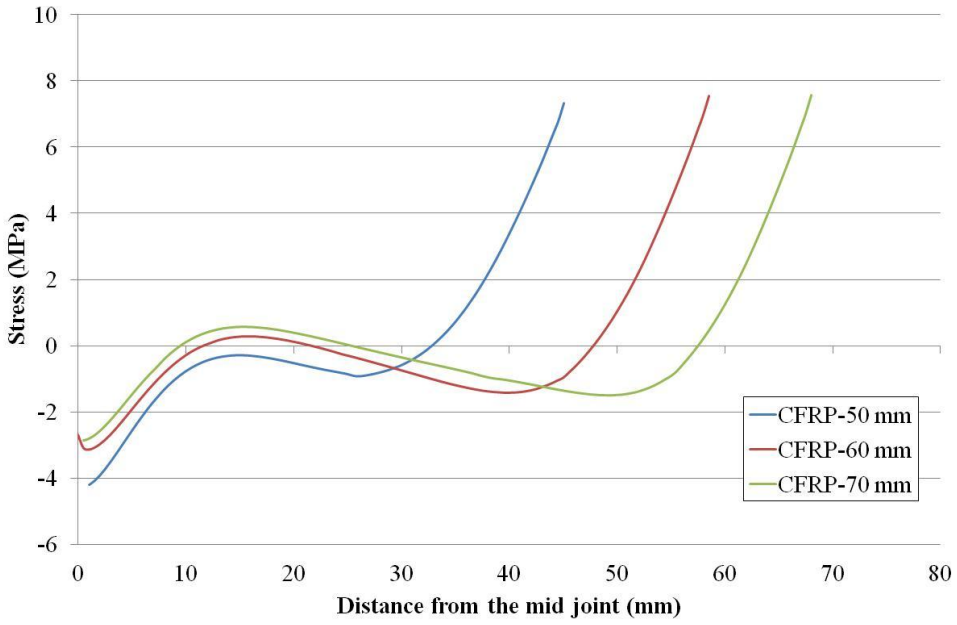

Figure 6.8: Distribution of normal stresses for different CFRP plate lengths at a maximum cyclic load of 30 kN and 40 °C

6.2.2.4 Failure modes

Two types of failure were observed from the fatigue tests of the double-lap shear specimens at different cyclic loading and temperatures. At 24 °C, debonding had occurred at the steel/adhesive and CFRP/adhesive interfaces for specimens subjected to the maximum applied loads of 30 and 40 kN, respectively (see Figure 6.9a). However, failure at the CFRP/adhesive interfaces was observed at 40 °C. The change in the failure mode is due to the change in the adhesive properties and in the distributions of the shear and normal stresses along the bonded joint (as shown in Figures 6.3 to 6.6).

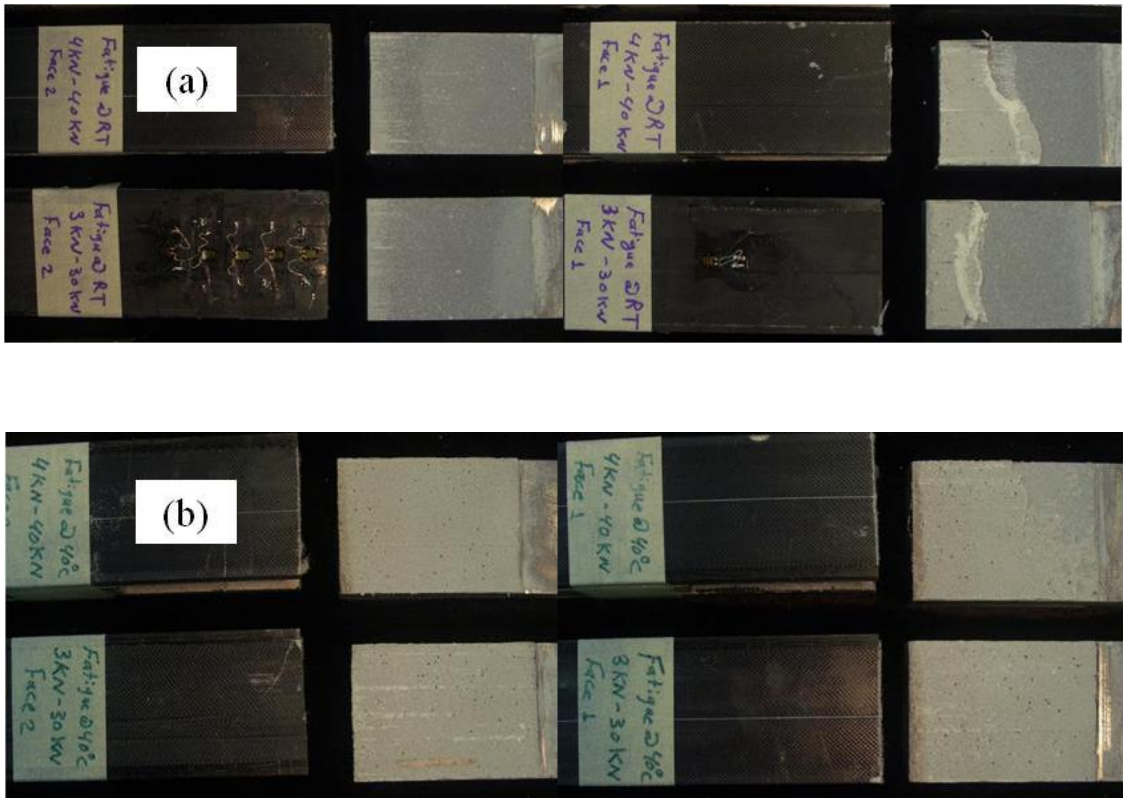

Figure 6.9: Fatigue failure modes for double-lap shear specimens (a) combined at the steel/adhesive and CFRP/adhesive interfaces at 24 °C and (b) at the CFRP/adhesive interface at 40 °C

6.3 Bending test

Three-point bending fatigue tests were carried out on eight steel beams strengthened with CFRP plates at different cyclic loading ranges and temperatures. The specimens were cyclically loaded at constant frequency until the CFRP plate debonding occurred. Three specimens were initially tested at different loading ranges at 20 °C as control specimens, and other specimens were subjected to the same loading ranges at elevated temperatures. The specimens were fabricated in the same way as described in section 4.3.1 in Chapter 4. The length of the CFRP plate chosen in the fatigue test was 600 mm instead of 700 mm due to the higher interfacial stresses at the ends of the shorter plate, since it terminated in regions of a large bending moment. Thus, the test running period till plate debonding was reduced.

Specimens were named in the form of FB N1-N2-T, where the letter 'F' stands for fatigue test, the letter 'B' refers to bending test, the numbers 'N1-N2' denote the minimum and the maximum flexural cyclic applied loads, respectively, and the last number 'T' refers to the testing temperature. For example, FB 5-70-20 represents a fatigue test on a CFRP strengthened steel beam specimen subjected to a minimum and a maximum bending loads of 5 and 70 kN at 20 °C.

6.3.1 Instrumentation and testing

The fatigue tests were carried out using the same servo-hydraulic machine and thermal chamber used in the static test, described in sections 4.3.2 and 4.3.3 in Chapter 4. A schematic of the test setup is shown in Figure 6.10. The load was applied at the mid-span using a pinned support consisting of a steel roller placed in between the steel plates with a counter seat to prevent any loading point movement while the fatigue test was in progress.

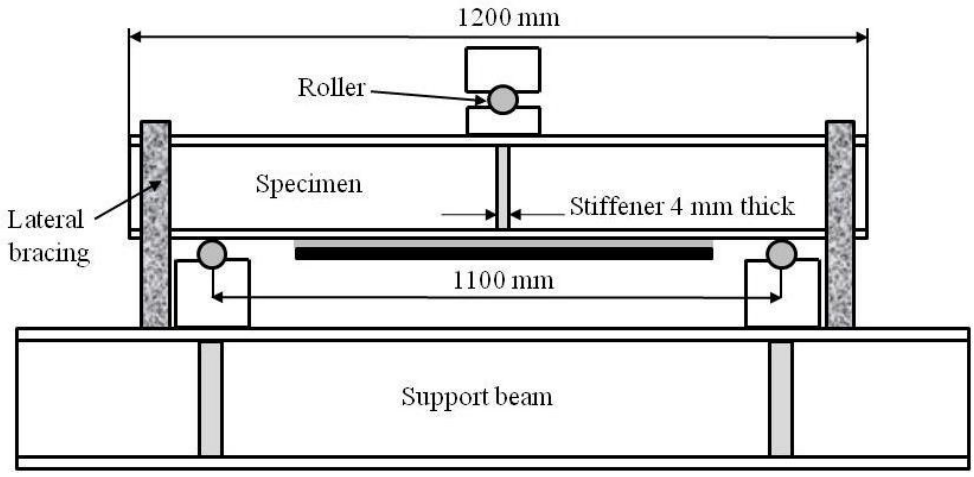

Figure 6.10: A schematic of the three-point bending test setup

Each specimen was bonded with five electrical resistance strain gauges (2 mm long) along the centre line of the CFRP plate to monitor the crack initiation and propagation in the adhesive. Due to the stress concentration at the plate ends, two gauges were mounted at 5 and 15 mm from each plate end, as shown in Figure 6.11. A linear potentiometer was used to measure the deflection at the mid-span, and two thermocouples (T_1 and T_2) were attached to the upper face of the bottom flange to control the temperature along the steel beam (Figure 6.11).

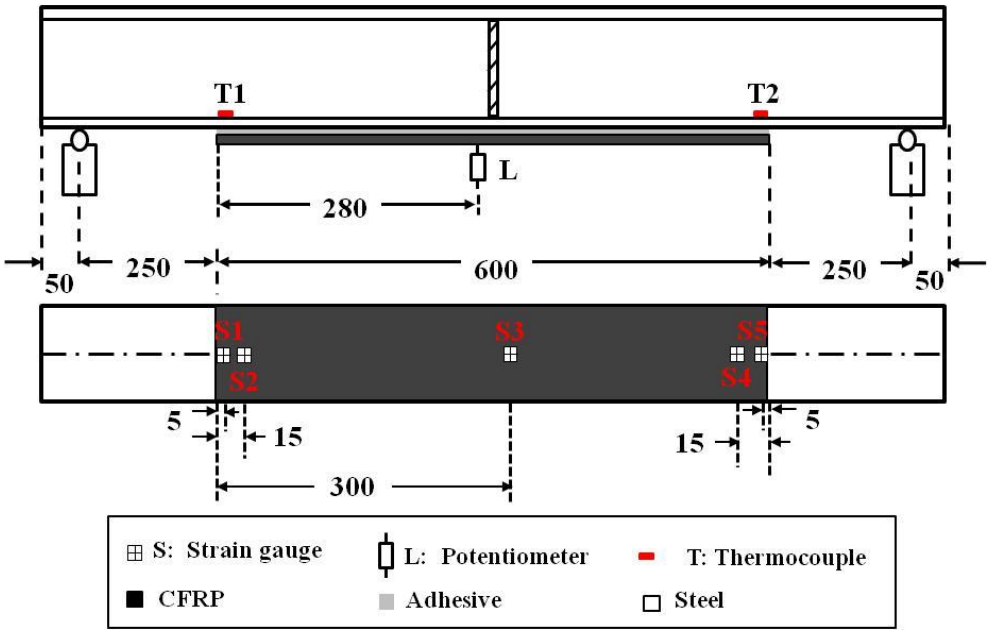

Figure 6.11: Instrumentations on the fatigue test specimen

Each beam was initially loaded with a minimum load of 5 kN to ensure a firm contact between the beam and the supports. The maximum applied loads were 70, 80 and 90 kN which are equivalent to 60, 69 and 78% of the static yielded load of the unstrengthened beam (116 kN, Figure 4.37 in Chapter 4). Tests were carried out at a low frequency of 1 Hz to avoid self heating of the adhesive bond. This frequency was chosen as the vehicle loading rate on highway bridges containing steel decks equivalent to the frequency of 1 Hz [133]. In addition, a beam loaded in flexure at a frequency of 2 Hz was unable to recover fully from one load application before reaching the next [134].

Each specimen was cyclically loaded using sinusoidal waveform in a load control mode until the CFRP plate debonding occurred. Test was frequently paused at different intervals and then three triangular waveform cycles were applied between the minimum and maximum applied loads at frequency of 0.5 Hz. This procedure was used to capture the strains at the maximum and minimum cyclic applied loading accurately, because a sinusoidal wave at a high frequency cannot produce consistent strain values. Figure 6.12 shows that the triangular waveform reached the maximum and minimum loads precisely as the sinusoidal waveform. The average of the maximum strain values was calculated from the three triangular waveform cycles at the maximum applied load. The relationship between the number of cycles and the average values of the maximum strains along the CFRP plate indicated the crack initiation, propagation and

plate debonding. In addition, visual observation was carried out using magnifying glasses at each pause to observe plate end debonding. These pauses were more frequent at the early stages of the cyclic life since the strains changed dramatically with the number of cycles.

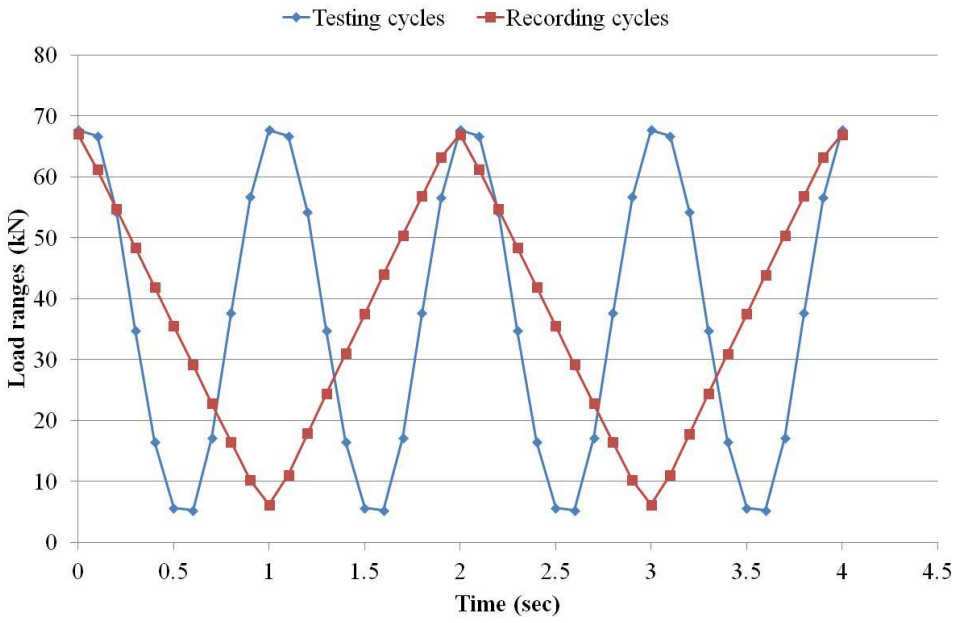

Figure 6.12: Comparison of the testing cycles (sinusoidal wave, 1Hz) and recording cycles (triangular wave, 0.5Hz)

6.3.2 Test results and discussion

6.3.2.1 Monitor cracks initiation and propagation

The initiation and propagation of fatigue cracks in the adhesive between a steel beam and a CFRP plate affects the strain values measured along the CFRP plate. Test results showed that the debonding failure initiated either at one or both plate ends, and then propagated to the mid-plate. Figure 6.13 shows the relation between the maximum strain (the average value obtained from the three triangular waveform cycles at the maximum applied loading) and the number of cycles. The strains (measured by S1 and S5 strain gauges, Figure 4.34) to number of cycle curve can be divided into three stages (Figure 6.13): First, crack initiation stage where the strain increased to the maximum negative value with the number of cycles. Second, crack propagation stage where the maximum strain decreased to a constant value. Finally, plate debonding occurred and the strain value remain constant with number of cycles.

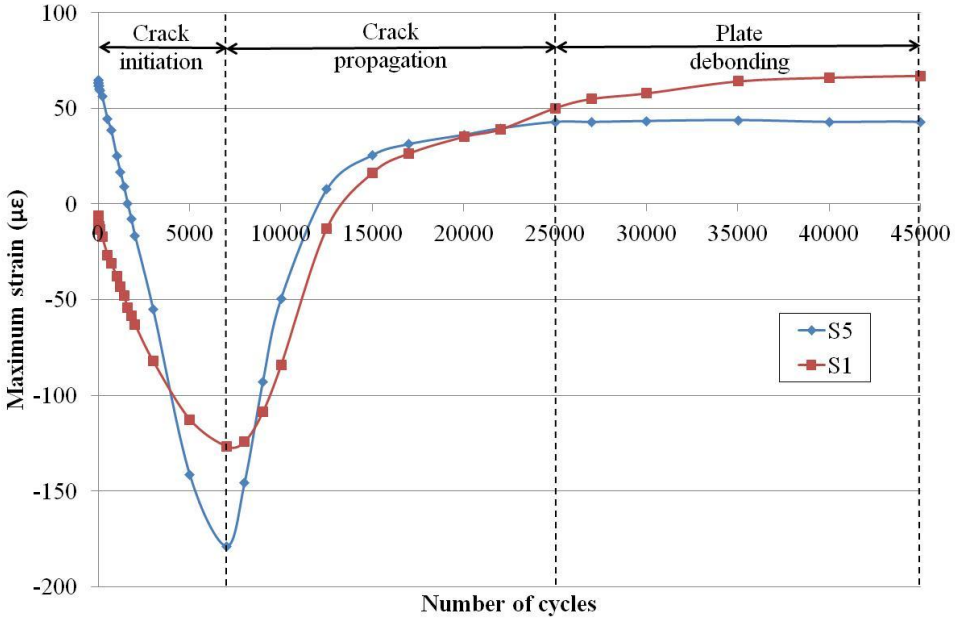

Figure 6.13: A CFRP plate debonding monitored using strain gauges measured at the plate ends of the FB 5-90-20 specimen

The strains measured along the CFRP plates in specimen FB 5-90-20 versus the number of cycle is shown in Figure 6.14. The crack initiated in this specimen at around 7500 cycles measured by strain gauge S5 (Figure 6.14) and grew by 10 mm (measured by strain gauge S4) after 15000 cycles. The crack reached mid-plate after 75000 cycles where the strain measured by the gauge S3 dropped suddenly from the maximum value.

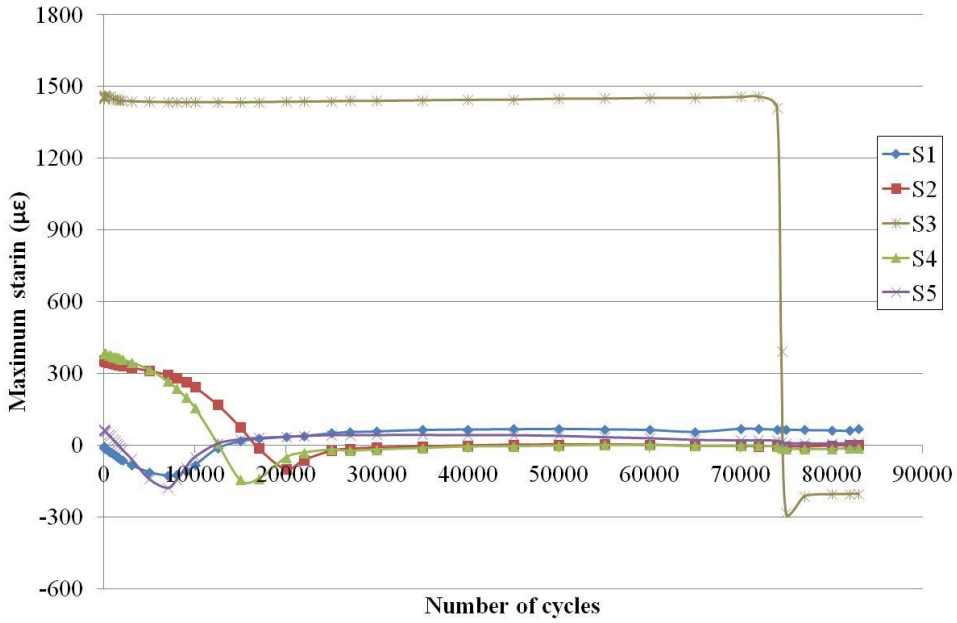

Figure 6.14: Strain measured along the CFRP plate end for the FB 5-90-20 specimen

Increase the applied load reduced the fatigue life of the CFRP strengthened beams at the same temperature, as shown in Figure 6.15. Crack initiating and propagation for specimens tested at different maximum applied loads (70, 80 and 90 kN) at a temperature of 20 °C occurred early at the higher applied load. This is because the higher load increased the stresses in the adhesive at the plate ends from which a longer plastic zone developed (as will be discussed in section 6.3.2.3). The fatigue lives of reinforced beams subjected to the same maximum applied load decreased significantly with increasing temperature, as shown in Figures 6.16 to 6.18. This is due to the reduction in the strength and stiffness of the adhesive with temperature increases thereby increase the length of the plastic zone (as will be discussed in section 6.3.2.3). Thus, the fatigue life of the reinforced beam is dependent upon both the applied load and the temperature, which it was similarly observed for the double-lap shear specimens as discussed previously in section 6.2.2.1.

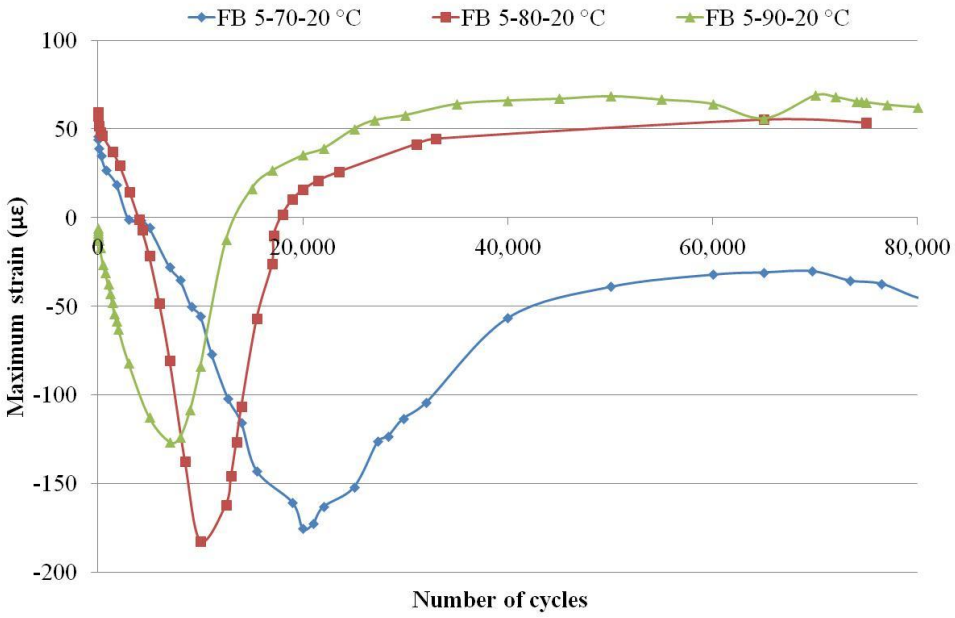

Figure 6.15: Comparison of the strain measured at the plate end for different specimens subjected to different maximum loads of 70, 80 and 90 kN at 20 °C

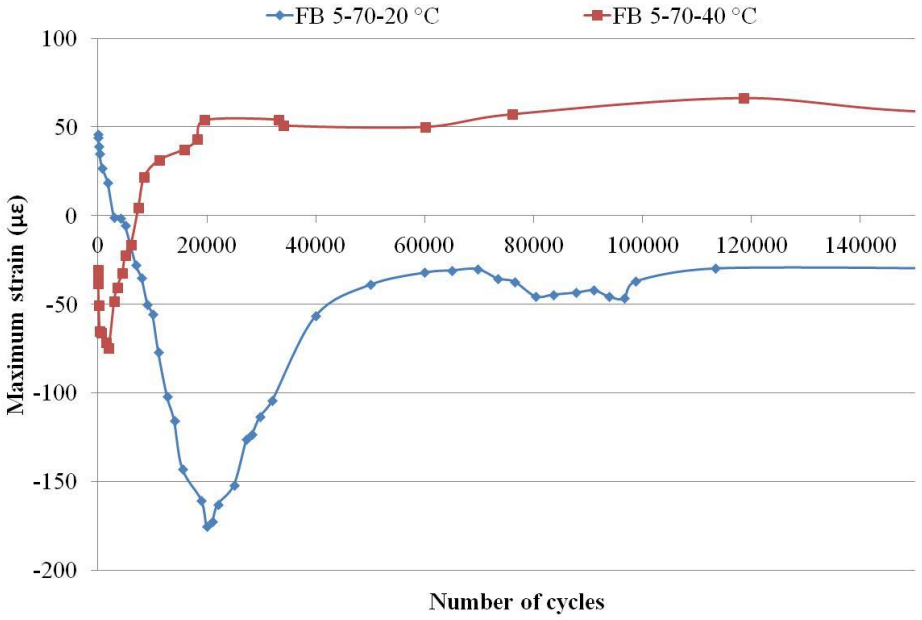

Figure 6.16: Comparison of the strain measured at the plate end for specimens cyclically loaded between 5 to 70 kN at 20 and 40 °C

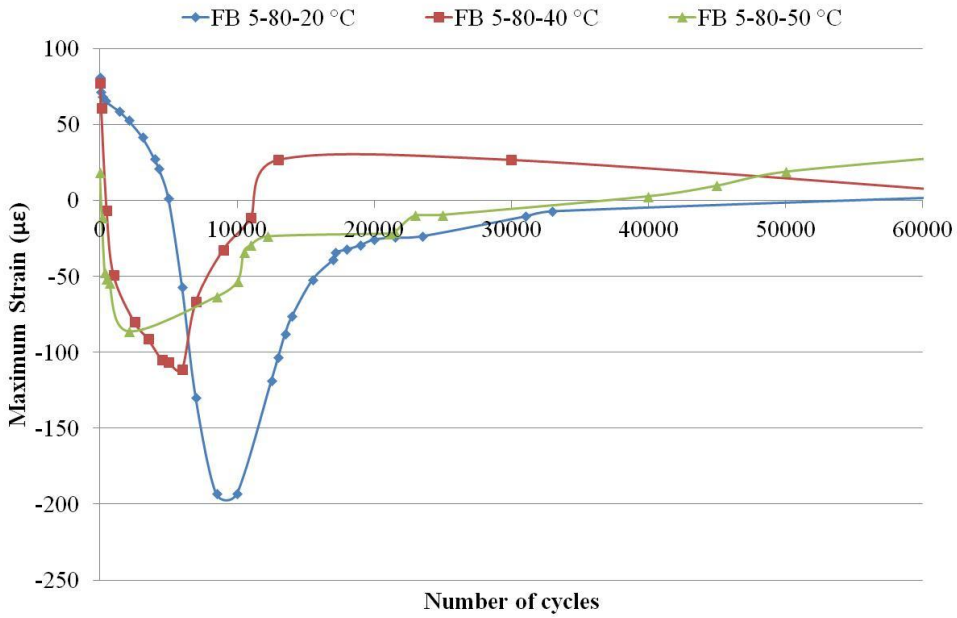

Figure 6.17: Comparison of the strain measured at the plate end for specimens cyclically loaded between 5 to 80 kN at 20, 40 and 50 °C

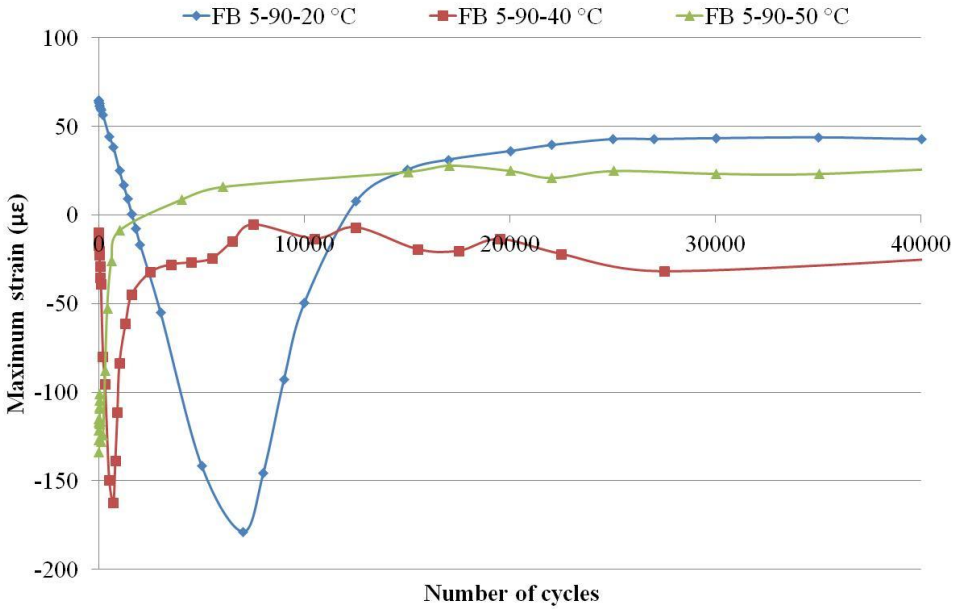

Figure 6.18: Comparison of the strain measured at the plate end for specimens cyclically loaded between 5 to 90 kN at 20, 40 and 50 °C

6.3.2.2 Fatigue life of the CFRP reinforced steel beam specimens

Test results of steel beams strengthened with CFRP plates cyclically loaded at different loading ranges and temperatures are summarised in Table 6.3. The table includes the operating temperatures, the maximum and minimum applied loads, the number of cycles and the crack location. In addition, the reduction in the numbers of cycles at elevated temperatures to that at room temperature at the same cyclic applied load are reported. Test results showed that the fatigue lives of the CFRP reinforced beams decreased by 61 to 76% due to temperature increasing.

Table 6.3: Three-point bending test results

Sample	Temperature °C	Loads ($P_{min} - P_{max}$)/ kN	Number of cycles N	Reduction in number of cycles %	Crack location
FB 5-70-20	20	5-70	66000	/	S5 > S1
FB 5-80-20	20	5-80	33000	/	S5 > S1
FB 5-90-20	20	5-90	25000	/	S5
FB 5-70-40	40	5-70	20000	70	S5 < S1
FB 5-80-40	40	5-80	13000	61	S5
FB 5-90-40	40	5-90	7500	70	S1
FB 5-80-50	50	5-80	11000	67	S5 ≫ S1
FB 5-90-50	50	5-90	6000	76	S5 ≪ S1

The relationship between the maximum applied load and the number of cycles at 20 and 40 °C is shown in Figure 6.19. The fatigue life decreased with the increase in loading levels at the same temperature due to the higher stress concentration in the adhesive bond at plate ends. Regression analysis was used to give the best fit S-N lines at 20 and 40 °C as follow:

$$P_{\max,20^{\circ}C} = 284.7 - 19.42\ln(N) \quad , \quad R^2 = 0.9424 \tag{6.3}$$

$$P_{\max,40^{\circ}C} = 271.4 - 20.29\ln(N) \quad , \quad R^2 = 0.9951 \tag{6.4}$$

where $P_{\max}$ is the maximum applied load and N is the number of cycles. These equations are applied only to the tested CFRP reinforced steel beam specimen's specifications to calculate the fatigue life at different temperatures. According to these equations the x-axis in Figure 6.19 should be in logarithmic scale.

The fatigue life of the reinforced beam decreased with the increase of temperature at the same maximum applied load. Figure 6.20 shows the temperature versus the number of cycle curves for the CFRP strengthened beams tested at the same applied load. Test results indicated that the influence of temperature on the fatigue life is more severe than that of the load e.g. the specimen FB 5-70-20 failed after 66000 cycles while the specimen FB 5-70-40 failed at 20000 cycles when the temperature was increased from 20 to 40 °C. However, the failure occurred at 33000 and 25000 cycles, respectively, when the load level was increased from 80 to 90 kN at 20 °C (specimens FB 5-80-20 and FB 5-90-20). Thus, the combined effects of high stresses and adhesive softening decreased the fatigue life of the reinforced beams significantly.

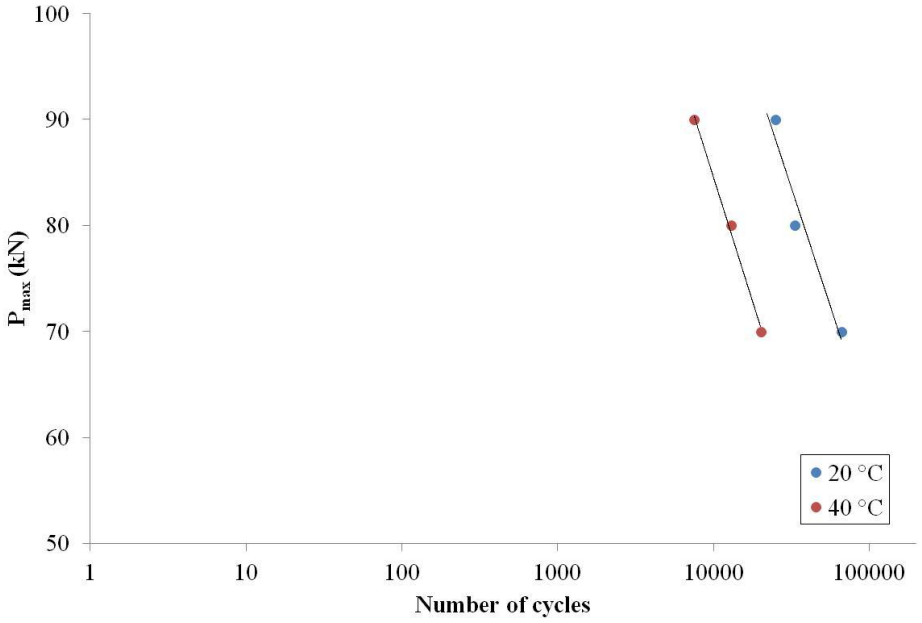

Figure 6.19: The maximum applied load versus the number of cycles curves for a steel beam reinforced with a CFRP plate at different temperatures

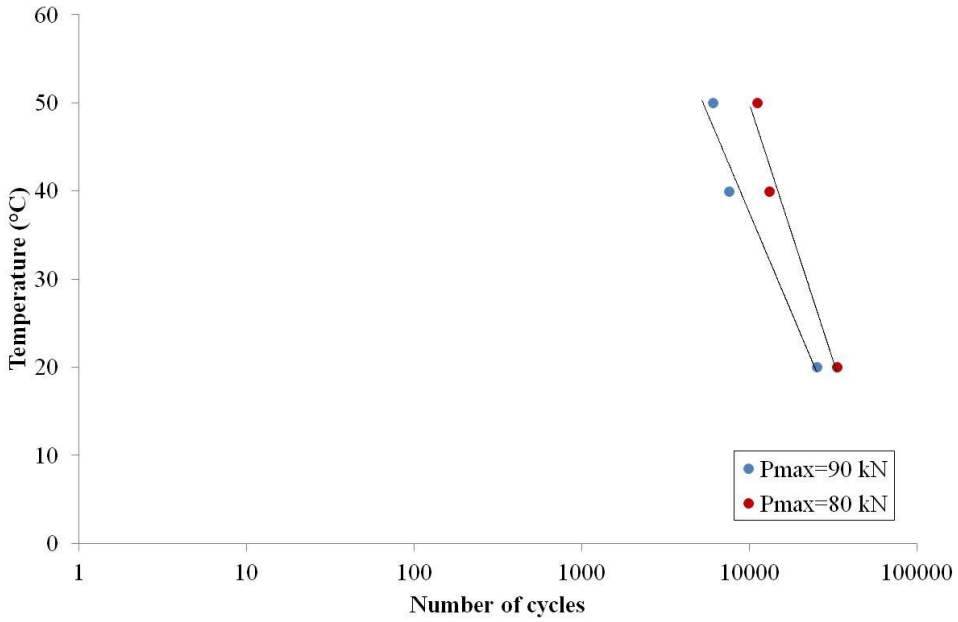

Figure 6.20: Temperature versus number of cycles curves for a steel beam reinforced with a CFRP plate tested at the same loading ranges

6.3.2.3 Stress analysis of the CFRP strengthened steel beam specimens

The distribution of the shear and the normal stresses in the adhesive between the steel beam and the CFRP plate at different applied loads and temperatures were calculated using the FE-model previously discussed in section 5.2.2 in Chapter 5. Figures 6.21 to 6.22 show the distributions of the shear and the normal stresses with a maximum applied load of 70 kN at 20, 40 and 50 °C. The shear stresses at the plate end exceeded the adhesive elastic limitation thus the plastic zones were created. The length of the plastic zone (Figure 6.21) increased with the increase of temperature at the same applied load due to the adhesive softening hence the fatigue life of the reinforced beam decreased.

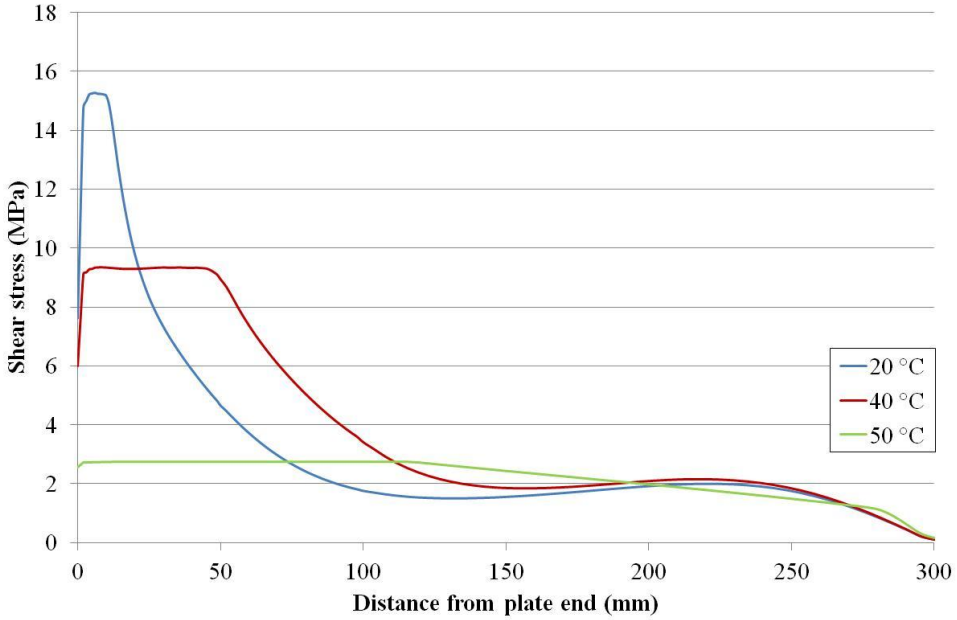

Figure 6.21: Distribution of shear stresses with a maximum applied load of 70 kN at different temperatures

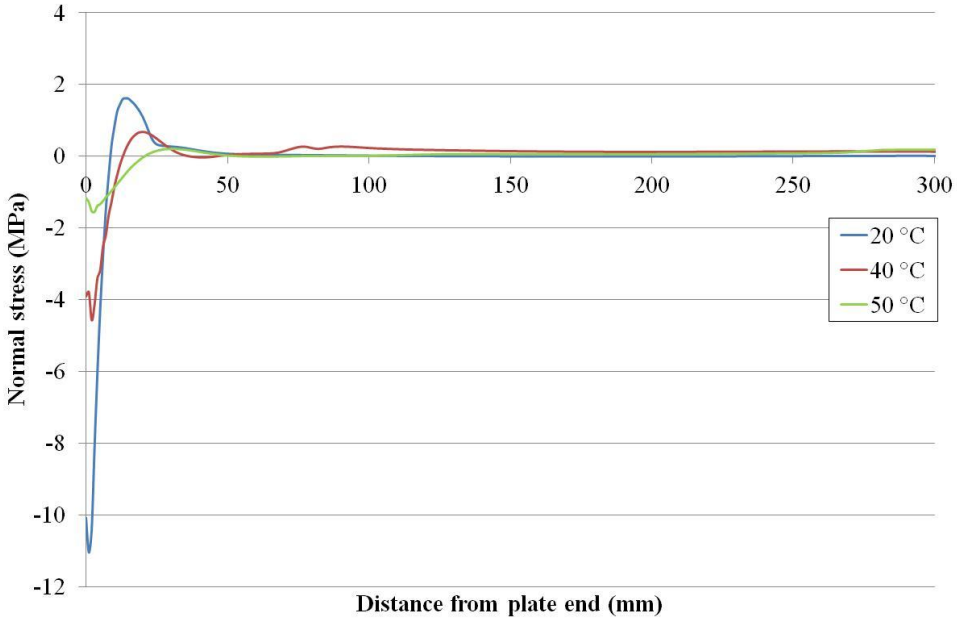

Figure 6.22: Distribution of normal stresses with a maximum applied load of 70 kN at different temperatures

6.3.2.4 Beam stiffness

The deflection values measured at the mid-span for the FB 5-70-20 specimen versus the number of cycles is shown in Figure 6.23. No change in the deflection observed after plate debonding because the elastic modulus of the CFRP plate was lower than that of the steel. Other specimens showed similar behaviour.

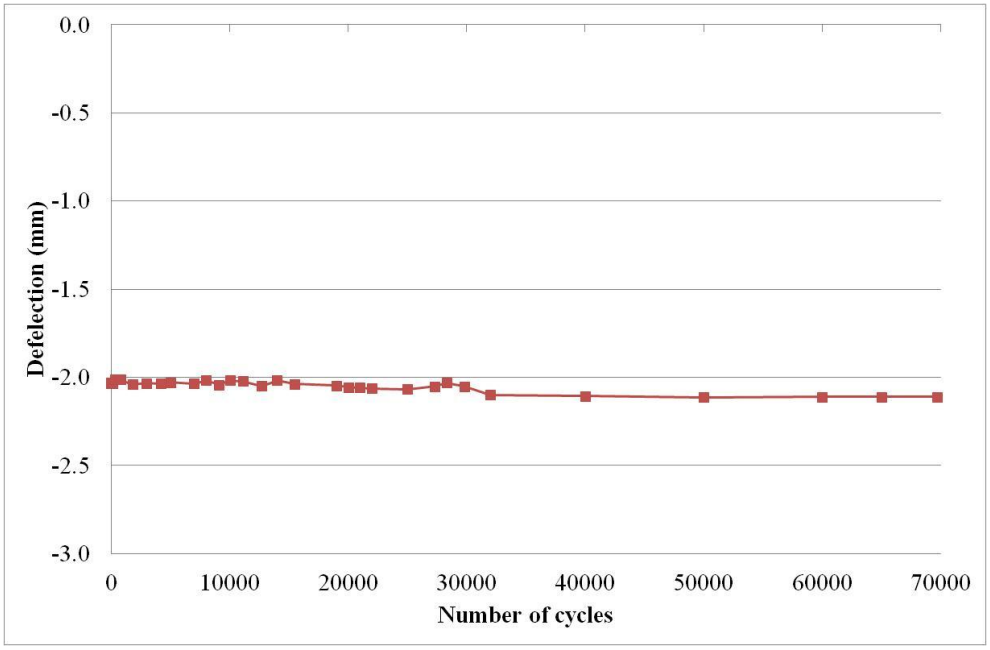

Figure 6.23: Deflection values measured at the mid-span for the FB 5-70-20 specimen

6.4 Conclusion

In this chapter, fatigue tests were carried out on both double-lap shear specimens and CFRP reinforced beams subjected to different cyclic applied loading ranges and temperatures. In addition, FE analyses were conducted to indicate the distribution of the shear and normal stresses in the adhesive and to determine the stress concentration zone (plastic zone) at the adherends discontinuity.

It was found that the fatigue life of the double-lap shear specimens was reduced with increasing both the load and the temperature. Increase the temperature to 40 °C decreased the fatigue life of the bonded joint within a range of 84-97%. However, Increase the bonded joint length from 50 to 70 mm increased the fatigue life even at elevated temperature. FE analyses on the double-lap shear joint showed that a longer plastic zone developed at the plate end when the temperature increased thus the fatigue life reduced. However, increasing the bonded joint length reduced the average shear stress along the bonded and the length of the plastic zone thereby the joint fatigue life increased.

The fatigue lives of CFRP reinforced beams decreased in the range 61-76% due to increase the temperature to around T_g . Strain gauges mounted along the CFRP plate were able to monitor the deterioration of the fatigue life of the strengthened beam. The strain versus the number of cycle curves indicated three stages to complete CFRP plate debonding. The length of the plastic zone at the plate end obtained from FE analyses increased with increase the temperature at the same applied load thus the fatigue lives of the reinforced beams were significantly reduced.

The relationship between the load versus the number of cycles at different temperatures for both the double-lap shear specimens and the reinforced beams obtained from the test results were given.

Chapter 7 Conclusions, recommendations and future work

7.1 Conclusions

The aim of this research is to evaluate the effects of temperature on the strength and the fatigue life of steel beams reinforced with CFRP plates. In this research, the properties of the adhesive materials were first obtained experimentally at temperature ranges from 20 to 60 °C. Static and fatigue tests were then carried out on double-lap shear specimens and CFRP reinforced beams within this temperature range. These were followed by analytical and FE analyses which calculate the interfacial stresses developed in the adhesive between the steel beam and the CFRP plate under different loading levels and temperatures. The research findings concluded the following:

- The effect of temperature up to 60 °C on CFRP and adhesive materials obtained experimentally showed that the CFRP mechanical properties were not affected because the CFRP matrix softened when the temperature exceeded 190 °C. However, the strength and stiffness of Sikadur-30 adhesive were significantly reduced at the glass transition temperature T_g . The T_g value obtained from the relation between the elastic modulus and the temperature was about 43 °C. In addition, the stress-strain curves of the adhesive changed from linear to nonlinear with temperature increase. The nonlinear curve was approximated as a bilinear elastic-plastic representation in the FE analyses of double-lap shear joints and CFRP reinforced beams. Plastic zones were found to be developed at the plate ends due to stress concentrations.

- The strength of double-lap shear joints was reduced by about 23% at T_g compared to that at 24 °C. Also the fatigue lives of the bonded joints were reduced by an average of 90 % when the temperature was increased from 20 °C to 40 °C. However, the fatigue life of the bonded joints at 40 °C was increased by extending the CFRP plate length. FE analyses on the double-lap shear joints showed that the reductions in the joint strength and fatigue life with the temperature increase were due to a reduction in the adhesive strengths, hence a longer plastic zone developed at the plate end at the same applied load. However, increasing the bonded joint length reduced the average shear stress along the bonded and the length of the plastic zone thereby increasing the

joint fatigue life. It has also found that the failure load of the bonded joint was not only temperature dependent but also time dependent due to the creep behaviour of the adhesive polymer. Finally, the failure mode changed from combined failures between steel/adhesive and CFRP/adhesive interfaces at 24 °C to just CFRP/adhesive interfaces failure at 60 °C.

- The flexural capacities of the CFRP reinforced beams increased with the length of the plate at 20 °C. This is because a longer plate reduced the bending moment at the plate ends and thus the stresses at theses ends were reduced. Although the flexural capacity of a steel beam reinforced with 700 mm CFRP plate was 35% higher compared to the unstrengthened beam, this increase in capacity was about 50% when the temperature increase to around T_g. The fatigue life of the reinforced beam decreased with increasing either the load or the temperature. Increase the temperature from 20 °C to around T_g reduced the fatigue life by an average of 67%. Stress analyses showed that the length of the plastic zone at the plate end increased with an increase in the temperature and the load, thus the strength and the fatigue life of CFRP reinforced beams were significantly reduced. In addition, the failure mode changed from CFRP/adhesive interface failure at 24 °C to steel/adhesive interface failure at 60 °C.

- The interfacial shear and normal stresses in the adhesive between a steel beam and a CFRP composite were calculated using analytical and FE models. The analytical model proposed by Deng et al. [11] was modified to consider the temperature dependency of the adhesive properties. The shear and the normal stresses obtained from that model terminated at the maximum adhesive shear and normal strengths calculated from the FE analysis on the double-lap shear joint, hence the length of plastic zones from the plate ends were determined analytically. FE analyses on CFRP strengthened beams determined the length of the plastic zone more accurately than the analytical model since it approximated the adhesive nonlinear stress-strain behaviours at elevated temperatures with bilinear elastic curves. The analysis showed that the plastic zone was increased if the stiffness and the thickness of the CFRP plates were increased. Also, a higher applied load caused higher interfacial shear stresses at the ends of a shorter plate which resulted in increasing of the length of the plastic zone. Increase the temperature at the same applied load increased the length of the plastic zone due to the softening of the adhesive. However, increase the plate length reduced significantly the length of the plastic zone even at temperatures above

the T_g . Thus, the analyses showed that it is possible to avoid CFRP plate debonding at high temperatures by using a longer CFRP plate.

7.2 Recommendations

The findings obtained from this research suggested the following:

It has been experimentally and analytically proven that an increase in the length of the CFRP plate to a lower bending moment region will mitigate the effect of adhesive softening due to temperature elevation on the strength and the fatigue life of a bonded joint and a reinforced beam. Therefore it is recommended that the CFRP plate lengths for reinforcing steel beams exposed to high temperatures should be extended by 30% compared to those exposed to 20 °C. It is also suggested to use an adhesive with a glass transition temperature (T_g) that exceeded the maximum expected structural temperature by at least 15 °C, which agreed with the design guidance recommendation given in CIRIA C595 report [27].

7.3 Future works

- This research was conducted on limited number of testing specimens using a normal modulus CFRP composite and one type of adhesive. Further investigations are required to consider different types of adhesive and using ultra high modulus CFRP composites which have higher elastic modulus than steel.
- The creep behaviour of the steel beams strengthened with CFRP composites at elevated temperatures should be experimentally examined. In addition, cycles of both the temperature and the loads for CFRP reinforced beams should be experimentally investigated as it simulates better the behaviour of the real structures exposed to continuous traffics and daily temperature changes.
- The temperature dependency of the adhesive material was considered in the current stress analysis of a steel beam strengthened with a CFRP composite. But their time and the temperature dependency on the interfacial stresses requires investigation to avoid creep failures.

Appendices

Appendix A: Tensile test on steel dogbone specimens

The tensile tests were carried out on dogbone steel specimens to determine the elastic modulus, the yield strain and the yield and ultimate strength. Test followed recommendations in the standard BS EN ISO 6892-1:2009 [116]. Three specimens, with serial numbers F1, F2 and F3 , were cut from the flange of a universal steel beam 127×76UB13 and manufactured to the specified dimensions as shown in Figure A.1.

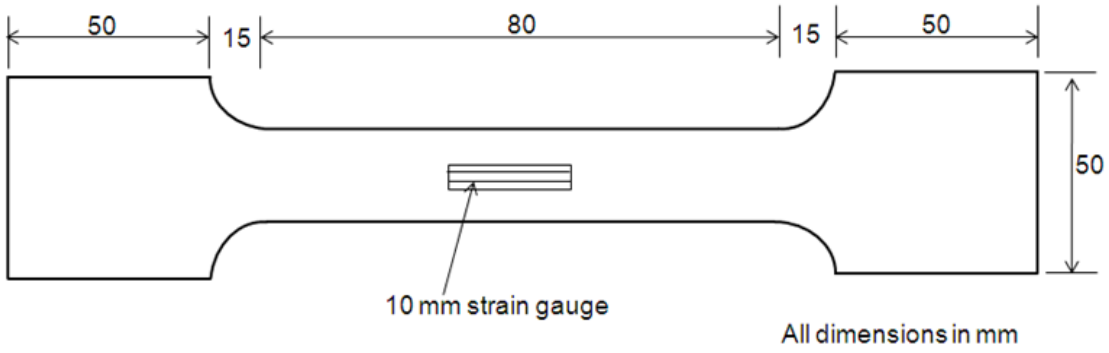

Figure A.1: Dimensions of steel dogbone specimen

Calculations:

The width (W), the thickness (t) and the sectional area (A) in the middle of each specimen were measured by a vernier caliper and reported in Table 3.1 in Chapter 3. The yield strength σ_y, and the ultimate tensile strength σ_u are given by Eq. (A.1):

$$\sigma = \frac{F}{A} \tag{A.1}$$

where F is the yield tensile load F_y or the ultimate tensile load F_u.

The elastic modulus, E_s, is given by Eq. (A.2):

$$E_s = \frac{\sigma_2 - \sigma_1}{\varepsilon_2 - \varepsilon_1} \qquad \text{A.2}$$

where σ_1 and σ_2 are the stresses measured at the strain values of ε_1=0.0005 and ε_2=0.0015, respectively. Test results of the three specimens are presented in Table 3.1 in Chapter 3.

Appendix B: CFRP plates manufacturing

The CFRP, 750×450 mm dimensions, panels were made by stacking seven layers of MTM46 prepreg unidirectional laminate 0.5 mm thick. The Initial cure was done using an autoclave under a controlled temperature and pressure of 120 °C and 6.2 bars, respectively. The manufacturer recommends a post curing at 180 °C to obtain the maximum mechanical properties and T_g [82]. The technique used to prepare the CFRP plates is as follows:

- The roll of MTM46 prepreg was taken out of the freezer in a sufficient time (at least 24 hours) to allow them to thaw and reach the room temperature,
- The prepreg laminates cut to the required length,
- Aluminium mould sprayed with three layers of bond release coat, and then prepreg laminates, peel ply layers, release film, breather and vacuum bag assembled as shown in Figure B.1,
- Temperature increased at a rate of 2 °C/min from ambient to 120 °C, consequently autoclave pressure elevated to 6.2 bar,
- The temperature and the pressure were held for 1 hour, and then specimen post cured at temperature of 180 °C for another 1 hour,
- Specimen temperature reduced at a rate of 3 °C/min to room temperature, before the vacuum bag released.

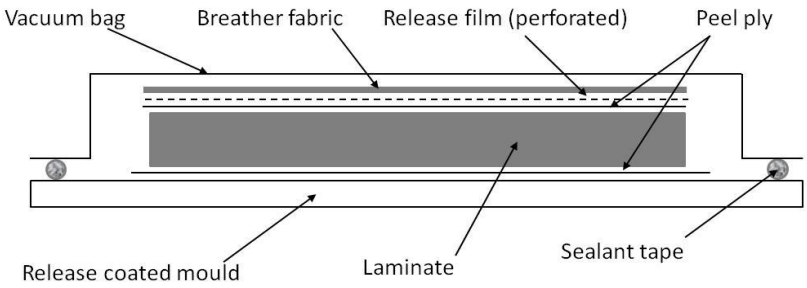

Figure B.1: Laminate bagging arrangement

Appendix C: Tensile tests on unidirectional CFRP specimens

The Tensile test on the CFRP specimens was made to obtain the elastic modulus and the ultimate tensile strength in the longitudinal fibre direction. Test was conducted according to the recommendations in the standard BS EN ISO 575-5:2009 at 23, 30, 40, 45, 50 and 60 °C. Specimens were cut to the specified dimensions (Figure C.1) from CFRP panel with a band saw and the specimens' edges were finished smoothly using sand papers. The width (W) and the thickness (t) in the middle of the specimen were measured by using a vernier caliper and presented in Table C.1.

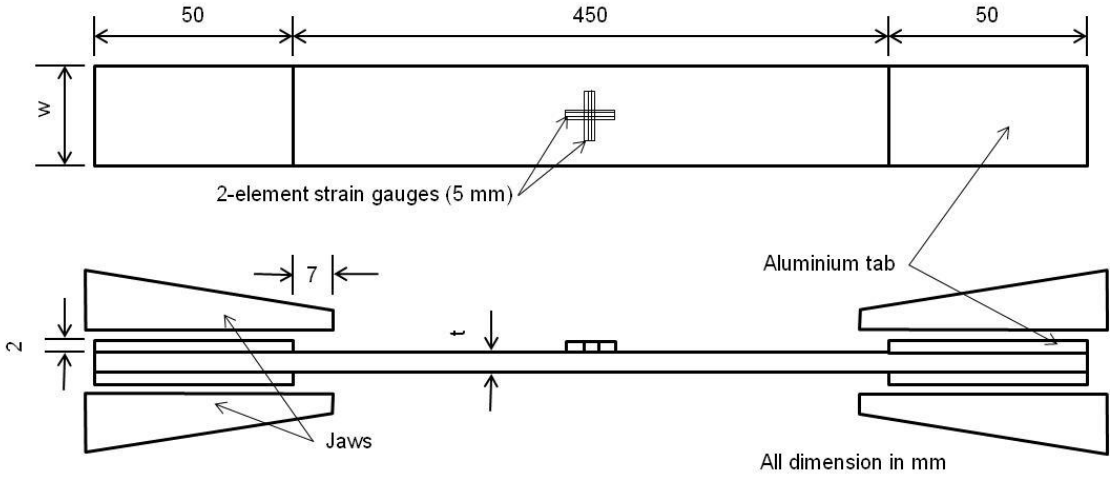

Figure C.1: CFRP specimen dimensions and strain gauges length

Calculations:

The ultimate tensile stress (σ_p) was calculated from Eq. (C.1):

$$\sigma_p = \frac{F_p}{A} \qquad \text{C.1}$$

where F_p is the failure load and A is the cross sectional area.

The elastic modulus (E_p) was calculated by Eq. (C.2):

$$E_p = \frac{\sigma_2 - \sigma_1}{\varepsilon_2 - \varepsilon_1} \qquad \text{C.2}$$

Where σ_1 and σ_2 are the stresses measured at the strain values of ε_1 =0.0005 and ε_2 =0.0025 respectively. Values of the elastic modulus and the ultimate tensile strength are summarised in Table C.1.

Table C.1: Dimensions and mechanical properties of the CFRP specimens.

Sample	Temp. (°C)	W (mm)	t (mm)	A (mm^2)	F_p (kN)	ε_u ($\mu\varepsilon$)	σ_p (MPa)	E_p (GPa)
CFRP 1	23	14.73	3.16	46.55	48.83	7996.62	1049.10	125.55
CFRP 2	23	14.77	3.22	47.56	49.01	8185.51	1030.52	121.78
CFRP 3	30	15.11	3.51	53.04	58.55	9402.21	1103.90	111.24
CFRP 4	30	14.62	3.43	50.15	63.51	/	1266.58	97.73
CFRP 5	30	15.52	3.68	57.11	67.21	11589.82	1176.84	94.16
CFRP 6	30	15.97	3.26	52.06	69.16	10175.02	1328.37	124.88
CFRP 7	40	14.41	3.16	45.54	64.16	11864.38	1409.05	109.74
CFRP 8	40	14.32	3.19	45.68	67.31	12742.50	1473.39	105.34
CFRP 9	40	16.03	3.32	53.22	63.65	9551.44	1196.02	118.16
CFRP 10	40	15.63	3.3	51.58	67.88	10315.25	1315.94	122.40
CFRP 11	45	15.18	3.3	50.09	73.62	13319.13	1469.41	110.82
CFRP 12	45	14.39	3.29	47.34	61.76	/	1304.58	107.01
CFRP 13	45	16	3.3	52.80	65.95	9450.74	1249.12	125.53
CFRP 14	45	15.93	3.31	52.73	67.19	10340.38	1274.28	125.03
CFRP 15	50	15.93	3.31	52.73	67.74	10288.55	1284.70	118.52
CFRP 16	50	16.02	3.37	53.99	71.12	11652.11	1317.35	105.61
CFRP 17	50	15.37	3.3	50.72	67.20	10158.01	1324.96	122.28
CFRP 18	60	14.77	3.22	47.56	71.55	11653.66	1504.50	123.83
CFRP 19	60	15.73	3.21	50.49	70.07	11060.66	1387.76	121.05
CFRP 20	60	15.83	3.31	52.40	63.88	9691.90	1219.10	119.32

Appendix D: Tensile test on bulk adhesive dogbone specimens

Bulk adhesive dogbone specimens were fabricated using silicon mould, as described in section 3.4.1.1 in Chapter 3. Specimens were tested in tension, according to the recommendations in the standard BS EN ISO 527-2 [123], to determine their elastic modulus, ultimate tensile strength and Poisson's ratio. Tests were performed 20, 30, 40, 45, 50 and 60 °C. Specimen held at that temperature for 15 minutes before loading to reach thermal stabilisation. The load was applied in a displacement control mode at a rate of 1 mm/min. Strains in the longitudinal and transverse directions were recorded by 2 mm long rosette strain gauges mounted to each specimen. The width (W) and the thickness (t) at the middle of each specimen were measured by a vernier caliper and summarised in Table D.1. Figure D.1 shows the stress-strain curves of adhesive specimens at different temperatures.

Calculation:

The adhesive tensile strength (σ_a) was calculated by Eq. (D.1):

$$\sigma_a = \frac{F_a}{A} \tag{D.1}$$

where F_a is the failure load and A is the cross sectional area.

The Young's modulus (E_a) was calculated by Eq. (D.2):

$$E_a = \frac{\sigma_2 - \sigma_1}{\varepsilon_2 - \varepsilon_1} \tag{D.2}$$

where σ_1 and σ_2 are the stresses measured at the strain values of ε_1=0.0005 and ε_2=0.0025 respectively.

At elevated temperatures, the Young's modulus was calculated from the slop of the stress-strain polynomial fitted curve at the origin.

The Poisson's ratio was calculated by Eq. (D.3):

$$\nu_a = \frac{\varepsilon_T}{\varepsilon_L} \qquad \text{D.3}$$

Where ε_T and ε_L are the strains in the transverse and the longitudinal directions, respectively, measured by strain gauges.

Table D.1: Dimensions and mechanical properties of the Sikadur-30 adhesive.

Sample	Temp. (°C)	W (mm)	t (mm)	A (mm2)	F_a (kN)	ε_a ($\mu\varepsilon$)	σ_a (MPa)	E_a (GPa)
S1	20	14.81	6.25	92.56	2.83	2814.02	30.61	10.85
S2	20	15.00	6.20	93.00	2.91	2474.39	31.34	12.90
S3	20	14.59	6.30	91.92	2.36	1938.44	25.68	12.87
S4	20	14.97	6.64	99.40	2.26	2383.15	22.77	11.62
S5	30	14.68	6.12	89.84	2.34	2496.42	26.05	12.60
S6	30	15.42	6.66	102.70	2.38	2001.22	23.19	10.31
S7	30	15.40	6.23	95.94	2.65	3401.68	27.63	12.45
S8	40	15.05	6.59	99.18	1.44	1722.56	14.53	10.41
S9	40	15.05	6.15	92.56	1.98	3119.83	21.37	10.32
S10	40	14.36	6.06	87.02	1.27	1781.48	14.63	10.38
S11	40	15.35	6.04	92.71	1.35	/	14.58	10.02
S12	45	14.83	6.80	100.84	0.84	/	8.35	0.93
S13	50	14.75	6.22	91.75	0.45	72703.70	4.89	0.32
S14	50	14.54	5.83	84.77	0.47	79384.55	5.56	0.39
S15	50	14.55	6.31	91.81	0.51	84617.57	5.60	0.38
S16	60	14.56	6.28	91.44	0.27	44698.72	2.97	0.16
S17	60	14.51	6.26	90.83	0.24	28311.82	2.68	0.20
S18	60	15.88	6.02	95.60	0.28	43345.10	2.97	0.20

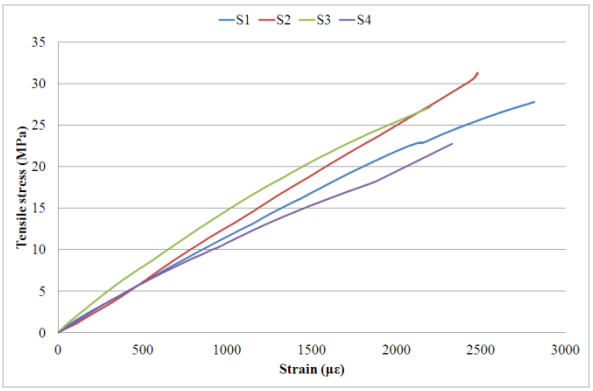

(a) T=20 °C

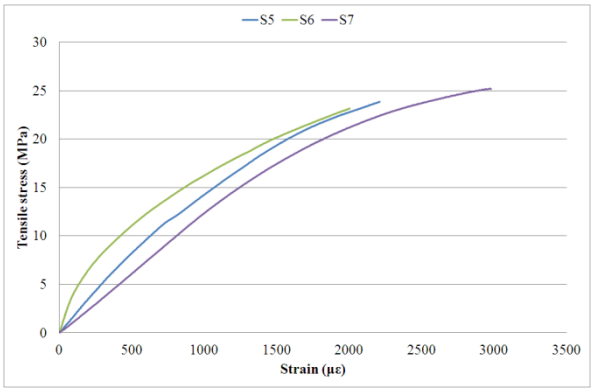

(b) T=30 °C

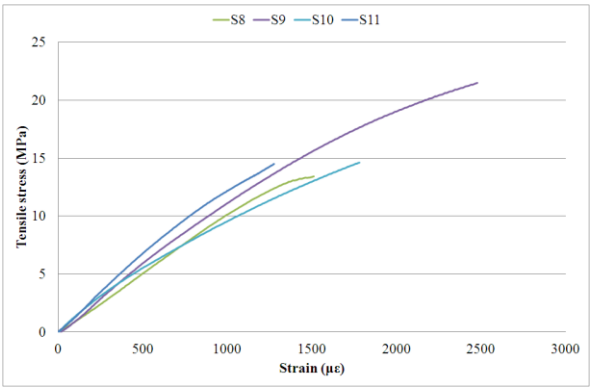

(c) T=40 °C

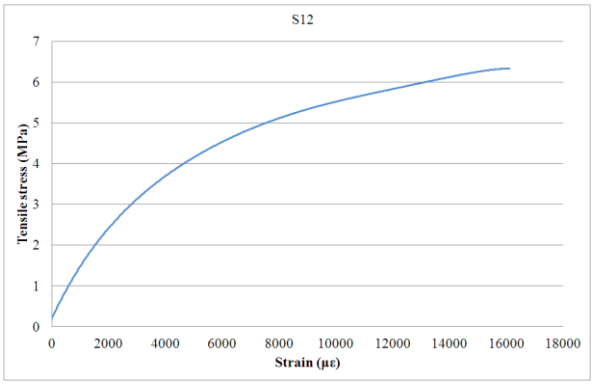

(d) T=45 °C

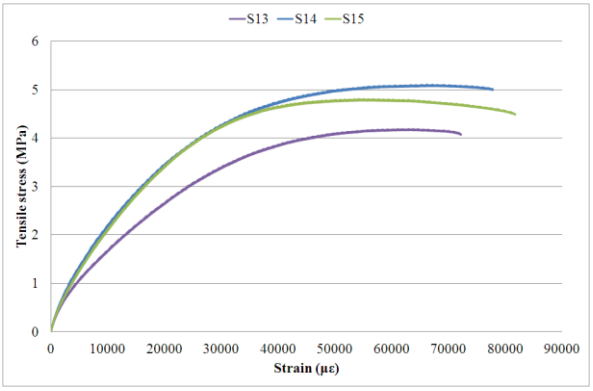

(e) T=50 °C

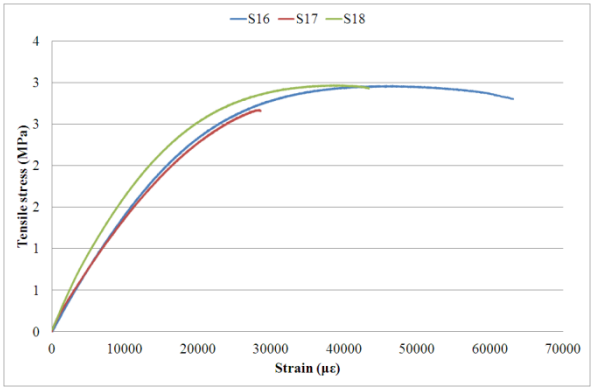

(f) T=60 °C

Figure D.1: Stress-strain curves for Sikadur-30 adhesive tension specimens at different temperatures.

Appendix E: Strains distributions along CFRP plate and mid span beam at different load levels and temperatures for all specimens

Steel beam strengthened with 450 mm CFRP and tested at 20 °C (SB 450-20)

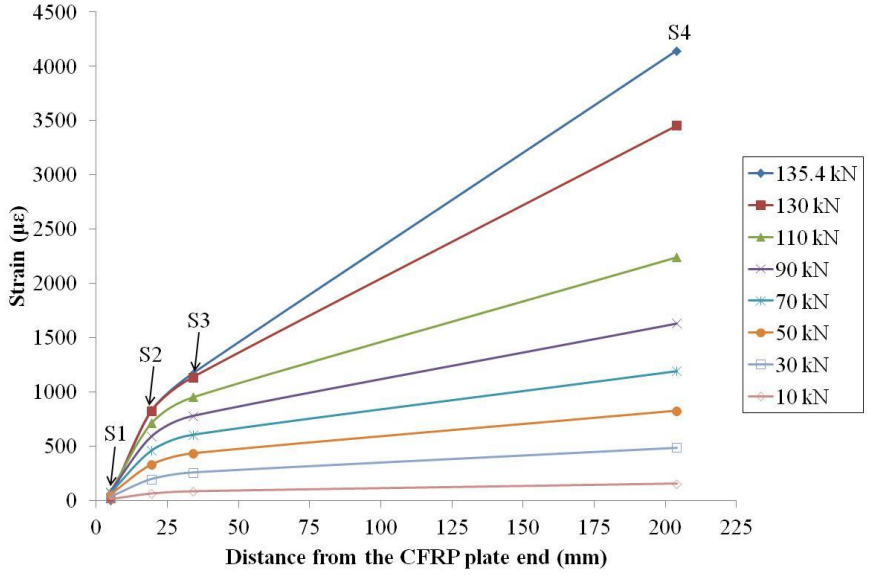

Figure E.1: Strain distribution along CFRP plate at different load levels for SB450-20 specimen

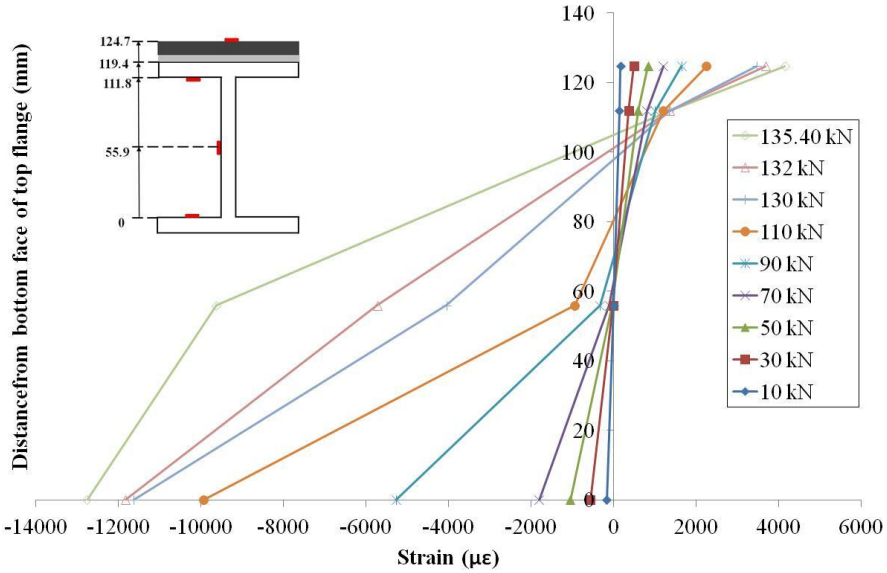

Figure E.2: Strain distribution across the middle of SB450-20 specimen at different load levels

Steel beam strengthened with 600 mm CFRP and tested at 20 °C (SB600-20)

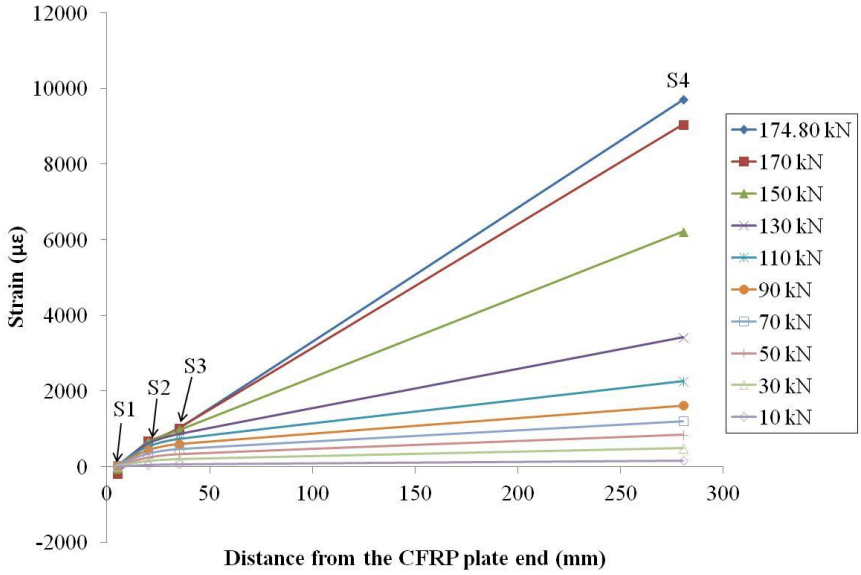

Figure E.3: Strain distribution along CFRP plate at different load levels for SB600-20 specimen

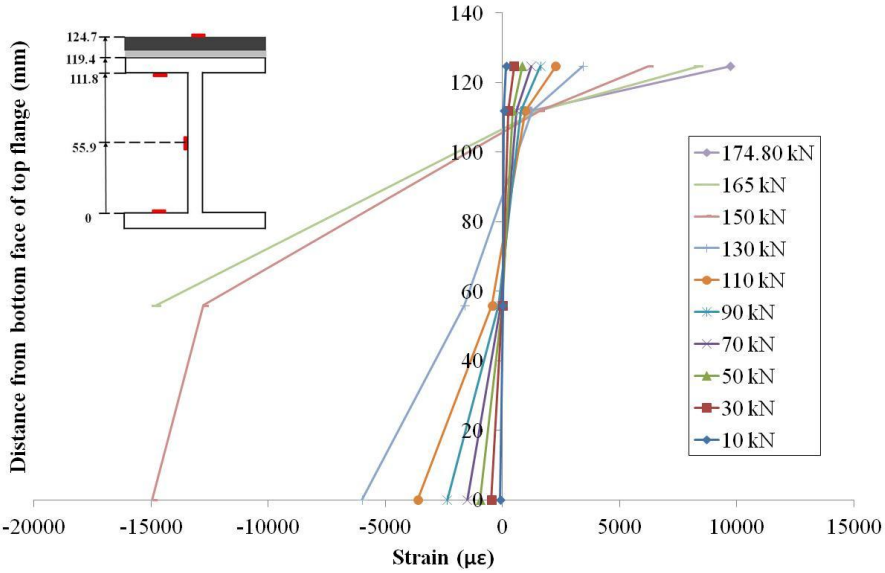

Figure E.4: Strain distribution across the middle of SB600-20 specimen at different load levels

Steel beam strengthened with 700 mm CFRP and tested at 42 °C (SB 700-42)

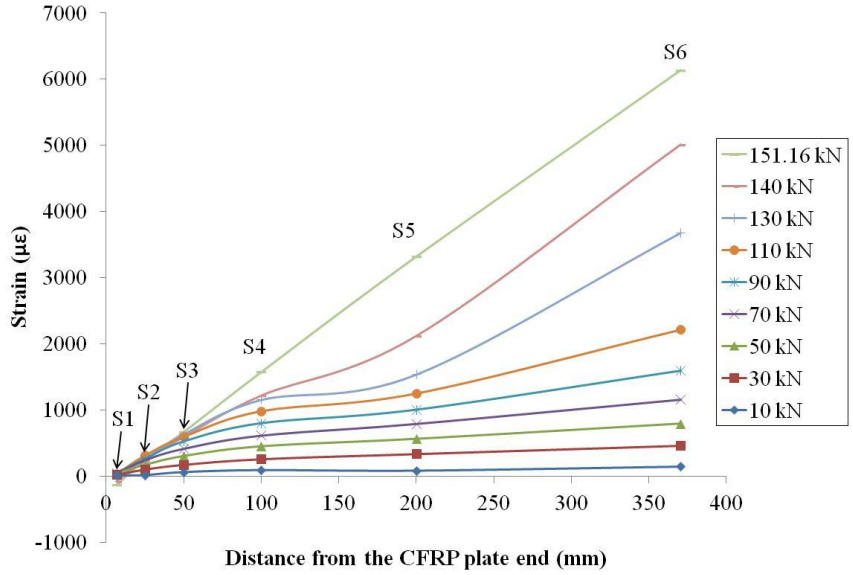

Figure E.5: Strain distribution along CFRP plate at different load levels for SB700-40 specimen

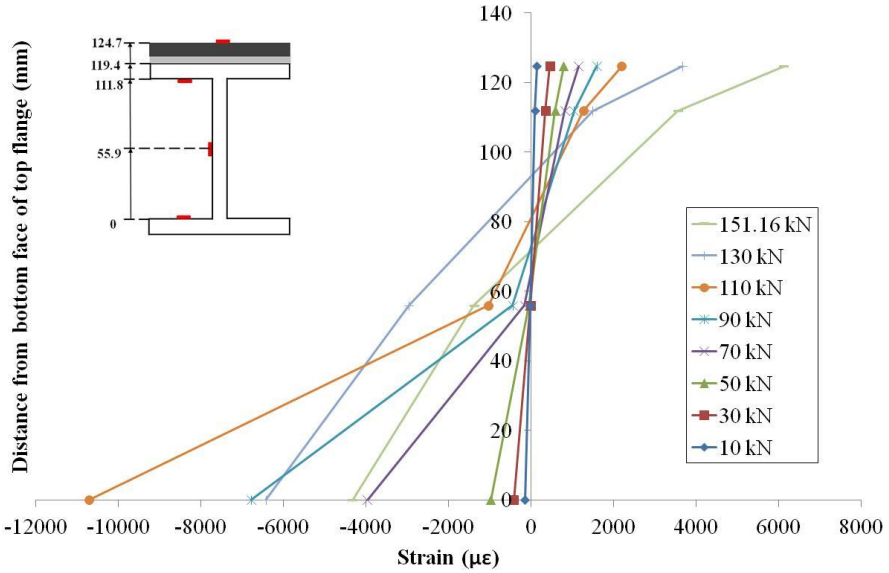

Figure E.6: Strain distribution across the middle of SB700-42 specimen at different load levels

Steel beam strengthened with 700 mm CFRP and tested at 45 °C (SB 700-45)

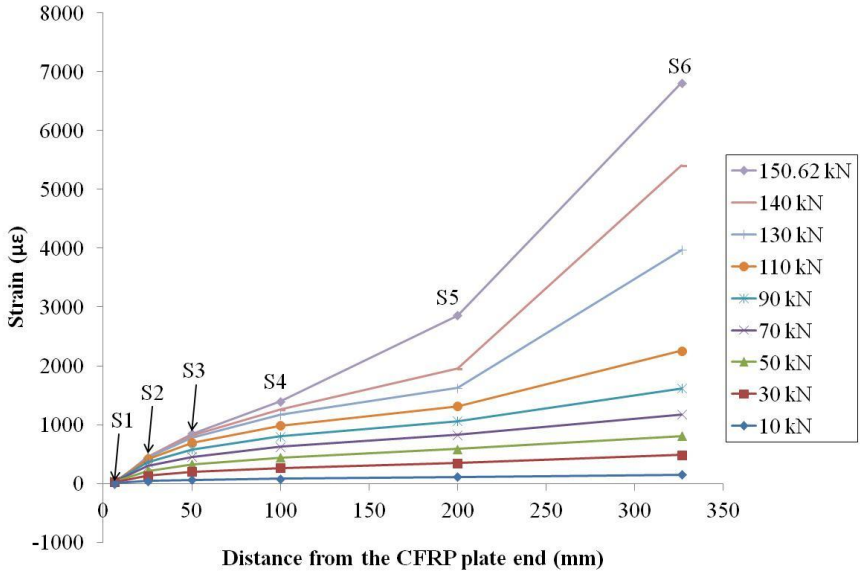

Figure E.7: Strain distribution along CFRP plate at different load levels for SB700-45 specimen

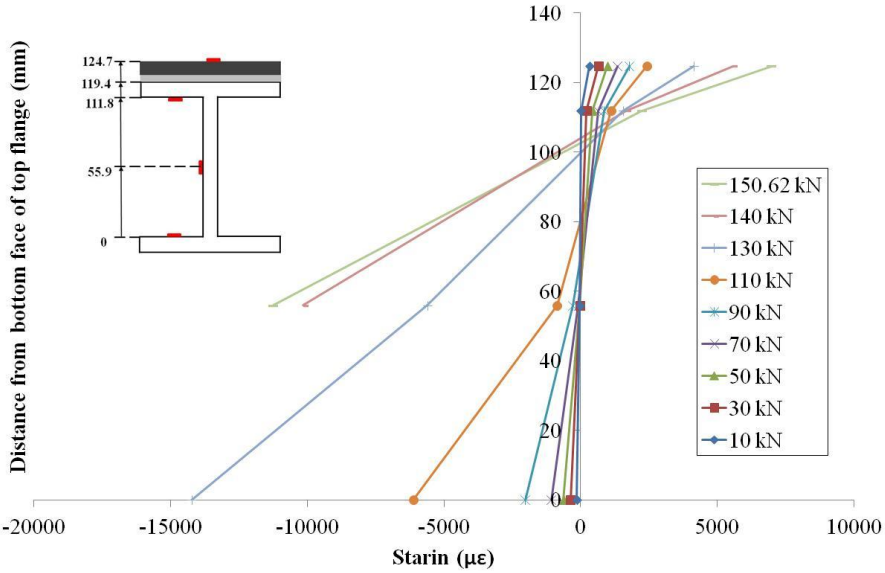

Figure E.8: Strain distribution across the middle of SB700-45 specimen at different load levels

Steel beam strengthened with 700 mm CFRP and tested at 60 °C (SB 700-60)

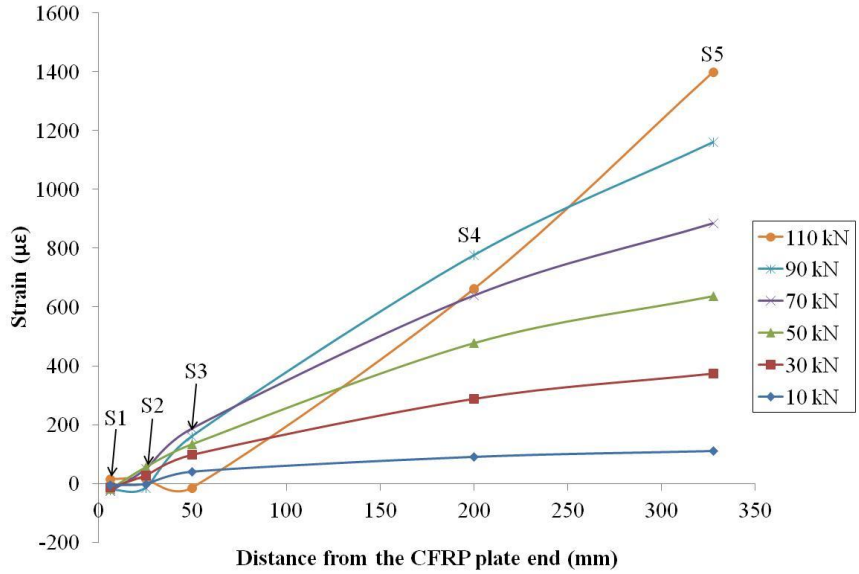

Figure E.9: Strain distribution along CFRP plate at different load levels for SB700-60 specimen

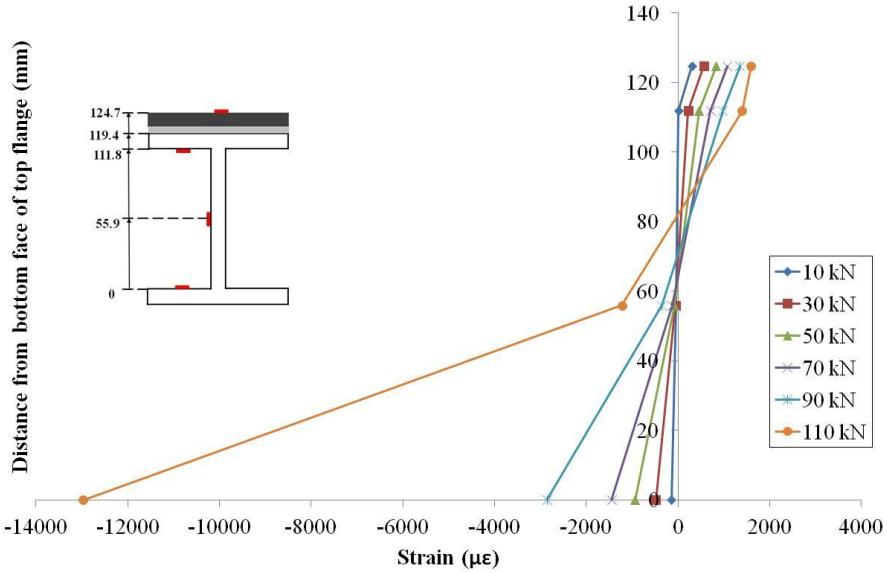

Figure E.10: Strain distribution across the middle of SB700-60 specimen at different load levels

References

1. Bussell, M.N., *Appraisal of existing iron and steel structures*. 1997, Steel Construction Institute

2. International Transport Forum, *Permissible maximum weights of trucks in Europe*. October 2011.

3. TREN/G3/318/2007, *Final report: Effects of adapting the rules on weights and dimensions of heavy commercial vehicles as established within Directive 96/53/EC* November 2008, TRANSPORT & MOBILITY LEUVEN.

4. Mays, G.L. and A.R. Hutchinson, *Adhesives in Civil Engineering*. 1992: Cambridge University Press.

5. Al-Shawaf, A., *Modelling wet lay-up CFRP-steel bond failures at extreme temperatures using stress-based approach.* International Journal of Adhesion and Adhesives, 2011. **31**(6): p. 416-428.

6. ACI-Committee-440, *Report on Fiber-Reinforced Polymer (FRP) Reinforcement for Concrete Structures.* American Concrete Institute (ACI), 2007.

7. BS 5400 part 2, *Steel, concrete and composite bridges. Part 2-Specification for loads* 2006, British Standard.

8. BS EN 1991, *Eurocode 1. Actions on structures. Part1-5: General actions. Thermal actions*. 2003.

9. BS EN 1994-2, *Eurocode 4. Design of composite steel and concrete structures.* , in *Part 2: General rules and rules for bridges*. 2005 a, BSI.

10. Ditcher, A.K. and J.P.H. Webber, *Nonlinear mechanical and thermal responses of a unidirectional carbon-fibre-reinforced plastic.* The Journal of Strain Analysis for Engineering Design October, 1979 **14**: p. 149-156.

11. Deng, J., M.M.K. Lee, and S.S.J. Moy, *Stress analysis of steel beams reinforced with a bonded CFRP plate.* Composite Structures, 2004. **65**(2): p. 205-215.

12. Stratford, T. and J. Cadei, *Elastic analysis of adhesion stresses for the design of a strengthening plate bonded to a beam.* Construction and Building Materials, 2006. **20**(1-2): p. 34-45.

13. Dawood, M. and M. El-Tahan. *Effect of Extreme Temperatures on the Bond Behavior of Steel Beams Strengthened with CFRP Plates*. in *Advanced Composites in Construction (ACIC)*. 2011. University of Warwick, UK: netcomposites limited.

14. Schnerch, D., et al., *Use of high modulus carbon fibre reinforced polymer (CFRP) for strengthening steel structures.* 2003.

15. Tavakkolizadeh, M. and H. Saadatmanesh, *Fatigue Strength of Steel Girders Strengthened with Carbon Fiber Reinforced Polymer Patch.* Journal of Structural Engineering, 2003c. **129**(2): p. 186-196.

16. Tavakkolizadeh, M. and H. Saadatmanesh, *Strengthening of Steel-Concrete Composite Girders Using Carbon Fiber Reinforced Polymers Sheets.* Journal of Structural Engineering, 2003b. **129**(1): p. 30-40.

17. Miller, T.C., et al., *Strengthening of a Steel Bridge Girder Using CFRP Plates.* Journal of Bridge Engineering, 2001. **6**(6): p. 514-522.

18. Hollaway, L.C. and J. Cadei, *Progress in the technique of upgrading metallic structures with advanced polymer composites.* Progress in Structural Engineering and Materials, 2002. **4**(2): p. 131-148.

19. Deng, J. and M.M.K. Lee, *Behaviour under static loading of metallic beams reinforced with a bonded CFRP plate.* Composite Structures, 2007. **78**(2): p. 232-242.

20. Deng, J. and M.M.K. Lee, *Fatigue performance of metallic beam strengthened with a bonded CFRP plate.* Composite Structures, 2007. **78**(2): p. 222-231.

21. Kim, Y.J. and G. Brunell, *Interaction between CFRP-repair and initial damage of wide-flange steel beams subjected to three-point bending.* Composite Structures, 2011. **93**(8): p. 1986-1996.

22. Kim, Y.J. and K.A. Harries, *Fatigue behavior of damaged steel beams repaired with CFRP strips.* Engineering Structures, 2011. **33**(5): p. 1491-1502.

23. Ghafoori, E., et al., *Fatigue strengthening of damaged metallic beams using prestressed unbonded and bonded CFRP plates.* International Journal of Fatigue, 2012(0).

24. Täljstena, B., C.S. Hansen, and J.W. Schmidt, *Strengthening of old metallic structures in fatigue with prestressed and non-prestressed CFRP laminates.* Construction and Building Materials, 2009. **23**(4): p. 1665-1677.

25. Smith, S.T. and J.G. Teng, *Interfacial stresses in plated beams.* Engineering Structures, 2001. **23**(7): p. 857-871.

26. Denton, S.N. *Analysis of stresses developed in FRP plated beams due to thermal effects.* in *Proceeding of the Conference on Composites in Civil Engineering* 2001. Hong Kong.

27. Cadei, J.M.C., et al., *Strengthening metallic structures using externally bonded fibre-reinforced composites (C595)*, in CIRIA, Editor. 2004: London. p. 234

28. Shen, H.-S., J.G. Teng, and J. Yang, *Interfacial Stresses in Beams and Slabs Bonded with Thin Plate.* Journal of Engineering Mechanics, 2001. **127**(4): p. 399-406.

29. Yang, J., J.G. Teng, and J.F. Chen. *Interfacial stresses in soffit-plated reinforced concrete beams*. in *Proceedings of the ICE- Structures and Buildings* 2004

30. Yang, J. and J. Ye, *An improved closed-form solution to interfacial stresses in plated beams using a two-stage approach.* International Journal of Mechanical Sciences, 2010. **52**(1): p. 13-30.

31. Zhao, X.-L. and L. Zhang, *State-of-the-art review on FRP strengthened steel structures.* Engineering Structures, 2007. **29**(8): p. 1808-1823.

32. Hollaway, L.C. and M.B. Leeming, *Strengthening of Reinforced Concrete Structures: Using Externally-Bonded FRP Composites in Structural and Civil Engineering*. 1999.

33. Dussek, I.J., *Strengthening of bridge beams and similar structures by means of epoxy-resin-bonded external reinforcement.* Transportation Research Board, Transportation Research Record. 785, Washington, D.C, 1980: p. 21-24.

34. Hutchinson, A.R., *Strengthening of the Quinton Bridges with externally bonded steel plate reinforcement: a durability appraisal after 19 years*. 1996, Bridge Management 3, eds. J E Harding, G A R Parke and M J Ryall, E & F N Spon. p. 743-750.

35. Kennedy Reid, I.L., D.M. Milne, and R.E. Craig, *Steel Bridge Strengthening: A Study of Assessment and Strengthening Experience and Identification of Solutions*. 2001: Thomas Telford Ltd.

36. Meier, U., *Strengthening of structures using carbon fibre/epoxy composites.* Construction and Building Materials, 1995. **9**(6): p. 341-351.

37. Meier, U., *Bridge repairs with high performance composite fibre materials.* Material und Technik, 1987. **15**: p. 225-228.

38. Hutchinson, A.R. and H. Rahimi. *Behaviour of reinforced concrete beams with externally bonded fibre-reinforced plastics*. in *Proc. 5th, Int. Conf. on Structural Faults and Repair*. 1993. Edinburgh: Engineering Technics Press,.

39. Hollaway, L.C. and M.B. Leeming, *Structural Strengthening with Bonded Fibre-Reinforced Composites.* Woodhead puplishing limited, 1998.

40. Mertz, D.R. and J.W. Gillespie, *Rehabilitation of Steel Bridge Girders Through the Application of Advanced Composite Materials* in *Final Report to the Transportation Research Board (Contract NCHRP-93-ID011)*. 1996: Washington, D.C. p. 30.

41. Mertz, D.R., et al., *The rehabilitation of steel bridge girders using advanced composite materials.*, in *IDEA Program Final Report NCHRP-98-ID051*. 2001.

42. Moy, S.S.J., *ICE Design and Practice Guides. FRP composites: Life extension and strengthening of metallic structures*. 2001: Thomas Telford.

43. Schnerch, D., M. Dawood, and S. Rizkalla, *Design Guidelines for the Use of HM Strips: Strengthening of Steel Concrete Composite Bridges with High Modulus Carbon Fiber Reinforced Polymer (CFRP) Strips*, T.R. IS-06-02, Editor. 2007a, Department of Civil, Construction and Environment Engineering, North Carolina State University.

44. CNR-DT202, *Guidelines for the design and construction of externally bonded FRP systems for strengthening existing structures- metallic structures*. 2007: Rome, Italy.

45. Moy, S.S.J. and A.G. Bloodworth, *Strengthening a steel bridge with CFRP composites.* Proceedings of the ICE - Structures and Buildings, 2007. **160**(2): p. 81-93.

46. Chajes, M., et al., *Application of Advanced Composites to Steel Bridges: A Case Study on the Ashland Bridge (Delaware-USA).* DELAWARE CENTER FOR TRANSPORTATION, University of Delaware, 2005.

47. Phares, B.M., et al. *Strengthening of Steel girder bridges using FRP*. in *Proceedings of the 2003 Mid-Continent Transportation Research Symposium*. 2003. Ames, Iowa.

48. Mosallam, A., *Structural Evaluation and Construction of Fiber-Reinforced Polymer Composites Strengthening Systems for the Sauvie Island Bridge.* Journal of Composites for Construction, 2007. **11**(2): p. 236-249.

49. Liu, X., P.F. Silva, and A. Nanni. *Rehabilitation of steel bridge members with FRP composite materials*. in *Proceedings of the International Conference on Composites in Construction,*. 2001. Porto, Portugal: J. Figueiras, L. Juvandes and R. Furia, eds.

50. Tavakkolizadeh, M. and H. Saadatmanesh. *Repair of cracked steel girder using CFRP sheet*. in *Creative Systems in Structural and Construction Engineering, Proceedings of the 1st International Structural Engineering and Construction Conference*. 2001a. Honolulu, Hawaii,: Amarjit Singh, ed., .

51. Tavakkolizadeh, M. and H. Saadatmanesh, *Repair of Damaged Steel-Concrete Composite Girders Using Carbon Fiber-Reinforced Polymer Sheets.* Journal of Composites for Construction, 2003a. **7**(4): p. 311-322.

52. Al-Saidy, A.H., F.W. Klaiber, and T.J. Wipf, *Repair of Steel Composite Beams with Carbon Fiber-Reinforced Polymer Plates.* Journal of Composites for Construction, 2004. **8**(2): p. 163-172.

53. Sen, R., L. Liby, and G. Mullins, *Strengthening steel bridge sections using CFRP laminates.* Composites Part B: Engineering, 2001. **32**(4): p. 309-322.

54. Shaat, A. and A. Fam, *Repair of Cracked Steel Girders Connected to Concrete Slabs Using Carbon-Fiber-Reinforced Polymer Sheets.* Journal of Composites for Construction, 2008. **12**(6): p. 650-659.

55. Rabinovich, O. and Y. Frostig, *Closed-Form High-Order Analysis of RC Beams Strengthened with FRP Strips.* Journal of Composites for Construction, 2000. **4**(2): p. 65-74.

56. Yang, J., J.F. Chen, and J.G. Teng, *Interfacial stress analysis of plated beams under symmetric mechanical and thermal loading.* Construction and Building Materials, 2009. **23**(9): p. 2973-2987.

57. Stratford, T. and L. Bisby, *Effect of Warm Temperatures on Externally Bonded FRP Strengthening.* Journal of Composites for Construction, 2012. **16**(3): p. 235-244.

58. BS EN 1994-1-2:, *Eurocode 4. Design of composite steel and concrete structures.* , in *General rules- Structural fire design.* 2005, BSI.

59. AS4100, S.A., *Steel structures*. 1998: Sydney, Australia

60. Ashby, M.F. and D.R.H. Jones, *Engineering materials 2 : an introduction to microstructures, processing and design* 2006: Butterworth-Heinemann Ltd.

61. de NÃ¨ve, B. and M.E.R. Shanahan, *Effects of humidity on an epoxy adhesive.* International Journal of Adhesion and Adhesives, 1992. **12**(3): p. 191-196.

62. BS ISO 11357-2, *Plastics. Differential scanning calorimetry (DSC). Determination of glass transition temperature*. 1999, BS.

63. BS EN ISO 6721-1, *Plastics. Determination of dynamic mechanical properties. General principles*. 2011, BSI.

64. Hollaway, L.C., *A review of the present and future utilisation of FRP composites in the civil infrastructure with reference to their important in-service properties.* Construction and Building Materials, 2010. **24**(12): p. 2419-2445.

65. Banea, M.D. and L.F.M.d. Silva. *The effect of temperature on the mechanical properties of adhesives for the automotive industry*. 2010: Proceedings of the Institution of Mechanical Engineers, Part L: Journal of Materials: Design and Applications.

66. Mahieux, C.A., K.L. Reifsnider, and S.W. Case, *Property Modeling across Transition Temperatures in PMC's: Part I. Tensile Properties.* Applied Composite Materials, 2001. **8**(4): p. 217-234.

67. Mahieux, C.A. and K.L. Reifsnider, *Property modeling across transition temperatures in polymers: application to thermoplastic systems.* Journal of Materials Science, 2002. **37**(5): p. 911-920.

68. Bai, Y. and T. Keller, *Effects of thermal loading history on structural adhesive modulus across glass transition.* Construction and Building Materials, 2011. **25**(4): p. 2162-2168.

69. Bai, Y., T. Keller, and T. Vallée, *Modeling of stiffness of FRP composites under elevated and high temperatures.* Composites Science and Technology, 2008. **68**(15-16): p. 3099-3106.

70. Sauder, C., J. Lamon, and R. Pailler, *The tensile behavior of carbon fibers at high temperatures up to 2400 ˚C.* Carbon, 2004. **42**(4): p. 715-725.

71. Bisby, L.A., M.F. Green, and V.K.R. Kodur, *Response to fire of concrete structures that incorporate FRP.* Progress in Structural Engineering and Materials, 2005. **7**(3): p. 136-149.

72. Saafi, M., *Effect of fire on FRP reinforced concrete members.* Composite Structures, 2002. **58**(1): p. 11-20.

73. Wang, Y.C., P.M.H. Wong, and V. Kodur, *An experimental study of the mechanical properties of fibre reinforced polymer (FRP) and steel reinforcing bars at elevated temperatures.* Composite Structures, 2007. **80**(1): p. 131-140.

74. Cao, S., Z. Wu, and X. Wang, *Tensile properties of CFRP and hybrid FRP composites at elevated temperatures.* Journal of Composite Materials 2009. **43**(4): p. 315-330.

75. Barker, A.J. and H. Vangerko, *Temperature dependence of elastic constants of CFRP.* Composites, 1983. **14**(1): p. 52-56.

76. Wang, K., B. Young, and S.T. Smith, *Mechanical properties of pultruded carbon fibre-reinforced polymer (CFRP) plates at elevated temperatures.* Engineering Structures, 2011. **33**(7): p. 2154-2161.

77. Chowdhury, E., et al., *Mechanical Characterization of Fibre Reinforced Polymers Materials at High Temperature.* Fire Technology, 2011. **47**(4): p. 1063-1080.

78. Keller, T., C. Tracy, and A. Zhou, *Structural response of liquid-cooled GFRP slabs subjected to fire- Part I: Material and post-fire modeling.* Composites Part A: Applied Science and Manufacturing, 2006a. **37**(9): p. 1286-1295.

79. Keller, T., C. Tracy, and A. Zhou, *Structural response of liquid-cooled GFRP slabs subjected to fire- Part II: Thermo-chemical and thermo-mechanical modeling.* Composites Part A: Applied Science and Manufacturing, 2006b. **37**(9): p. 1296-1308.

80. Gibson, A.G., et al., *Laminate Theory Analysis of Composites under Load in Fire.* Journal of Composite Materials 2006. **40**(7): p. 639-658

81. Bai, Y. and T. Keller, *Time dependence of material properties of FRP composites in fire.* Journal of Composite Materials, 2009. **43**(21): p. 2469-2484.

82. Umeco, *MTM46, PDS1191/03.12/6a*. 2012, Advanced Composites Group Ltd.

83. Engineering ToolBox *Resources, Tools and Basic Information for Engineering and Design of Technical Applications*, in *http://www.engineeringtoolbox.com/*. 24.11.2012.

84. Zuk, W., *Thermal Behavior of Composite Bridges - Insulated and Uninsulated*. 1965, Highway Research Board. p. 231-253.

85. Emerson, M., *The Calculation of the Distribution of Temperature in Bridges*, in *TRRL laboratory report 561*. 1973: Crowthorne, Berkshire.

86. Emerson, M., *Extreme Values of Bridge Temperature for Design Purpose*, in *TRRL laboratory report 744*. 1976: Crowthorne, Berkshire.

87. Adams, R.D., et al., *The effect of temperature on the strength of adhesive joints.* International Journal of Adhesion and Adhesives, 1992. **12**(3): p. 185-190.

88. Ashcroft, I.A., et al., *Effect of Temperature on the Quasi-static Strength and Fatigue Resistance of Bonded Composite Double Lap Joints.* The Journal of Adhesion, 2001. **75**(1): p. 61-88.

89. Harris, J.A. and P.A. Fay, *Fatigue life evaluation of structural adhesives for automative applications.* International Journal of Adhesion and Adhesives, 1992. **12**(1): p. 9-18.

90. Blontrock, H., *Analysis and modeling of the fire resistance of concrete elements strengthened with externally bonded FRPs*. 2003, Ghent University. p. 414.

91. Klamer, E.L., D.A. Hordijk, and C.S. Kleinman, *Debonding of CFRP laminates externally bonded to concrete specimens at low and high temperatures*, in *Third International Conference on FRP Composites in Civil Engineering (CICE 2006).* 2006: Miami, Florida, USA p. 35-38.

92. Di Tommaso, A., et al., *Behavior of Adhesively Bonded Concrete-CFRP Joints at Low and High Temperatures.* Mechanics of Composite Materials, 2001. **37**(4): p. 327-338.

93. Ferrier, E., G. Lagarde, and P. Hamelin, *Concrete beams reinforced by fibre-reinforced plastics: the effect of temperature on the adhesive layer.* Composites Science and Technology, 2001. **61**(3): p. 425-431.

94. Aguiar, J., A. Camões, and N. Vaz, *Effect of temperature on RC elements strengthened with CFRP.* Materials and Structures, 2008. **41**(6): p. 1133-1142.

95. Klamer, E.L., D.A. Hordijk, and M.C.J. Hermes. *The influence of temperature on RC beams strengthened with externally bonded CFRP reinforcement*. 2008.

96. Huang, P.Y., et al., *Fatigue lives of RC beams strengthened with CFRP at different temperatures under cyclic bending loads.* Fatigue & Fracture of Engineering Materials & Structures, 2011. **34**(9): p. 708-716.

97. Jiao, H. and X.L. Zhao, *CFRP strengthened butt-welded very high strength (VHS) circular steel tubes.* Thin-Walled Structures, 2004. **42**(7): p. 963-978.

98. Yong-xin, Y., Y. Qing-rui, and P. Peng Fu-ming. *Experimental Research on Bond Behavior of CFRP to Steel*. in *Proceedings of the International Symposium on Bond Behaviour of FRP in Structures (BBFS 2005)*. 2005. Hong Kong, China: Chen and Teng (eds): International Institute for FRP in Construction.

99. Al-Zubaidy, H., R. Al-Mahaidi, and X.-L. Zhao, *Experimental investigation of bond characteristics between CFRP fabrics and steel plate joints under impact tensile loads.* Composite Structures, 2012. **94**(2): p. 510-518.

100. Fawzia, S., R. Al-Mahaidi, and X.-L. Zhao, *Experimental and finite element analysis of a double strap joint between steel plates and normal modulus CFRP.* Composite Structures, 2006. **75**(1-4): p. 156-162.

101. Fawzia, S., et al., *Bond characteristics between CFRP and steel plates in double strap joints.* The International Journal of Advanced Steel Construction, 2005. **2**: p. 17-27.

102. Fawzia, S., X.-L. Zhao, and R. Al-Mahaidi, *Bond–slip models for double strap joints strengthened by CFRP.* Composite Structures, 2010. **92**(9): p. 2137-2145.

103. Zhao, X.-L., D. Fernando, and R. Al-Mahaidi, *CFRP strengthened RHS subjected to transverse end bearing force.* Engineering Structures, 2006. **28**(11): p. 1555-1565.

104. Hashim, S., et al., *Design and analysis of DLS steel/composite thick-adhernd adhesive joints*, in *17th International Conference on Composite Materials (ICCM-17)*. 2009.

105. Fawzia, S., et al., *Strengthening of circular hollow steel tubular sections using high modulus CFRP sheets.* Construction and Building Materials, 2007. **21**(4): p. 839-845.

106. Crasto, A.S. and R.Y. Kim, *Environmental durability of a composite-to-composite adhesive bond in infrastructure applications*, in *28th international SAMPE technical conference*. 1996. p. 837-849.

107. Clarke, H., *Reinforcing Wrought Iron with Carbon Fibre Reinforced Polymers* in *School of Civil Engineering and the Environment*. 2006, UNIVERSITY OF SOUTHAMPTON.

108. Colombi, P., et al., *Durability of steel elementsstrengthened by FRP plates subject to mechanical and environmental loads* in *CCC2005:Third international conference composites in construction.* . 2005, composites in construction: Lyon, France. p. 291-298.

109. Colombi, P., G. Fava, and C. Poggi, *Durability of steel members strengthened by CFRP strips under mechanical and environmental loadings* in *CICE2006: Third International Conference on FRP Composites in Civil Engineering* 2006: Miami, Florida, USA.

110. Kinloch, A.J., *Durability of Structural Adhesives*. 1983: Applied Science.

111. Zhang, Y., A.P. Vassilopoulos, and T. Keller, *Effects of low and high temperatures on tensile behavior of adhesively-bonded GFRP joints.* Composite Structures, 2010. **92**(7): p. 1631-1639.

112. Al-Shawaf, A., R. Al-Mahaidi, and X.L. Zhao, *Effect of Elevated Temperature on Bond Behaviour of High Modulus CFRP/Steel Double Strap Joints*, in *Australian Structural Engineering Conference*. 2008: Melbourne p. 1-14.

113. Nguyen, T.-C., et al., *Mechanical characterization of steel/CFRP double strap joints at elevated temperatures.* Composite Structures, 2011. **93**(6): p. 1604-1612.

114. Hart-Smith, L.J., *Adhesive-bonded double-lap joints* 1973b, Langley research centre, Hampton, Virginia. p. 123

115. Nguyen, T.-C., et al., *Time-dependent behaviour of steel/CFRP double strap joints subjected to combined thermal and mechanical loading.* Composite Structures, 2012. **94**(5): p. 1826-1833.

116. BS EN ISO 6892-1, *Metallic materials. Tensile testing. Method of test at ambient temperature*. 2009, BSI.

117. BS 5950-1, *Structural use of steelwork in building. Code of practice for design. Rolled and welded sections*. 2000, BSI.

118. ASTM D696-08, *Standard test method for coefficient of linear thermal expansion of plastics between -30˚C and 30˚C With a Vitreous Silica Dilatometer*. 2009, ASTM.

119. Lanza di Scalea, F., *Measurement of thermal expansion coefficients of composites using strain gages.* Experimental Mechanics, 1998. **38**(4): p. 233-241.

120. Vishay-Tech Note-513-1, *Measurement of Thermal Expansion CoefficientUsing Strain Gages*. 2010.

121. Kreuzer, M., *Comparing the effect of lead and switch resistances on voltage- and current-fed strain-gage circuits*. 1985, Reports in Applied measurement. p. 13-18.

122. Special Metals, *The NILO and NILOMAG Nickel-Iron Alloys*. 2004.

123. BS EN ISO 527-2, *Plastics. Determination of tensile properties. Test conditions for moulding and extrusion plastics*. 1996.

124. Sikadur-30, *Adhesive for Bonding Reinforcements, product data sheet*. 2006.

125. BS ISO 11003-2, *Adhesives- Determination of shear behaviour of structural adhesives- part 2: tensile test method using thick adherends*. 2001.

126. ABAQUS, *ABAQUS/Standard User's Manual. Version 6.10, Hibbitt, Karlsson & Sorensen*. 2010.

127. BS EN 1542, *Products and systems for the protection and repair of concrete structures. Test methods. Measurement of bond strength by pull-off*. 1999, BSI.

128. DIN EN 24624, *Paints And Varnishes - Pull-off Test For Adhesion*. 1992.

129. Hart-Smith, L.J., *Adhesive-bonded single-lap joints* 1973a, Langley research centre, Hampton, Virginia. p. 123

130. Abaqus, *ABAQUS analysis user's manual, version 6.7-EF1*. 2007.

131. Narmashiri, K., N.H. Ramli Sulong, and M.Z. Jumaat, *Failure analysis and structural behaviour of CFRP strengthened steel I-beams*. Construction and Building Materials, 2012. **30**(0): p. 1-9.

132. Lenwari, A., T. Thepchatri, and P. Albrecht, *Debonding Strength of Steel Beams Strengthened with CFRP Plates*. Journal of Composites for Construction, 2006. **10**(1): p. 69-78.

133. Tilly, G.P., *Fatigue problems in highway bridges*, in *Transportation Research Board*. 1978.

134. Emberson, N.K. and G.C. Mays, *Significance of property mismatch in the patch repair of structural concrete. Part 3: Reinforced concrete members in flexure*, in *Magazine of Concrete Research*. 1996. p. 45-57.